FIBRE ORIENTATION AND BREAKAGE IN GLASS FIBRE REINFORCED POLYMER COMPOSITE SYSTEMS: EXPERIMENTAL VALIDATION OF MODELS FOR INJECTION MOULDINGS

B. PARVEEN

Ph.D

2014

Fibre Orientation and Breakage in Glass Fibre Reinforced Polymer Composite Systems: Experimental Validation of Models for Injection Mouldings

Validation of Short and Long Fibre Prediction Models within Autodesk Simulation Moldflow Insight 2014

Bushra PARVEEN

(B.Eng) Hons

Submitted for the degree of

Doctor of Philosophy

Faculty of Engineering and Informatics

University of Bradford

2014

Abstract

Bushra Parveen

Fibre orientation and breakage in glass fibre reinforced polymer composite systems: experimental validation of models for injection mouldings.

Keywords: Fibre, orientation, length, prediction, Moldflow, long fibre, short fibre, injection moulding.

End-gated and centre gated mouldings have been assessed with varying thickness and sprue geometries for the centre gate. Alternative image analysis techniques are used to measure the orientation and length of injection moulded short and long fibres composite components. The fibre orientation distribution (FOD) measurements for both geometries have been taken along the flow path. In shear flow the FOD changes along the flow path, however the FOD remains relatively constant during expansion flow. The core width and FOD at the skin within a long glass fibre (LGF) specimen is different in comparison to a short glass fibre (SGF) specimen. Fibre length measurements have been taken from the extrudate, sprue and 2 positions within the centre gate cavity. The size of the sprue has little influence on fibre breakage if the moulding is more than 1 mm thick

The SGF FOD prediction models within Autodesk Simulation Moldflow Insight 2014 (ASMI) have been validated against measured SGF data. At present, by default, the models over-predict the $<\cos^2\theta>$ for most geometries. When the coefficients are tailored for each model, drastic improvements are seen in the FOD prediction. The recently developed SGF RSC model accurately predicts the FOD in shear, in a thin geometry, whereas the Folgar-Tucker model predicts the FOD accurately in expansion flow.

The measured LGF fibre length distribution (FLD) and FOD have been validated against the LGF prediction models. The LGF models are currently under-

predicting the breakage and over-predicting $\langle \cos^2\theta \rangle$. The breakage prediction improves if measured FLD of the extrudate is input into the model.

Dedicated to my cousin and childhood friend who died at a tender age in the midst of the PhD. He has instilled within me the meaning of life he will always be missed.....

Naveed Ahmed

1987-2012

Acknowledgements

I would like to thank Almighty Allah, the most gracious and merciful for giving me the strength, courage and ability to achieve success in life.

The work described in report was carried out under the supervision of Dr. Phillip Caton-Rose and Professor John Sweeney at the Polymer IRC. I would like to thank both supervisors for their continuous support and encouragement during the course. I would like to extend a special appreciation to Dr. Phillip Caton-Rose for giving me this opportunity and for instilling within me confidence, patience and clarity.

The work carried out in this project is sponsored by Autodesk Ltd, I would like to offer a special thanks to Dr. Franco Costa and other members of the Autodesk team, for their efforts in coordinating the programme and instant responses. I would like to express my appreciation to Dr. Peter Hine at the University of Leeds for his research and involvement in the project. I would like to thank Dr. Dave Brands and other members of the SABIC Innovative Plastics for their contribution.

Special thanks go to Mr. Glen Thompson, Mr. Roy Dixon and other members of the technical staff team who have given me invaluable technical support. I would like to thank Professor Phillip Coates, colleagues and friends at the Polymer IRC who have kept me going throughout the programme, with their encouragements, banter and sometimes tantrums.

Last but not least I would like to thank my parents and the other members of my family and friends for all the support, love and motivation to get me through all the struggles in life.

Table of Contents

List of Figures

List of Tables

Nomenclature

θ	Angle theta (º)
φ	Angle Phi (º)
X	X-axis
Y	Y-axis
Z	Z-axis
A_{ij}	Second order orientation
$\dot{\gamma}$	Strain Rate (s^{-1})
C_i	Coefficient of interaction
D_Z	Thickness interaction coefficient
K	Reduced strain scalar factor
L_n	Average length (mm)
L_W	Weighted average length (mm)
L (b)	Length (mm)
D (a)	Diameter (mm)
Wt (%)	Weighted (%)
C_B	Breakage coefficient
D_g	Breakage drag coefficient
S	Breakage shape coefficient
$\cos^2\theta$	Average fibre orientation (tensor component)
SGF	Short glass fibre
SFT	Short fibre thermoplastic
LGF	Long glass fibre
LFT	Long fibre thermoplastic
FT	Folgar -Tucker
MFT	Modified Folgar -Tucker
RSC	Reduced Strain Closure
ARD	Anisotropic Rotary Diffusion
FOD	Fibre Orientation Distribution
FLD	Fibre Length Distribution
2-d/3-d	2-dimensional and 3-dimensional

Chapter 1 Introduction

Polymers, materials commonly referred to as plastics, are widely used in everyday life in applications such as food packaging, toys, medical devices and many more. The ability to rapidly and easily transform polymers into complicated shapes at low cost is one of the main reasons why polymers are widely used today. Within the last few decades there has been a rapid increase in the production of synthetic composites, as it is possible to obtain new materials with tailored applications. A composite is a material having two or more distinct constituents or phases, the constituent that is usually continuous and present in the greater quantity in the composite is termed matrix (Matthews and Rawlings, 1994). When fine fibres are incorporated into a polymer matrix this results in a reinforced composite. Enhanced performance and mechanical properties are the reasons behind the growth and development of reinforced composites material (Rhode et al., 2011).

Mechanical properties of the composite as a whole are defined by the matrix system, type of fibre reinforcement, fibre content, fibre length and orientation shown by Thomason, (2002; 2008). Fibres are produced using glass material, although where increased performance is desired, carbon and Kevlar reinforcement are available for application. For short or long glass filled polymers the parameters fibre length distribution (FLD) and fibre orientation distribution (FOD) are influenced by the process conditions, part design and processing technologies. Injection moulding process is the most common, cost effective process technique available to manufacture glass fibre reinforced thermoplastic (GFRP) products. For injection moulding of GFRP the average fibre length of a pellet is between, 2-3 mm for short glass fibre (SGF) and 12 to 25 mm for long glass fibres (LGF).

High fibre content and sufficiently high aspect ratio (length/diameter) are desired properties to enhance mechanical performance of a composite part. Short fibre thermoplastics (SFTs) have been used in the automotive industry for many years, there has recently been a strong growth in long fibre

thermoplastics (LFTs) to reduce cost in production of vehicles by replacing structural metallic parts (Thattaiparthasarathy et al., 2007). The automotive industry is utilizing increasing amounts of long glass/carbon fibre reinforced plastics with the aim to decrease vehicle weight and boost fuel efficiency. The majority of plastic components can be formed using injection moulding (Gauthier, 1995).

The essence of injection moulding is injection of molten polymer within a closed split mould which completely defines product dimensions. During the polymer melt flow, SFT experience shear and elongation stresses that distribute and orient the fibres along preferential directions. LFTs in some cases behave as short fibre composites, however fibre interactions are more complicated due to long length, and this may change the FOD. In SGF and LGF thermoplastics the moulding conditions, polymer rheological behaviour, gate shape, nozzle and screw design affect the FLD which in turn influences FOD. All parameters which decrease the shear stresses in the polymer melt generally decrease fibre degradation such as low back pressure and slow screw speed etc. Some authors Lafranche et al., (2005); Bijsterbosch and Gaymans, (1995) have shown how the injection moulding process affects the fibre degradation and advised on methods to optimize the FLD.

In order to make use of injection moulded composites effectively, there is a great need to develop process constitutive models, as well as computational tools to predict microstructure of the composite (Nguyen et al., 2005). The resulting property from processing can be used to produce reliable macroscopic or microscopic predicted responses of the final product. Otherwise the mechanical state of a component must be assumed, resulting in over-engineering and the increase in manufacturing costs.

Currently there are commercial computer aided engineering (CAE) software packages available which simulate the injection moulding process and predict the structural properties of the component. Software or modelling packages are usually based upon finite element (FE), approximate solutions of partial differential equations. Geometries can be represented as shell or 3-d models and the solver uses a mesh to break the model into smaller elements and

nodes. Models (equations) have been derived and incorporated into the software to predict the processing parameters and composite structure outcome of injection moulding i.e. fibre orientation (VerWeyst et al., 1999). In order to enhance the accuracy of property prediction, constant development of mathematical models is required as well as further research to understand the effect injection moulding has on the product properties. Software like Autodesk Simulation Moldflow Insight 2014 (ASMI) can be an extremely useful tool; however it requires an expert user to identify areas where accuracy may be lost.

1.2 Aims and Objective

The aim of the project is to study how injection moulding affects the properties of short and long glass fibre (SGF and LGF) composite components, using both experimental and computational methods. The literature review will identify how the micro structural characteristics of glass FLD and FOD affect the mechanical properties of a composite structure. The next step is to understand the effect moulding process, parameters, mould design and material behaviour has on the glass FOD and FLD.

The objectives of the study are broken into sub-tasks;

- Understand the fibre prediction models in Autodesk Moldflow Simulation Insight 2014 (ASMI).
- Injection mould simple test geometries using short and long glass fibre material.
- Find suitable methods to measure FLD and FOD.
- Produce 2-dimensional (2-d) and 3-dimensional (3-d) models in ASMI 2014 to asses FLD and FOD prediction models.
- Compare the measured FOD with predicted FOD (short and long).
- Compare the measured FLD with the predicted fibre breakage.
- Assess fibre orientation and breakage models, find limitations and possible solutions to improve prediction.

1.3 Outline of Thesis

This thesis has been divided into 7 chapters. **Chapter one** gives a brief introduction to the subject and outlines the key objectives of the thesis. **Chapter two** covers the detailed literature review related to the aim of the project. **Chapter 3** includes the experimental methodologies used to obtain measured and predicted data. The focus of **Chapter 4** is on SGF measured and predicted average FOD. The investigation of measured and predicted LGF average FOD and FLD is found in **Chapter 5.** Chapter 4 and 5 consist of detailed analysis, discussion and conclusions. **Chapter 6** presents the general discussion and conclusions. **Chapter 7** establishes areas where there is further scope of research.

Chapter 2 Background

2.1 Structure and Properties of Polymers

A polymer is a large macromolecule built up from repeated single structural units (monomers). The physical characteristic of a polymer depends on the configuration of the molecular chain. It can be assumed that the molecules are not generally straight and in a tangled mass, but in some cases the molecules consist of linear and branched chain networks. The degree of polymerisation (number of monomers incorporated) is a term used to express the length of a polymer chain. The length of the chain affects the degree of interactions between molecules, therefore influencing mechanical and physical properties.

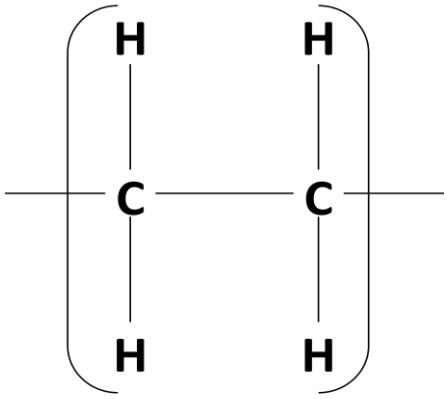

Figure 2.1 Molecular structure of Polyethylene

Thermoplastic are linear polymers. They do not crosslink to form a rigid network although the chains may be branched. The bonding in thermoplastic chains is weak and is easily broken by the combined action of high temperature and applied stress (McCrum et al., 1997).

Thermoplastics polymers soften when heated, eventually liquefying and hardening when cooled (this process is reversible). Over 80% of plastics are thermoplastic in nature, some of the commodity polymers include polyethylene (PE), polypropylene (PP), Polyvinyl chloride (PVC) and polystyrene (PS) (Powel and Housz, 1998). The semi-crystalline polymers polyethylene (PE),

polypropylene (PP) and Polyamides (PA) are currently the most popular matrixes used in industry. The major advantage of the polymer matrix is that it can be economically manufactured in vast quantities and find wide application in areas like automotive engineering as well as packaging.

2.1.1 Semi-crystalline and Amorphous Structure

Polymers as completely amorphous solids have no order in their structure so polymer chains have a random orientation. Cross linked plastics and rubber are some of the forms of amorphous polymer. The microstructure of crystalline polymer depends on the packing of polymer molecule crystals. Some material such as polypropylene, polyethylene and polyamide can form semi-crystalline structures. Narrow and regular linear polymer chains can form ordered arrangement of molecules which pack closely together below a certain temperature. The close packing confers on the crystallite a higher density, higher axial and transverse stiffness and strength. Semi-crystalline structures are an intimate mixture of ordered crystallites, suspended in a matrix of randomly structured amorphous material of the same polymeric type Figure 2.2.

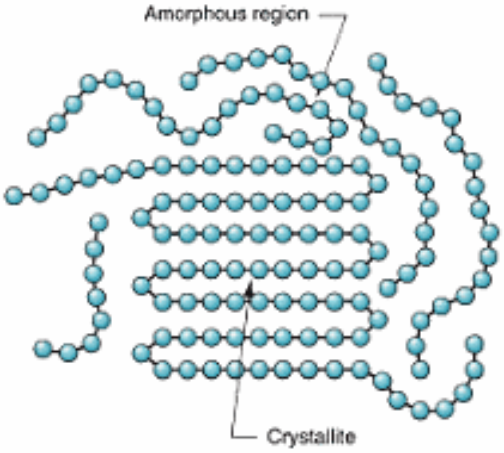

Figure 2.2 Long molecules forming crystals randomly mixed in with the amorphous material (Groover, 2010)

2.1.2 Mechanical properties

There are a number of standard tests which can be carried out in order to investigate the mechanical properties of polymers. The tensile test (material is placed under uniaxial tension until failure) is most widely used test, which is performed on dumbbell shaped tensile bars; the dimensions of these comply with industry standards (ISO). The dumbbell specimen with a narrow waist is preferred in testing for rubbers and thermoplastic material. Often single tests are conducted at one temperature to obtain stress-strain curves, from which a number of significant mechanical properties can be calculated.

Many different terms exist to describe the mechanical behaviour of materials, which can be explained using the characteristics of the stress/strain curves. The ultimate strength of a sample is the stress required to make it fail. The Young's modulus also known as the tensile modulus is the gradient of the linear proportion of the stress strain curve. This is a measure of the stiffness of an elastic material. The toughness is the amount of energy absorbed before failure occurs, the area under the stress /strain curve.

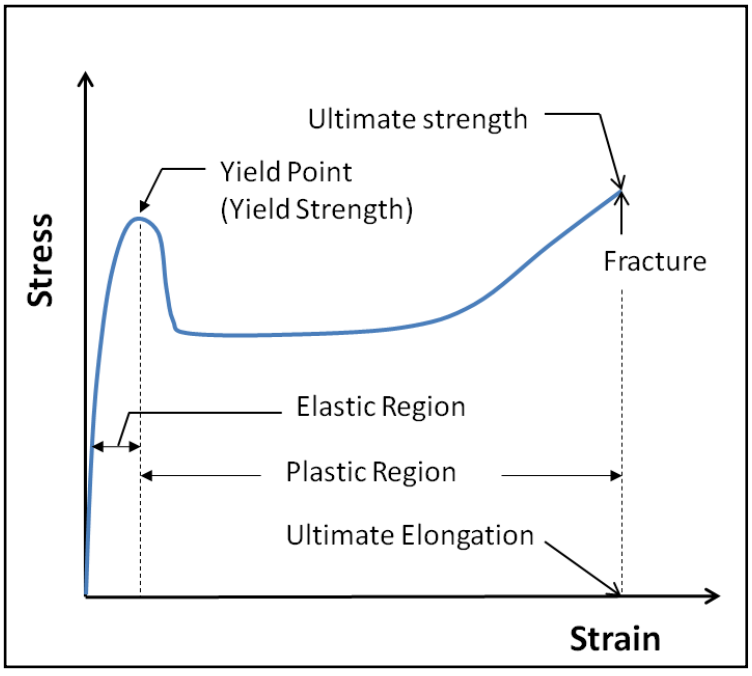

Figure 2.3 Shows stress /strain curve for crystalline material.

The material deforms up to the yield point, whereupon there is a drop in stress and the material starts to neck. The neck forms as the chain segments move past each other to form crystalline regions. This continues as plastic deformation where the molecules tend to uncoil until the molecules assume a fully stretched conformation and failure occurs. The stress that induces yielding is called the yield stress.

Polyamides are high performance semi-crystalline thermoplastics, with attractive high strength, resistance, wear and cost properties important for many industrial applications (Table 2.1). Kagan, (2003) and Nelson, (1976) have reported polyamides as a class are more moisture sensitive, than most thermoplastics, and will absorb water vapour when exposed to air. An increase of moisture absorption for PA6 and PA66 of 1% may result in 0.2% to 0.3% increase in dimension. This means that the drying process prior to moulding must be controlled to avoid differences within each moulded batch.

	ASTM test	**PP**	**PA6.6**	**HDPE (high density polyethylene)**	**uPVC**
Relative price		1.0	2.9	1.0	0.7
Young's modulus (GPa)	D790	1.5	2.8	0.8	3.0
Yield/fracture stress (MPa)	D638	33	83	28	55
Notched Izod impact strength J m^{-1}	D256	150	53	>1300	70
Heat distortion temperature (°C)	D648	<23	90	<23	55

Table 2.1 Properties of thermoplastic polymers with testing conditions specified in ASTM standard (McCrum et al., 1997).

2.2 Fibre Composites

The major problem with polymers in engineering is their low strength and stiffness. Two methods used to make up for these deficiencies include; changing the design of the component and the other is the addition of reinforcing material more commonly known as adding fillers to the resin (Matthews and Rawlings, 1994). Adding fillers or fibres is the means to increasing the strength and stiffness of a thermoplastic material at low cost. Most commercial composite grades are based on polypropylene and PA6 matrices. Synthetic inorganic fibres such as glass and carbon are examples of reinforcements. The use of carbon fibre is limited to high performance applications due to the high cost. Glass-fibre reinforced systems are responsible for the majority of the fibre reinforced plastics (FRP) and polymer matrix composite (PMC) market (Sims and Broughton, 2000). E-glass material is commonly used due to its low cost and reasonably high modulus. The unique properties obtained from the glass include high strength, heat resistance, flexibility and yielding (Wambua et al., 2003). Applications for glass fibre reinforced composites include; automotive and aerospace bodies, construction and pressure vessels.

2.2.1 Composite Mechanical Properties

The orientation and length of fibres in an injection moulded component varies through the thickness of the specimen. There are areas where fibres align parallel or perpendicular to the principal axis, therefore the mechanical properties are different in each direction. In theory the idealised composite would consist of continuous aligned fibres in one direction i.e. unidirectional with perfect interfacial bonding between fibre and matrix (Piggot, 1989). The material is orthotropic where the elastic properties are symmetric with respect to the chosen (1, 2 and 3) axis as shown in Figure 2.4 (Ward and Sweeney, 2013).

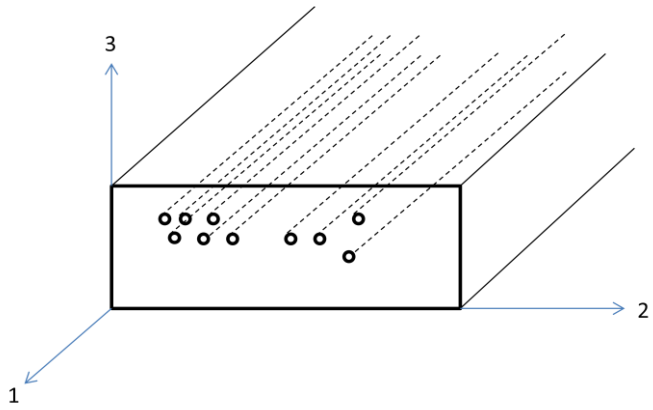

Figure 2.4 Orientation of principal composite material axis

The idealised composite obeys the Rules of Mixtures (Equation 2.1). If a load is applied parallel to the direction of fibres the mechanical properties are described by the tensile strength (fibre and matrix) and the volume fraction (Templeton, 1990).

$$E_c = V_f E_f + V_m E_m \qquad \textbf{2.1}$$

E_c = Composite Modulus, V_f = Fibre volume fraction, V_m = Matrix volume fraction, E_f = Fibre Modulus and E_m = Matrix Modulus.

The Modified Rule of Mixtures (MROM) (Equation 2.2) is used to model the effects of parameters on the stiffness of short fibre composites (Hine et al., 2014). The Krenchel orientation factor η_0 represents the average value of the fourth order orientation tensor in respect to the testing direction and the η_L represents the fibre reinforcing efficiency, where $\eta_L = 1$ for a unidirectional fibre.

$$E_c = \eta_0 \eta_L V_f E_f + V_m E_m \qquad \textbf{2.2}$$

2.2.2 Discontinuous Fibre Reinforcement

When a single fibre of length L (discontinuous fibre) is embedded into a polymer matrix and subjected to a tensile load in the fibre direction, there is a transfer of stress from fibre to matrix interface (Cooper and Kelly, 1969; Kelly

and Davis 1965). A greater aspect ratio (Equation 2.3) increases the fibre and matrix interface and the ability to transfer stresses across the fibre-matrix. The matrix and the fibre will experience different tensile strains as the fibre is strong and stiff (has a higher Young's Modulus). Interfacial shear stress acts in the direction of the fibre axis and the fibre is stressed in tension. A study carried out by Piggot and Harris, (1980) shows the matrix is stronger in compressive load compared to glass, which has no relative strength against compression.

$$\text{Aspect ratio} = \frac{\text{Fibre length}}{\text{Fibre Diameter}} \qquad \textbf{2.3}$$

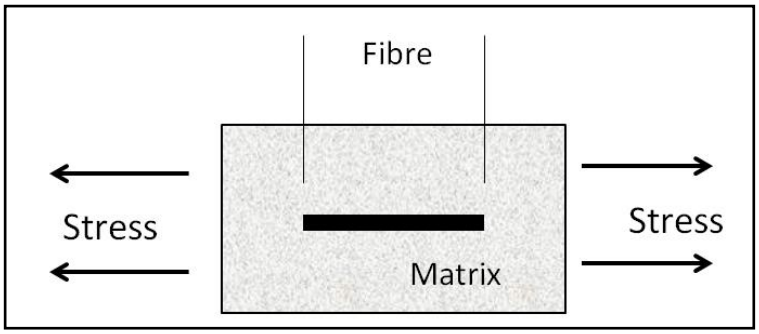

Figure 2.5 Discontinuous fibre in matrix subjected to tensile load stress

The efficiency of fibres also depends on interface strength as load transfer from polymer to fibre requires a strong interfacial bond (Greszczuk, 1969). A feature which influences the interface region is the fibre surface coating applied by the manufacturer, before integrating into the plastic matrix and protecting from surface damage. Thomason and Schoolenberg, (1994) show that the interfacial strength increases if a commercial coating is applied to the glass fibre compared to a standard silane coupling agent. Gupta et al., (1989) confirms the interfacial bonding is greater for long glass fibre material as there is greater interaction.

2.2.2.1 Fibre Length and Content

Short glass fibre composites have been used in the industry for many years, however recently there has been an increasing growth in the use of long fibre thermoplastics composites in engineering applications. The growth of

polypropylene based long fibre compounds has been due to excellent levels of performance, productivity and process-ability of these materials (Thomason, 2008). This section will discuss the differences before and after processing in SGF polyamide and long fibre polypropylene (LG-PP) pellets.

Continuous filaments of glass fibre are initially manufactured as bundles. Each filament normally has a round cross-section and the bundle consists of large number of strand filament (1000 – 10000). The major use of glass fibres is still as chopped strands into lengths of 3.2 mm, 6.4 mm, 12.7 mm or 25.4 mm (Mallick, 2000). Conventional method of extrusion or screw compounding, with a dry blend of the chopped glass fibres and polymer is used to produce 2-3 mm in length polymer-coated pellets for injection moulding (Wolf, 1994). Lunt and Shortall, (1979) have done a study to show the glass fibre degradation in PA66 caused by extrusion compounding, followed by injection moulding of 3 mm in length glass fibres. The results highlight even before injection moulding the length in the pellet ranges between 3 mm to 0.03 mm. Kamal et al., (1986) carried out injection moulding using pellets with an average fibre length of 0.710 mm, after injection moulding the average fibre length in the sample was 0.274 mm.

In recent years new processing techniques such as wire coating, cross-head extrusion or thermoplastics pultrusion have received more attention to create long fibre polypropylene injection moulding pellets (Ahmadi et al., 2000 and Schijve, 2000). In the process of pultrusion impregnation continuous fibre strands are pulled through liquid polymer in a die located at the end of an extruder, the coated fibres are then pelletized into 12.7 or 25.4 mm lengths. An adapted wire coating method is introduced by Schijve, (2000) whereby each glass fibre filament is coated (polymer/additives), the coated filaments are then wire-coated (bundled) with additional polymer and then cut into 12 mm and 25 mm pellet lengths. Traditional wire coated materials may not have coating on each filament. Due to the aligned nature of fibre in LG-PP compounds, it is possible to produce pellets with higher fibre concentration (Thomason, 2005). Two alternative studies show the average measured fibre length after injection moulding is 4.40 mm from a wire coated pellets compared to pultrusion

compounded pellets with an average fibre length of 3.54 mm. (Ward et al., 1993 and Schijve, 2000).

Figure 2.6 illustrates the FOD in short and long glass fibre pellets. As a result of the different methods of pellet manufacture the orientation of fibres is random in a short fibre pellet and parallel in a long glass fibre pellet. In production the glass fibre diameter will typically range between 10-17 µm for SGF pellets and 16 -20 µm for LGF pellets (Thomason, 2002).

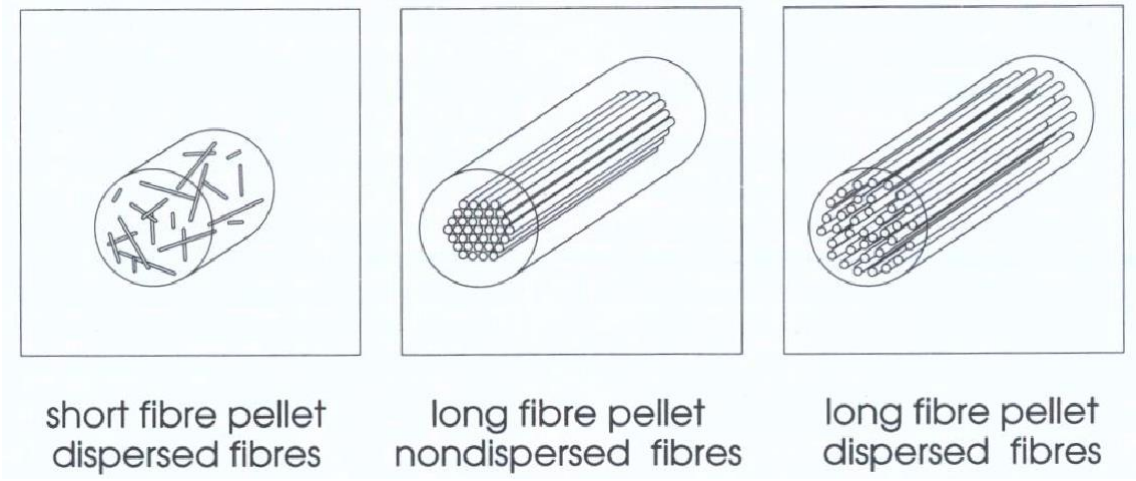

Figure 2.6 Short and long fibre thermoplastic composite pellets used for injection moulding (Wolf, 1994)

Thomason, (2002 and 2008) has compared the effect of fibre length on mechanical properties based on polyamide and polypropylene composites, at the same fibre diameters over a range of fibre contents. In these studies long fibre polypropylene showed a significant improvement in tensile and flexural strength, for both notched and un-notched impact resistance. Long fibre samples have a higher modulus over short glass fibre as the strain increases, this is highlighted in Figure 2.7.

However many of these mechanical properties reach maximum performance between 40-50 wt% fibre content range. In another study carried out by Thomason, (2005) on injection moulded 12.5 mm long glass fibre polypropylene, the modulus increases as the fibre content increases, but the strength and impact properties decrease between 40-50 wt% by fibre content. Implementing a small concentration of glass fibre into the matrix is a process of improving

interfacial shear strength between fibre and matrix. This reduction in interfacial strength with increasing fibre content is investigated by Thomason, (2007) on injection moulded 12.5 mm LGF polypropylene.

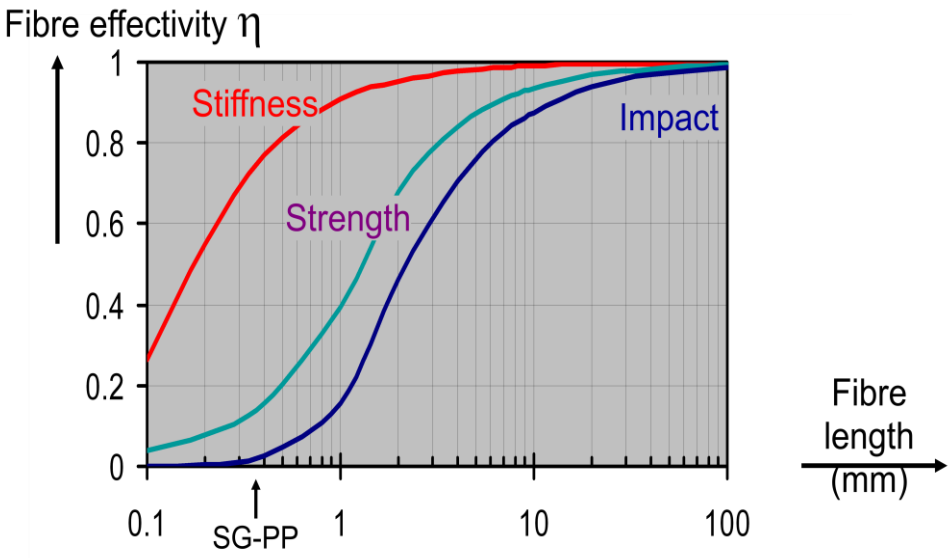

Figure 2.7 Effectiveness of fibre is proportional to the length (Schijve, 2010)

In discontinuous fibre reinforced composites as shown in Figure 2.5 there is a critical fibre length (l_c). The Kelly and Tyson (1965) theory assumes the critical length, is the length required for the fibre to reach the maximum stress condition within the matrix if the composite is loaded in tension. High shear stresses are developed at the fibre ends, the shear stress increases with decreasing fibre length. Consequently the critical fibre length (Equation 2.4) is dependent on the fibre diameter (d_f), ultimate fibre tensile strength (σ_{fu}) and the fibre-matrix interfacial shear stress (τ_i).

$$l_c = \frac{\sigma_{fu}}{2\tau_i} d_f \qquad \textbf{2.4}$$

Figure 2.8 illustrates the stress distributions which occur when a single fibre is loaded for failure at different fibre lengths. A value lower than the critical length, will result in a stress condition and the fibre will not fracture in tension. In this case failure may be a result of matrix cracking, debonding or fibre pull-out. If the fibre length is greater than the critical fibre length the central portion of the fibre will attain uniform stress level, which will allow effective use of the fibre.

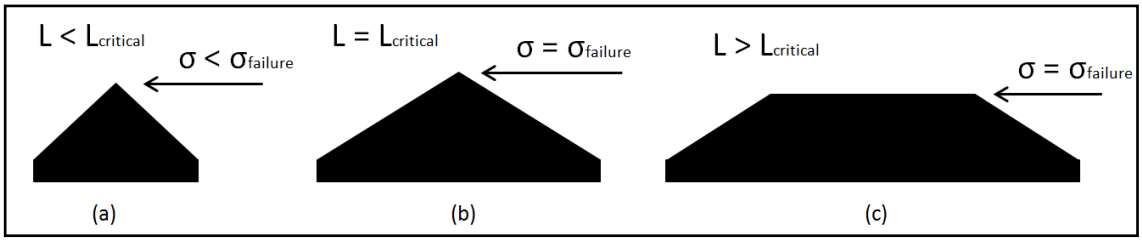

Figure 2.8 Normal stress distribution along the length of a short fibre at the point of composite failure (a) $l < l_c$ (b) $l = l_c$ (c) $l > l_c$

Templeton, (1990) has calculated the critical fibre length for short glass fibre polypropylene to be 1.4 mm; however it is hard to use this value as an indicator for the critical fibre length. The critical fibre length can vary from the grade or length of the raw material and the process settings (Schijve, 2000 and Wolf, 1994).

2.2.2.1.1 Fibre Dispersion

Lafranche et al., (2007) highlights characteristics seen in injection moulded long glass fibre thermoplastics. Areas of fibre clusters as shown in Figure 2.9 and porosity exist in certain locations of the specimen, reducing the flexural properties. Also more bundling occurs at the centre (core) of the part. Although the influence of segregation has never been measured, it is unclear if this is directly linked with the injection moulding process or resultant of the flow. According to Gupta et al., (1989) the dispersion of fibres is non-uniform and this uneven dispersion does not allow every fibre to act independently. Bijsterbosch and Gaymans, (1995) highlighted fibres can be well dispersed during injection moulding but at the cost of degradation.

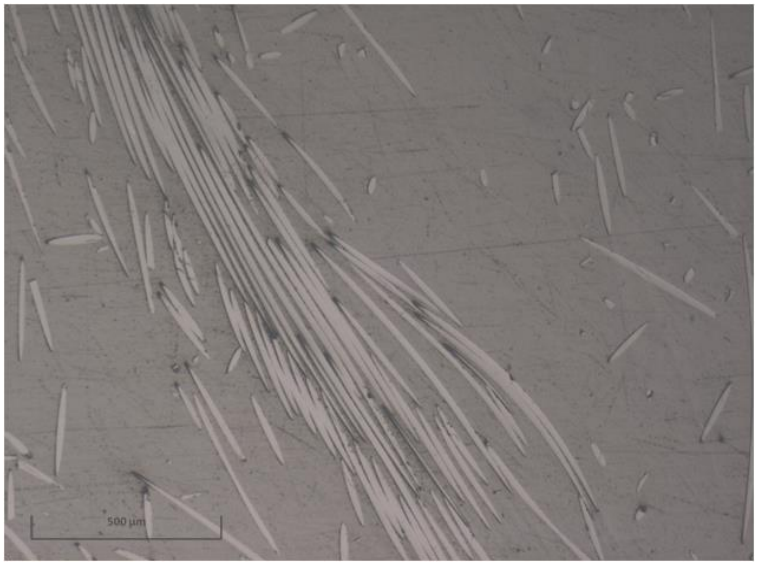

Figure 2.9 Bundling of fibres in a long glass fibre sample

2.3 Injection Moulding

Injection moulding is a traditional method used to form thermoplastic glass fibre composite components (Bijsterbosch and Gaymans, 1995). Once the component is manufactured the injection moulding process does more than shape the component, it also positions the reinforcing particles and fixes their orientation (Templeton, 1990). The shear stresses and flow results are an important characteristic of the reinforced polymer as the material exhibits anisotropy in its physical properties.

The injection moulding process can be divided into four stages: preparing the melt, filling, packing causing pressure build up and solidification by cooling (Olmsted and Davis, 2001). These stages are very important as they affect the performance of the finished product. The filling phase occurs at a pressure only sufficient to cause the viscous melt to completely occupying the mould cavity. To compensate for the significant thermal contraction of the polymer melt it is necessary to force additional material at higher pressure into the cavity. The packing and solidification determines the final dimensions i.e. tolerances, as well as the orientation of molecules or fibres and anisotropy. The material enters the mould cavity through a single or multiple injection points which is

usually a gate. The width, size and position of the gate are dependent upon the part and desired mechanical properties.

2.3.1 Overview of Process

Injection moulding is a recurring process which has very short cycle times (commonly within in the range of 10 s to 30 s and is used to produce identical, thin walled components, whose structure may consists of complex geometry. The diagram in Figure 2.10 below illustrates the main stages of an injection moulding process.

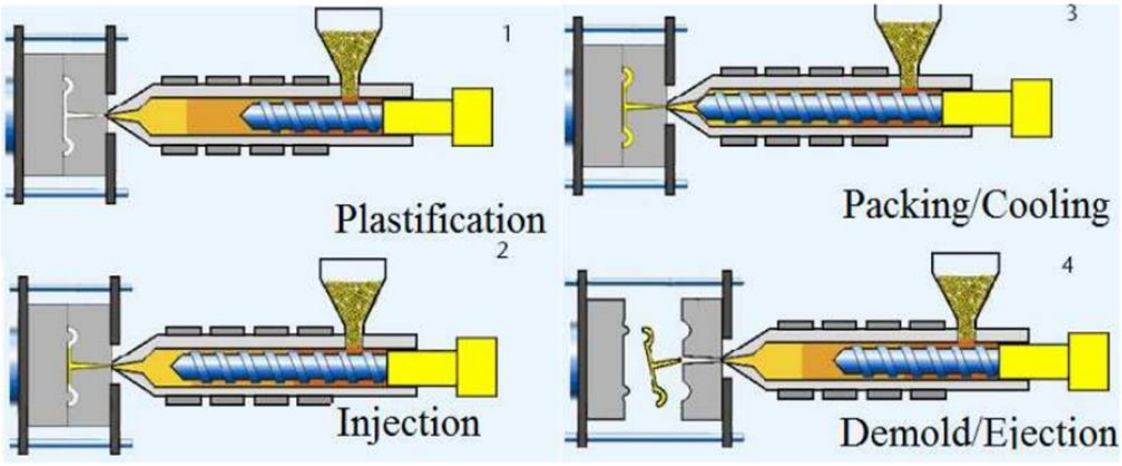

Figure 2.10 Pictorial of stages in an injection moulding process (Toolcraft Plastics, 2014)

The technique of injection moulding is simply a quantity of plastic pellets being gravity fed through a feed hole into a barrel. The material is blended into a viscous liquid, softened by the means of heat and shear by the screw (plastification). The screw has helical flights when the screw rotates backwards, the plastic moves forward and becomes a melt. The volume of the melt builds up in front of the screw; it forces the screw to the rear of the barrel against an adjustable "back pressure". The screw stops rotating once it reaches the position assigned; the machine is now ready for injection. The screw is then forced forward and material is injected at high pressure (typically, 70 to 205 MPa) under shear and guided through the nozzle and runner or gate system into the mould cavity (Gauthier, 1995). The design of the runner or gate is

dependent on the mould geometry and is required to provide the best flow to the cavity. The time taken for the material to fill the cavity is referred to as injection time. The mould temperature is held constant using a heat exchanger and typical mould temperatures vary from 10 ºC to 120 ºC. Temperatures are kept lower than the melting point of the material therefore the allowing the polymer to solidify as the mould fills.

The machine then switches over from velocity to pressure control, to hold the screw in the forward position to permit packing. A greater pressure is maintained to ensure polymer continues to flow as the solidifying material shrinks. The mould opens once the part has solidified and then it is ejected. While the part cools and the mould opens, the screw is drawn back for a new cycle to begin. It is important to consider the time taken for the part to cool as it is dependent on the nature of the cooling system, material and the mould size or shape. A compromise may be necessary between product quality and production economics, as low melt temperatures reduce cycle times. Avoidance of thermal degradation is another reason for reducing processing temperatures, especially in the high softening glassy plastics.

2.3.2 Fibre Length Degradation

Severe fibre breakage occurs in the injection moulding process resulting in shorter FLD. After injection moulding the average fibre length delivered for short glass components are < 1 mm and > 1 mm for long glass. The screw rotates and the granules undergo extreme shear and heat. As the granules melt a thin film of molten polymer builds up in the barrel. Thus the fibres experience shear and drag forces along the length.

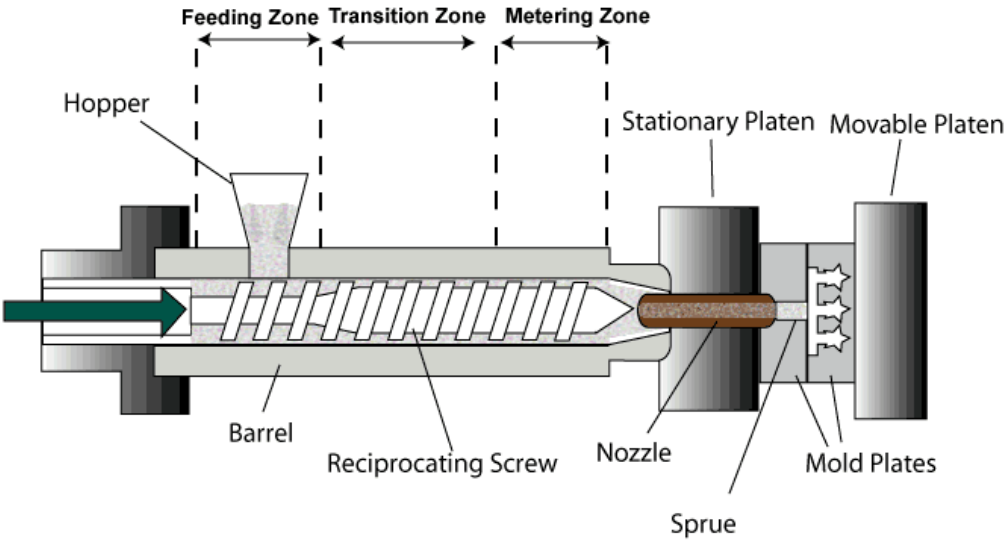

Figure 2.11 Detailed representation of the injection moulding mechanism (Hoshen, 2009)

Fibre attrition occurs at the following stages of the injection moulding cycle shown in Figure 2.11; screw pre-plasticisation, nozzle tip, injection of melt through narrow channels like runner or gate and through cavity surface (Bailey and Kraft, 1987 and Gupta, 1989). Previous work done by Lafranche et al., (2005) and Patcharaphun and Opaskornkul, (2008) has shown the majority of fibres breakage occurs in the feed and transition (compression) zone of the screw due to the high shear rates (Figure 2.12), such that the final length of long glass fibre reduces to 70% and short to 10% of its initial length. More fibre breakage occurs in LGF material; this is due to the solid-melt interface and increased fibre-fibre and fibre-wall interactions causing fracture (Rostato, 1996).

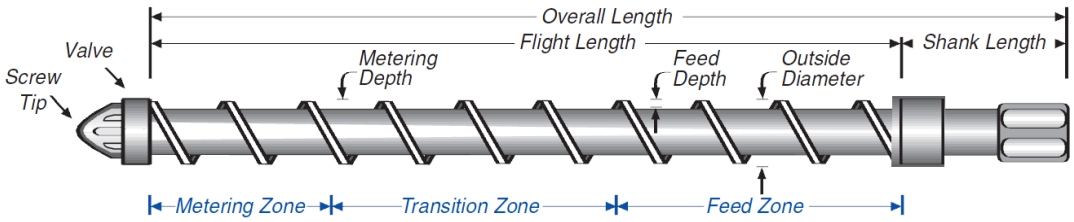

Figure 2.12 General purpose screw (Ticona, 2011)

As majority of fibre breakage occurs in the transition (compression) zone of the screw, material producers usually recommended a screw profile adapted to their LFT material (Sabic, 2011). In order to decrease shear stresses within the barrel during the plasticising stage material suppliers recommended a screw

with lower compression ratio, longer compression section and higher flight depth. However, most plastic part manufacturers choose to use a general purpose screw due to cost and multi material processing capabilities. Work carried out by Lafranche et al., (2007) and Nomoto et al., (2012) conclude using a LFT dedicated screw profile decreases the fibre breakage amount by 80% at the nozzle exit.

Once the material comes out of the screw tip it purges into the nozzle through to the cavity by means of gate or runner system. O'Regan and Akay, (1996) show LGF FLD exhibits particular sensitivity to nozzle arrangement, mould geometry and position in the moulding. They have found a hydraulic shut off nozzle leads to increased fibre breakage compared to a standard nozzle, due to the reduced orifice dimensions Figure 2.13. A larger gate dimension also increases the fibre volume average compared to a smaller gate (Bailey and Kraft, 1987).

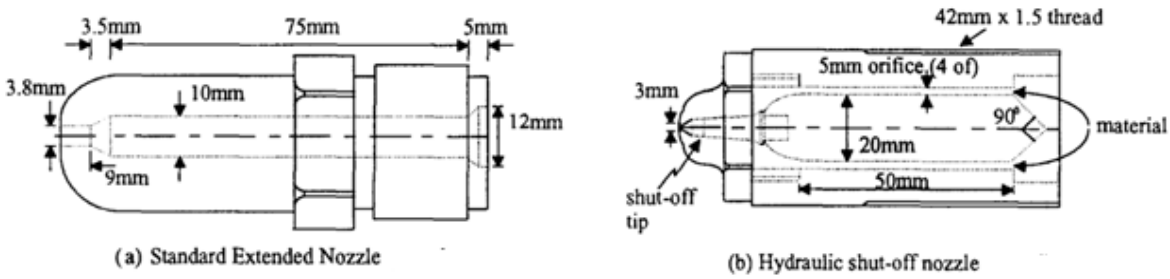

Figure 2.13 Comparison of shut-off and standard nozzle (O'Regan and Akay, 1996)

Some injection moulding parameters affect the overall FLD in a moulded component (Bailey and Kraft, 1987). During the plastification stage of injection moulding the backwards rotation of the screw is opposed by a pressure this resistance is termed 'back pressure'. The back pressure has the greatest impact on fibre length than injection speed or pressure (Rhode et al, 2011 and Bailey et al, 1989). However some researcher's debate screw rotational speed has a stronger effect on fibre breakage than back pressure (Lafranche et al., 2005). Although it is recommended by suppliers to keep both the back pressure and screw rotational speed low when processing glass fibre material (Sabic, 2011).

2.3.3 Characteristic of melt flow in the injection moulding process

There are 3 main flow regions that generally occur within injection moulded parts are skin (frozen) layer, shear layer and core layer as shown in the Figure 2.14. The mould filling stage involves a non-isothermal and non-steady melt flow shown in research carried out by Bright and Darlington, (1980), Brydson, (1970) and Bay et al., (1992).

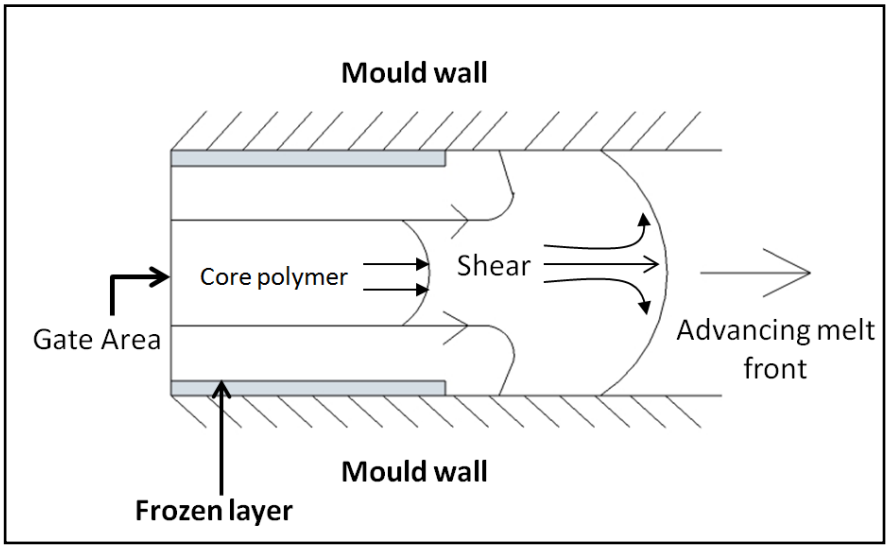

Figure 2.14 Fountain flow effect in the cavity

The material is stretched as it flows forward at the gate of the cavity and polymer viscosity reduces as it shears. A shear flow occurs at the flow front and accounts for the majority of flow during injection moulding.

The flow front region is referred to as the fountain flow as shown in Figure 2.14. The melt moves forward and rapidly cools when it comes into contact with the cold mould walls, which are below the freezing temperature of the melt. When the melt cools it solidifies forming a thin frozen/skin layer of fibres, either oriented randomly or in the direction of flow depending on the width of the mould (Vincent and Agassant, 1986). The shell layer is below the frozen region, where fibres are predominantly parallel to the flow direction. The inner or core layer orientates fibres transverse to the flow direction. Fresh material then flows between the frozen surface layers to create a new melt front. This cycle

continues until the mould is full. The flow of the polymer has a considerable effect on the fibre orientation this will be discussed further in the next section.

2.3.3.1 Influence of polymer flow on glass fibre orientation distribution

Figure 2.15 illustrates the various fibre orientation distributions which might occur during the injection stage:

1. A totally random alignment found at the entrance.
2. Flow aligned fibres are found in the converging flow area.
3. Highly aligned fibres in the principal direction are found in restricted flow or areas where high shear is experienced in a constant wall thickness.
4. Transversally aligned fibres are found in the diverging flow area.

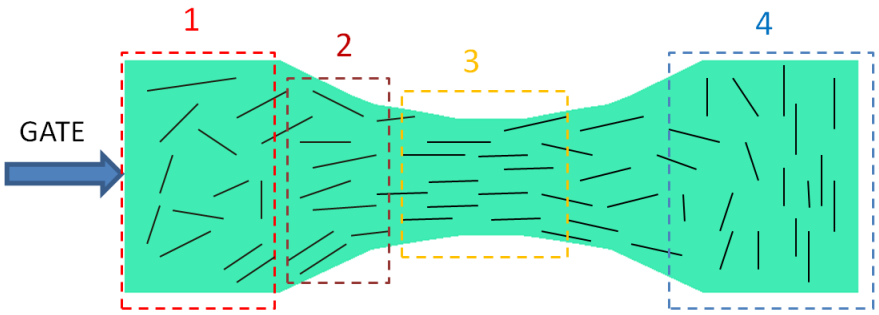

Figure 2.15 Schematic of a plan view illustrating the influence flow pattern has on the FOD

Orientation of fibres has a considerable influence on the strength and stiffness of the fibre reinforced composite. Akay and Barkley, (1991) have examined the influence of FOD on mechanical properties at different position in an injection moulded sample. Their findings show mechanical properties are enhanced in areas where fibres are orientated in the direction of flow, over those areas where fibre alignment is transverse.

The final FOD within an injection moulded part depends on the details of mould geometry, part thickness and injection moulding parameters. The resultant flow within the cavity is the main factor which influences the FOD predominantly at the core. A secondary factor is the velocity profile (Bright and Darlington, 1980).

In a centre gate disc geometry the radial flow causes the fibres at the core to align transverse to the flow direction (Bay and Tucker, 1992). High injection speeds give alignment of fibres transverse to the flow direction and at slow injection speeds the fibres align parallel to the flow (Bright et al., 1978). Therefore high injection speeds result in a larger core compared to slow injection speeds.

The FOD changes through the thickness of the mould and from place to place in the mould. This is due to the fibres aligning in layers through thickness, consisting of skin/shell/core (Figure 2.16). The mid-plane of the mould will normally be a lower shear region; principally fibres tend to align in the direction perpendicular to flow direction in the core. For many polymers the fibres in the shell regions tend to align in the main direction of melt flow, however there are very few occasions where this is not the case in some polymers. The orientation in skin region (frozen layer) depends completely on the state caused by the fountain flow front. As the thickness of the mould increases, the width of the core region gets wider. Reference to the graph in Figure 2.16 the orientation below 0.5 ($\cos^2\theta$) is identified as the core and the frozen skin layer has a lower orientation compared to the shell (Bay and Tucker, 1992). The average FOD at various positions through the thickness is described by the orientation tensor component $\cos^2\theta$.

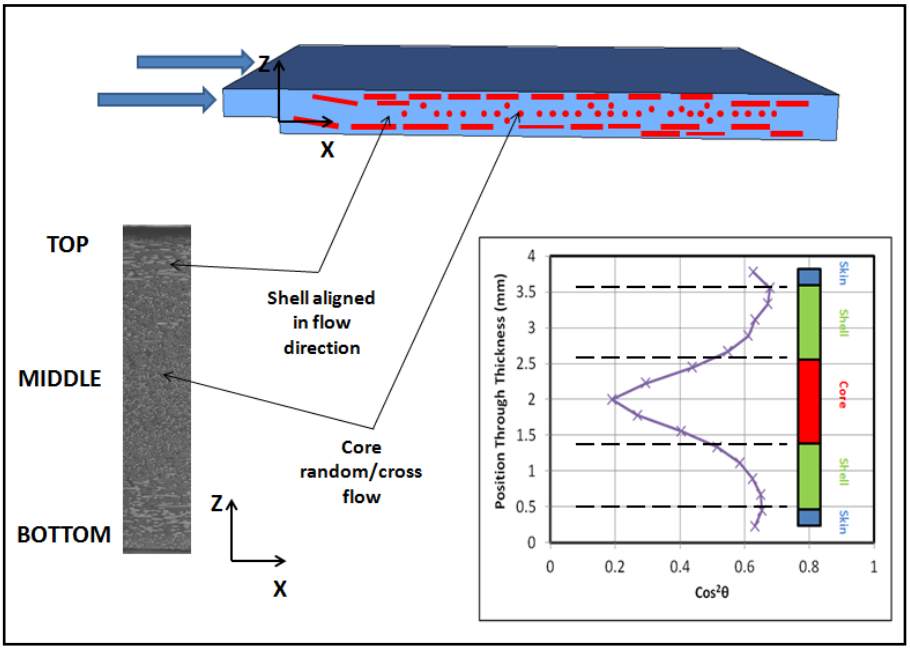

Figure 2.16 Example of skin, shell and core layer FOD in a simple component

2.3.4 Effect of Fibre Orientation on Fibre Length

Research carried out by Bailey and Kraft, (1987) on 10 mm LGF material indicates that a higher average length was found in the core compared to the skin. This is due to the mould filling characteristics, where the core of the component is filled with high velocity and little deformation due to the shear forces being retained within the surface regions. As the overall average fibre length increases the rheological properties of the composite change, this has an impact on the fibre mobility and its ability to orient. A study carried out by Thomasset., et al (2004) confirms that the viscosity of long fibre-filled PP is slightly larger in comparison to the short fibre-filled PP.

Lafranche et al., (2007) measured the fibre orientation distribution within a 10 mm long glass fibre injection moulded plate, changes were noticed in the skin layer which is made up of 2 regions. The relative thickness of core layer increases; this is illustrated with 2 injection mouldings of the same geometry using a long and short glass fibre material (Figure 2.17). Hoffmann, Meyer and Baird, (2008) made a comparison between the same geometry injection moulded with short and long glass fibre. The FOD data for the centre-gated disc suggests that short glass fibre develops into the expected core-shell layer structure while the long glass fibre evolve slower and to a much higher transverse alignment. An irregular flow field is also seen near of the fountain flow front for the long fibre system.

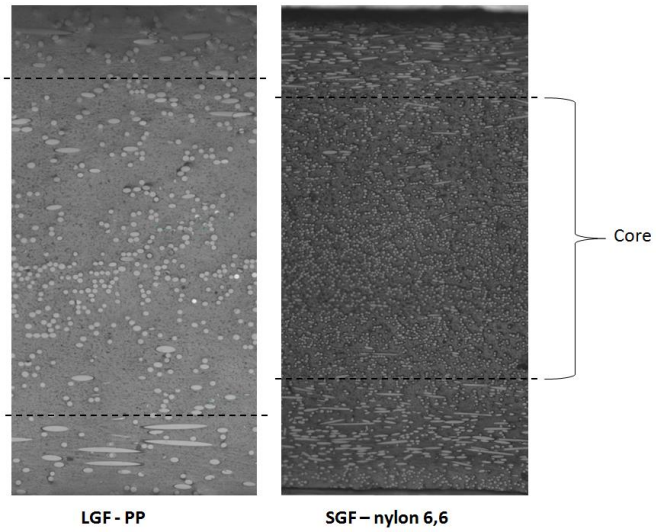

Figure 2.17 A wide core is present within the LGF sample

2.4 Polymer Rheology

Rheology is the behaviour of viscous liquids under deformation. Knowledge of flow behaviour is important in processing and proves useful as a quality control tool to modellers.

The melt flow describes the viscosity of the plastic material during the process of injection moulding. The melt flow index (MFI) is the most popular method available in industry to measure the rate of melt flow of thermoplastic molten polymer. As the material is injected through the mould it occupies a certain flow. This flow determines many mechanical properties of the component. The melt flow depends on various variables like; fill time, velocity, pressure, momentum, and temperature. These functions can be altered to suit the specification during the injection moulding process.

Thermoplastic materials, including the ones in the study are classified as non-Newtonian, viscoelastic or time-dependent fluids, these materials display a non-linear response to stress. These Non-Newtonian fluids exhibit a pseudoplastic behaviour, the apparent viscosity of a pseudoplastic fluid decreases with increasing shear rate, and hence these materials are referred to as shear thinning (Cheremisinoff, 1993). As shown in Figure 2.18 very high or low shear regions are the exceptions, where the flow behaviour is Newtonian.

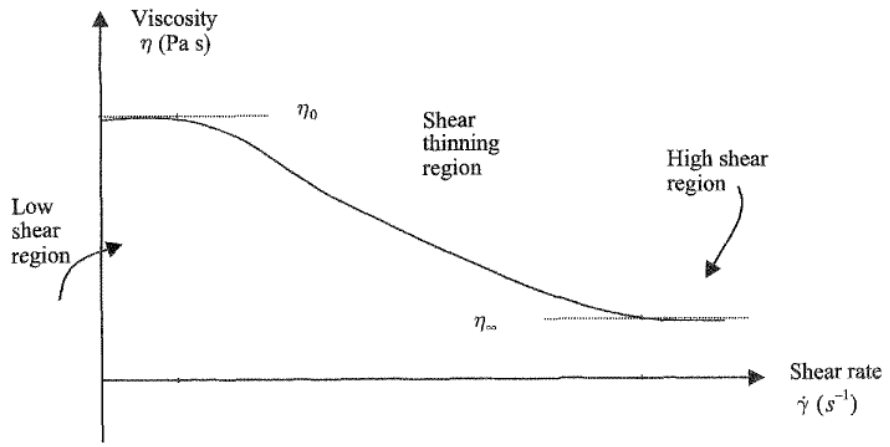

Figure 2.18 Shear thinning behaviour of pseudoplastic fluids (Nassehi, 2002)

A generalised Newtonian viscosity model for polymer melts is widely accepted for injection moulding simulations. The model is simple and accurate for injection moulding process where the shear deformation dominates the flow (Park and Park, 2011). There are a few models which provide a good prediction for shear thinning viscosity of polymers these include the Power-Law and Cross-WLF model. The Cross-WLF model (Equation 2.5) is incorporated within ASMI 2014 and relates critical shear stress (τ^*) to viscosity. The shear stress is at the transition between Newtonian and power law behaviour. The values n <1 denote thermoplastic material.

$$\eta = \frac{\eta_0}{1 + \left(\frac{\eta_0 \dot{\gamma}}{\tau^*}\right)^{1-n}} \qquad \textbf{2.5}$$

For modelling injection moulding ASMI 2014 uses the zero-shear viscosity model in Equation 2.7. The model can reflect the viscosity with temperature, pressure and in which A_1, A_2, D_1, D_2, and D_3 are material parameters.

$$\eta_0 = D_1 exp\left[-\frac{A_1\left(T - (D_2 + D_3 P)\right)}{A_2 + T - D_2}\right] \qquad \textbf{2.6}$$

2.5 Analysis of fibre orientation

2.5.1 Short Glass Fibre

A description of fibre orientation distribution must begin by considering the motion of a single fibre and the Euler angles to define the orientation of a rigid body (Jeffery, 1922). The orientation of a single fibre can be described by the angles (ϕ, θ) (Advani and Tucker, 1987) shown in Figure 2.19. Phi (ϕ) is defined as the angle the projection of the fibre in the YX plane makes with the X-axis and θ is the angle which the fibre makes with the Z-axis (normal to the sectioned surface) (Hine, 2004). A pictorial description of fibre orientation distribution relative to axis 1 is shown in Figure 2.20.

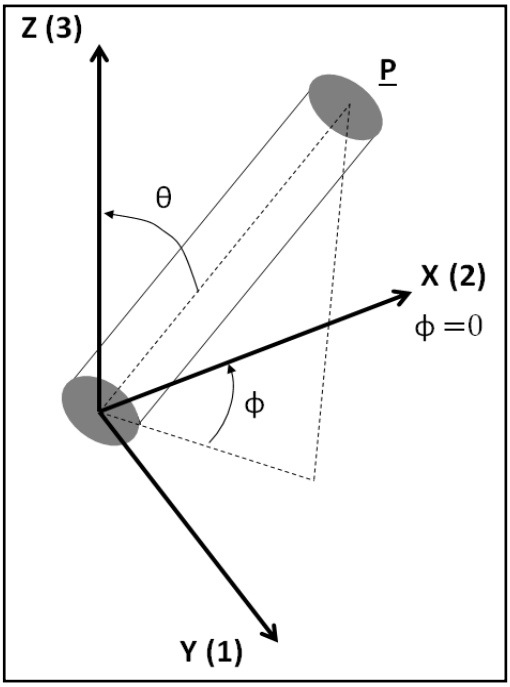

Figure 2.19 Axis of fibre orientation distribution.

If a unit vector **p** is associated with the direction of the fibre, the Cartesian components are given by 2.7 -2.9.

$$p_1 = \sin\theta\cos\varphi \quad \textbf{2.7}$$

$$p_2 = \sin\theta\sin\varphi \quad \textbf{2.8}$$

$$p_3 = \cos\theta \quad \textbf{2.9}$$

The second order tensor for describing fibre orientation is symmetric ($a_{ij} = a_{ij}$), so it possesses 3 eigenvalues.

$$a_{ij} = \begin{bmatrix} a_{11} & a_{12} & a_{13} \\ a_{21} & a_{22} & a_{23} \\ a_{31} & a_{32} & a_{33} \end{bmatrix} \qquad \textbf{2.10}$$

A normalization condition (Equation 2.11) reduces 9 components down to 5 independent components. A mathematical description is given for each of these tensor components in Section 3.2.3.3 Calculation of orientation averages.

$$(a_{11} + a_{22} + a_{33} = 1) \qquad \textbf{2.11}$$

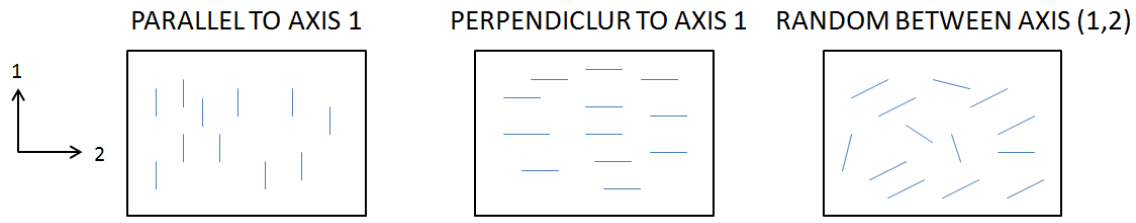

Figure 2.20 Fibre orientation distribution relative to axis 1

2.5.2 Capturing the flexibility of Long Glass Fibre

In the case of short fibres where length < 1 mm the fibres can be treated as rigid particles and the structure is characterized by simply the orientation of the fibres. In the case of long fibres > 1 mm, their characterisation is more complex due to the semi-flexibility caused by the length of the fibre.

Theories have been established to predict the flexibility of long glass fibre (Keshtkar et al., 2010). The flexibility of a fibre is dependent on the length and this varies after the process of injection moulding, Figure 2.21 shows example of curved fibres. Hence in some cases long glass fibre cannot be represented as a rigid ellipsoid particle in 3-d space. A clear solution is currently required to calculate the average fibre orientation of a curved fibre. Alternatively

experimental work at present is based on the rigid fibre assumption referred as segmental orientation (Nguyen et al., 2005, 2008; Lafranche et al., 2007). The long fibre is divided into straight segments or rigid ellipses and the average fibre orientation is calculated for the complete fibre. Another similar investigation was carried out by Hoffmann et al., (2013) this also applies the rigid ellipse method to analyse a centre-gated disc. Findings show the rigid ellipse method was sufficient for the centre-gated disc, as majority of the fibre alignment is transverse to the shear flow especially in the core region and majority of curved fibres are not visible.

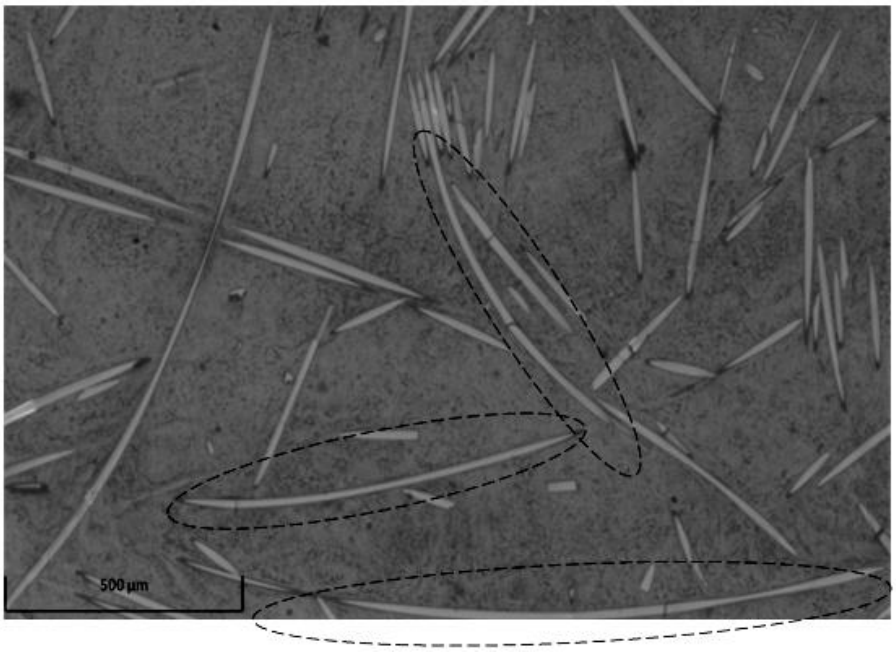

Figure 2.21 Example of curved fibres in a long glass fibre sample

Constructing 3-d projections of the sample using plane to plane reconstruction is another method under a great deal of interest to study fibres and particles. McGrath, (1995) and Clarke et al., (1995, 1999) have applied different image analysis techniques to quantifying the fibre orientation distribution. The different techniques include optical, confocal and tomography microscopy. High resolution X-ray computed tomography (XCT) is becoming an established solution as quantitative data like fibre orientation, filler content, 3-d distribution of fillers and filler size distribution function can be extracted from a 3-d image (Kastner et al., 2012).

The principle applied to CT (computed tomography); 3-d micro structural image data is produced using a wide X-ray beam (or scanned through a narrow beam). The data is then used in reconstruction calculations to generate cross-sectional images (Rochow and Tucker, 1994). 3-d scans of a sample (Figure 2.22) are analysed further using a mathematical algorithm to compute fibre length and orientation (Monnich, 2004). The term micro-CT is used to indicate that the voxel size (size of the 3-d pixel) of the cross sections is in micrometer range. Synchrotron scanning must be applied to produce images with higher resolution and enhanced accuracy. These sub-micro-CT devices are capable of producing resolutions down to 1 µm or smaller, but devices like these are expensive (Salaberger et al., 2011). Salaberger et al., (2011) shows FOD results from CT increase in error with increasing complexity of fibre network and higher fibre content.

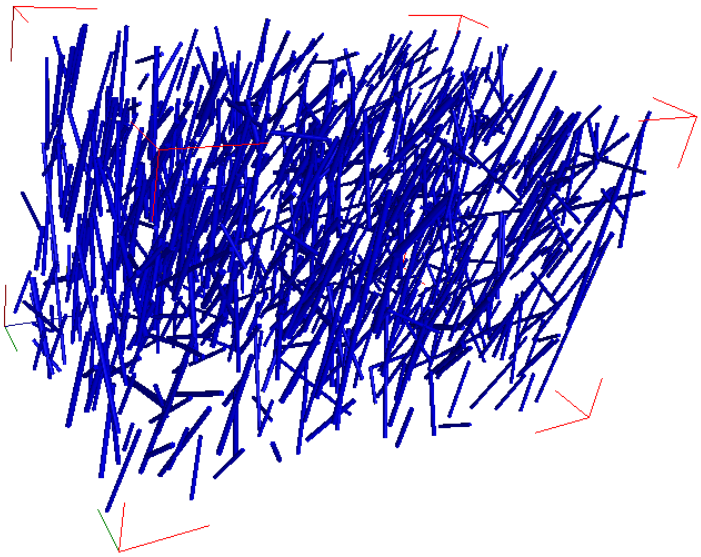

Figure 2.22 Example of CT scan and detected fibres in a polyamide 6 30% SGF

Although successful results have been found from using micro-CT for short glass fibre composites (Bernasconi et al., 2012), there is no practical and cost-effective solution which can describe the fibre orientation accurately for a long glass fibre sample.

2.6 Simulation Software

In the past injection moulding and mechanical property prediction was a trial and error process. This would cost a company producing vast amount of components a lot of time and money, as an engineer would have to go through many unsuitable parts to arrive at the solution.

The first commercial injection flow prediction Computer Aided Engineering (CAE) software appeared around 30 years ago (Shen et al., 2005). Packages available now are developed using the finite element or volume method in two and three dimensional models. At the core of the finite analysis is a numerical method which determines the accuracy and speed of the analysis. There are a number of software products on the market such as; Moldex3D, CADMould and Autodesk Simulation Moldflow Insight 2014 (ASMI), which aim to simulate the injection moulding process. ASMI has become one of the leading softwares in predicting polymer flow during the injection moulding process. ASMI 2014 has introduced a range of modules which allow engineers to simulate and optimize the plastic, mould and tool design before manufacturing begins (Huilier and Patterson, 1991). The numerical prediction models mentioned in the next chapter have been incorporated into ASMI 2014.

2.6.1 Finite Element Method

The basic principle of finite element method (FEM) is the division of domains into a set of simple sub-regions without any gaps called 'finite elements' (Reddy, 1993). Together the finite elements provide a finite element mesh for the domain which is connected at points called nodes. The elements can have different sizes but usually they have a common shape (linear, quadratic, triangular and quadrilateral) and equal number of nodes when applied to the geometry. Nodes are the points where the numerical values like; Temperature, velocity and pressure flow are calculated for each element within the mesh in order to solve mathematical equations. The generated mesh can be coarse (have a few elements) or refined (have many elements). As the number of elements increase the approximations improves resulting in reduced error. The

main disadvantage of all 3-d numerical simulations is high computational cost of and constant validation of prediction.

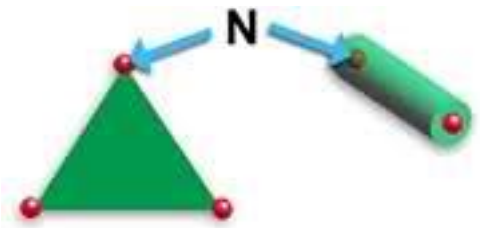

Figure 2.23 Representation of triangular element and nodes (ASMI, 2014)

Commercial software can predict filling conditions on the distribution of flow patterns as well as flow vectors, shear stress, optimum number of injection points, fill time, frozen skin, clamping force required, weld lines, pressure, fibre orientation, velocity, temperature distribution, shrinkage and warpage and many other injection moulding results (ASMI, 2014).

To practically model injection moulded three-dimensional complex geometries the rheological behaviour of the melt is described as non-isothermal generalised Newtonian (for more information reference can be made to Section 2.4 Polymer Rheology). In a non-isothermal system the viscosity is directly dependent on the change in temperature. There are three kinds of models available in most commercial packages, including the mid-plane, surface and 3-d (solid) model. The surface approach is currently unique within ASMI 2014.

2.6.2 Geometric Solutions

Three different models and mesh techniques are utilized within ASMI to computationally analyse the model:-

2.6.2.1 Mid-plane

Hieber and Shen, (1980) first proposed the ideas, which have later attributed in today's finite element flow simulation packages. The Hele-Shaw approximation of non-isothermal flow is based on their theoretical studies of filling flow in thin cavities. As most injected parts are thin walled, this means the gap height (h) in

the thickness direction is very small compared to other attributes such as the length and width of the part. The Hele-Shaw approximation models the cavity as 2-d flow problem, the mean velocities are averaged through the cavity gap-width, which is related to the pressure gradient through a quantity called 'measure of fluidity' representing the sum of the effect of changing temperature and viscosity across a gap (Cardozo, 2008).

The arbitrary planar geometry at the centre/mid-plane of the cavity, with a defined thickness is used to represent the 3-d geometry. Consequently the flow is symmetric about the mid-plane and the z- axis is equal to zero. The model assumes pressure does not vary in the z-direction and velocity is negligible in the z-direction compared to in-plane velocities (V_X and V_Y) (Altan, 1990). Therefore the model is unable to calculate the velocity and pressure fields in 3-d features such as corners, gates, ribs and junctions.

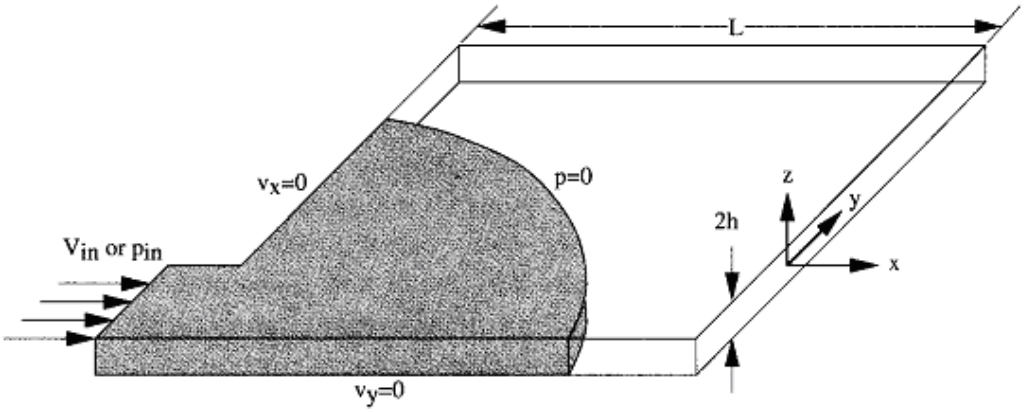

Figure 2.24 Example of thin (narrow gap) geometry as analyzed by Hele-Shaw approximations (Dantzig and Tucker, 2001)

Another limitation of this model is that, non-slip boundary condition cannot be placed on the outer boundary of the cavity in the x-y plane because viscous diffusion is not taken into account for in this region. A solution has been incorporated into Moldflow software; in order to model the effect fluid velocity has along the edges and on fibre alignment predictions. An edge effect is integrated into ASMI 2014, which constrains orientation along the free edges causing fibres to align with flow direction. In a more advanced Hele-Shaw simulation, special formulae have been developed, to correctly predict the temperature and orientation in the fountain flow region. As long as the basic

assumptions of the Hele-Shaw model are met the fibre orientation prediction should provide a good solution (VerWeyst et al., 1999).

A CAD model is converted, using the mid-plane generator. Mesh consists of tri-node triangular elements that form a 2.5 D representation of the part though the centre (Figure 2.25). Each element also has a number of shell layers, ranging from 6-20.

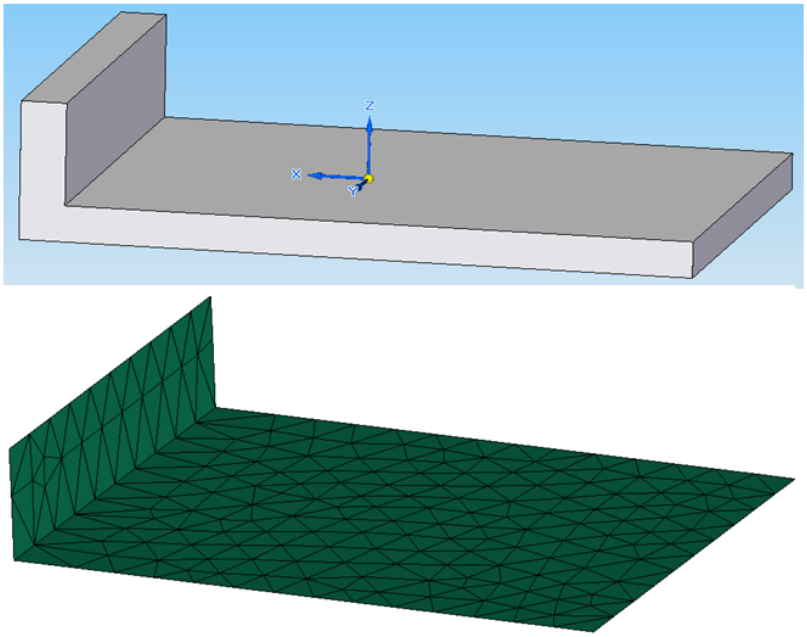

Figure 2.25 CAD part converted into a 2.5 D mid-planer mesh

2.6.2.2 Surface or dual-domain

Surface models or dual domain technology as known in ASMI 2014 is a finite element representation of a 3-d part with a boundary on the outside surface. The first mathematical surface model was presented by Yu and Thomas, (1997). This model was widely accepted as it allows users to directly examine complex 3-d geometries, which is very difficult and time consuming when examining the 2-d geometry. The surface model adopts Hele-Shaw approximations and is very similar to the mid-plane model (Figure 2.26); as a result of this the whole cavity is divided into two equal parts in the gap-wise direction. Triangular elements are generated on the surface and the gap-wise direction is only employed from one wall to the centre of the boundary condition (z = 0 to z = b) (Zhou and Li, 2001).

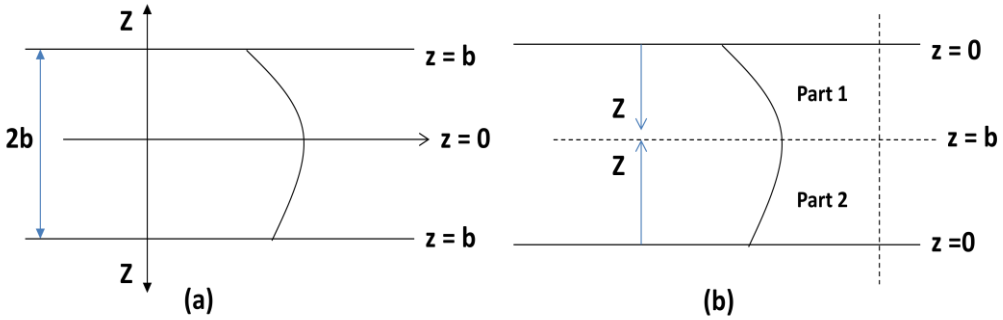

Figure 2.26 Schematic for boundary condition in a gap-wise direction (a) the mid-plane model and (b) of the surface model

The elements on the opposite surfaces of both walls are matched and aligned. The surface mesh is easily visualised as a hollow body as shown in Figure 2.27. When a rib or any discontinuity is introduced in the 3-d geometry the flow on the opposite surface may not match, in this case an extra connector element is introduced from the unmatched point through the thickness to the other side.

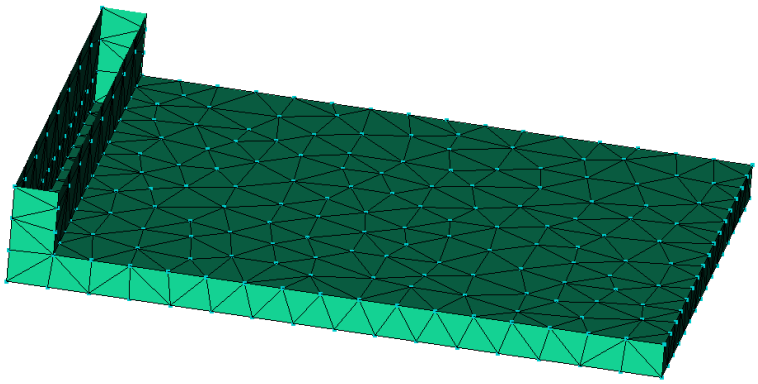

Figure 2.27 Dual domain mesh is applied to the surfaces of a model (hollow shell)

2.6.2.3 3-dimensional

Interest in 3-d simulation of injection moulding has increased rapidly in the last 10 years. More injection parts are large, complex 3-d geometries which are either thick or have a non-uniform thickness. There are many situations occurring during the mould filling which cannot be accurately predicted by the Hele-Shaw approximation. Amongst the most significant include the fluid flow behaviour at the free surface (flow front), the fluid flow behaviour near and at the solid walls, the phenomenon occurring at the merging of two or more fluid streams (weldlines) and the kinematics in areas where shear and extensional deformations contribute significantly to stress fields (gate and ribs) (Zhou, 2005).

The fountain flow effect occurs at the flow front, where the fluid near the centre is moving faster than the average velocity across thickness (Steinbach, 2002). A combination of extensional and shear flow causes the material from the core area to move towards the wall and solidify (a thin layer). In most injection moulding applications the influence of the 'fountain flow' region increases according to sudden thickness changes i.e. ribs. Therefore the effects in the fountain region cannot be represented by the Hele-Shaw approximations.

A 3-d mesh solver represents the solid CAD model by filling the volume of the model with 4-noded solid tetrahedral elements. Increase in the number of elements makes 3-d modelling computationally intensive. However with development of computer technology, 3-d simulation has become a promising solution and the first 3-d model was incorporated by ASMI 2014 (Talwar et al., 1997). For 3-d simulation the polymer flow is assumed to be compressible and non-isothermal during filling, hence the conservation equations for mass and momentum (equations that govern motion of viscous fluid) are described by the Navier -Stokes derivation (Navier, 1823). In this derivation the velocity and pressure are the only prime field unknowns. Tracking of the melt front (fluid free surfaces) is important in 3-d filling simulation. The boundary tracking flow problem is modelled using the level set method (LSM) algorithm (Osher and Sethian, 1988). Moldflow uses a fixed grid LSM approach to solve the tracking fountain flow, where the fluid moves within a single fixed mesh one element to the next over time. The technique has been successful in handling possible topological complexities such as corners, interface splitting and merging (Zhou, 2013)

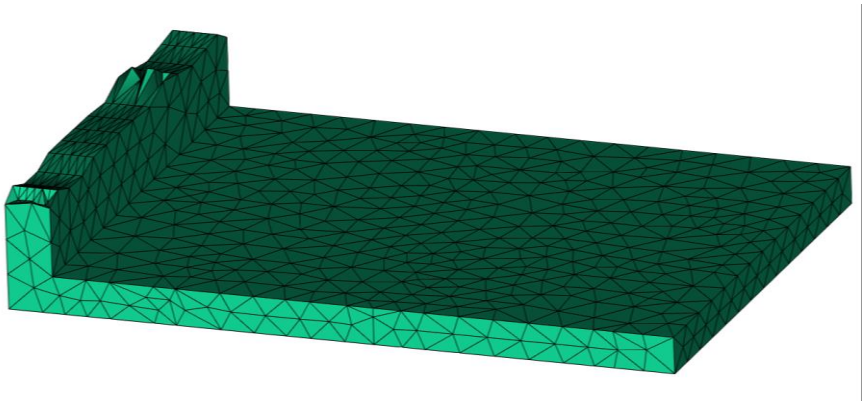

Figure 2.28 3-d mesh the cross-section shows the internal nodes (volume mesh)

2.7 Fibre Prediction Model

In recent years there has been a rapid development in the ability to model the orientation structure in fibre reinforced composites. This is seen by the increase of computer simulations, which predict the fibre orientation and polymer flow in injection moulded parts. The equation(s) which allow this prediction have been built upon work spanning the last half-century.

2.7.1 Short Fibre Prediction

2.7.1.1 The Folgar-Tucker Equation

Folgar – Tucker, (1984) model is widely used to predict fibre orientation in injection moulded composites. The Folgar- Tucker model uses the principles of Jeffery's equation, (1922) to predict the orientation of a single fibre immersed in viscous fluid. The model provides a better prediction for fibres in dilute fibre suspensions and can over-predict orientation in concentrated suspensions, as the model cannot account for fibre-fibre interactions. The Folgar Tucker (FT) suggests amendments by representing flow effects and adding a rotary diffusion term, to represent fibre-fibre interactions.

The models use a second order tensor (Advani and Tucker, 1987) to represent the fibre orientation at a single point this is defined in 2.12.

$$\mathrm{A} = \langle \mathrm{pp} \rangle \qquad \textbf{2.12}$$

The orientation of a single, rigid fibre can be characterised by a unit vector **p** directed along the fibre length and the bracket is the average over a volume. The changes in the orientation due to flow can be predicted in terms of second - order tensor. The FT model in terms of the orientation tensor **A** 2.13.

$$\frac{DA}{D_t} = (\mathrm{W}.\mathrm{A} - \mathrm{A}.\mathrm{W}) + \xi(\mathrm{D}.\mathrm{A} + \mathrm{A}.\mathrm{D} - 2\mathbf{A}\!:\!\mathrm{D}) + 2\mathrm{C_I}\dot{\gamma}(\mathrm{I} - 3\mathrm{A}) \qquad \textbf{2.13}$$

Hence DA/Dt is the material derivative of A (the second order tensor); W and D are vorticity and the rate of deformation tensors the terms were introduced by the Jeffrey's, (1922) equation. Correspondingly ξ is the shape parameter and is dependent upon the fibre length to radius ratio. The term $C_{\mathrm{I}}\dot{\gamma}$ gives the model proposed by Folgar and Tucker, (1984) for fibre – fibre interactions. Coefficient C_{I} is the interaction coefficient and a larger value implies more fibre-fibre interactions (increase fibre concentration); and $\dot{\gamma}$ is strain rate. Each interaction between two fibres produces an orientation change in both fibres. The frequency of these interactions is proportional to the strain rate and the change in orientation per collision is independent of $\dot{\gamma}$ (Phelps and Tucker, 2008). **A** is the fourth order orientation tensor is defined as $\mathrm{A} = \langle \mathrm{pppp} \rangle$ (Wang, 2010).

Setting $\mathrm{C_I} = 0$ sets the model back to the Jeffery form. Work carried out by Folgar and Tucker (1984) show that it is very difficult to determine an appropriate value for the $\mathrm{C_I}$, which is related to the fibre aspect ratio and fibre volume fraction. Curve fitting with experimental orientation data is one method to determine the $\mathrm{C_I}$ value (Bay and Tucker, 1992). Tucker and Advani, (1994) proposed an empirical expression (2.14) if there is no experimentally determined coefficient. Where V_f is the volume fraction of glass fibres, L is the fibre length and D is the fibre diameter.

$$c_i = 0.0184 \exp\left(-0.7148 \mathrm{V}_f \frac{\mathrm{L}}{\mathrm{D}}\right) \qquad \textbf{2.14}$$

The $\mathrm{C_I}$ value can change with different flow geometries, making it difficult to predict a solution. The interaction coefficient C_{I} takes on values much less than 1 to match experimental findings (Nguyen et al., 2010 and Phelps and Tucker, 2009). Bay and Tucker, (1992) carried out one of the early studies on the effects of the interaction coefficient in simple shear flow. They found as the value of C_{I} decrease (fibres do not interact with each other), the orientation in the shell layer becomes more aligned in the flow direction and the orientation in the core is perpendicular to the flow. On the other hand if the value of C_{I} increases, the core decrease and the shell thickness increases.

Within ASMI, (2014) software, for the mid-plane and dual domain mesh, the classical FT (Equation 2.13) is further developed by a introducing a $\mathrm{D_Z}$ coefficient term (Wang and Jin, 2010). The $\mathrm{D_Z}$ term sets the significance of the randomizing which is a result of the coefficient of interaction. For the modified FT model (2.15 the boundary conditions for D_Z ($0 \leq D_z \leq 1$).

$$\frac{DA}{D_t} = (\mathrm{W.A - A.W}) + \xi(\mathrm{D.A + A.D - 2\mathbf{A}:D}) + 2\mathrm{C_I}\dot{\gamma}(\mathrm{I - (2 + D_Z)A}) \qquad \textbf{2.15}$$

Setting $\mathrm{D_Z} = 1.0$ gives the classic Folgar-Tucker orientation model for the 3-d problem and if $\mathrm{D_Z} = 0$ gives the modified Folgar-Tucker model for the 2-d problem. The hydrodynamics cause the fibres to lie parallel to the flow direction; hence decreasing $\mathrm{D_Z}$ parameter reduces the out of plane orientation but increases the thickness of core layer.

The low $\mathrm{D_Z}$ model results in reduced error levels for thin parts (thickness less than 2.5 mm). For parts with thickness of greater than 2.5 mm the revised model with $\mathrm{D_Z} = 1.0$ is used. The value of $\mathrm{D_Z}$ has been shown to increase rapidly with part thickness. This increasing trend is constant with the expectations that out of plane fibre orientation would increase with increasing part thickness.

2.7.1.2 Closure Approximation

A closure approximation is essential to use the fibre orientation tensor to predict the effects of flow on the fibre orientation. The model contains a fourth order tensor a_{ijkl} and is not yet suitable as a second order tensor derivative. A solution to this problem is to use a closure approximation, a formulae which approximates the unknown fourth order tensor, into a known second order tensor. The following conditions must be satisfied in order to construct closure approximations for the orientation tensor.

- The approximation must be created only from the lower order orientation tensor and the unit tensor δ

- It must satisfy normalization conditions such as $a_{ijkl} = a_{ij}$
- It must maintain the symmetries of the orientation tensors.

One method to form a closure approximation was proposed by Hand, (1962). This linear closure approximation is accurate for a completely random distribution of fibre orientation. While the quadratic closure approximations are exact for perfect aligned fibres. Therefore it would be sensible to combine both approximations to obtain a more accurate solution known as the hybrid closure approximation. Experiments show the hybrid closure provides the most simple and steady state solutions, modelling a range of orientation levels (Advani and Tucker, 1987). The hybrid method has been adopted in the software for this study. The presence of the approximation itself may introduce some small errors or oscillations in the simulation.

Although the hybrid closure is a stable model it tends to over-predict the level of orientation. Therefore the search for a closure approximation, which offered better accuracy, was still active. The best available closure are the family of approximations, known as orthotropic closures (Cintra and Tucker, 1995) and the natural closure proposed by Verleye and Dupret, (1993). However both of these models are not computationally efficient as they require additional time and computer power to solve (Park and Park, 2011).

2.7.1.3 Reduced Strain Closure Model

Recent findings have shown that the rate of orientation development in short glass fibre thermoplastics is much slower than the current model predicts. Wang, (2008, 2010) has introduced the reduced-strain closure (RSC) model, which slows the orientation kinetics in order to get a better correlation between experimental and prediction.

The Folgar-Tucker model was modified with two assumptions; reducing the growth rates of the eigenvalues (λ) of orientation tensor by a slip factor $k \leq 1$, but the eigenvector rotation rate factor is unchanged. This results in what is now known as the RSC model Equation 2.16.

$$\frac{DA}{D_t} = (\mathrm{W}.\mathrm{A} - \mathrm{A}.\mathrm{W}) + \xi(\mathrm{D}.\mathrm{A} + \mathrm{A}.\mathrm{D} - 2[\mathbf{A} + (1-\kappa)(\mathbf{L} - \mathbf{M}:\mathbf{A})]:\mathrm{D}) + 2\kappa \mathrm{C_I}\dot{\gamma}(\mathrm{I} - 3\mathrm{A}) \quad \textbf{2.16}$$

Here L and M are also the fourth order tensors; they are functions of eigenvalues and the eigenvectors so no closure approximation is required (Wang et al., 2008). In comparison to the standard Folgar-Tucker 2.13 the RSC model has a diffusion term reduced by the scalar factor k (this controls rate of orientation development). Setting k = 1 reduces RSC model Equation 2.16 back to the FT model Equation 2.13. Using experimentally determined orientation recent publications have suggested the values of k could be set at 0.05 for thin geometries and 0.03 for thick geometries (Wang and Jin, 2010).

2.7.2 Long Fibre Prediction

This section will cover the theory behind long fibre prediction models incorporated in ASMI 2014. These include the long fibre anisotropic rotary diffusion orientation model (ARD) and the long fibre breakage model.

2.7.2.1 ARD Model

Fibres longer than 1 mm are generally considered as long fibres. The fibre alignment in the flow direction is weaker; due to the characteristics of long fibre material compared to short fibre injection moulded parts. The isotropic diffusion used in the Folgar-Tucker and RSC models is unable to capture the fibre-fibre interaction in long fibres. Therefore the current models cannot accurately predict the orientation of long fibres; therefore a new anisotropic rotary diffusion model (ARD) for long fibre composites has been developed by Phelps and Tucker (2008).

The first concept of the ARD model was introduced by Koch (1995), who considered the influence of long-range hydrodynamic fibre-fibre interactions on orientation in a partially diluted fibre suspension. This idea was later developed by Fan et al., (1998) and Phan-Thien et al., (2002). This model was tested as a

direct simulation in simple shear flow. The rotary diffusion for fibre orientation is defined two-dimensionally in orientation space. The model developed by Phelps and Tucker, (2008) incorporates a good 2-d understanding of the rotary diffusion.

The ARD model is defined on the surface of the unit sphere traced by all possible orientations and not in the direction the unit is pointing. The coefficient C_I is replaced by C rotary diffusion tensor in the ARD model (2.17). The C tensor can depend on orientation state and flow type, the C tensor is made up of 5 scalar parameters in Equation 2.18 (b_1, b_2, b_3, b_4 and b_5).

$$\dot{A} = (\mathrm{W.A} - \mathrm{A.W}) + \xi(\mathrm{D.A} + \mathrm{A.D} - 2\mathbf{A}\!:\!\mathrm{D}) + \dot{\gamma}(2\mathrm{C} - 2(\mathrm{trC})\mathrm{A} - 5(\mathrm{CA} + \mathrm{AC}) + 10\mathrm{A}\!:\!\mathrm{C}) \quad \textbf{2.17}$$

$$C = b_1 I + b_2 A + b_3 A^2 + b_4 \frac{D}{\dot{\gamma}} + b_5 \frac{D^2}{\dot{\gamma}^2} \quad \textbf{2.18}$$

An ARD – RSC model which slows the kinetics of the ARD model Equation 2.19 is applied using the RSC treatments.

$$\begin{aligned} \dot{A}^{ARD-RSC} = {} & (\mathrm{W.A} - \mathrm{A.W}) \\ & + \xi(\mathrm{D.A} + \mathrm{A.D} - 2[\mathbf{A} + (1-\kappa)(\mathbf{L} - \mathbf{M}\!:\!\mathbf{A})]\!:\!\mathrm{D}) \\ & + \dot{\gamma}\{2[\mathrm{C} - (1-\kappa)\mathrm{M}\!:\!\mathrm{C}] - 2\kappa(\mathrm{trC})\mathrm{A} - 5(\mathrm{CA} + \mathrm{AC}) \\ & + 10[\mathrm{A} + (1-\kappa)(\mathrm{L} - \mathrm{M}\!:\!\mathrm{A})]\!:\!\mathrm{C}\} \end{aligned} \quad \textbf{2.19}$$

Setting κ (reduced strain factor) equal to 1 reduces the ARD-RSC model to the ARD model. The 5 parameters are set as defaults in ASMI 2014 as follows; b_1 = 0.0001924, b_2= 0.005839, b_3= 0.04, b_4= 1.168 x 10^{-5} and b_5= 0, poor choices of the ARD parameters can give non-physical behaviours in orientation. The rotary diffusion tensor Equation 2.19 is purely phenomenological, it would be better to have a mechanistic model that would give the rotary diffusion as a function of local fibre orientation state, and type of deformation (Phelps and Tucker, 2008).

2.7.2.2 Fibre Breakage Model

Autodesk Moldflow has incorporated the first quantitative fibre breakage model proposed by Phelps and Tucker (Phelps, 2009). This statistical model describes the probability of a fibre breaking, due to buckling and shearing forces in the flow field. The fibre breakage rate, at which fibres break, can be defined with probability P_i of length segment l_i at time Δt and a probability R_{ik} of creating a fibre of length segment l_j from breaking a fibre of length l_k. Combining the loss caused by breakage (growth due generation of children) gives a basic conservation (Equation 2.20) fibre length N_i.

$$\frac{dN_i}{dt} = -P_i N_i + \sum_k R_{ik} N_k \qquad \textbf{2.20}$$

The left hand side of the Equation 2.20 represents the change rate in the numbers of fibres, with fibre length l_i in a unit of volume. The first term on the right hand side is for representing the loss of fibres due to breaking and the second term represents the creation of child fibres due to the breakage of longer fibres.

The next part will describe the equation which gives the breakage rate P_i as a function of flow conditions and fibre properties. The free moving fibres interact with fluid in laminar shear motion; axial forces arising due to the velocity component load the fibre in compression or tension. The model assumes that even a small amount of contact may trigger buckling from the compressive forces of a hydrodynamic loaded fibre. Therefore this model is based on Dinh and Armstrong, (1984) arguments for the effect of hydrodynamic compression of fibres on bulk viscosity. The criterion in 2.21 can be used to describe the force required to break a single fibre under hydrodynamic compression.

$$\frac{F_i}{F_{crit}} = \hat{\gamma}\left(-2\widehat{D} : pp\right) \geq 1 \qquad \textbf{2.21}$$

For a single fibre, represented by vector P, of length l_i in a polymer melt of viscosity η_m, the buckling forced F_i (2.22) is considered from the hydrodynamic compression force given in terms of the deformation rate tensor $\widehat{D}$.

$$F_i = \frac{D_g \eta_m l_i^2}{8}\left(-\widehat{D}: pp\right) \qquad \textbf{2.22}$$

The critical buckling force is calculated using 2.23.

$$F_{crit} = \frac{\pi^3 E_f d_f^4}{64 l_i^2} \qquad \textbf{2.23}$$

E_f and d_f are fibre elastic modulus and diameter, respectively. It is not computationally feasible to track each fibre individually through the flow simulation. Therefore to get a statistical average of the fibre orientation the pp in 2.21 is replaced by fibre orientation tensor $\hat{A}$. Now the probability of fibre breakage under the hydrodynamic buckling force can be expressed with shear strain rate influence, over a period of time (2.24) as a function of fibre dimensions and properties.

$$P_i = C_b \dot{\gamma}\left\{0, \left[1 - \exp\left(1 - \frac{F_i}{F_{crit}}\right)\right]\right\} \text{ for } \hat{\dot{\gamma}} \geq 1 \qquad \textbf{2.24}$$

Where scalar parameters;

- C_b= a scalar rate constant which controls the overall rate of change of fibre length.
- D_g = dimensionless fiber drag coefficient, which controls the length below which fibres do not break
- S = affects the shape of the fibre length distribution by changing the distribution of child fibres when fibres break
- $\dot{\gamma}$ = the shear strain rate (additional force in the flow field)

Default values for each of these are set in ASMI 2014 (C_b= 0.002, D_g = 3 and S = 0.25)

In Equation 2.24 the buckling criterion dominates the probability form, if it is less than one; P_i is zero this means there is no chance for a fibre to break. A fibre will only break if the hydrodynamic compression force is higher than the critical buckling force $F_i > F_{crit}$. Finally, the normal distribution function is used to describe the probability R_{ik} with consideration that breakage is most likely to occur at the midpoint of a fibre of length l_k, and scaling factor S changes the shape of the FLD curve by affecting the distribution of child fibres as fibres break in 2.25.

$$R_{ik} = N_{norm}\left(l_i, \frac{l_2}{2}, Sl_k\right) \qquad \textbf{2.25}$$

Although some initial results have shown this is a good mathematical model (Equation 2.20) (Wang and Jin, 2011). There is additional fibre breakage caused by the melting zone of the screw, geometric features like gates and sharp bends in runners and these need to be incorporated into the model (Tucker et al, 2010).

2.8 Outcome from Literature Review

This section will outline the areas where there is very little or no literature available, this assessment will narrow down the areas where some advancement in knowledge is possible.

There is intensive literature based on the properties of short fibre composites but there is very little understanding of the properties and behaviour of long fibre injection moulded composites. More investigation is required to obtain accurate data on FOD and FLD for long fibre composites. Researchers are currently trying to find a novel or existing method to capture and measure the flexibility of long fibres. Solutions such as micro CT allow detailed 3-d analyses of FLD and FOD but this option is expensive and not easily accessible. There is very little measured data comparing the difference in FOD as result of fibre length (short fibre and long fibre), geometry shape and thickness. Fibre length degradation has a negative impact on the mechanical properties of long fibre injection

moulded components. Therefore it is important to find means of reducing this degradation and the resultant effect of process parameters have on fibre length. The same can be said for the fibre prediction models, the short fibre models (the FT to the RSC) have been under intensive development for over 30 years. However the long fibre prediction models including the ARD and fibre breakage model were recently (within last 3 years) incorporated into ASMI 2014. As of yet the long fibre models are under mathematical review and development, although early validation of the long fibre FOD show good agreement with measured data. Measured FOD and FLD data is important to assess the accuracy and to find possible areas of improvement within the prediction. Each model has optimum coefficients but these are found through fitting measured data against predicted to both 2-d and 3-d geometries. Apart from the FT model there is a lack of understanding of how these coefficients influence the prediction. The long fibre breakage model is dependent on a user to input the measured FLD at inlet; this means the model needs to incorporate the fibre breakage taking place within the screw.

Chapter 3 Experimental Methodology

This section covers the specification of the components, which have been injection moulded and evaluated in ASMI 2014 as part of the project. This includes the overview of injection moulded short and long glass fibre material components, the methods of obtaining fibre orientation and fibre length data (for long glass fibre material). Simple geometries including a fan-gate and a centre-gate scenario were evaluated in order to study the effect geometry has on the fibre length and fibre orientation. The components include a 1, 2 and 4 mm thick centre gate-disc, 2 mm plaque and a 4 mm thick plaque with a rib. Modifications were made to the sprue of the centre gate disc component for further study using long glass fibre material. The mid-plane of the fan-gate and centre geometries was investigated in ASMI 2014, to assess the limitations of the fibre prediction models.

3.1 Injection Moulded Geometries

3.1.1 Material

Short glass fibre PA6 and long glass fibre polypropylene reinforced materials were used to mould the components as part of the study. These two thermoplastic materials have a distinct difference in fibre length and this is the primary reason they were selected for injection moulding. The reason for selecting a short and a long glass fibre reinforced material is, to understand the effect processing and geometry has on the fibre orientation distribution including fibre degradation in the case of LGF material. Processing conditions during injection moulding influence the resultant fibre breakage before and after material enters the mould cavity. Processing parameters and design modifications were recommended by SABIC® (material supplier) to preserve fibre length during injection moulding of LGF material.

3.1.1.1 Short Glass Fibre

Rhodia Technyl C216 V40 (previously known as Nyltech Sniamid C216), which is 40% (by weight) glass fibre (E-glass) reinforced PA6. The 3 mm long pellets are manufactured using the conventional method of extrusion compounding more information is found in Section 2.2.2.1 Fibre Length and Content. The material is reinforced with chopped glass fibres with an average length of 350 µm and 14 µm diameter. The distribution of fibres within the pellet is random. The glass fibre within the material is coated but details of the coating are unavailable. Glass fibre reinforced PA6 provides mechanical properties such as; greater dimensional stability under heat compared to unfilled material, advanced short term strength/stiffness and long term fatigue/creep (Rhodia, 2011). Recommended processing settings for the material are shown in Table 3.1.

	Minimum	**Maximum**
Pre drying conditions	In the case virgin material has absorbed moisture; it must be dried with a dehumidified air drying equipment. Drying conditions of 80 **º**C for 3-4 hours	
Melt Temperature (º C)	260	280
Mould Temperature (º C)	80	120

Table 3.1 Processing guide for Rhodia Technyl C216 V40 (Rhodia, 2011)

3.1.1.2 Long Glass Fibre

This project was carried in collaboration with the SABIC®, therefore they have provided the SABIC®, Stamax 30YM240, a 30% (by weight) long glass fibre (E-glass) polypropylene reinforced material. The 12 mm long pellet is manufactured using wire coating process where continuous bundles of glass fibre with an average diameter of 20 µm are wired together like a cable. The cable then passes through 2 % by mass chemical coating (thickness of coating is confidential), the coated cable is then encapsulate with polymer and after passing through the water bath pellets are cut down to the final size. The fibres are parallel and have the same length as the pellet. In order to achieve high

stiffness and strength, the glass fibres are chemically coupled (silane coating) to the polypropylene matrix as shown in Figure 3.1.

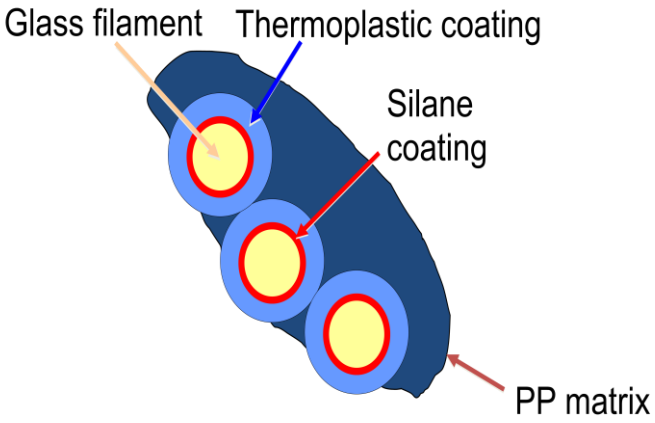

Figure 3.1 Structure of the LGF material (Schijve, 2000)

The advantages of LGF PP over SGF material include; low cost performance material (PP resin), good mechanical properties at both low and high temperatures, high toughness and low warpage (Sabic, 2013). In order to preserve the fibre length SABIC® has recommended limits for specific processing parameters these are provided in Table 3.2.

	Minimum	**Average**	**Maximum**
Melt Temperature (°C)	220	250	280
Cylinder settings (°C)	Flat temperature profile		
Back pressure (Bar)	0 (preferred)	As low as possible (e.g. 10 bar)	150 (only for specific screws)
Screw speed	As low as possible Target: Plasticizing complete during cooling and machine times.		
Injection speed	Moderate		

Table 3.2 Sabic recommendation to process Stamax 30YM240 (Sabic, 2011)

3.1.2 Injection Moulding Apparatus

Test geometries used in this study were injection moulded using the Battenfeld BA750/315 CDK shown in Figure 3.2. This was the only machine available with a 40 mm diameter general purpose screw. The mould was connected up to temperature control units to regulate the temperature within the mould. Machine specifications are included in Table 3.3.

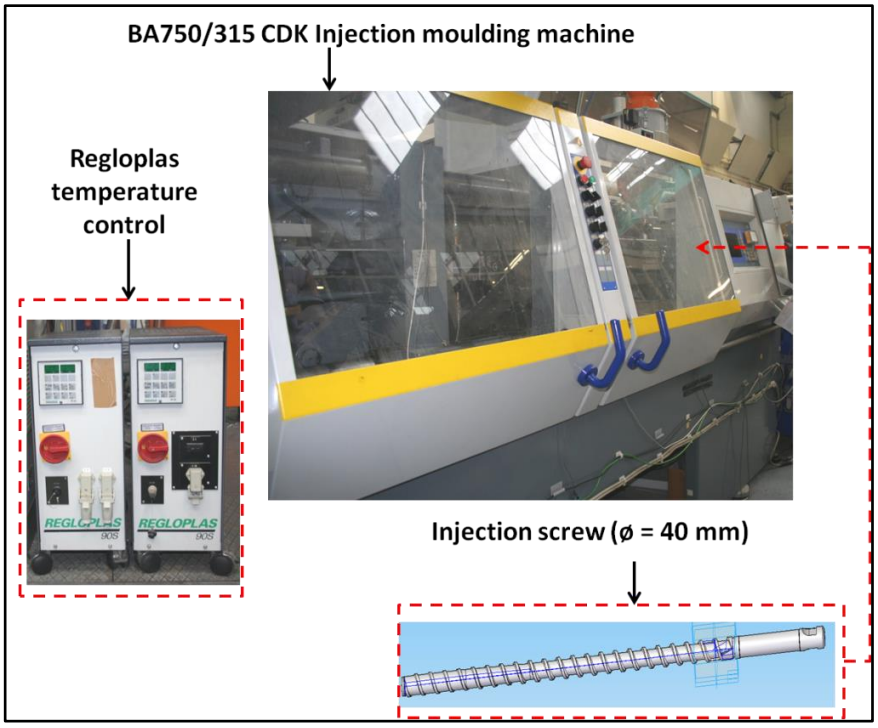

Figure 3.2 Injection moulding apparatus

Equipment	Details
Moulding machine	750 kN of clamp force Battenfeld BA750/315 CDK Driving power hydraulics with screw diameter 40 mm and length:diameter ratio (L/D) of 20:1 Max injection speed - 106 (mm/s) Max screw speed - 215 (rpm) Back pressure range - 0 to 40 (bar) Injection pressure - 1575 (bar) Specific holding pressure -140 (bar) with an intensification ratio of 11.25
Mould Temperature Controller	Regloplas 90S temperature control units Maximum temperature 90 (ºC)

Table 3.3 Moulding equipment

3.1.3 Geometries and Moulding Conditions

The geometries including fan gate and centre gate with varying thickness were investigated as part of this study. The flow in both of these geometries is different, this is the primary reason they were selected. The difference in the flow made an interesting study for FOD and FLD.

3.1.3.1 Fan Gate

The schematic of the 4 mm thick transverse ribbed plaque shown in Figure 3.3 has a 6 mm diameter sprue and a complex gating system, which consists of a fan shaped gate with a 4 mm thick well. The dimensions of the plaque are 120 x 40 mm and it contains a reinforcing rib 40 x 12 x 2.5 mm, which is protruding 40 mm from the gated end of the plaque and is perpendicular to the direction of flow. The gate and sprue dimensions are the same for the 2 mm transverse plaque but without a protruding rib shown in Figure 3.4**.**

The 4 mm thick ribbed plaque and 2 mm thick plaque are injection moulded using Rhodia Technyl C216 V40 material. The injection moulding conditions for both are found in Appendix 1.

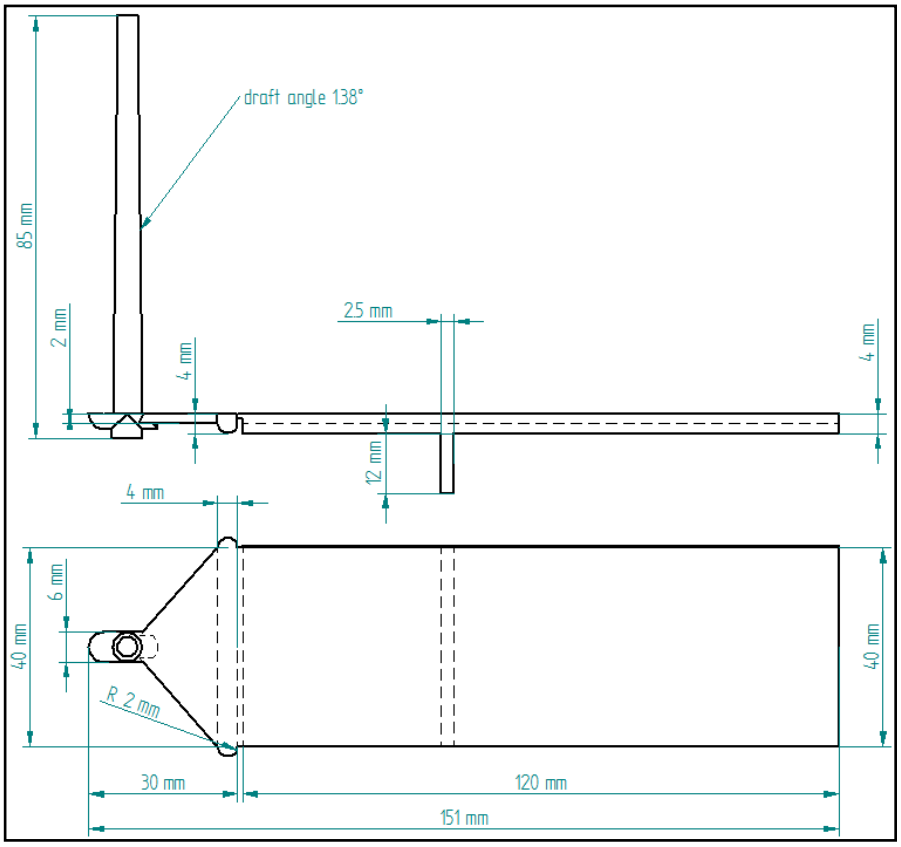

Figure 3.3 2-d drawing of transverse ribbed plaque.

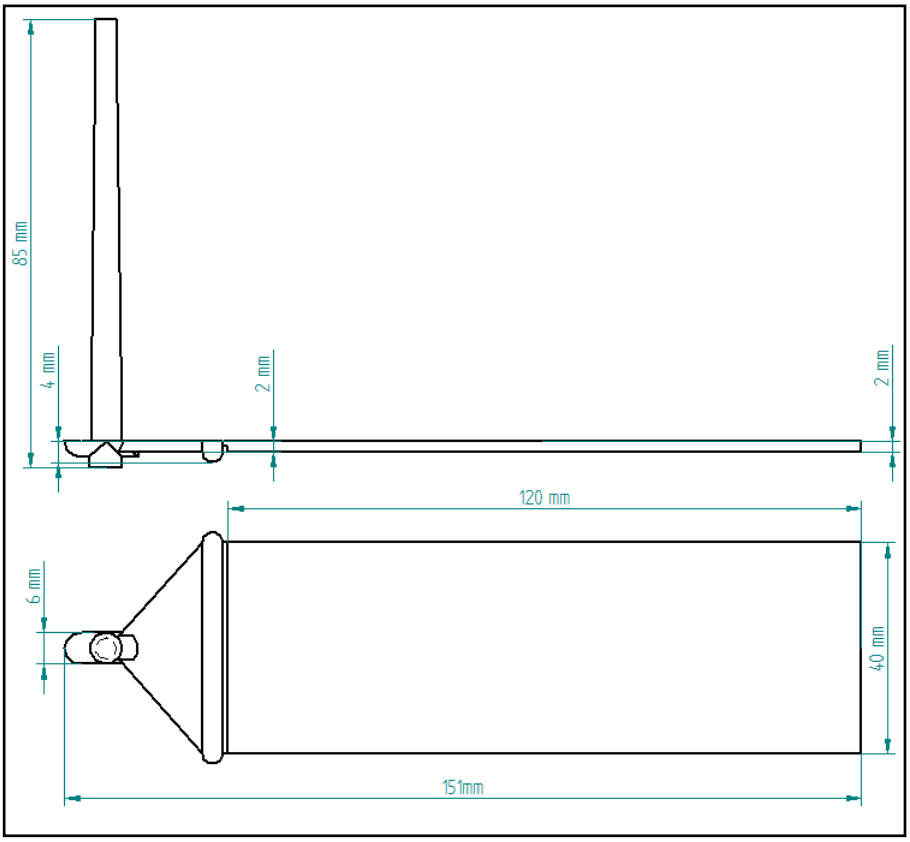

Figure 3.4 2-d drawing of flat plate 2 mm

3.1.3.3 Centre Gate

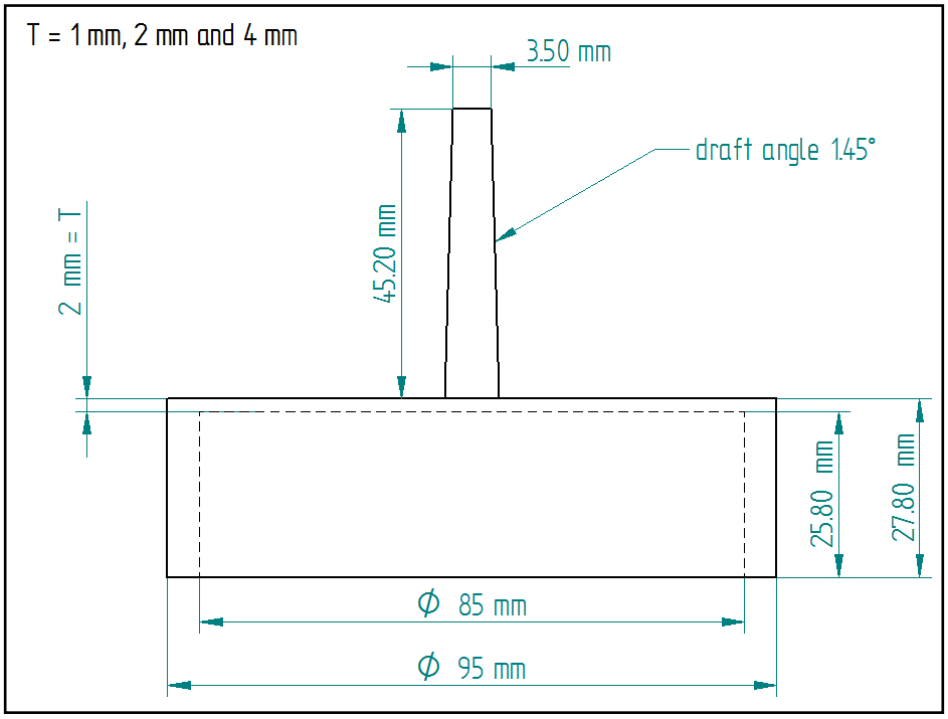

Figure 3.5 2-dimensional drawing of centre gate disc component

The centre gate disc component has a variable base thickness which is shown in diagram Figure 3.5. The disc consists of a sprue with a diameter of 3.50 mm, has an outer diameter of 95 mm and a 5 mm thick circular section protruding from the edge with a height of 27.80 mm. This geometry was injection moulded using both the short and long glass fibre material. The disc was injection moulded with Rhodia Technyl material for each thickness available (1, 2 and 4 mm) moulding conditions for these geometries are found in appendix 1. However only the 1 and 2 mm thick geometries were injection moulded using the long glass fibre Stamax material, the injection moulding conditions for these geometries are found in appendix 1. To process the LGF material the screw speed, back pressure were kept low (50 rpm and 3 bar) and the injection speed was set to a moderate speed less than 50% capacity of the machine (45.6 mm/s) as recommended by SABIC®.

3.1.3.2 Modifications

Shear is experienced during injection moulding, this results in fibre degradation while processing long glass fibre material, which in turn affect the mechanical properties. Apart from adjusting the processing conditions to reduce breakage in the LGF material, modifications can be made to design of the nozzle and sprue. SABIC® has recommended using a standard extended nozzle and increasing the size of the sprue (Sabic, 2011). Justification of possible processing and design suggestions to reduce fibre degradation are discussed in Section 2.3.2 Fibre Length Degradation. The Battenfeld injection moulding machine was installed with a 3 mm diameter standard extended nozzle (Figure 3.6), to injection mould the 3.5 mm sprue centre gate geometries.

To preserve the fibre length the size of the sprue and nozzle exit was increased to 6 mm diameter (Figure 3.7). A large nozzle and sprue diameter should reduce the amount of shear the material experiences between the nozzle and sprue before it gets to the cavity. To examine the total fibre breakage which occurs as the material is plasticised in the screw, fibre length measurements were carried out on the material which purges out of the nozzle. For the modified configuration, only the 1 and 2 mm thick geometries were injection moulded using the long glass fibre Stamax material. The injection moulding conditions with this geometry for both materials are found in appendix 1.

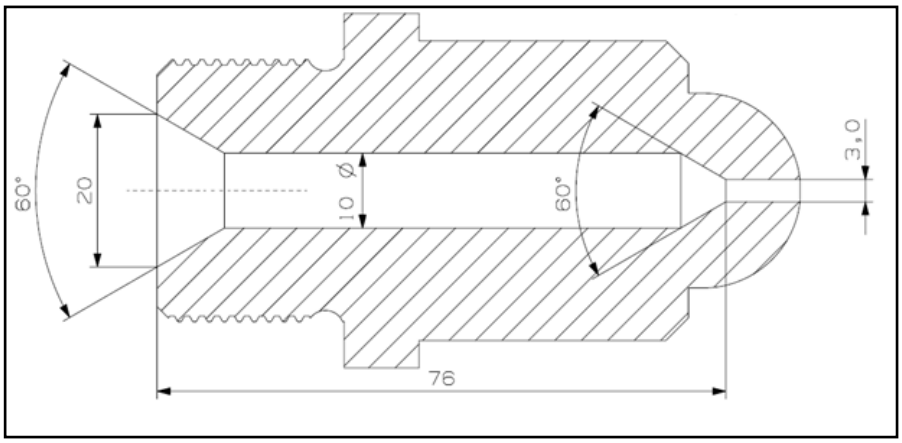

Figure 3.6 Cross-section drawing of 3.0 mm diameter nozzle

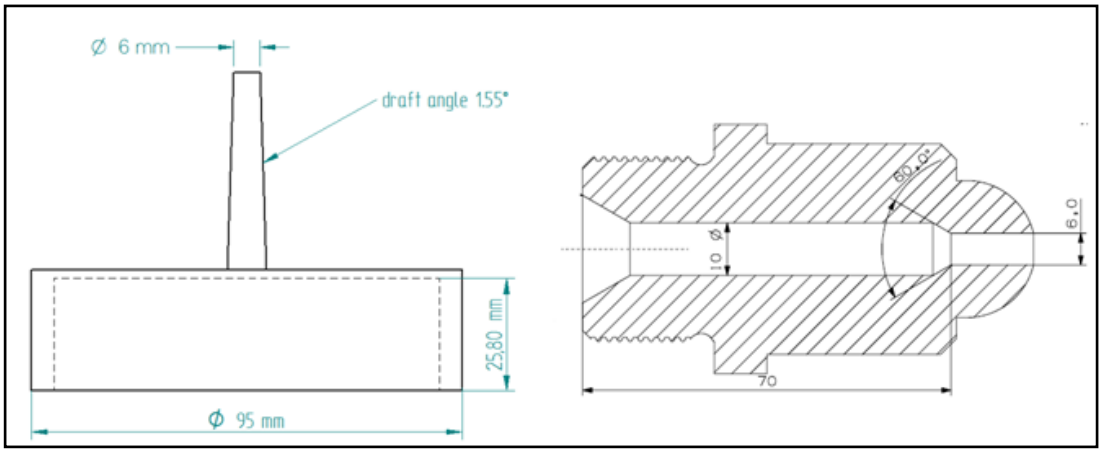

Figure 3.7 Drawing of modified centre gate component and nozzle

3.2 Fibre Orientation Distribution Measurement

As discussed in 2.5.1 Short Glass Fibre the fibre orientation distribution of a short and long glass fibre is at present represented in a 3-d space using uniquely defined by two polar angles θ and ϕ. FOD data can be derived from either polished 2-d sections using reflective microscopy (Vincent and Agassant, 1986) or from microtomed slices (20-30µm) using CMR (contact micro-radiography) (Darlington and Mcginley, 1975; Kamal et al., 1986). Making the 3-d problem into a 2-d problem considerably simplifies the data extraction process and makes it easier to automate. The University of Leeds currently offers a reflective microscopy-based system; this offers accurate 3-d characteristics of fibre orientation using 2-d images over small size areas (Davidson, 1993; 1997 and Hine et al., 1993; 1995). The system is controlled by a PC and allows samples containing tens of thousands of fibres to be analysed. Regions of interest can be analysed after careful sample preparation. Alternate methods such as micro-CT were not investigated here but may be part of future work.

3.2.1 Sample preparation

Sample preparation steps include cutting, marking, mounting, grinding, polishing and etching (Valez-Garcia et al., 2012). The end result is a polished cross-section ready to analyse using optical microscopy (Bay et al., 1992).

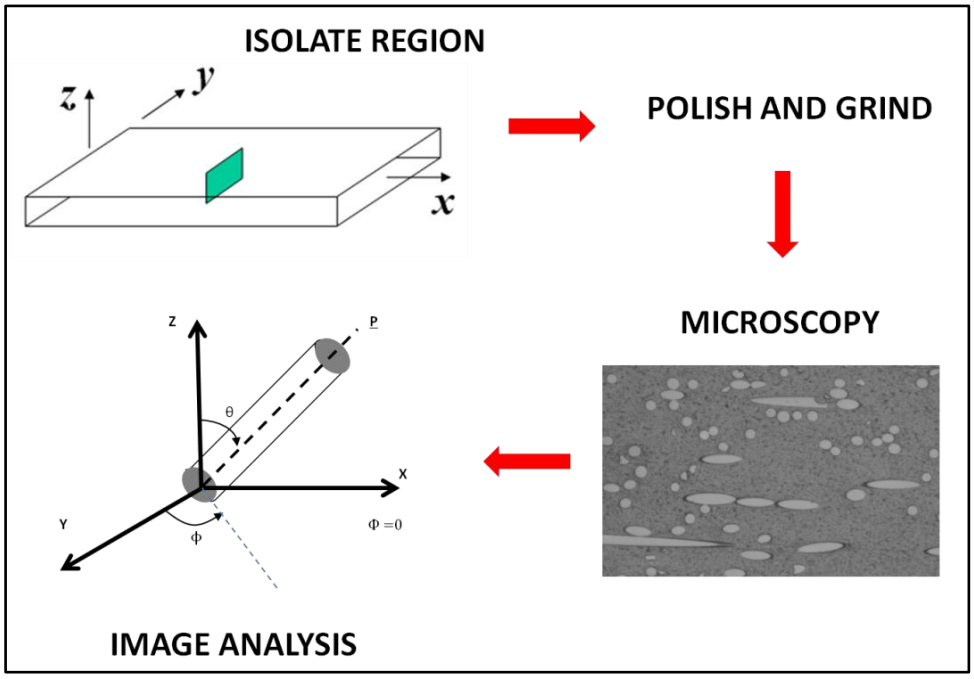

Figure 3.8 Procedure to measure fibre orientation distribution

3.2.1.1 Mounting sample

The specimen needs to be clearly marked and a section from the region of interest cut using saw blade dia. 120 x 1.7 mm. However a relevant margin (2 mm has been sufficient) needs to set between the measurement plane and cutting lines, as well as performing the cut using low speeds to prevent fibre damage (Bates and Wang, 2003 and Hayes and Gamon, 2010). The material in the margin is easily removed during the machining step. The sample is then placed into a 40 mm diameter plastic mould; the region of interest must be placed flat against the bottom cover shown in Figure 3.9. To ensure the sample does not move it is secured using either a plastic support clip or double sided tape. Mould release is sprayed on to the base and mould combined thus ensures the sample can be easily retrieved once it hardens. A mixture of EpoThin Resin and EpoThin hardener with a ratio of 5:2 is mixed together, from a cloudy to a clear mixture which is then poured into the mould and left to cure for 9 hours. Once the epoxy has cured the edge showing the sample is machined removing a maximum of 0.2 mm of material to give a flat surface to polish and grind as shown in Figure 3.9.

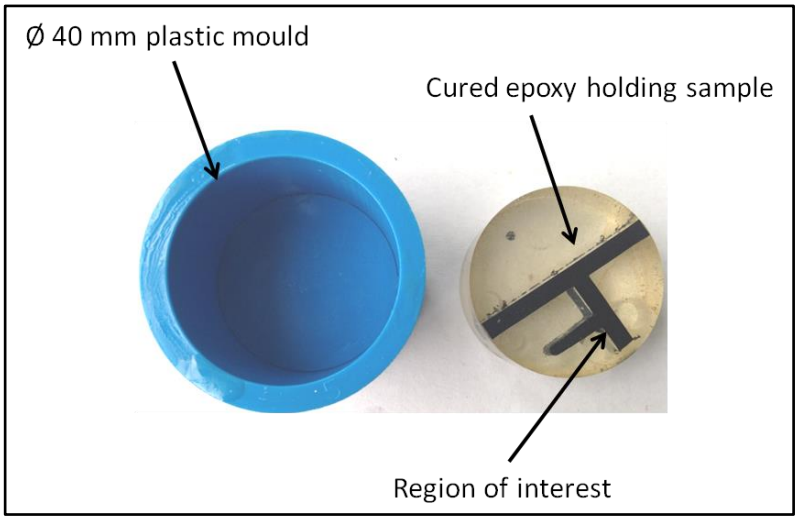

Figure 3.9 Example of cured sample

3.2.1.2 Grinding and Polishing

To ensure a parallel grinding and polishing process the specimen is clamped by apparatus discussed in Section 3.2.1.2.1 Apparatus. To reveal the composite structure standard grinding and polishing techniques were used prior to etching (Sawyer and Grub, 1994; Hayes and Gamon, 2010). The grinding process is essentially the removal of material; the amount of material removed is dependent on the coarseness of silicon carbide (SiC) paper, pressure and velocity. The abrasive (grit) size determines how much material is removed by the SiC paper. The abrasive standard FEPA (Federation of European Producers of Abrasives) denotes a letter P after the abrasive size, a larger size removes less material (finer paper). Water is used as lubricant during grinding (wet grinding) to carry debris away. Polishing involves the removal of material on a microstructure level, using a polishing cloth and slurry of alumina (aluminium oxide) suspension containing finer abrasive particles. To create a smooth and shiny surface it is important to change polishing cloths between different alumina suspensions. Natural or synthetic silk cloths come in different forms and have the fastest removal rates.

3.2.1.2.1 Apparatus

Buehler Metaserv automated grinder/polisher (Figure 3.10) consists of a rotating head and a rotating wheel. The rotating head can operate in a clockwise or counter clockwise direction. The wheel has a rotational speed between 25 to 300 revolutions per min (rpm) this is user controlled. Interchangeable 8 inch platens/disks can be placed on the wheel to accommodate for the silicon carbide paper or polishing pads. An adjustable pneumatic force creates downward motion of the rotating head; this is indicated in lbf on the pressure gauge with a maximum value of 60 lbf (266.89 N). There is a small water supply to the rotating platens, the release of water is user controlled. There is an option to have a timer controlled cycle. A central force specimen holder was used to hold three 40 mm specimens at one time. It is best to fill the circular cavities with three specimens, with the same hardness to create an even pressure distribution each time the procedure is carried out.

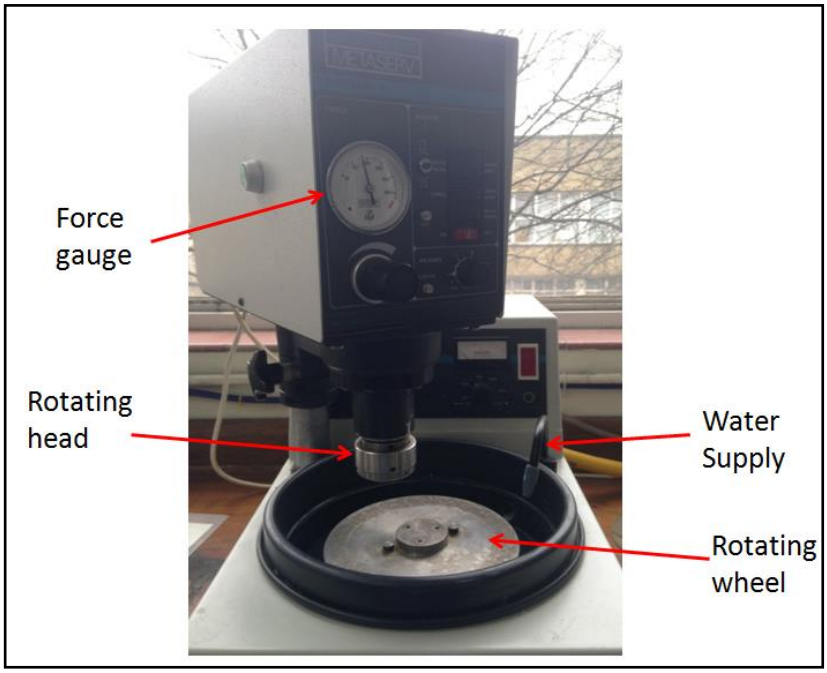

Figure 3.10 Buehler Metaserv automated grinder/polisher

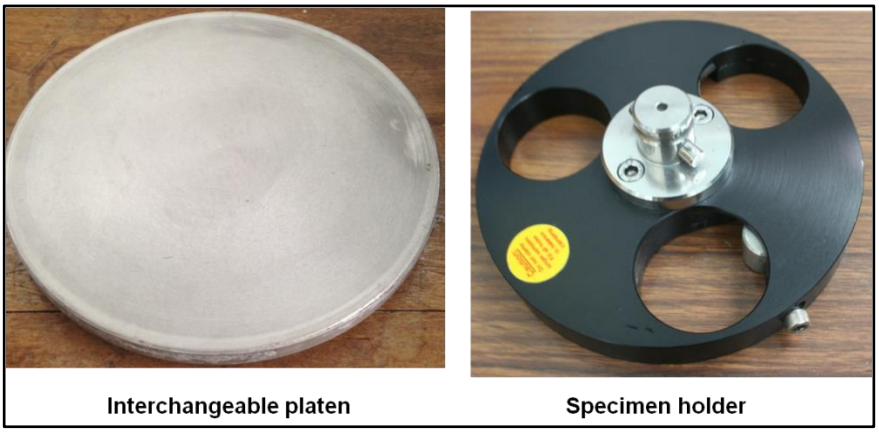

Figure 3.11 Platen and specimen holder

3.2.1.2.2 Procedure

After each step the specimen holder is removed and the specimens are rinsed with distilled water to remove debris and dirt. It is important to study the samples using optical microscopy at x100 magnification at the end of each step to determine if enough material has been removed (fibres are visible). More time may be required to grind and polish the sample if the sample area increases. Table 3.4 to Table 3. 7 indicate the operating parameters to carry out each step.

SiC paper (Ø 8 inch)	P 600
Lubricant	Wet Grinding (water on)
Wheel speed	300 rpm
Force	8 lb (35.6 N)
Time	2 minutes

Table 3.4 Rough grind parameters

SiC paper (Ø 8 inch)	P 800
Lubricant	Wet Grinding (water on)
Wheel speed	300 rpm
Force	8 lb (35.6N)
Time	4 minutes

Table 3.5 Fine Grind parameters

Polishing cloth (Ø 8 inch)	Buehler Texmet 1000
Lubricant (spread over cloth)	1 μm alumina suspension Diluted with distilled water ratio (1:5)
Wheel speed	150 rpm
Force	10 lb (44.5 N)
Time	15 minutes

Table 3.6 Rough Polish parameters

Polishing Cloth (Ø 8 inch)	Buehler Soft, synthetic MicroCloth
Lubricant (spread over cloth)	0.3 μm alumina suspension Diluted with distilled water ratio (1:5)
Wheel speed	150 rpm
Force	6 lb (26.7 N)
Time	15 minutes

Table 3. 7 Fine Polish parameters

3.2.1.3 Etching Sample

The polished sample is investigated under an optical microscope although the fibres and matrix can be seen; there is difficulty in distinguishing between the glass fibres and matrix as a result of the similar contrast. To overcome this problem the sample is etched in an oxygen rich environment; plasma etching is the most preferable method of etching thermoplastic glass fibre composites (Hine and Duckett, 2004 and Valez-Garcia, 2012). Energised oxygen ions bombard the polymer surface removing < 1 mm of material (Egitto, 1990). Etching creates a rough surface this gives a good contrast between the fibres and matrix.

3.2.1.3.1 Apparatus

Edwards Sputter Coater/Etcher - S150B (Figure 3.12) was used to etch the samples. The samples are placed into a glass chamber with 150 mm dia. and 115 mm high. The lid of the chamber has an electrode comprising of a platinum 60 mm diameter target. The coater is connected to an oxygen gas cylinder; a built in vacuum pump draws the oxygen into the chamber. The vacuum pressure is regulated using a pressure gauge with maximum pressure of 5 mbar. High voltage is supplied to the electrode this is user controlled, the current and voltage range from 0 -100 mA and 0 - 2.5 kV.

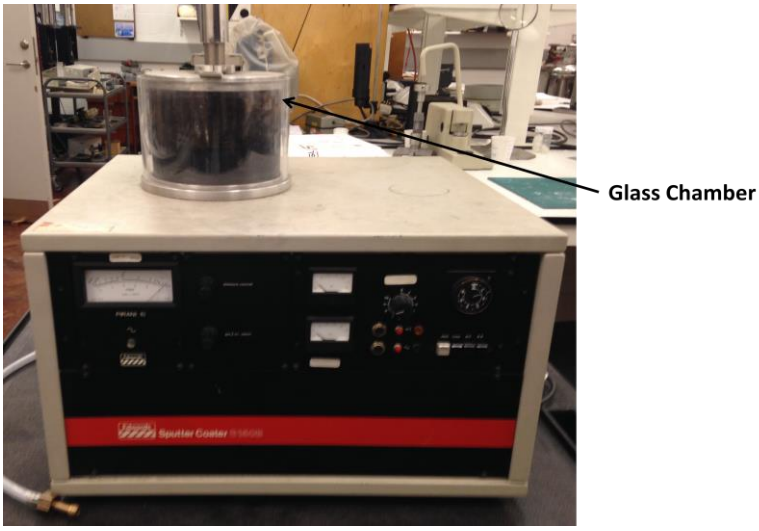

Figure 3.12 Sputter Coater/Etcher

3.2.1.3.2 Procedure

One sample should be placed into the glass chamber to ensure plasma etching is even, the region of interest should be facing the lid. The following steps are taken to etch polymer from the surface.

1. The lid is tightly closed to prevent any leaks.
2. The valves are closed and the RP (roughing pump) button is pressed to create a vacuum in the chamber.
3. Open the main valve (counter-clockwise) on the oxygen cylinder to a pressure of 0.8 atm (atmosphere).

4. Flush the chamber with oxygen several times and gradually turning the pressure control until pressure rises to 0.2 atmosphere.
5. Press the HT button use the pressure control to set the HT (high tension) to 1 kV (voltage) and 50 mA (current).
6. A white glow strikes the chamber once the oxygen ratio is correct (purple glow donates excessive amounts of nitrogen). The sample etching time for PA6 and PP samples was 15 minutes; this gives enough time for the matrix to degrade.

Figure 3.13 shows a clear difference in an etched and non-etched sample, the dark background allows the image analyser to detect the fibres.

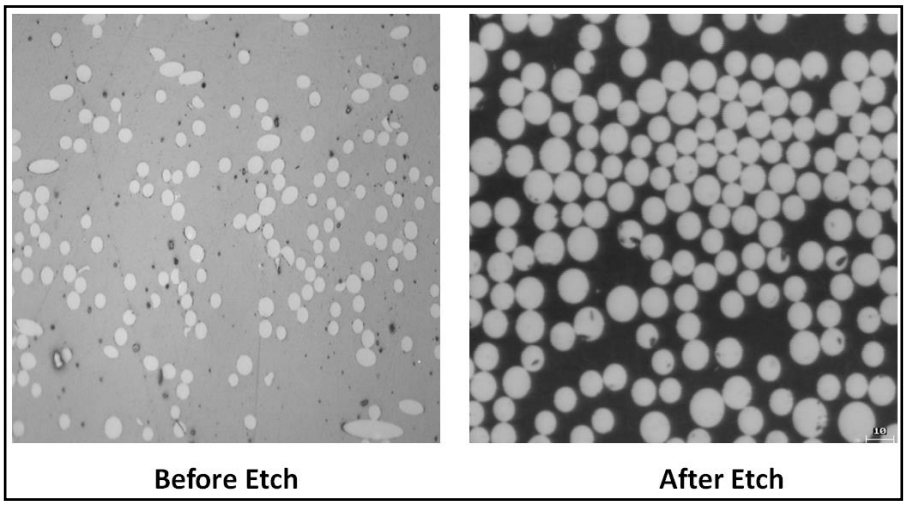

Figure 3.13 Optical images of glass fibre sample before and after etch

3.2.2 Fibre Images

The samples are analysed using an Olympus BX41 reflective optical microscope with x20 objective power and x2.5 eye piece. The microscope is mounted with a Prior Scientific XY translation stage and autofocus unit. To gain suitable images of the samples a Sony square pixel CCD camera is mounted on top of the Olympus camera adapter attached to the microscope. Figure 3.14 shows the schematic of the automatic image analyser system and the layout of the microscope unit. As a result of pixilation and lack of detail an x12.5 magnification power will not provide suitable images to process at a later stage. The magnification was increased to x50 magnification to capture accurate

elliptical parameters for each fibre. This magnification produces an image field view of 560 µm in the x direction and 430 µm in the y direction example of one frame is shown in Figure 3.15.

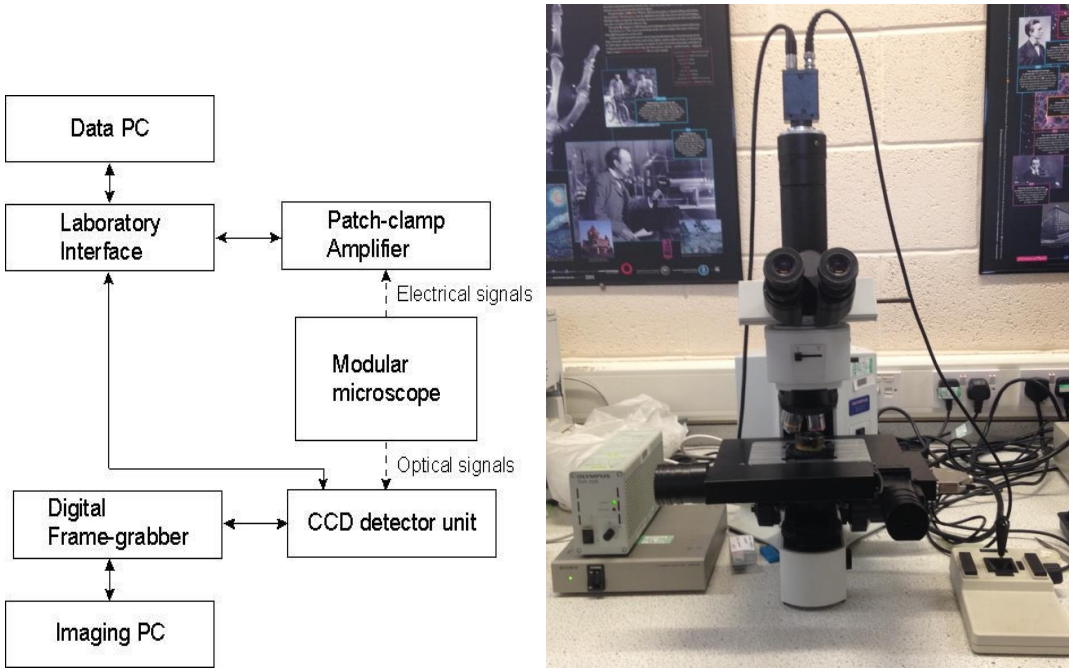

Figure 3.14 Schematic and image showing functions of image analysis system

The output of the camera is to a computer as there is a clear difference between the bright fibres and dark matrix; primary objects are isolated using a threshold technique. To compress the data two possible grey levels are associated on each digitized frame. The threshold is set such that a value above this is a fibre pixel and below is recognized as the matrix (Hine and Ducket, 2004). Elliptical parameters are found for every group of pixels recognised as a fibre. During processing the fit to each ellipse is shown by an ellipse outline example of a live image is shown in Figure 3.15.

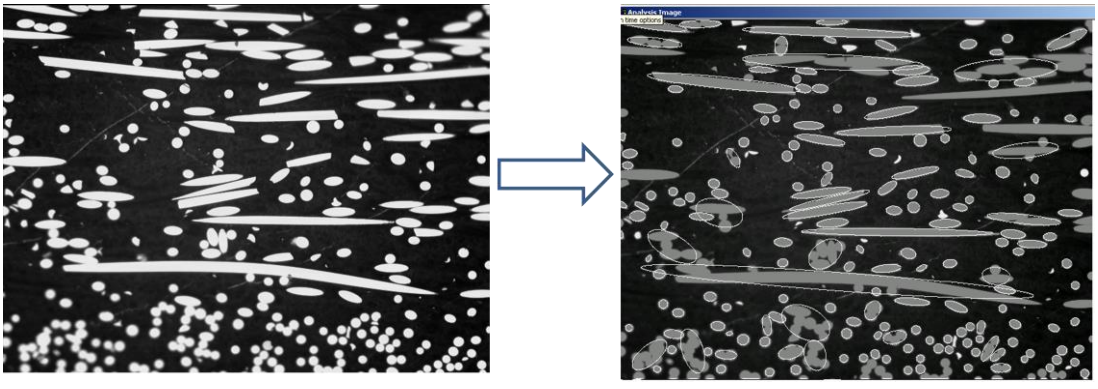

Figure 3.15 Recognition of bright fibres during image analysis

The threshold was systematically altered from pixel intensity of 150 to 210. An image is built up for large areas, through a series of stage movements and image captures using a computer controlled XY stage. Images are saved in the memory as the stage moves through frames. The number of frames in x and y direction are dependent on the magnification and region of interest. For example a 3 x 3 area (Figure 3.16) at x50 magnification is equal to 1.68 mm in the x direction and 1.29 mm in the y direction. An autofocus algorithm is included this ensures the sample remains in focus during image capture.

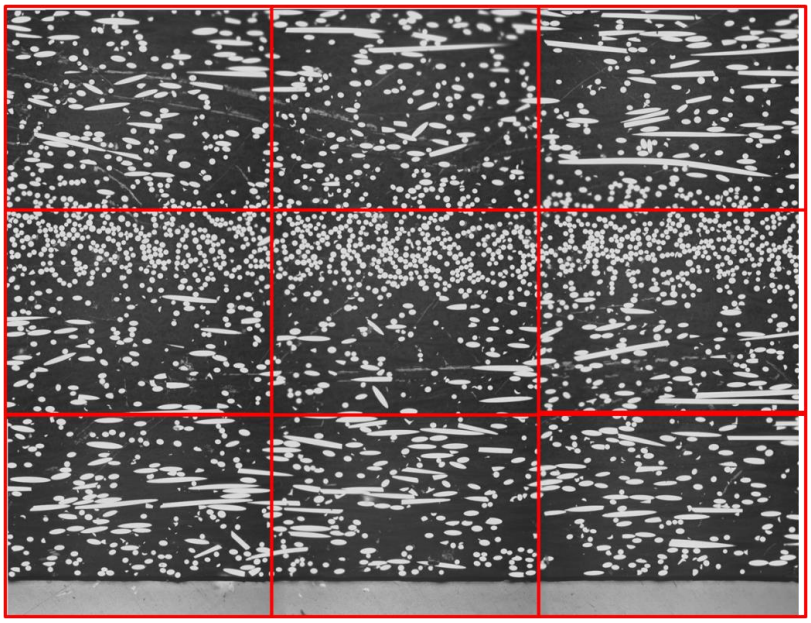

Figure 3.16 FOD Image analysed as 3 x 3 frames

It is possible that some fibre images will overlap the edge of the current field of view (Figure 3.17). The probability of overlapping increases with the presence of long glass fibres, which could cross up to 3 frames if the fibre is flat in the measurement plane. These partial fibre images on the edge must be reconstructed if the elliptical measurements are to be achieved. The image analysis stores data on the partial image until the image sort process recognises the next part of the partial image within adjacent frames with the same central coordinates. The data for each complete particle/ellipse is stored in a file the next step is to analyse the data.

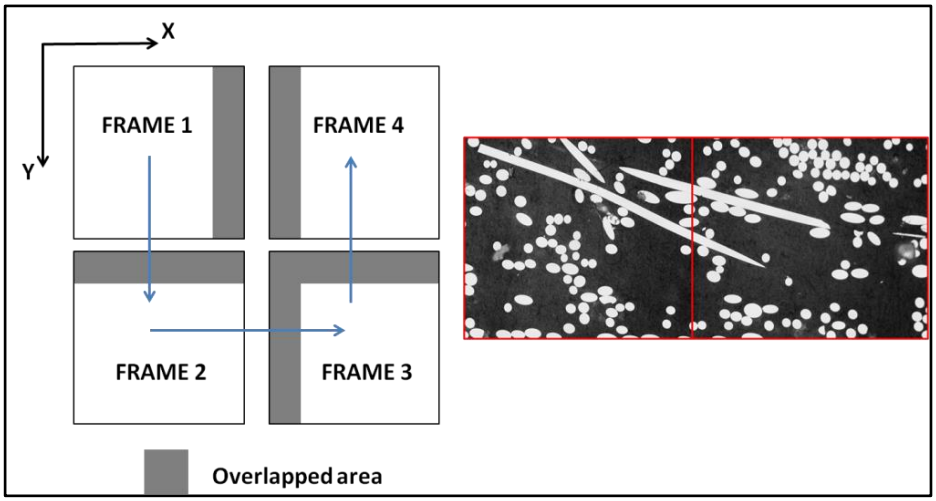

Figure 3.17 Overlap area and an example of overlap in x50 mag LGF sample

3.2.3 Processing Images

3.2.3.1 Orientation Calculation

In processing the images, the data characterising all the ellipses passes through an algorithm which calculates the angles of orientation. The out of plane angle is theta (Equation 3.1) is determined from the elliptical footprint shown in Figure 3.18. The measurements represent the semi-major axis length a, and semi-minor axis length b respectively.

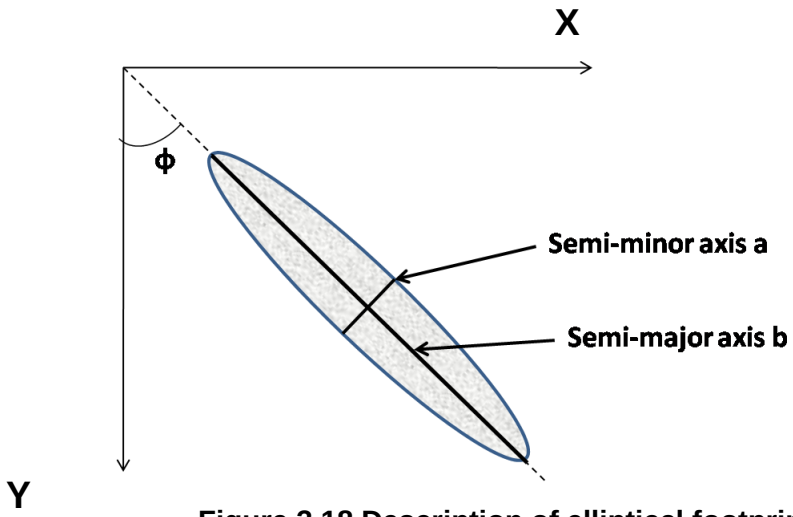

Figure 3.18 Description of elliptical footprint

$$\theta = \cos^{-1}\left(\frac{b}{a}\right) \qquad \textbf{3.1}$$

A problem with 2-d polished surface is that there is an 180^{O} ambiguity in the angle to the section normal to the axis 3 Figure 3.19. The only way to determine this is to scan the sample at relative displacements through the thickness making sure that the position remains the same. Some researchers propose a method which derives a 3-d FOD by combining data from orthogonal plane sections (Zhu et al., 1997). Although it would be interesting to know the ambiguity in the in-plane angle the exercise of combining data from orthogonal planes is very time consuming and it is outside the scope of this study.

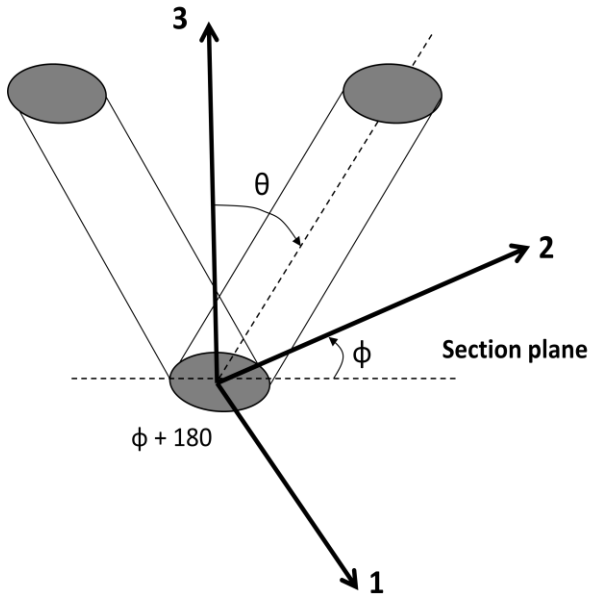

Figure 3.19 Two possible fibre orientations based on the same elliptical cross-section

3.2.3.2 ANALYSE

Analysis of data is carried out in "ANALYSE" software developed by Davidson, (1993). The image analyser stores all the information from one complete scan into an assigned folder. The information stored for each particle/ellipse during the scan includes; the central co-ordinates, semi-minor (a), semi-major (b), theta angle, phi angle and total number of pixels for each particle. Once the files are extracted the distribution for each ellipse angle (θ and ϕ) and length (semi-minor and major) (pixels) is displayed as shown in Figure 3.20.

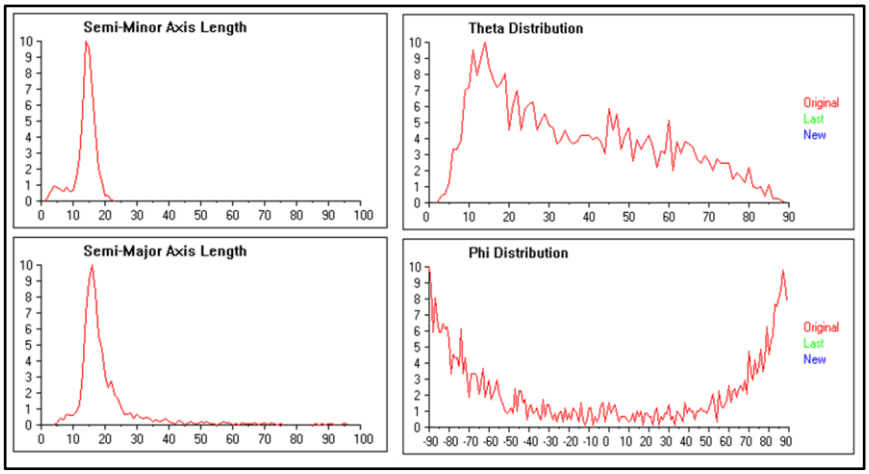

Figure 3.20 Example of data gathered from the scan in ANALYSE before filter

Although the samples are prepared by polishing there may be some redundant particles present including, fibre fragments, build up of debris on the surface of the sample as shown in Figure 3.21. This unwanted data is easily removed by defining upper and lower limits for the semi-minor length in pixels and a fit factor depending on the angle theta. The semi-minor axis length distribution has two tails as shown in Figure 3.20. The distribution under the tail to the left represents small fragments and the distribution under the tail to the right represents merged fibres. In this example choosing a minimum value of 11 and a maximum value of 20 will remove any small fragments and merged fibres. Example of a merged fibre and fragment is shown in Figure 3.21.

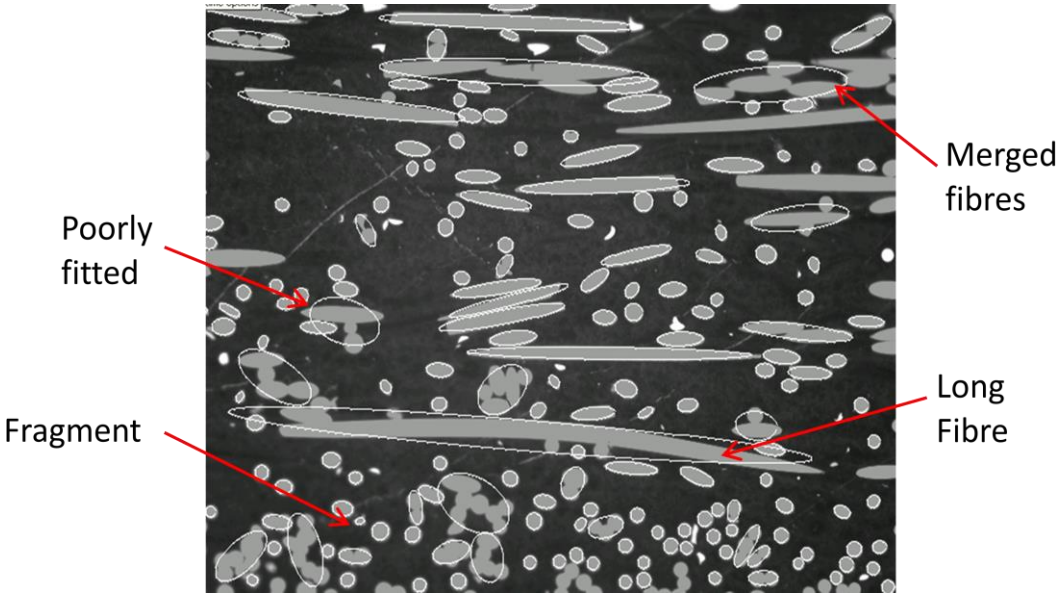

Figure 3.21 Example of particles recognised during live image process

Each particle is fitted with an ellipse even if the shape of the particle does not correspond to the shape of an ellipse. The difference between the computer reduced area and the total number of pixels for each particle (fit factor) must be less than 5% to accept the particle. The fit factor in (Equation 3.2) found with the semi-minor axis length (a), semi-major axis length (b) and the total number of pixels. Choosing a fit factor of 0.05 (5%) will remove particles including holes, fragments, incomplete or poorly fitted fibres as shown in Figure 3.21. A long fibre as shown in Figure 3.21 could be disregarded as a poorly fitted fibre by the fit factor calculation. If the fibre is very long and lying in the plane of measurement the angle theta is usually above 80 degrees. To overcome this problem and to keep the long fibres in the orientation calculation the fit factor condition is declined if the angle theta for the particle is above 80 degrees.

$$\text{Fit Factor} = \frac{(\text{Total number of pixles} - \pi ab)}{(\text{Total number of pixels})} \qquad \textbf{3.2}$$

3.2.3.3 Calculation of orientation averages

Once the raw data has been processed it can then be used to describe an orientation distribution using the second order tensor system. The Leeds FOD system calculates the orientation tensor components using the following relations (Bay and Tucker, 1992).

$$a_{xx} = \langle \sin^2\theta \cos^2\phi \rangle \qquad \textbf{3. 3}$$

$$a_{xy} = a_{yx} = \langle \sin^2\theta \cos\phi \sin\phi \rangle \qquad \textbf{3.4}$$

$$a_{xz} = a_{zx} = \langle \sin\theta \cos\theta \sin\phi \rangle \qquad \textbf{3. 5}$$

$$a_{yy} = \langle \sin^2\theta \sin^2\phi \rangle \qquad \textbf{3. 6}$$

$$a_{yz} = a_{zy} = \langle \sin\theta \cos\theta \sin\phi \rangle \qquad \textbf{3. 7}$$

$$a_{zz} = \langle \cos^2\theta \rangle \qquad \textbf{3. 8}$$

The calculated average orientation tensor in each axis is output in the form of a graph or contour plot as shown Figure 3.22. The plots represent the FOD over a number of strips through thickness and as this number increase the number of data points increase. The data from the graph is extracted and taken to Excel for further evaluation.

The angled brackets relates to the average taken over every fibre in the sample area. The 180° ambiguity in phi means that a_{yz} and a_{xz} terms are much more susceptible to errors. Therefore an accurate orientation may be given by considering the remaining terms.

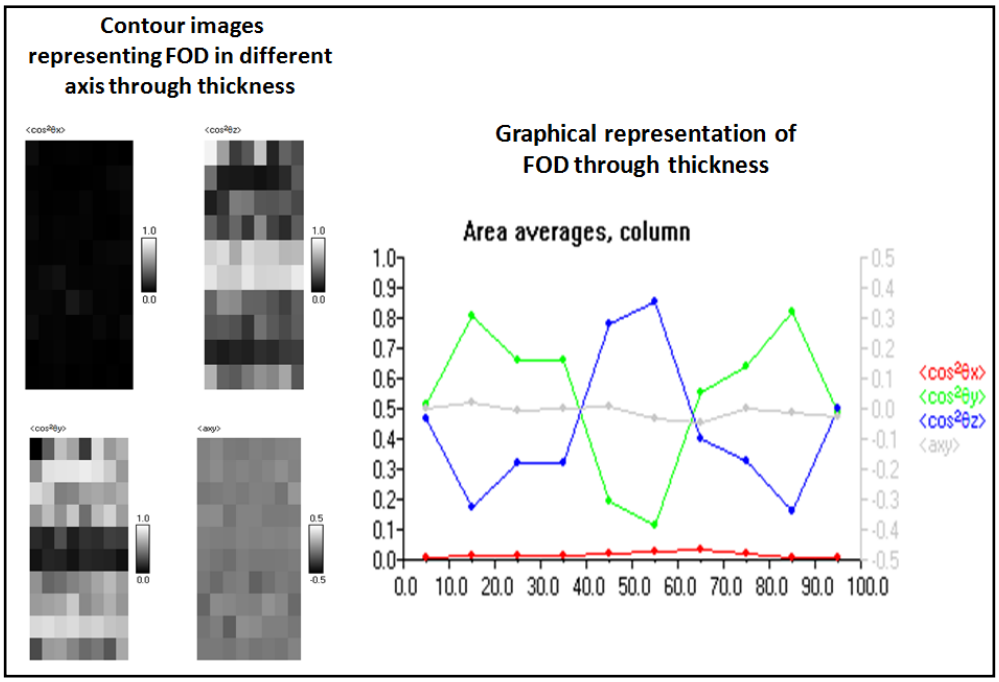

Figure 3.22 Output of FOD data in ANALYSE

3.3 Fibre Length Distribution Measurement

Over recent years fibre length measurements have been taken from pyrolised composite specimens (Vaxman and Narkis, 1988). After matrix removal it is important to disperse the fibres preferably without physical contact. It is common to disperse fibres extracted from SGF injection moulded specimens in a glass dish containing water (Fu et al., 2000). Dispersion of fibres extracted from LGF injection moulded specimens is much more difficult as fibres are bundled together. Research carried out by Kunc et al., (2007) discusses successful dispersion of long glass and carbon fibres on either a glass dish or laminating film.

Capturing 2-d images by the means of optical microscopy is a typical method of measuring the fibre length of short fibres (Fu et al., 2000, 2002). However this method is not suitable to capture long fibres, with lengths > 1 mm which could extend beyond the field of view at a higher magnification. Negating long fibres would bias the resultant length distribution and increase the level of error. Dahl et al., (2011) and Kunc et al., (2007) have found the use of a scanner to be an effective method to capture dispersed long and short fibres. Alternative methods to this include manual stitching of 2-d images or the automated reflective microscopy system; this was controlled by a PC and was capable of measuring the length of thousands of fibres over a large area (Davidson, 1999). The semi-automated FLD system present at the University of Bradford captures high resolution images of fibres with an A3 Epson Expression 10000XL Pro scanner with maximum optical resolution of 9600dpi (dots per inch). The images are then processed with an open source software package (ImageJ), using an in-house algorithm to measure the length of each straight fibre.

3.3.1 Matrix removal

Fibre length measurements are taken from the raw material, section of interests isolated from the component and extrudate within the plasticating phase (without injection) as shown in Figure 3.23. The specimen is enclosed in aluminium sheet, where the dimensions correspond to the shape of the cut

specimen. In order to allow expansion of long fibres during burn off there is a slight gap left between the aluminium sheet and the specimen. The specimen is then placed in a vacuum oven at 480ºC for 5 hours. The duration and environment in the oven will allow complete matrix removal leaving behind an entangled mass of fibres.

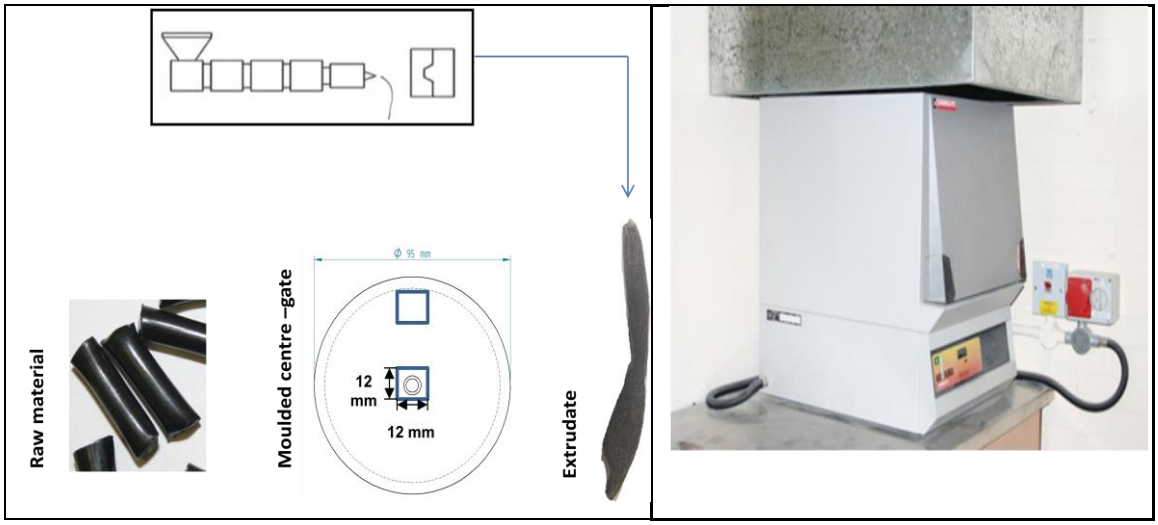

Figure 3.23 Samples isolated in vacuum oven

3.3.2 Fibre Images

There are two stages in creating suitable fibre images for processing, the first involves dispersing the fibres onto thin film and the second is capturing these images. Long glass fibres are susceptible to breakage therefore care has to be taken while dispersing. The burn-off contains an entangled mass of fibres and a small volume of very short fibres which have fallen to the bottom. The entangled mass of fibres is taken and placed onto a 215 x 266 mm transparent film 0.05 mm thick. To avoid physical contact with fibres a small hand held suction pump uses air to separate and disperse the fibres. This process is repeated until all the fibres are spread out sufficiently across a number of films if required. In some cases it is difficult to separate the fibres at the core because curved long fibres increasingly intertwined. In this scenario mechanical action is required to gently loosen the fibres, under a magnifying glass, using a thin bristle from a brush or a thin wooden stick. In the best possible situation fibres do not overlap but this cannot be avoided with a large number. The sample is

spread out over a number of films to reduce fibres crossing over. An example of ineffective fibre arrangement for image analysis is shown in Figure 3.28.

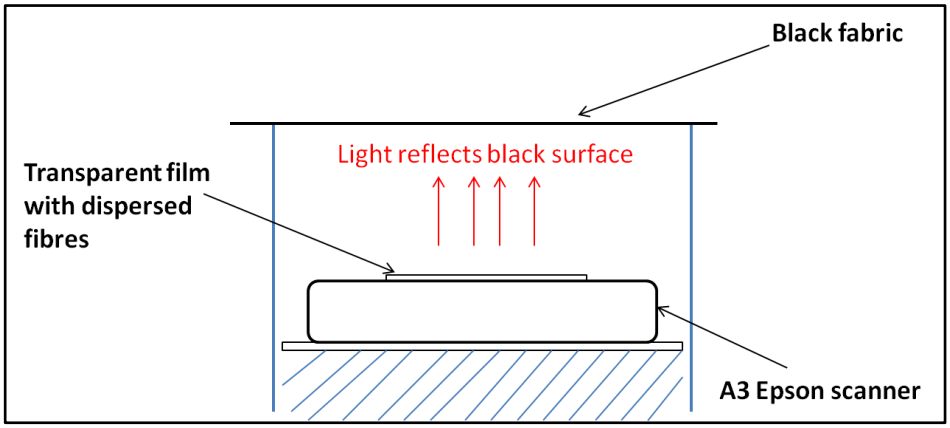

Figure 3.24 Cross-section schematic of the fibre length image system

Next step is to place the thin film onto the scanner table (Figure 3.24). The glass surface of scanner table should be clean and free of any dust or scratches. The scanner is able to capture all the fibres at a high resolution. The glass fibres are transparent this makes them difficult to capture if the scanner cover is in use during the scan. Therefore the scanner cover is removed and the scanner is completely isolated by a 0.2 mm thick black fabric, creating a contrast between glass fibres and the transparent film. Addition of any colour in the image is not necessary as this increases the size of the image. The end result is an 8-bit gray-scale image with an 8 µm (3200 dpi resolution) pixel size. Example of a typical image in ImageJ is shown in Figure 3.25.

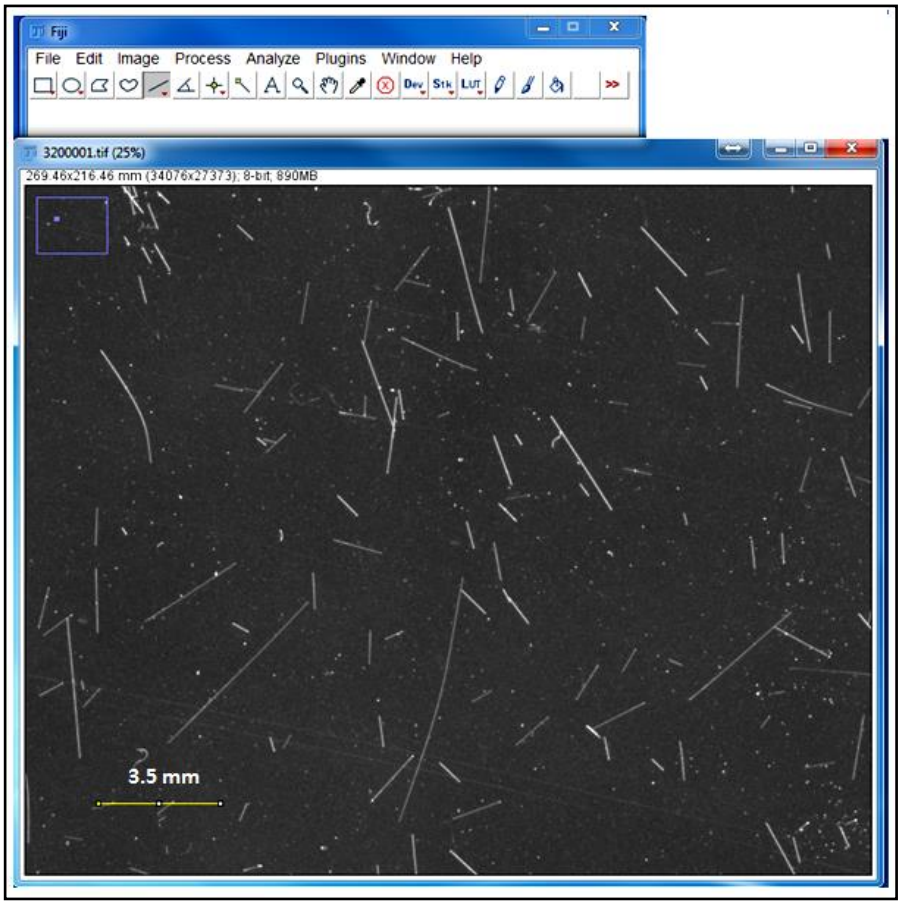

Figure 3.25 Example of fibre length image exported into ImageJ

3.3.3 Processing Images

3.3.3.1 Image filter

Before the image is processed the appropriate scale needs to be set according to the resolution of the image. A calibration piece was used to determine the distance of 1 pixel into mm. If the scale is not set the distance will simply be measured in the units of pixels. The image then goes through a series of manipulations, first the image is converted into a black and white (binary) image, where the fibres (high-aspect ratio) particles will be represented as long thin clusters of black pixels on white background. The next step involves removing small particles like dust. The fibre length of 0.02 mm was found to be the minimum length after investigating 3 different samples. Once the user has input the value an algorithm detects the particles smaller than 0.02 mm and they are removed from the image. Prior to applying the fibre length algorithm each

object in thinned down to a path of pixels, with a single pixel thickness (skeletonize), each fibre is described as a straight or curved line.

3.3.3.2 Line Detection

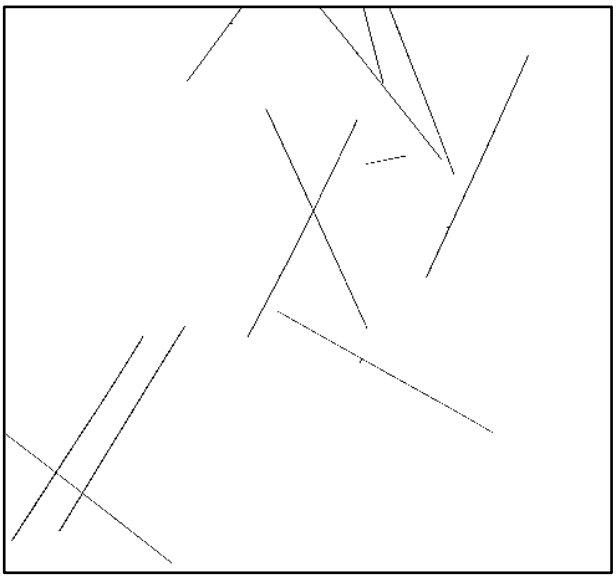

Figure 3.26 Thinned down image of straight glass fibres

The algorithm automatically recognises the backbone of high-aspect ratio straight particles visible in digital images, where particles may cross each other shown Figure 3.26. Hough transformation (Gonzalez, 1993) is a general technique employed to recognise lines within noisy images. The Hough transform is a practical method adopted for this application, Equation 3.9 represents an infinitely long straight line through x-y space using polar form. The relative difference between two lines (r_1, θ_1) and (r_2, θ_2) is denoted by Δr and $\Delta\theta$.

$$r = x\cos(\theta) + y\sin(\theta) \qquad 0 \leq \theta < \pi \qquad \textbf{3.9}$$

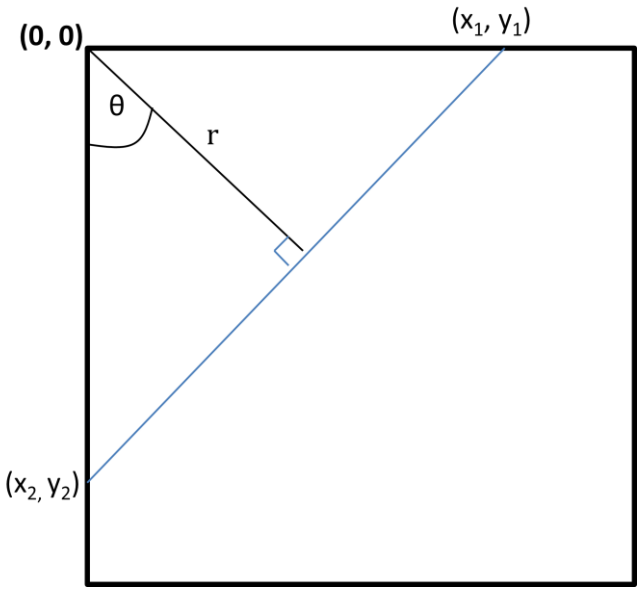

Figure 3.27 Parametric representation of a straight line using the polar form

Where r is the perpendicular distance from the line to the origin (top-left corner of the image), and θ is the angle this perpendicular makes with the y-axis. Each line is broken into smaller segments equal to 10 pixels, a line segment is a portion of a line that is bounded by a pair of distinct end points (x_1, y_1) and (x_2, y_2). The algorithm uses a line-segment merging operation based on iteratively joining pairs of line-segments that have values of r and θ, within specified values Δr and $\Delta\theta$ whose endpoints are within a distance u. Stating these 3 conditions allows lines crossing to be recognised with low probability of false-detection. The algorithm continues to join lines; if all three conditions are met the algorithm does not stop until the line-segments are replaced by equivalent single straight segments. The end-points of the new line should be the two original end-points. Analysis is performed on detected lines, using the list of end-point coordinates to output fibre length distribution.

The algorithm cannot distinguish between fibres which increasingly overlap and a curved fibre examples of these arrangements are shown in Figure 3.28. The software will process each curved fibre as multiple straight line - segments, therefore each curved fibre is measured manually.

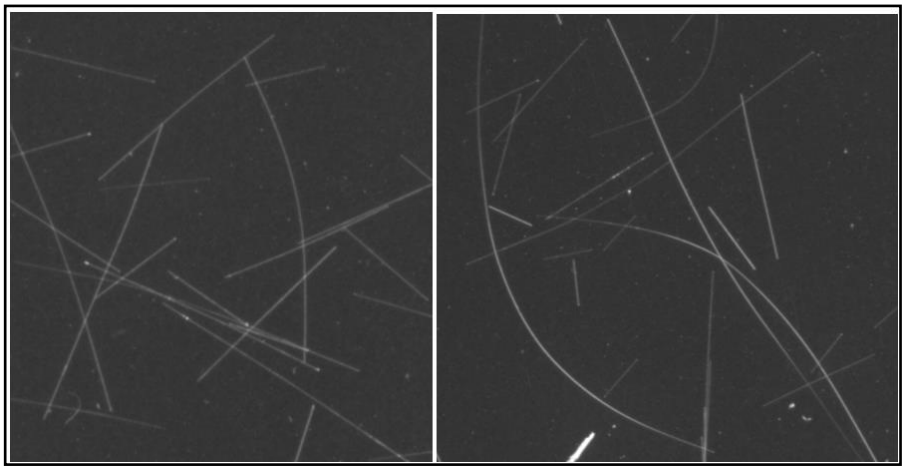

Figure 3.28 Example of curved fibres and ineffective arrangement of fibres

ImageJ has a solution to measure curved lines using a segmented-line feature. This feature allows users to superimpose a curved line and record this additional measurement. Figure 3.29 shows the image after semi-automatic analysis; the yellow lines denote a measured fibre.

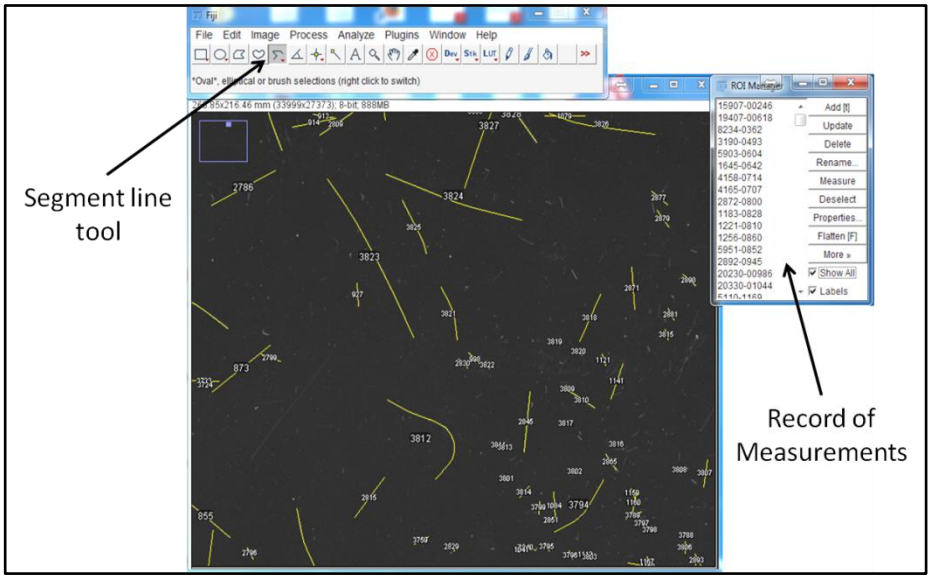

Figure 3.29 Example of fibre length image including manual measurements

3.3.4 Analysis of Data

The FLD data is output from the software and taken into excel for statistical analysis. The raw data is represented as a fibre length distribution plot. The minimum number, the maximum number, number average length (L_N) 3.10, the weighted average length (L_w) 3.11 and number of measurements are the output.

$$L_N = \frac{\sum L_i}{n} \quad \textbf{3.10}$$

$$L_w = \frac{\sum L_i^2}{\sum L_i} \quad \textbf{3.11}$$

The number average gives more emphasis to the shorter fibres as there are more in quantity, however long fibres exert a disproportionate influence on mechanical properties. A method which one can attribute the relative importance of measurements in a given sample is to calculate a "weighted average". To give more emphasis to the long fibres an appropriate characteristic of "weighting factor" for these fibres should be determined. A clear weighting factor is the weight of the fibres, but determining the weight of each fibre is not statistically possible. An explicit mathematical derivation Equation 3.11 of the weighted average length is only based on the fibre length, where fibres have a constant diameter.

Where L_i is actual measured length of the fibre and n is the number of fibre length measurements. Example of the L_N and L_w calculation Equation 3.12 to 3.13 using a real data set shown in Table 3.8.

Number	Length
1	0.12
2	0.29
3	2.66
4	1.95

Table 3.8 Example of fibre length data

$$L_N = \frac{0.12 + 0.29 + 2.66 + 1.95}{4} = 1.26 \quad \textbf{3.12}$$

$$L_w = \frac{0.12^2 + 0.29^2 + 2.66^2 + 1.95^2}{0.12 + 0.29 + 2.66 + 1.95} = 2.19 \quad \textbf{3.13}$$

3.4 Autodesk Simulation Moldflow Insight

This section will outline the key details of how to create geometries, extract and analyse 2-d solver predictions in ASMI 2014. A clear method of presenting the predicted and measured FOD and FLD data is described in this section.

3.4.1 Creating Geometries

3.4.1.1 Mid-plane

Simple 2-d surfaces which approximate the sections in the actual geometries are created in ASMI 2014. All 2-d geometries are made up of curves, boundaries and beams illustrated in Figure 3.30. The curves give the outline of the geometry and the surface is initially made up of a boundary layer. However for this study the boundary layer was constrained by nodes at locations in purple, these are the areas where data was extracted for both FLD and FOD predictions. The relevant thickness is assigned to the collapsed surface and mesh. The last step is to incorporate the runner or sprue system using the beam tool.

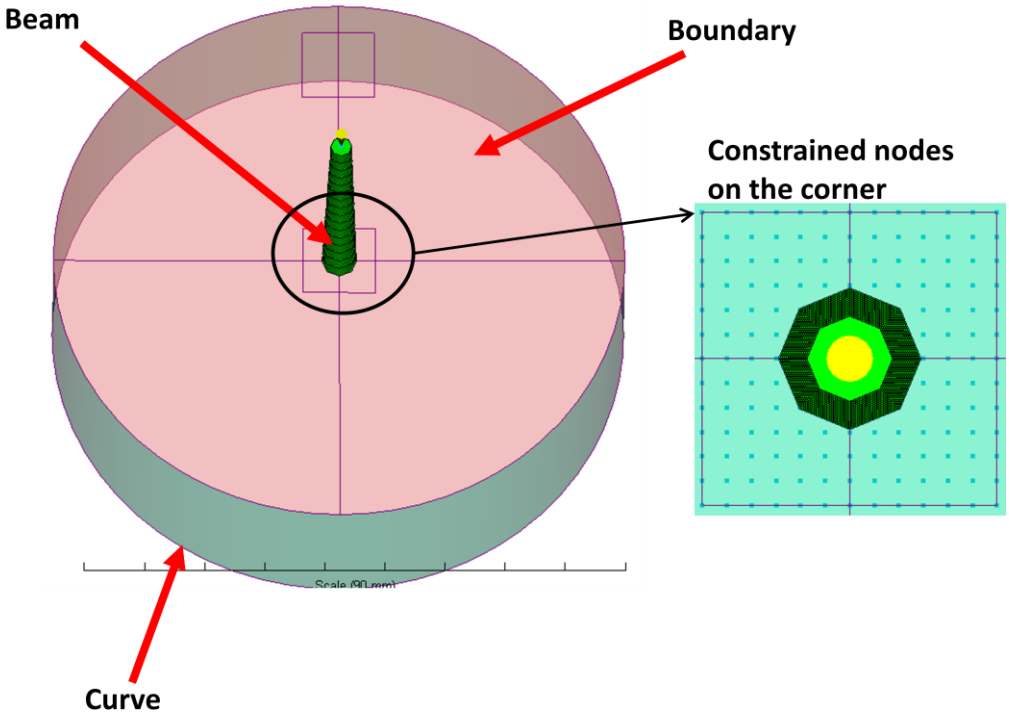

Figure 3.30 Components of a mid-plane model created in ASMI 2014

3.4.1.2 Mesh

The geometry is broken down into a mesh consisting of triangular elements before any analysis is carried out within ASMI 2014, example of this is shown in Section 4.3.1 Mesh Study. Each triangular element is described by a list of 3 nodes numbers which lie upon the element vertices.

In ASMI 2014 the meshing process is semi -automated and requires small amounts of user input, more information on the mesh solvers can be found in Section 2.6.2 Geometric Solutions. To generate a 2-d mesh a reasonable global edge length (mesh density) and the number of laminae (number of layers through thickness) are set. The global edge length is important as it determines the average length of each edge within a triangular element. As the global edge length decreases the mesh gets finer in theory this should enhance the prediction results. The laminae (normalized thickness) are invisible layers which spilt across the part thickness (z-axis). The relative accuracy and the number of data points across the thickness increase as the number of laminae increase. The normalized coordinates of grid points are listed in (Figure 3.31) for 20 laminae. The normalized thickness zero is at the centre line and 1 is at the wall of the thickness.

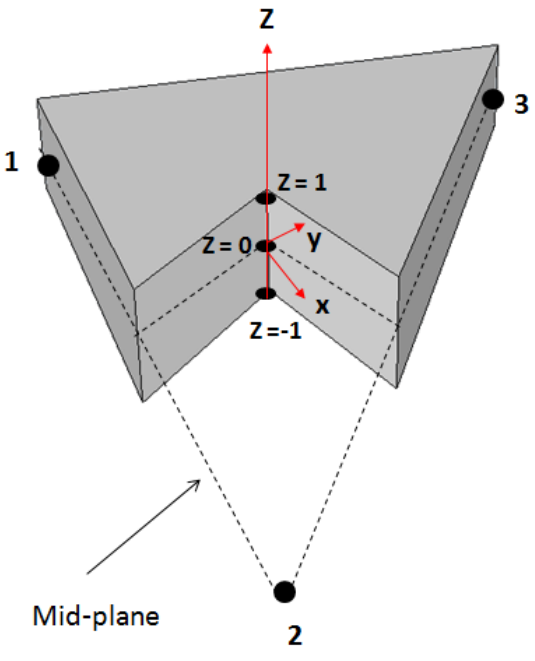

20 Laminae
1.000
0.938
0.864
0.779
0.685
0.583
0.474
0.36
0.243
0.123
0.000
0.123
0.243
0.360
0.474
0.583
0.685
0.779
0.864
0.938
1.000

Figure 3.31 Schematic of normalized thickness and grid points

Once the mesh is created the software shows the amount of triangular elements the model consists of; more elements increase the complexity of the model and more calculations are processed by ASMI 2014. To evaluate the effect edge length has on the prediction a review of 3 mesh densities were carried out on the mid-plane model of the centre gate disc examined edge lengths include; 0.5 mm, 1 mm and 2 mm. A comparison of the mesh densities is found in Section 4.3.1 Mesh Study.

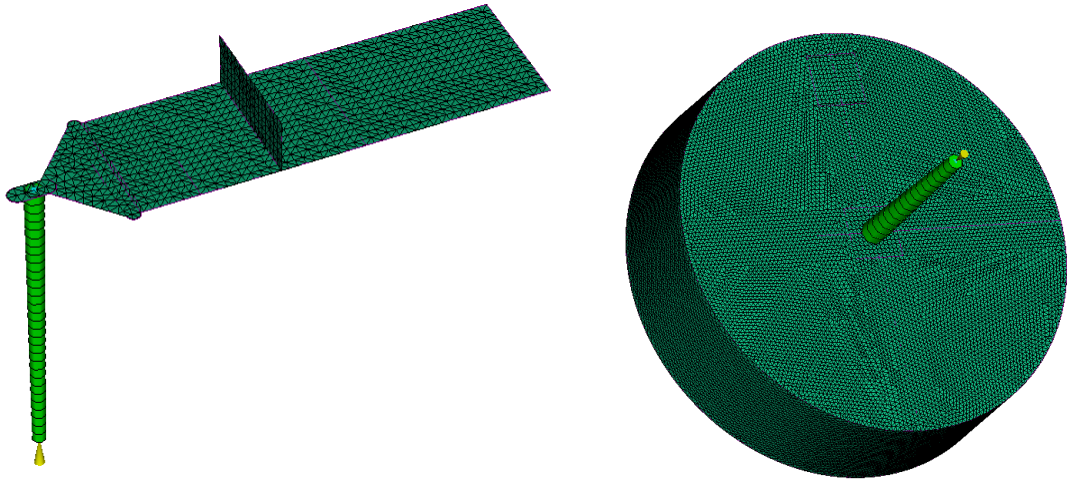

(a) **(b)**

Figure 3.32 (a) 2-d geometry of the 4 mm ribbed plaque (b) 2-d geometry of the 2 mm centre gate.

Each model consists of a single or multiple injection point. This is where the polymer injection would take place during the moulding process. Next the analysis sequence is selected to get the necessary output. This sequence mimics the injection moulding process, where the important stages of injection and packing occur. The manufacturer and grade of material is selected from the material database. The process settings allow the user to configure the injection moulding parameters, consisting of machine limitations and melt /mould surface temperature. The injection time, pressure settings and other variables are specified according to machine setting. Any changes to the fibre solver parameters are made through the settings, there is an option to select and change the variables within various models.

3.4.2 Extracting Predicted FOD

There are different means to extract the FOD prediction for the 2-d geometry. The "settings" fibre solver parameters allow users to change coefficients within the model. There is an option available to toggle between the FOD in the preferred axial direction. The option allows users to view the fibre orientation distribution in the various tensor components i.e. XX, YY, ZZ. This tool will be of an advantage to compare the FOD in the same axial direction as the experimental data.

3.4.2.1 Prediction Models and Coefficients

The SGF FOD prediction models (FT, MFT and RSC) and the long glass fibre prediction models (ARD -RSC and fibre breakage) are dependent on user defined coefficients. Each model has default coefficients defined by Moldflow. Many coefficients were assessed to understand the effect each coefficient has on the prediction and to find the best possible combination for each model.

3.4.2.1.1 Folgar Tucker Model

Reference to Equation 2.13 the FT model, when the value of $D_z = 1$ the model is dependent on the parameter $C_{i.}$ Table 3.9 contains the various input parameters into the FT model.

Model	C_I
1	0.1
2	0.01
3	0.001
4	0.0001
5	0.00001

Table 3.9 Input parameters FT model

3.4.2.1.2 Modified Folgar Tucker Model

Reference to Equation 2.15 the MFT model is dependent on both the D_z and C_i parameters. Table 3.10 contains the various input parameters into the MFT model.

Model	D_Z	C_i	Model	D_Z	C_i
1	0.8	0.1	11	0.4	0.1
2	0.8	0.01	12	0.4	0.01
3	0.8	0.001	13	0.4	0.001
4	0.8	0.0001	14	0.4	0.0001
5	0.8	0.00001	15	0.4	0.00001
6	0.6	0.1	16	0.2	0.1
7	0.6	0.01	17	0.2	0.01
8	0.6	0.001	18	0.2	0.001
9	0.6	0.0001	19	0.2	0.0001
10	0.6	0.00001	20	0.2	0.00001

Table 3.10 Input parameters MFT model

3.4.2.1.3 RSC Model

Reference to Equation 2.16 the RSC model is dependent on both the K and C_i parameters. Table 3.11 contains the various input parameters into the RSC model.

Model	K	C_i	Model	K	C_i	Model	K	C_i
1	0.8	0.1	21	0.1	0.1	41	0.00001	0.1
2	0.8	0.01	22	0.1	0.01	42	0.00001	0.01
3	0.8	0.001	23	0.1	0.001	43	0.00001	0.001
4	0.8	0.0001	24	0.1	0.0001	44	0.00001	0.0001
5	0.8	0.00001	25	0.1	0.00001	45	0.00001	0.00001
6	0.6	0.1	26	0.01	0.1			
7	0.6	0.01	27	0.01	0.01			
8	0.6	0.001	28	0.01	0.001			
9	0.6	0.0001	29	0.01	0.0001			
10	0.6	0.00001	30	0.01	0.00001			
11	0.4	0.1	31	0.001	0.1			
12	0.4	0.01	32	0.001	0.01			
13	0.4	0.001	33	0.001	0.001			
14	0.4	0.0001	34	0.001	0.0001			
15	0.4	0.00001	35	0.001	0.00001			
16	0.2	0.1	36	0.0001	0.1			
17	0.2	0.01	37	0.0001	0.01			
18	0.2	0.001	38	0.0001	0.001			
19	0.2	0.0001	39	0.0001	0.0001			
20	0.2	0.00001	40	0.0001	0.00001			

Table 3.11 Input parameter RSC model

3.4.2.1.4 ARD-RSC Model

Reference to 2.19 the ARD-RSC model is dependent on both the K factor and the 5 scalar parameters. The 5 scalar parameters are set at default values and the various K parameters input into the ARD-RSC model are in Table 3.12.

Model	K	Model	K
1	0.01	5	0.6
2	0.05	6	0.8
3	0.2	7	1.0
4	0.4		

Table 3.12 Input parameters ARD-RSC model

3.4.2.2 Translation of data

Data for FOD 2-d analysis are output in the form of patran (.ele) text file for each cavity laminate (normalized thickness) within each element. The files are simple data files containing element number and the five independent orientation tensor components for each element in the model. The orientation from the files is not ready for processing immediately as it requires some conversion in excel. The average tensor component for each element is converted into an ellipse to describe the orientation angle over a given position. The definition of orientation is found in Section 3.2.3.1 Orientation Calculation. This process is repeated for the selected elements through the laminate thickness (Figure 3.33). This process is made easier using a macro which repeats each step for each laminate.

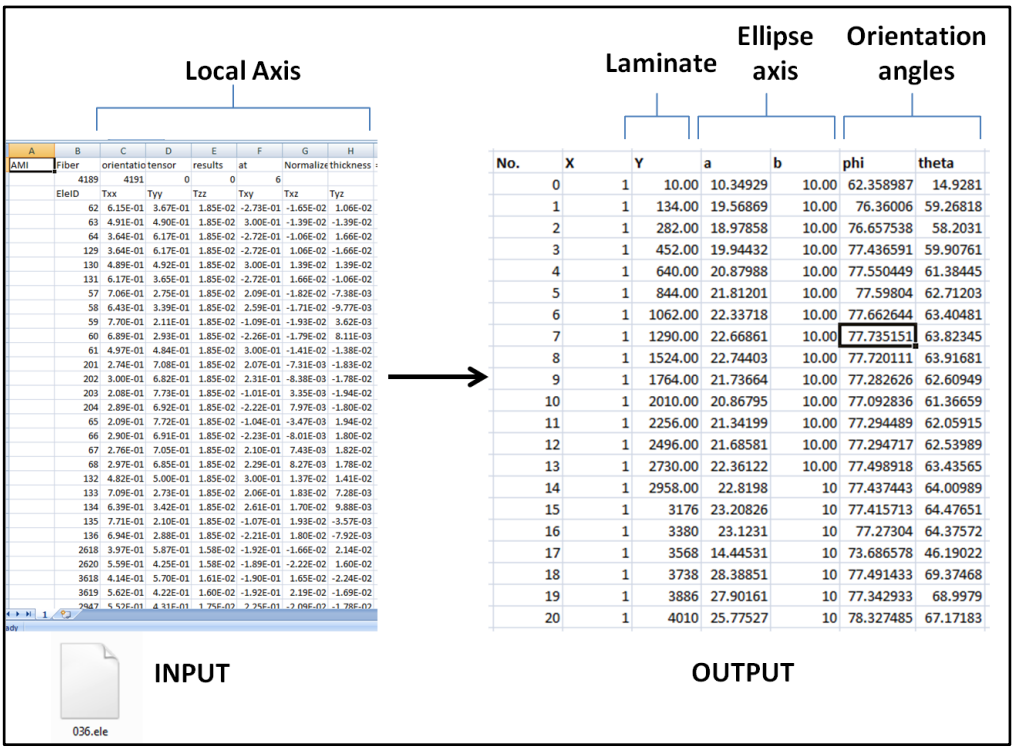

No.	X	Y	a	b	phi	theta
0	1	10.00	10.34929	10.00	62.358987	14.9281
1	1	134.00	19.56869	10.00	76.36006	59.26818
2	1	282.00	18.97858	10.00	76.657538	58.2031
3	1	452.00	19.94432	10.00	77.436591	59.90761
4	1	640.00	20.87988	10.00	77.550449	61.38445
5	1	844.00	21.81201	10.00	77.59804	62.71203
6	1	1062.00	22.33718	10.00	77.662644	63.40481
7	1	1290.00	22.66861	10.00	77.735151	63.82345
8	1	1524.00	22.74403	10.00	77.720111	63.91681
9	1	1764.00	21.73664	10.00	77.282626	62.60949
10	1	2010.00	20.86795	10.00	77.092836	61.36659
11	1	2256.00	21.34199	10.00	77.294489	62.05915
12	1	2496.00	21.68581	10.00	77.294717	62.53989
13	1	2730.00	22.36122	10.00	77.498918	63.43565
14	1	2958.00	22.8198	10	77.437443	64.00989
15	1	3176	23.20826	10	77.415713	64.47651
16	1	3380	23.1231	10	77.27304	64.37572
17	1	3568	14.44531	10	73.686578	46.19022
18	1	3738	28.38851	10	77.491433	69.37468
19	1	3886	27.90161	10	77.342933	68.9979
20	1	4010	25.77527	10	78.327485	67.17183

Figure 3.33 Conversion of predicted orientation from Moldflow to defined orientation angles for specified elements

Converting the average orientation tensors into orientation angles and ellipses means the data can be processed through "ANALYSE". This software was used to process the measured data from the fibre orientation distribution image analysis. The software calculates the orientation tensors and converts this

information into relevant plots, more information on how the software functions is found in Section 3.2.3.2 ANALYSE

3.4.3 Extracting Predicted FLD

3.4.3.1 Breakage Model

Referencing equation 2.20, the breakage model is dependent on 3 scalar parameters: C_b, D_g and S. The default values of each parameter as follow C_b = 0.002, D_g = 3 and S = 0.25. For this study the coefficients remain at default for all fibre breakage predictions. The effect each coefficient has on the prediction remains an area for further study.

The fibre breakage model is able to determine the fibre breakage, when a long glass fibre material datasheet is incorporated into ASMI 2014. The initial fibre length and aspect ratio values are input into the datasheet if they are not already present. The model gives the user the flexibility to change the fibre length distribution at inlet. The default settings run the model with the initial 12 mm long pellet length. However, in this study FLD measurements are taken from the extrudate, sprue and at two locations from the cavity. The FLD measurements taken from the sprue and extrudate are input into the fibre breakage model as part of the initial inlet setup. Table 3.13 shows an example of the measured FLD, taken from the 3 mm nozzle extrudate (refer to Section 3.1.3.2 Modifications) and input into AMSI. A comparison is made between the predicted breakage and the measured fibre length in the cavity.

Number	Length	Distribution (%)	Number	Length	Distribution (%)
1	0	0	15	6.75	1.17
2	0.25	7.98	16	7.25	1.11
3	0.75	19.36	17	7.75	0.92
4	1.25	21.63	18	8.25	0.71
5	1.75	11.69	19	8.75	0.84
6	2.25	7.26	20	9.25	1.14
7	2.75	4.93	21	9.75	0.85
8	3.25	4.26	22	10.25	0.64
9	3.75	3.28	23	10.75	0.7
10	4.25	2.79	24	11.25	0.64
11	4.75	2.15	25	11.75	0.47
12	5.25	1.69	26	12.25	0.69
13	5.75	1.57	27	12.75	0.32
14	6.25	1.23			

Table 3.13 Example of measured LGF extrudate FLD input into ASMI 2014

It is possible to output the overall FLD prediction through the thickness at any area. If the fibre length distribution is required over a given area, individual sets of data (15 nodes per dataset) are taken into excel and an average is taken over each node (Figure 3.34).

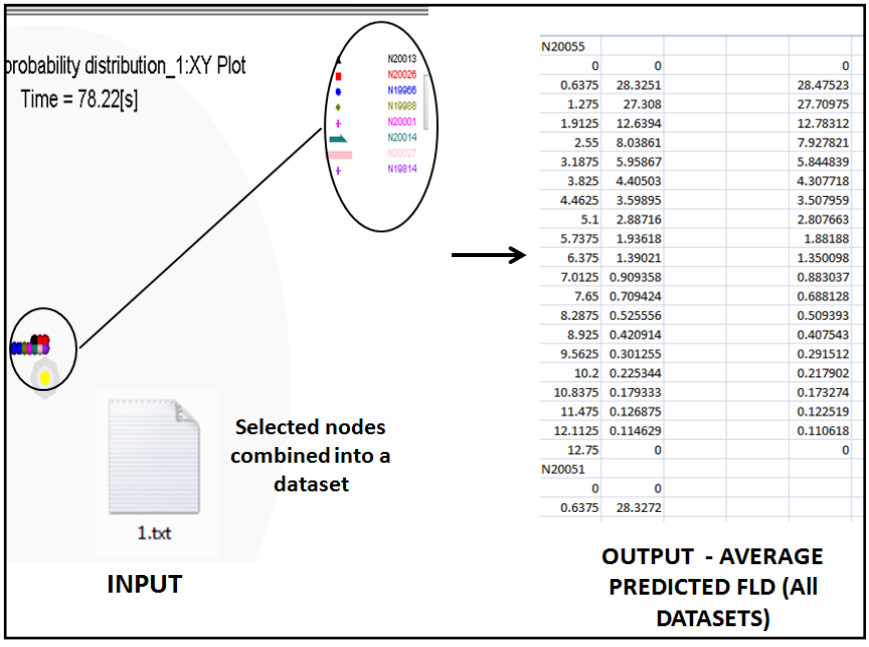

Figure 3.34 A group of nodes selected for FLD data extraction

3.4.4 Representation of Data

There are different ways of presenting the FOD and FLD data, this section introduces the techniques which will be adopted into the results chapter.

3.4.4.1 Fibre Orientation Distribution

A contour plot can indicate results using either greyscale or a range of colours, however sometimes the data can be presented more clearly through X-Y plots (Figure 3.35). The X-Y plot illustrates position through sample thickness versus average fibre orientation. It is more practical if the X-Y plot is in one direction and through a section as this will clearly illustrate levels of orientation through the part.

A typical FOD X-Y plot consists of three regions skin, shell and core. In the shell layer the average orientation of fibres is parallel to the direction of flow, the core is identified as $\cos^2\theta$ below 0.5, fibres oriented random in plane, and fibres at the skin layer have a marginally lower $\cos^2\theta$ compared to the shell layer (Bay and Tucker, 1992). Each layer is easily distinguished for example the markings above the graph in Figure 3.35 show where each layer starts and finishes, the thickness of each layer as follows; 0.35 mm thick skin layer, 1.1 mm thick shell layer and 1 mm thick core layer for a 4 mm thick plate.

Results from a number of experiments or simulation prediction are plot on to the same set of axis. The disadvantage of using this method to display FOD data is that it can only illustrate the average distribution across a section of elements in a defined area.

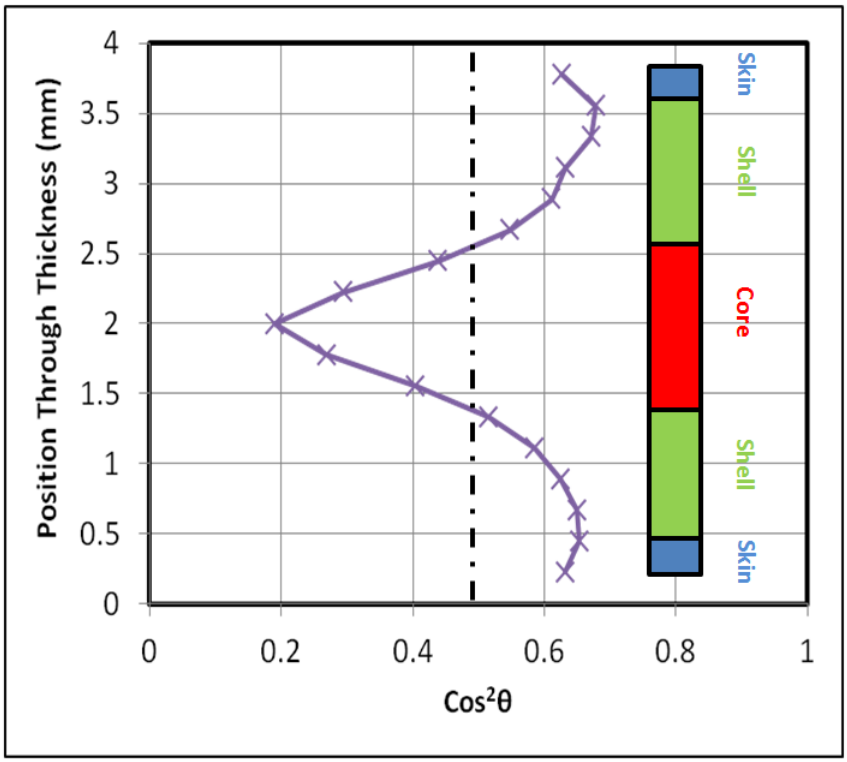

Figure 3.35 Example of a typical average X-Y FOD plot through the thickness

3.4.4.2 Fibre Length Distribution

The FLD data is presented using distribution plots fibre length distribution in % against the fibre length in mm (Figure 3.36). It is possible to have number of results on the same plot from both measured and predicted data. It is good practice to adopt the same frequency intervals (bins) to get a good comparison between the measured and predicted.

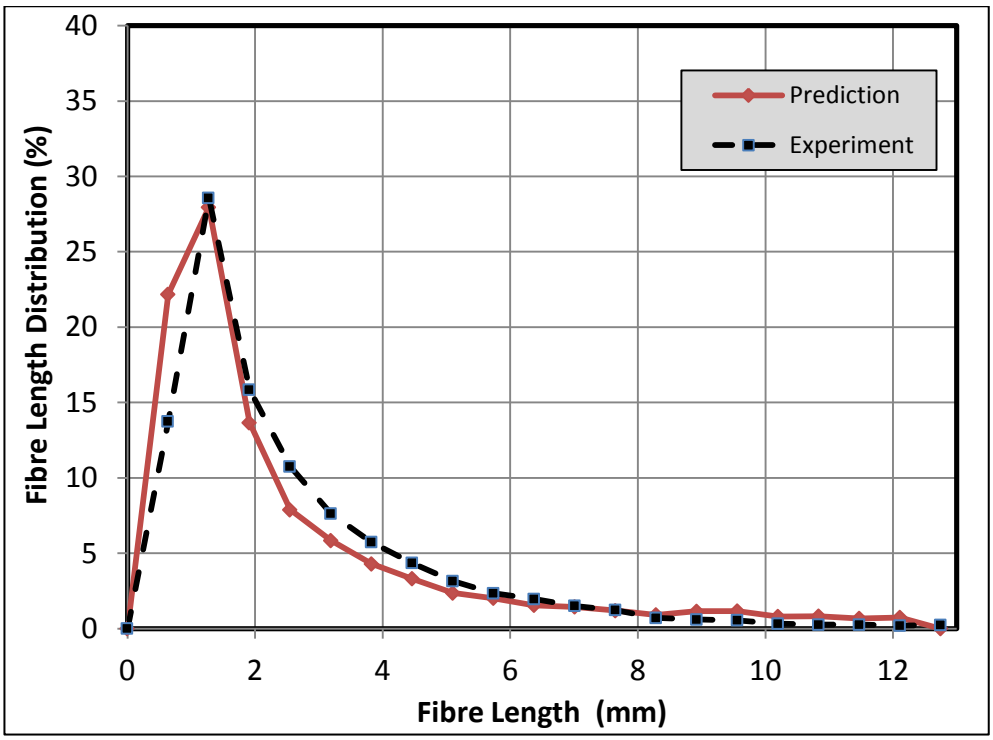

Figure 3.36 Example of the FLD distribution plot

3.5 Summary

This chapter outlines the material, experimental and simulation techniques which are part of this study. This study will focus on injection moulded fan gate and centre-gate SGF PA6 and LGF PP centre gate geometry with alternate dimensions. Clear guidelines were given by SABIC® to process the LGF STAMAX material. For this study the FOD analysis on LGF and SGF components was carried out on a recognized system available at the University of Leeds. The samples were prepared using polishing techniques before they were analysed using the optical reflective microscopy. Fibre length analysis was carried out on the LGF raw material, extrudate and components. Fibre length measurements were carried out using a semi-automatic system, where straight fibres were measured using an in-house algorithm but curved fibres were measured manually.

The 2-d geometry solutions were created to evaluate the fibre orientation and breakage models in ASMI 2014. Geometries with different thickness are

investigated to get a good overview of the limitations for each fibre prediction. To evaluate a model the correct measured data is required; this data is easily obtained using the measurement procedures in this chapter. The models under investigation include the fibre breakage, short glass fibre (FT, MFT and the RSC) and the ARD-RSC long glass fibre orientation more information on these is found in Section 2.7 Fibre Prediction Model. The measured FOD and FLD data is vital to assess the accuracy and limitations of the fibre prediction models, including observation of essential coefficients which can influence the prediction.

Chapter 4 Short Glass Fibre Results

4.1 Introduction

The work carried out in this study was a continuation of previous collaborative research carried out by Whiteside, (2001) and Hine et al., (2004 and 2005). Initial investigation was carried out on the injection moulded 4 mm thick ribbed plaque fan gate geometry by Whiteside, (2001). At a later stage Hine et al., (2004) examined the 2 mm thick fan gate geometry to study the FOD within a thick plaque. The measured data for the 2 mm and 4 mm end-gate geometries was inherited from these studies. A previous study carried out by Bubb, 2001 suggests there is an image analysis measurement error of $\pm$ 0.02 for any second order orientation tensor. His study was carried out using the same measurement technique while investigating SGF 2 mm and 4 mm thick plaques. The measured SGF FOD for the 2 mm thick plaque and the 1 mm thick centre gate geometry is currently being used to validate the ASMI 2014 fibre prediction models for both 2-d and 3-d solvers. Through the current and next chapter constant mention is made to the skin, shell and core layers within the FOD distribution plots. Definition of each layer is given in the previous chapter Section 3.4.4.1 Fibre Orientation Distribution.

4.1.1 Fan Gate

The classical Folgar-Tucker (FT), modified FT and RSC models have been applied to the 2 mm and 4 mm plates in mid-plane analyses, enhanced solutions were found for individual models by comparing fibre orientation distribution at locations A (16.5 mm from flow path) and B (67 mm from flow path) shown below in Figure 4.1.

Various D_z (significance of the randomizing coefficient) and (coefficient of interaction) C_i values are examined for both the classic/modified Folgar-Tucker (2.13 and 2.15) shell model. The findings from the 2 mm plate were then used

to tailor the solutions for the different thickness and geometries. The examined parameters are specified in Section 3.4.2 Extracting Predicted FOD.

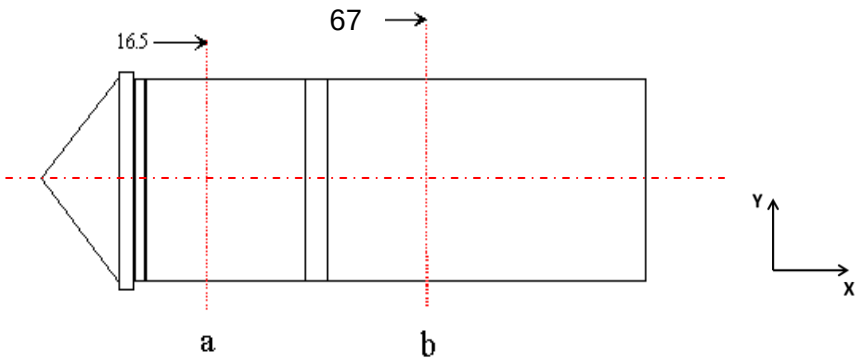

Figure 4.1 Diagram showing experiment locations A and B for end gate geometries

Figure 4.2 illustrates the filling pattern within thin and thick fan gate geometries. Within the thin geometry polymer enters from the sprue and the flow expands through the part. This type of shear flow (through the thickness) usually creates a skin/shell/core formation where the fibres at the skin and shell are aligned in the direction of polymer flow and the fibres at the mid-plane align perpendicular to the direction of flow. Previous research carried out by Tucker, (2013) and Whiteside, (2001) confirms that an expansion flow comes in through the gate within a thick plaque.

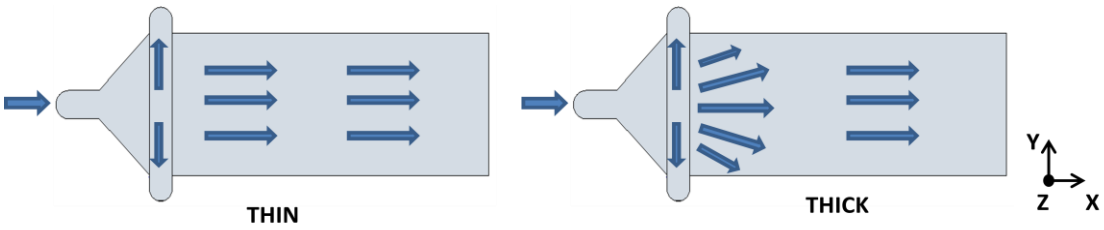

Figure 4.2 Diagram showing flow of polymer through thin and thick fan gate geometry

4.1.2 Centre Gate

The classical Folgar-Tucker (FT), modified FT and RSC models have been applied to the 1, 2 and 4 mm thick base centre gate geometries in mid-plane analyses, enhanced solutions were found for individual models by comparing fibre orientation distribution from location 3 locations along the radial flow path.

They are shown below in Figure 4.3; Location A (16 mm from the sprue); B (25 mm from the sprue); and C (36 mm from the sprue).

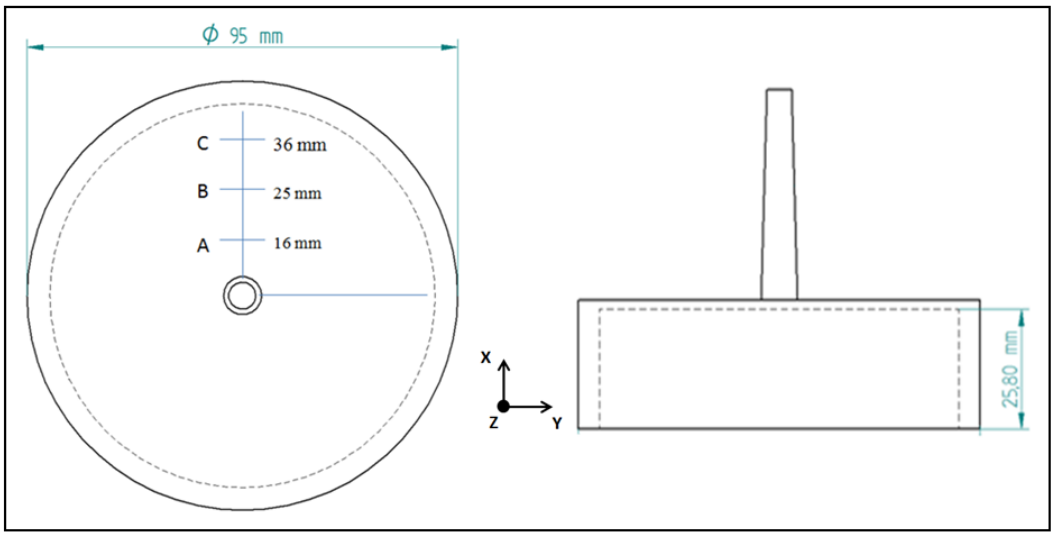

Figure 4.3 Diagram showing experiment locations A, B and C for centre gate

The filling pattern through the centre gate geometry during injection moulding is observed in Figure 4.4. The short shots show the polymer melt comes through the sprue located in the centre and fills the cavity in a radial form. This creates significant in-plane stretching at the base, which causes the fibres at the core to align in the principal stretching direction (Bay and Tucker, 1992). The gap-wise shearing causes the fibres at the shell to align in the direction of flow.

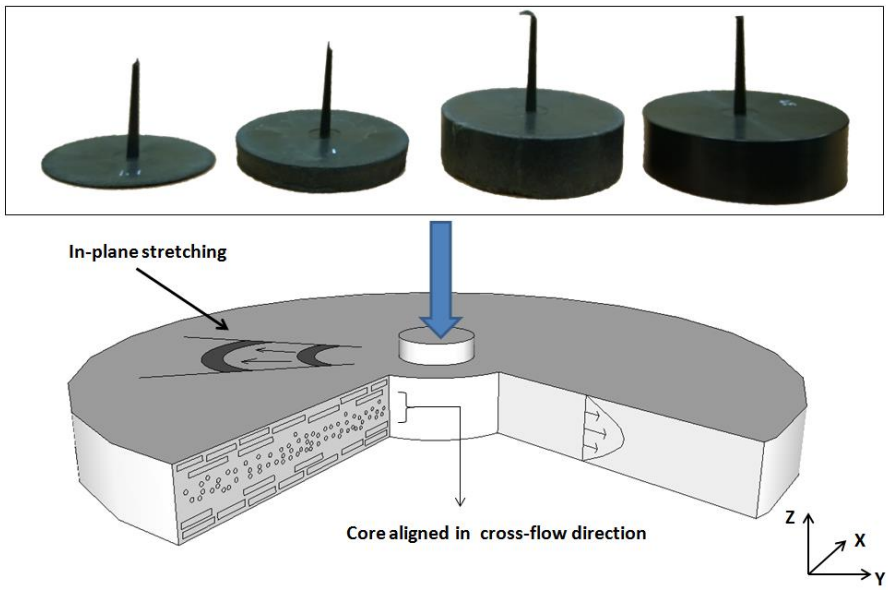

Figure 4.4 Filling and orientation pattern of centre gate geometry

4.2 Experiment

4.2.1 2 mm Thick Plate Measured

The FOD distribution does not change drastically at the skin and shell within the 2 mm end geometry as shown between location A and B in Figure 4.5. At location A the width of the core is 0.3 mm. However there is a change in the average orientation ($\cos^2\theta$) at the core further on in the flow (location B). There is no apparent core at location B; hence the value of $\cos^2\theta$ does not go below 0.5. The change within the core is clear in the contour plots in Figure 4.6, where 1.0 on the scale refers to fibres aligned parallel to the flow and 0 refers to the fibres aligned perpendicular to the flow direction. A discontinuous core is seen in the contour plot for location B, although this is contradicting Figure 4.6 there is a logical argument to explain the difference. The average orientation is taken across the width of each strip and the majority of the middle layer is highly oriented in the direction of flow. As a result the Figure 4.5 is the average orientation across the strip.

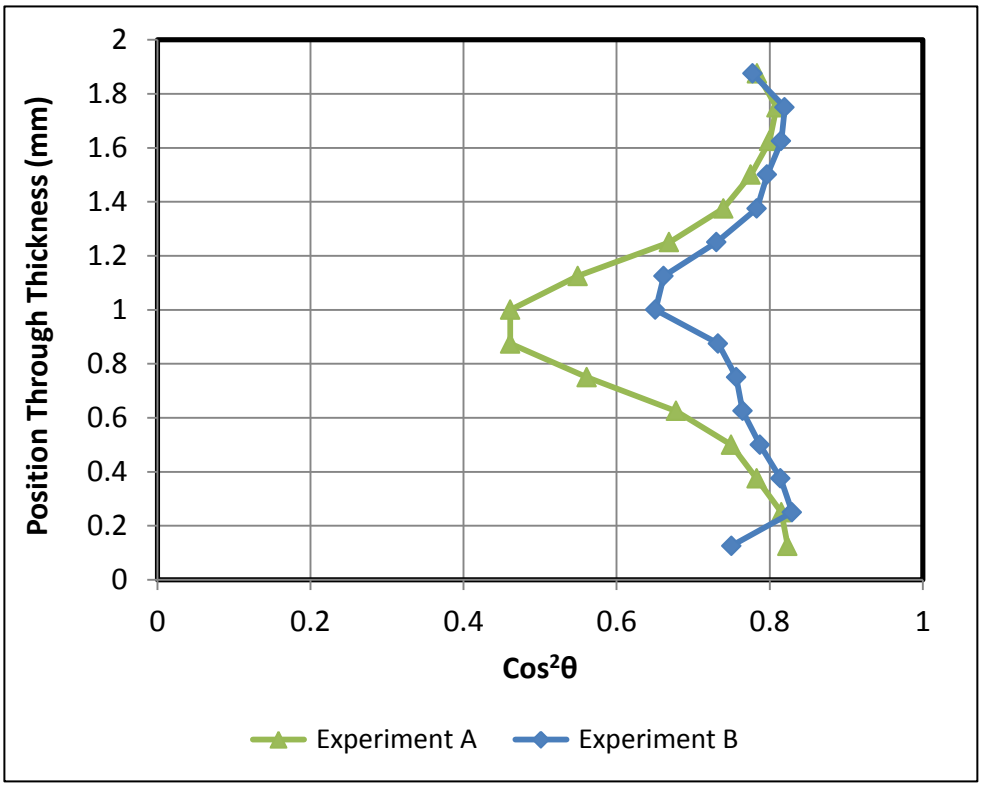

Figure 4.5 Measured average FOD within 2 mm plate at location A and B

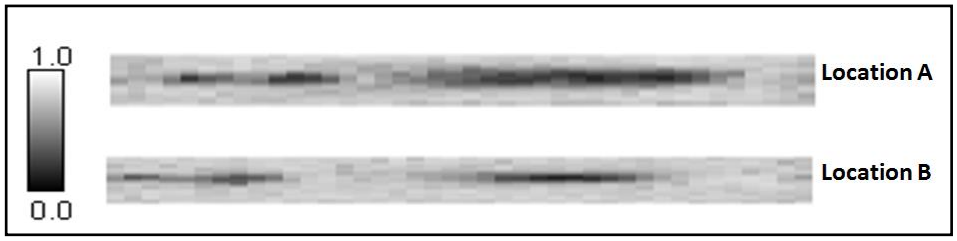

Figure 4.6 Contour plots of 2 mm plate at location A and B

4.2.2 4 mm Thick Ribbed Plate Experiment

The average FOD within the 4 mm plate changes at the skin, shell and core layers from position A to B (Figure 4.7). The fibres in the skin and shell layers become more aligned in the direction of flow at location B, with a $\cos^2\theta$ of 0.65 at the shell layer. This change is clear in the contour plots in Figure 4.8. Although the thickness of the core reduces from 2.20 mm at location A to 1 mm at location B, $\cos^2\theta$ remains at 0.2 where the fibres are aligned transverse to the flow direction.

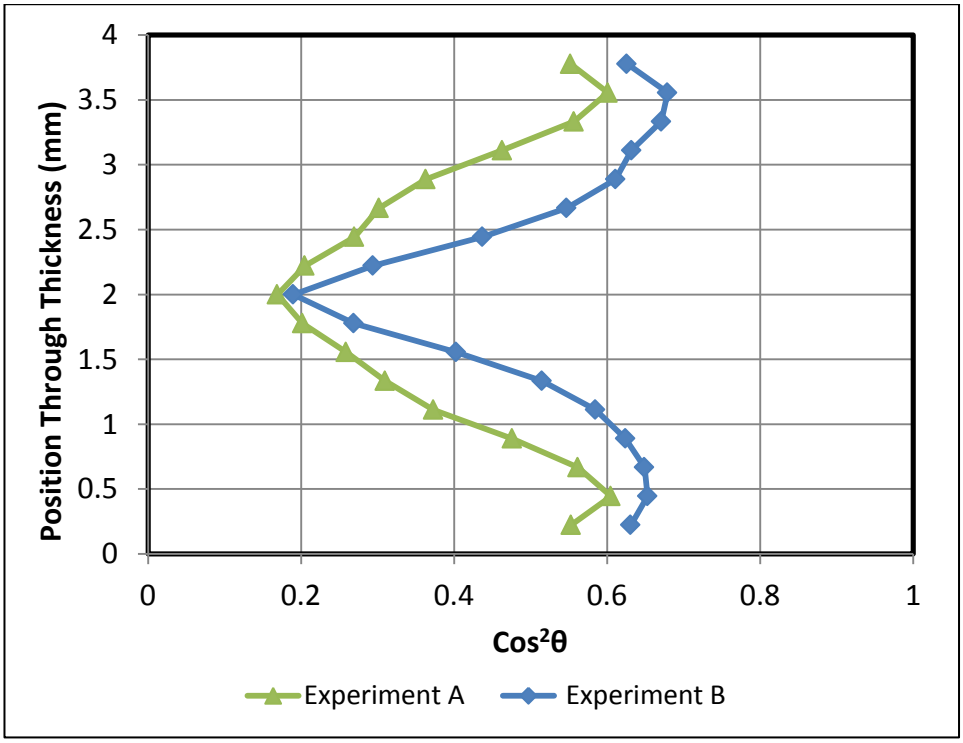

Figure 4.7 Measured average FOD within 4 mm plate at location A and B

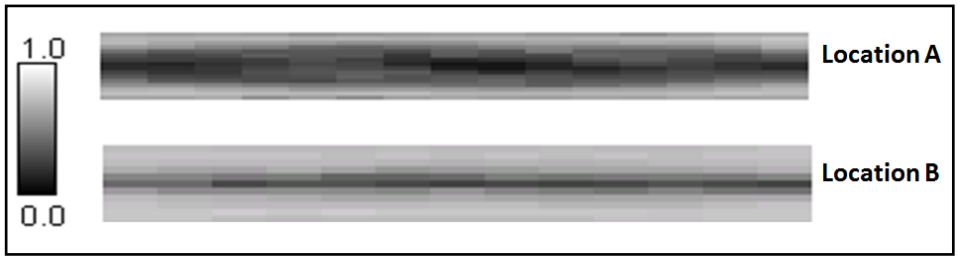

Figure 4.8 Contour plots of 4 mm plate at location A and B

4.2.3 Variation

The FOD will vary from sample to sample therefore it is important to assess the overall relative difference within the centre gate components. Fibre orientation measurements were taken from two 1 mm thick SGF centre gate samples along the same flow path. These tests were carried out on the same batch of injection moulded samples. Figure 4.9 shows the data for both samples at location A, B and C. To increase the data points or variation the FOD through thickness was split over 16 strips. A better comparison can be made between the two samples with more data points. Table 4.1 shows the standard deviation at each location and the average standard deviation.

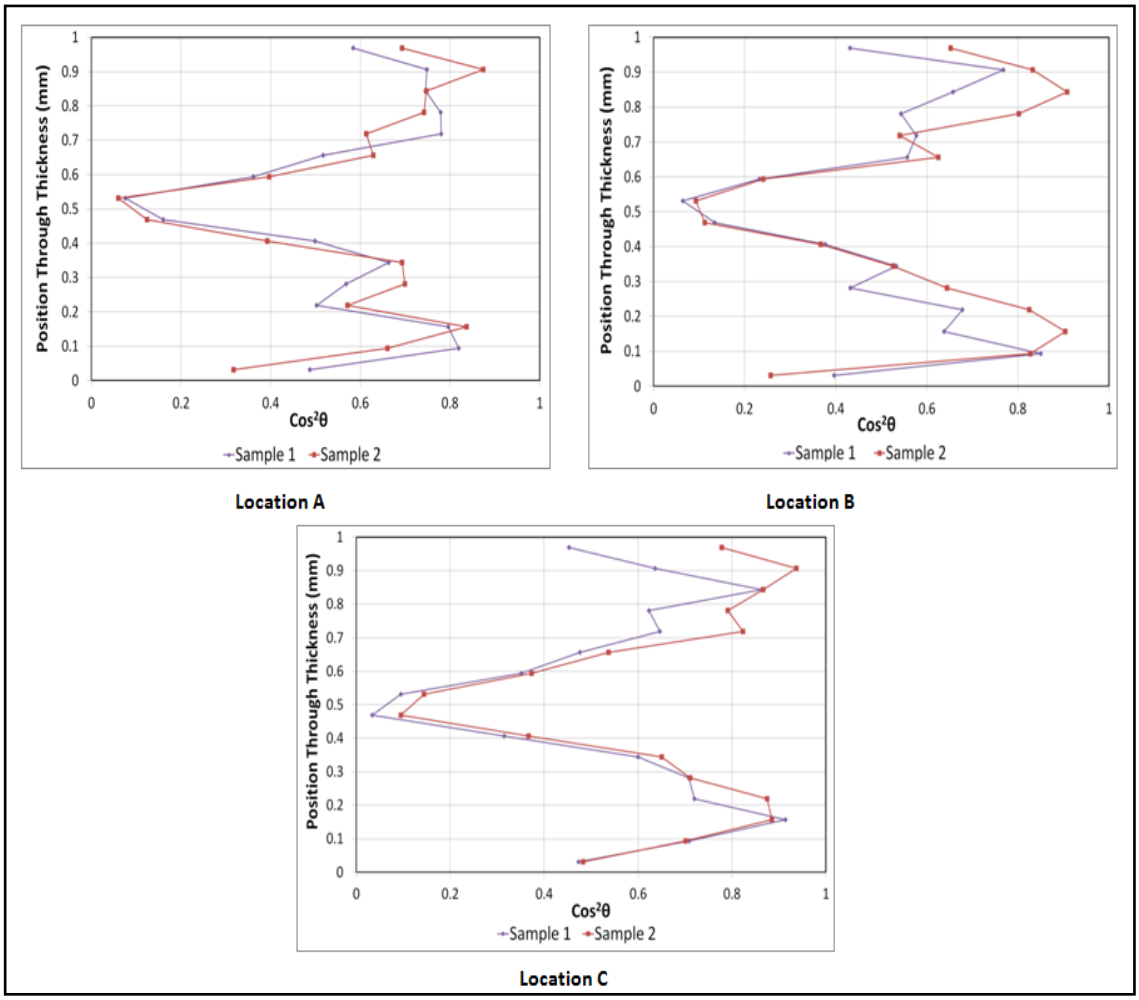

Figure 4.9 The measured average FOD from sample 1 and 2 taken from the SGF 1 mm thick centre gate at location A, B and C

Location A	Location B	Location C	Average
0.06	0.078	0.065	0.068

Table 4.1 Standard deviation between sample 1 and 2 at location A, B and C

A greater variation is found at location B compared to location A and C. The variation at each location occurs within the shell of the sample and the orientation within the core is the same. The increases in variation could be a result of the slight deviation in positioning the sample. The average variation of $\pm$ 0.07 in FOD is small but this includes an error in measurement of $\pm$ 0.02 which is a result of the image analysis system (Bubb, 2001). The remaining $\pm$ 0.05 random variation can be attributed to the variation in the injection moulding process conditions.

The number of strips dictates the random variation seen within the sample. Reducing the number of strips is one method of reducing this random variation. Decreasing the number of strips will average a larger number of fibres. The FOD data for the 1 mm thick centre gate shown at a later stage is spread over 12 strips. The example in Figure 4.10 at location A shows the difference between the FOD spread over 16 strips and 12 strips. Some of the random variation has been removed at the skin but the orientation and width of the core remains the same. The measurements with less variation make a better comparison with the predicted FOD.

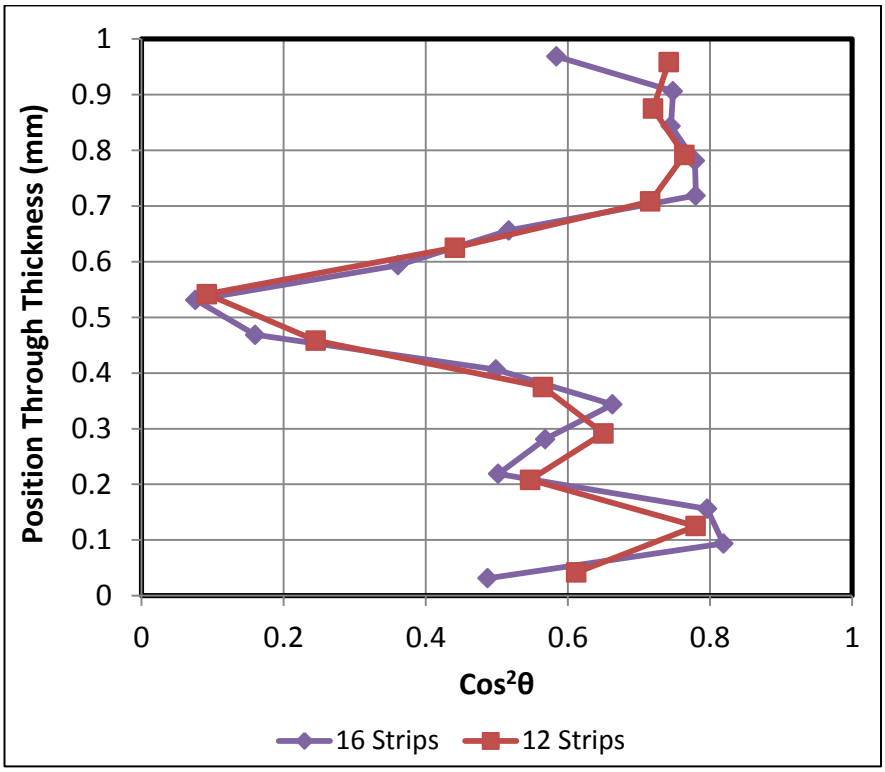

Figure 4.10 The measured average FOD taken over 16 and 12 strips at location A for 1 mm thick centre gate

4.2.4 1 mm Thick Centre Gate Experiment

Polymer fills the thin centre gate cavity at high shear this causes the majority of fibres to align parallel to the direction of flow this is illustrated by average FOD at location C Figure 4.11. As a result of high shear the core represents 1/5 of the total thickness of the sample at locations A, B and C with fibres aligned perpendicular to the flow direction with $\cos^2\theta$ below 0.1. The difference in the thickness of each layer is clearly shown in the contour plots of FOD through thickness in Figure 4.12. The average orientation at location A, B and C is very similar in respect to the $\pm$ 0.07 variation. The effect of in-plane stretching decreases towards the end of the flow path and shearing increases at location C, causing the fibres to align parallel to the direction of flow within the shell layers where $\cos^2\theta$ reaches above 0.8. The orientation at location C within the shell layers is parallel to the direction flow compared to location B this is clearly illustrated in Figure 4.12.

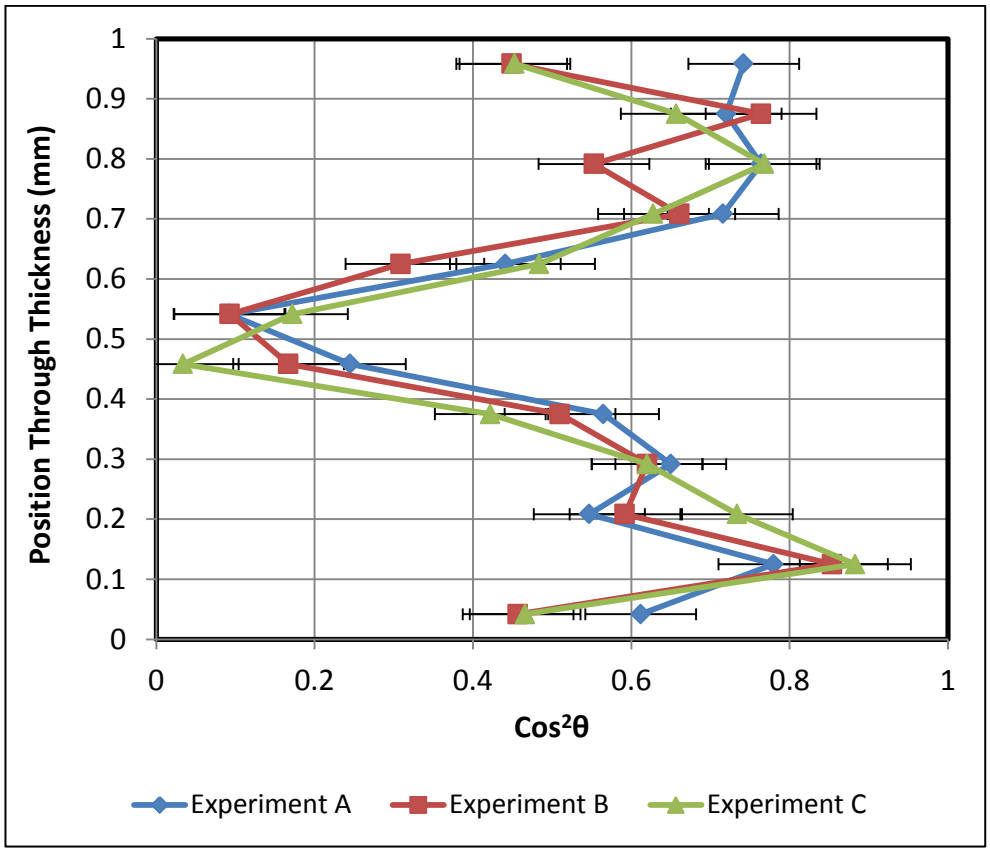

Figure 4.11 Measured average FOD within 1 mm centre gate at location A, B and C

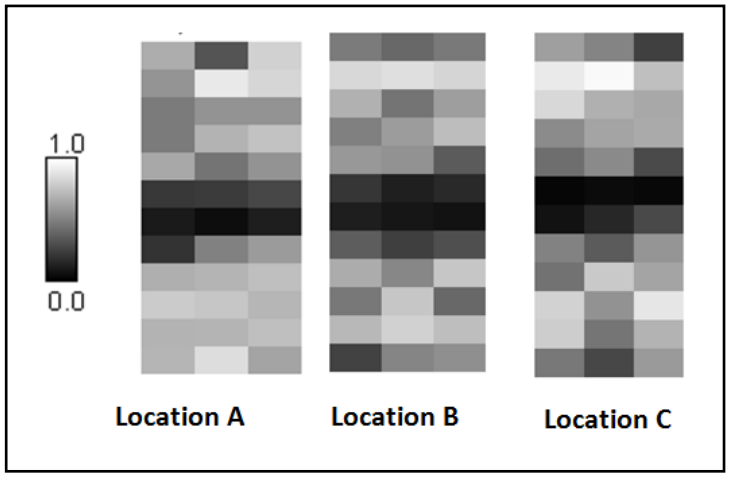

Figure 4.12 Contour plots of 1 mm centre gate at location A, B and C

4.2.5 2 mm Thick Centre Gate Experiment

The average FOD does not vary across the radial path within the 2 mm centre gate geometry Figure 4.13. The average orientation at the skin is between 0.6 - 0.68 and above 0.8 for the shell layer. The only noticeable change is in the width of the core from location B to C. The thickness of the core reduces from 1 mm at location B to a minimum of 0.8 mm at location C, this change is apparent in the contour plot Figure 4.14. Although there is less in-plane stretching towards the end of the flow path the $\cos^2\theta$ of the fibres at the core for all locations still remains below 0.1.

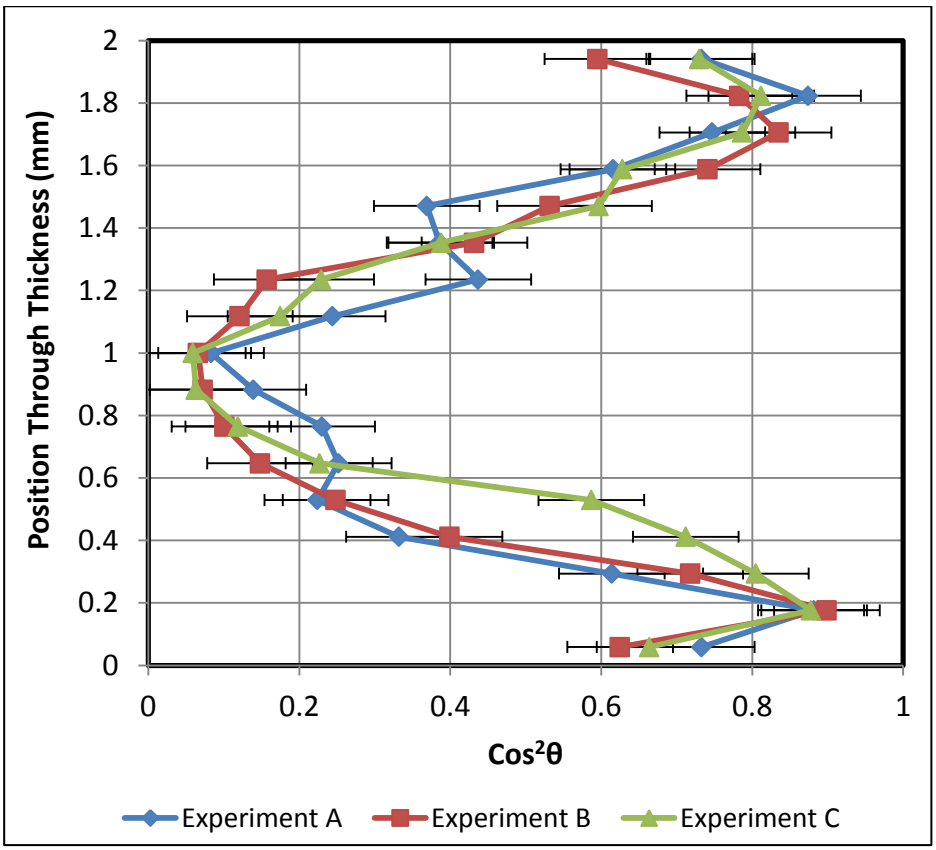

Figure 4.13 Measured average FOD within 2 mm centre gate at location A, B and C

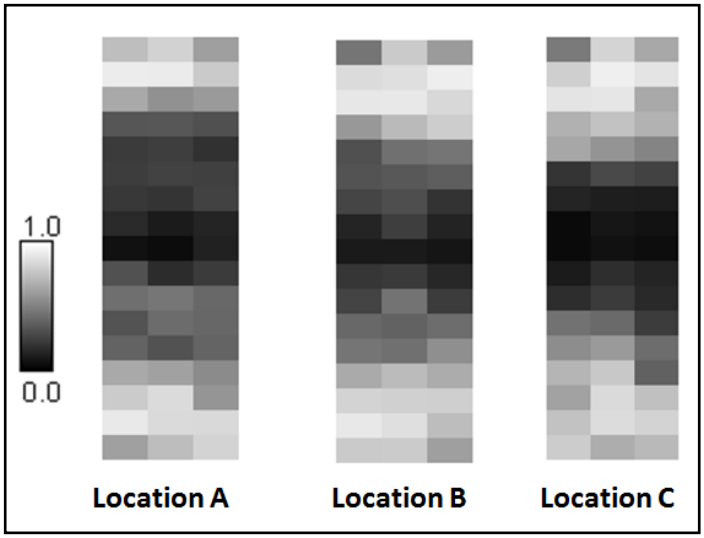

Figure 4.14 Contour plots of 2 mm centre gate at location A, B and C

4.2.6 4 mm Thick Centre Gate Experiment

In Figure 4.15 there is a similar trend in the average FOD through the radial flow path (locations A, B and C) within the 4 mm thick centre gate. The core represents 3 mm of the overall thickness of the sample, as a result the skin and

shell layers are thin with fibres aligned parallel to the flow direction with $\cos^2\theta$ above 0.7. At all locations the fibres are oriented perpendicular to the direction of flow with a $\cos^2\theta$ of below 0.2. The large area representing the highly transverse core is clearly illustrated in the contour plots in Figure 4.16.

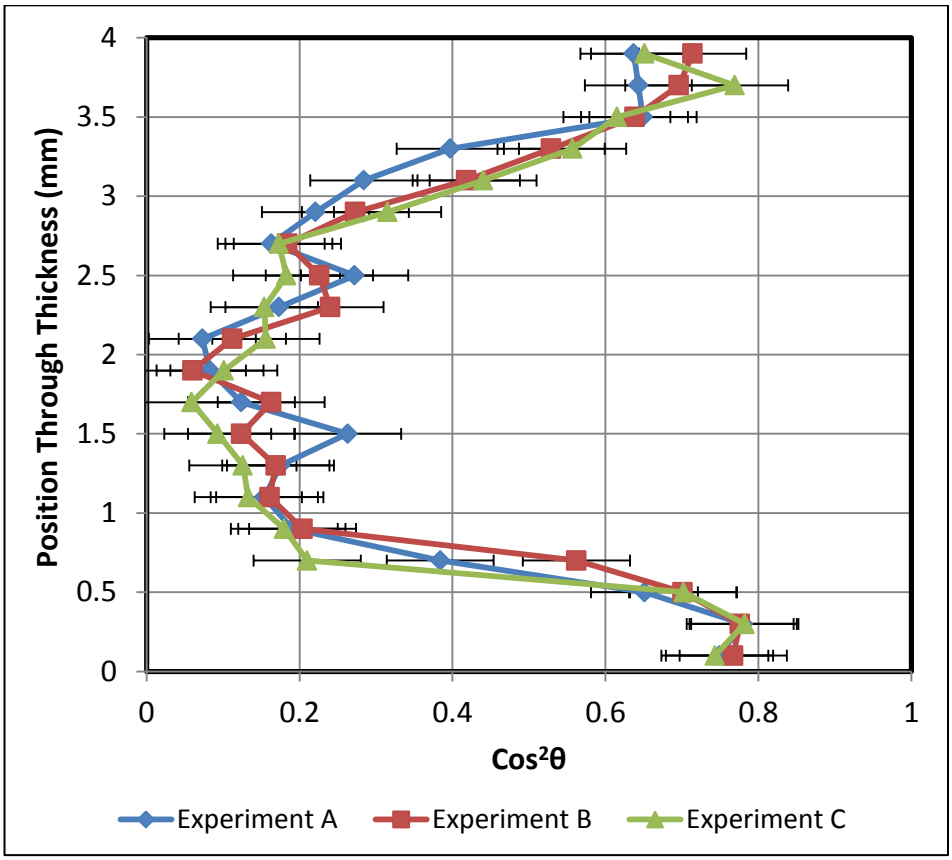

Figure 4.15 Measured average FOD within 4 mm centre gate at location A, B and C

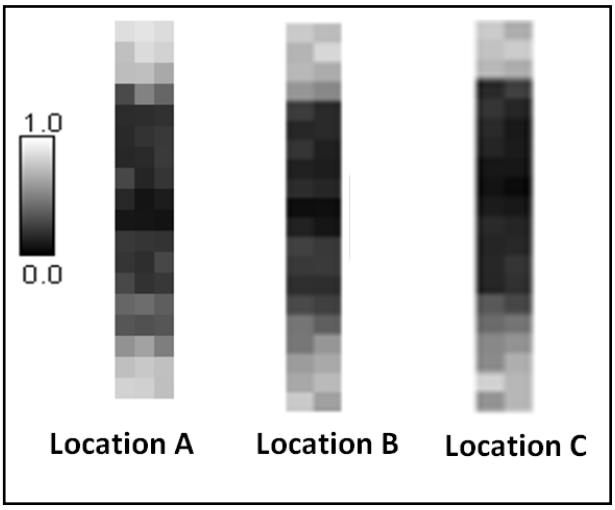

Figure 4.16 Contour plots of 4 mm centre gate at location A, B and C

4.2.7 Evaluation

It is apparent from Figure 4.5 to Figure 4.16 that the average FOD varies with thickness and geometry. Comparison is made between some data sets to investigate these changes.

4.2.7.1 Influence of Geometry Thickness

4.2.7.1.1 Fan-gate

To examine the difference in average FOD within the fan gate geometries, as a result of thickness a comparison is made between data sets, the 2 mm and 4 mm thick plaques in Figure 4.17 and Figure 4.18. As the thickness of the geometry increases, $\cos^2\theta$ decreases at the skin and shell layers. For example the alignment at the skin and shell reduces to around 0.65 and 0.62 in the 4 mm plaque compared to 0.79 and 0.81 in the 2 mm geometry at location B. At location A there is a 1.90 mm difference between the core width of the 2 mm and 4 mm geometries. The core is aligned perpendicular to the direction of flow with a $\cos^2\theta$ of 0.2 for the 4 mm plaque, compared to a potential random orientation within the core of the 2 mm plaque. However at location B there no core observed for the 2 mm plaque compared to the 1 mm thick transverse core observed for the 4 mm plaque.

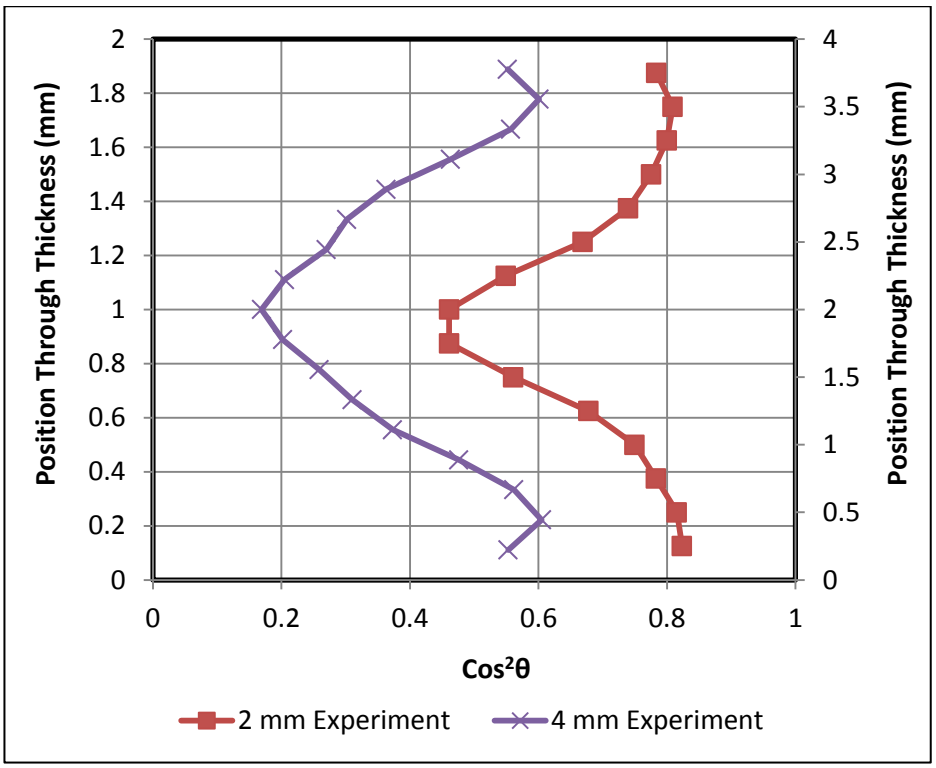

Figure 4.17 Measured average FOD 2 mm and 4 mm plates at location A

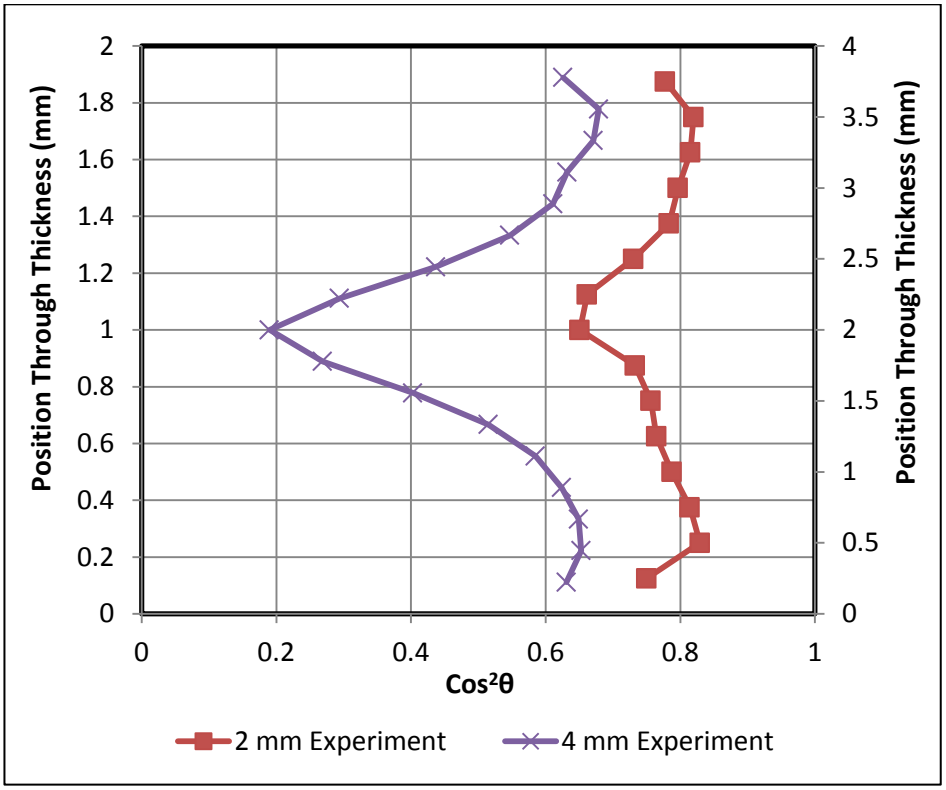

Figure 4.18 Measured average FOD 2 mm and 4 mm plates at location B

4.2.7.1.2 Centre Gate

The difference in the average FOD within the 1 mm, 2 mm and 4 mm centre gate geometries at location B is shown in Figure 4.19. The average FOD at the shell layer and skin layer is similar for all three geometries. However there is a significant change within the width of the core, which increases with increasing thickness. Figure 4.19 represents the core width as a percentage of the actual width in mm. Without taking the variation into consideration the actual core width for each centre gate component as follows; 0.25 mm width for the 1 mm geometry, 1 mm width for the 2 mm geometry and 3 mm thick for the 4 mm geometry. The changes in the width illustrate the core layer represents a bigger proportion of the overall width as the sample thickness increases.

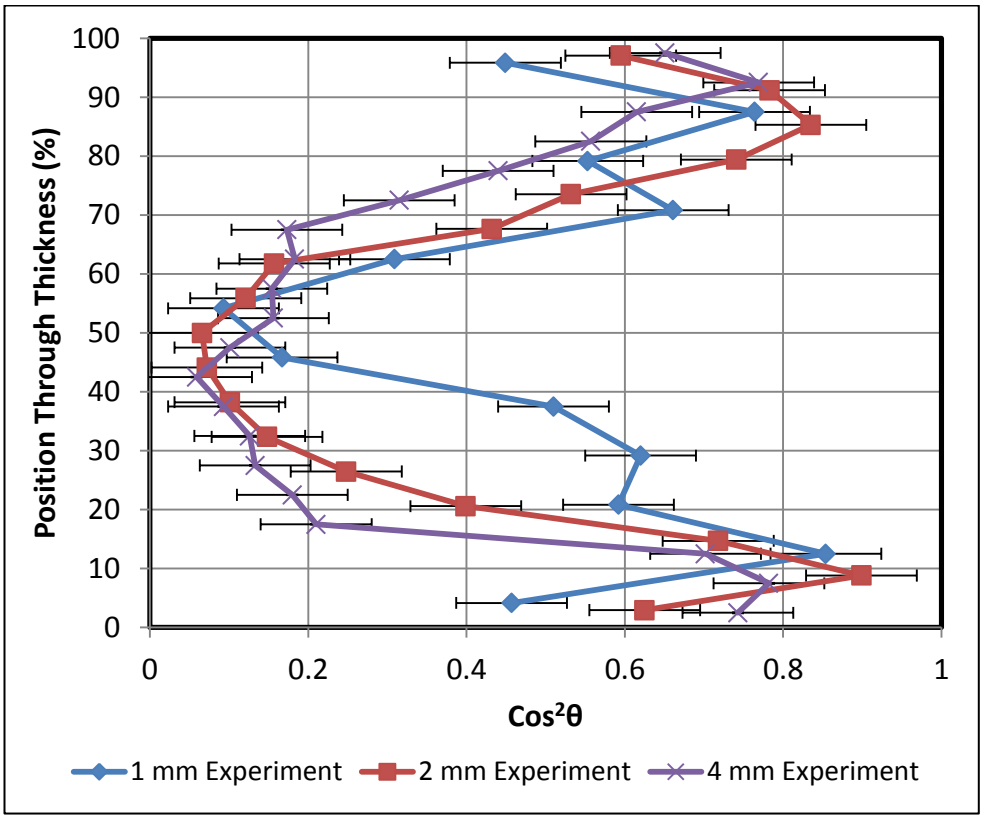

Figure 4.19 Measured average FOD 1 mm, 2 mm and 4 mm centre gate at location B

4.2.7.2 Influence of Geometry

Figure 4.20 and Figure 4.21 compare the FOD between the 2 mm and 4 mm plate and centre gate geometries, at the position closest to the end of the flow path in both geometries. It is clear that the average FOD within the 2 mm plate is higher compared to a 2 mm centre gate. The 2 mm centre gate consists of a highly transverse core layer with a 0.8 mm width. The $\cos^2\theta$ within the shell layer is similar for both geometries in the 2 mm case but this is not case in the 4 mm thick geometries. There is a maximum 2 mm difference between the core width of the 4 mm centre gate and plaque Figure 4.21. This illustrates the core is wider in a thick centre gate component compared to a thick plaque.

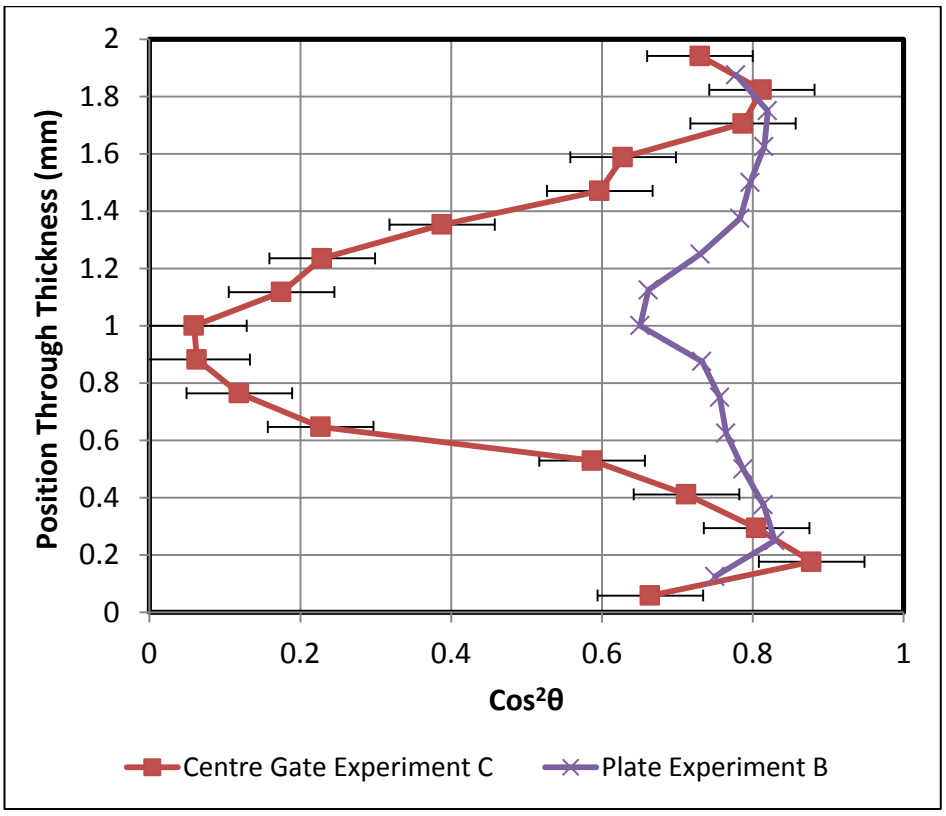

Figure 4.20 Measured average FOD 2 mm thick centre gate and end gate

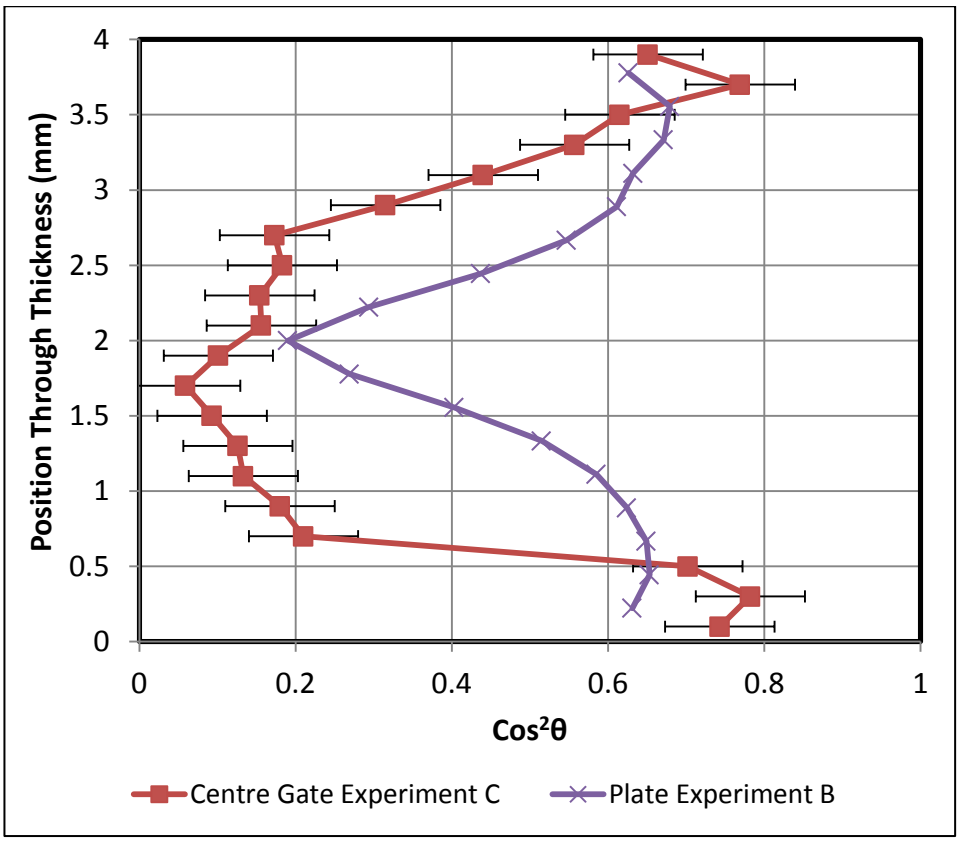

Figure 4.21 Measured average FOD 4 mm thick centre gate and end gate

4.2.7.3 Summary

The average FOD within the different components show a core, skin and shell layer formation. The skin layer has a lower orientation compared to the shell layer, as the skin is already frozen before shearing flow is able to align fibres in the direction of flow. The FOD within the centre gate disc is independent and does not change significantly after 16 mm along the radial flow path; however the same cannot be said for the end gate geometries. Within a thin centre gate cavity (1 mm) high shearing aligns fibres parallel to the direction of flow, as the thickness of the part increases the core width increases. However the average FOD reduces at the skin, shell and core layers as the thickness of the plaque increases. The change in the fan-gate component is a result of the shear flow which comes in through the gate within a thicker plaque creating a transverse aligned core. As a result of the principal stretching within the centre gate geometry the core is wider, transversely aligned to the direction of flow compared to the plaque where fibres align in the direction of shear flow.

4.3 Prediction

4.3.1 Mesh Study

To investigate the fibre prediction models incorporated in ASMI 2014, the 2-d geometry needs to be meshed accordingly. The background on finite element method (mesh type and element size) is discussed in Section 2.6.1 Finite Element Method. In this section a comparison is made between 3 mesh studies (Figure 4.22), created for the 1 mm centre gate geometry. The mesh studies consist of a coarse (fewer elements) and fine (more elements) mesh, the edge length and the number of elements for each study is found in Table 4.2.

Global Edge Length	Number of Elements
2.5 mm	4196
1 mm	32828
0.5 mm	133647

Table 4.2 Number of elements created for each mesh study

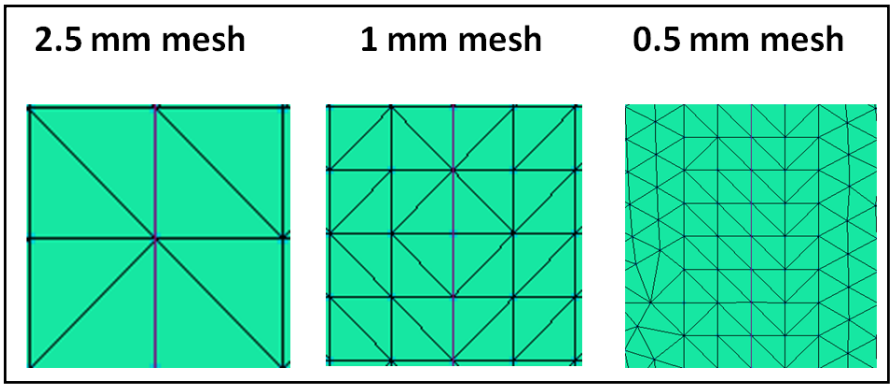

Figure 4.22 The mesh studies 0.5 mm, 1 mm and 2.5 mm

A comparison has been made between the different mesh and the influence on the FOD prediction against measured FOD at location A (16 mm), B (25 mm) and C (36 mm) along the radial flow path, a detailed schematic of this is shown previously in Figure 4.3. All three models FOD predictions are using classic Folgar-Tucker model with the (coefficient of interaction) $C_i = 0.03$. The results in Figure 4.23 and Figure 4.24 show small differences occur in the skin and core regions between the mesh solutions. At the end of the flow path/location C (Figure 4.25) the fine mesh (0.5 mm global edge length) generates a closer

solution to the measured FOD at the shell layer compared to the other two mesh solutions.

The finer mesh computes the average FOD within a fraction of the shell layer with greater accuracy at location C towards the end of the radial flow. However the predicted FOD is the same for all the other layers for each mesh at location A, B and C. As a result any of the global edge length solutions are adequate to investigate the accuracy of the fibre prediction models within ASMI 2014. For this project the shell models were meshed with a 1 mm global edge length. I have evaluated the simulations using the maximum 20 laminates.

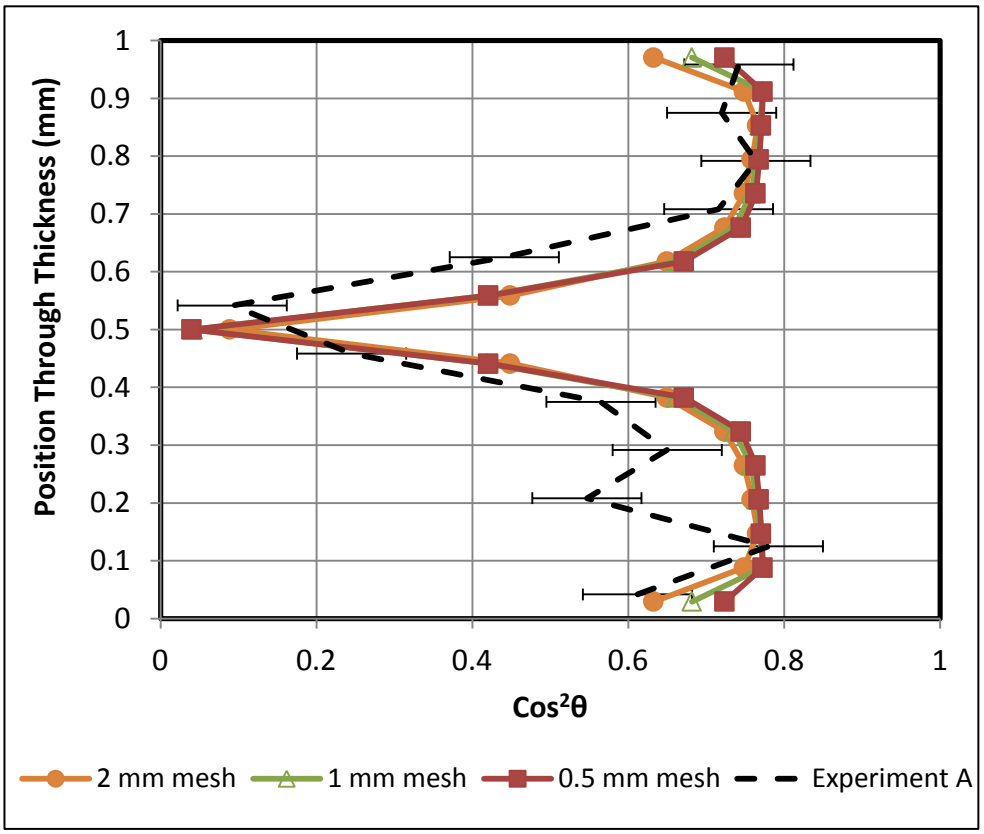

Figure 4.23 Evaluation of mesh studies 1 mm thick centre gate at location A

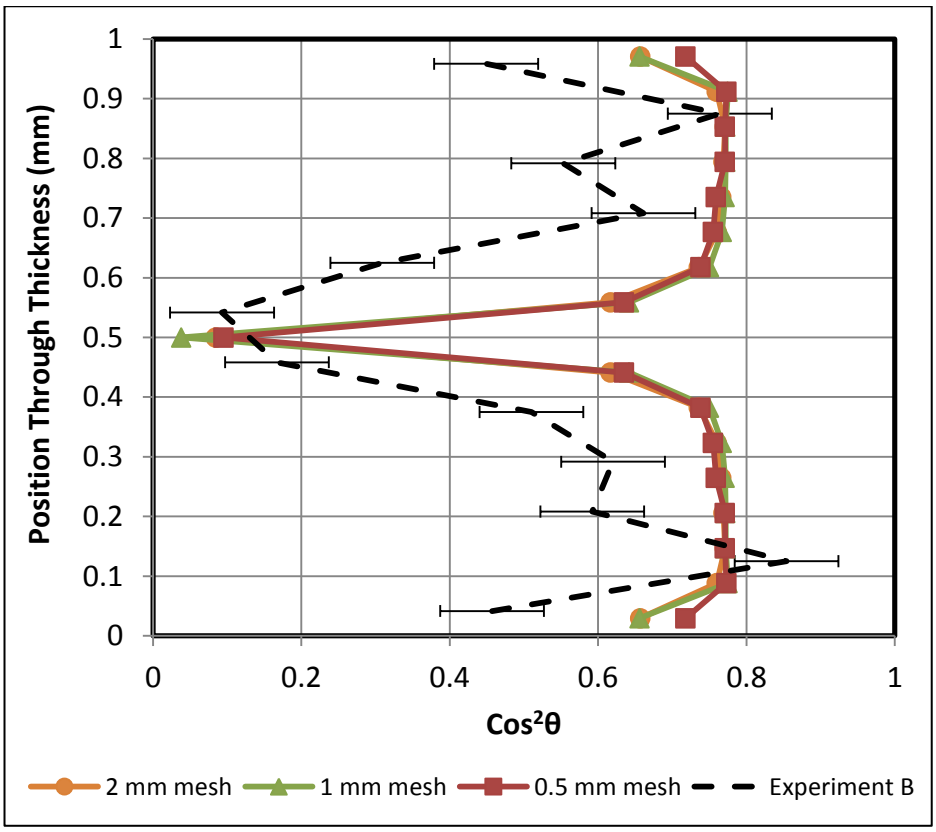

Figure 4.24 Evaluation of mesh studies 1 mm thick centre gate at location B

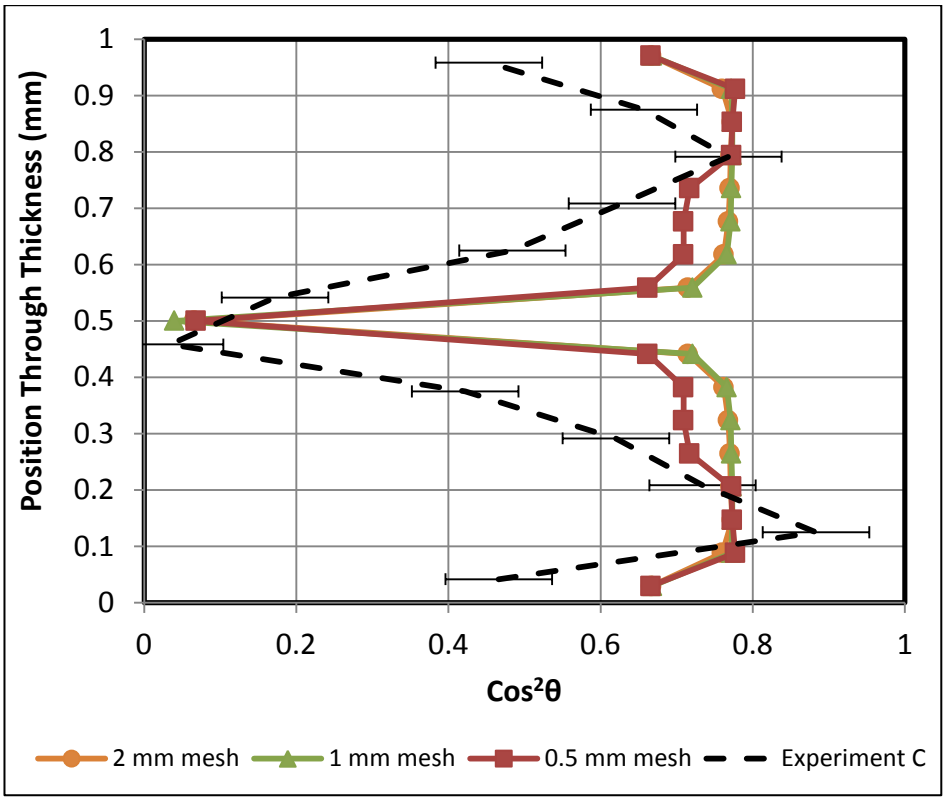

Figure 4.25 Evaluation of mesh studies 1 mm thick centre gate at location C

4.3.2 Flat Plate 2 mm

4.3.2.1 Classic Folgar-Tucker and Modified Folgar-Tucker

Figure 4.26 shows the effect of changing the C_i parameter within the classic Folgar-Tucker model. Table 4.3 contains the width of the core and the average FOD ($\cos^2\theta$) for the skin, shell and core layers for each C_i parameters in Figure 4.26. Results show 3 critical changes as the coefficient of interaction increases while FOD at the core remains the same, majority of the influence is on the orientation and thickness of the shell layer. Between coefficients, 0.00001-0.0001 the fibres at shell are highly aligned in the direction of flow and the core width ranges from 1.4 to 0.3 mm. A further increase in the interaction coefficient causes fibres in the shell to come out of the plane as shown by 0.001-0.01, the thickness of the shell increases and consequently decreasing the thickness of the core to 0.1 mm. At C_i = 0.1 the alignment of the shell and skin layer is random and the same. The fibre orientation at location B is over predicted at the core. The C_i between 0.001-0.01 at location A and B provide the closest prediction to the measured data.

C_i	Skin	Shell	Core	Core Thick (mm)
0.1	0.54	0.54	0.38	0.4
0.01	0.72	0.85	0.41	0.1
0.001	0.78-0.79	0.98	0.41	0.2
0.0001	0.7-0.72	0.98	0.41	0.3
0.00001	0.63 - 0.62	0.98	0.41	1.4 - 0.8

Table 4.3 Average FOD at each layer and core width for varying C_i

Figure 4.27 and Figure 4.28 shows the effect of changing the D_z parameter between 0.8 - 0.1, within modified Folgar-Tucker model at locations A and B. The results show a clear indication that the D_z parameter only starts to make a noticeable difference when D_z < 0.4. Decreasing the magnitude of D_z parameter below 0.4 increases the thickness of the core and reduces over prediction at the shell layer caused by the C_i above 0.1. The D_z parameter does not influence the orientation when C_i = 0.1, the shell layer remains random in

orientation at location A and B. The D_z parameter is known to control the "randomizing effect" to expand on this fact, the fibres are less parallel to the flow direction (randomizing effect increases) as D_z decreases (Wang and Jin, 2010). At both locations a smaller value of D_z between 0.2-0.1 would satisfy as good solution. The best solution for C_i remains between 0.001-0.01.

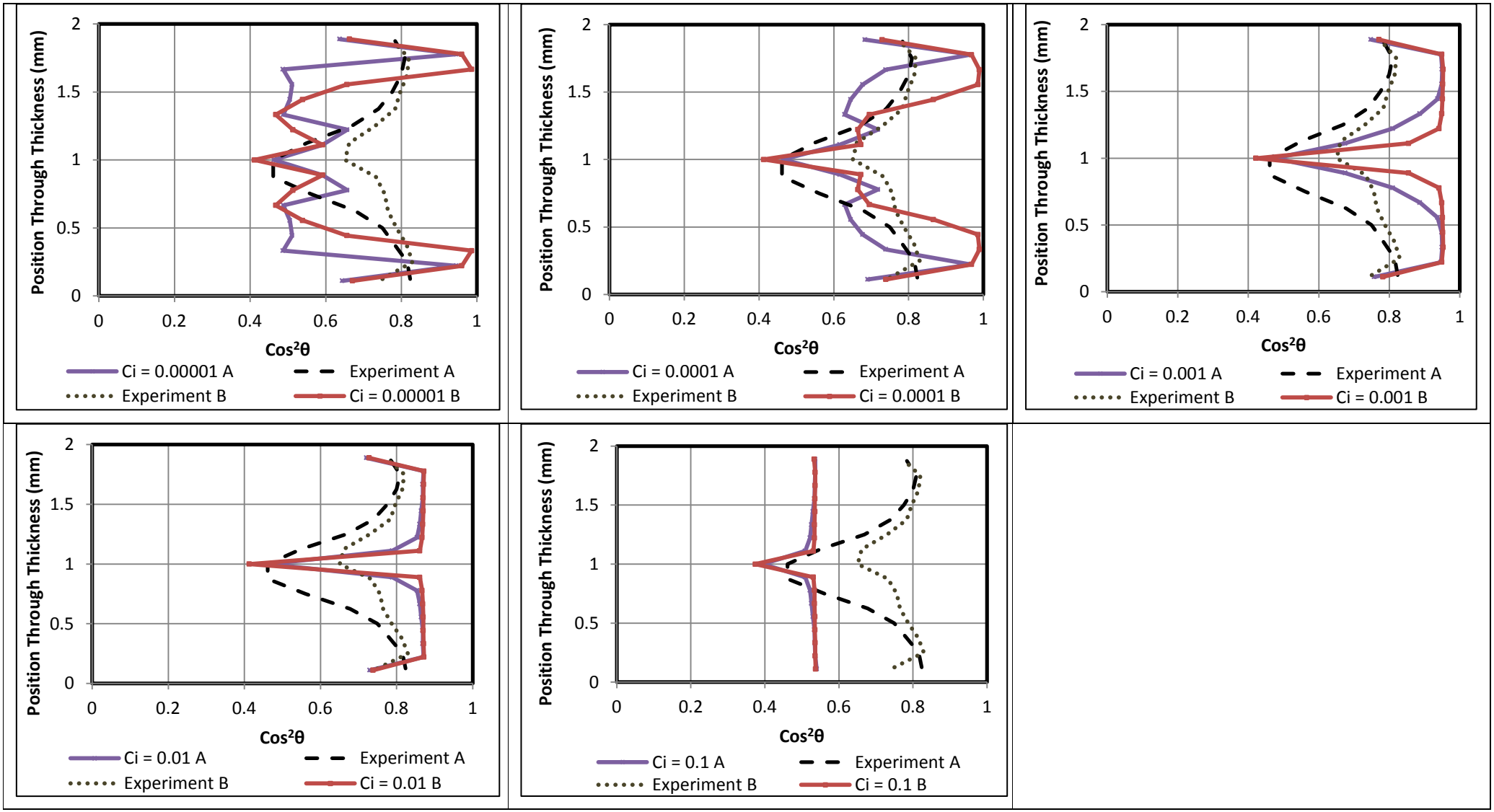

Figure 4.26 The graphs show the effect of changing the C_i coefficient within classic Folgar Tucker model $D_z = 1$ at 2 mm plate location A & B

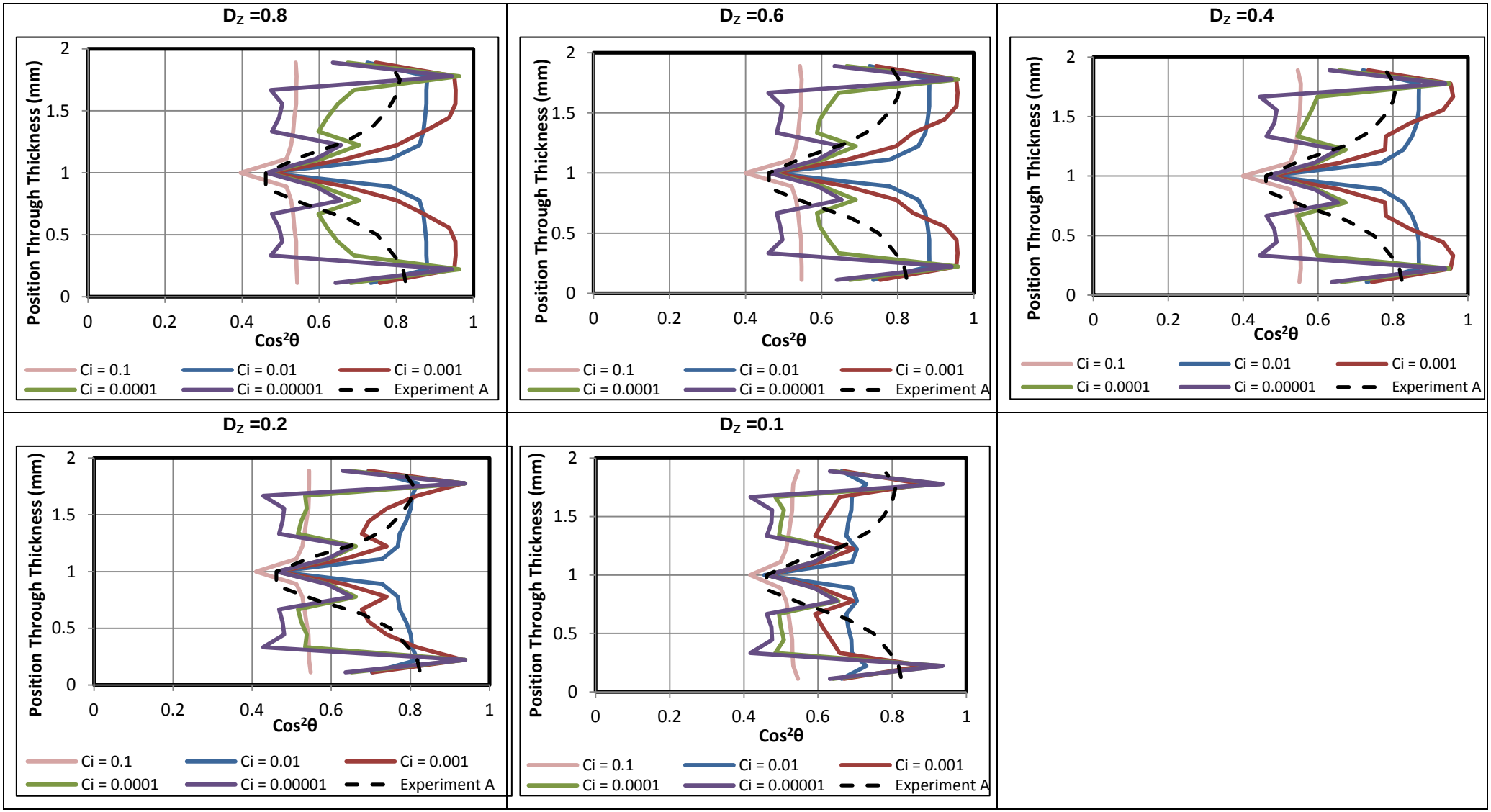

Figure 4.27 The effect of changing the C_I coefficient within the modified Folgar-Tucker model, when varying D_z at 2 mm plate location A

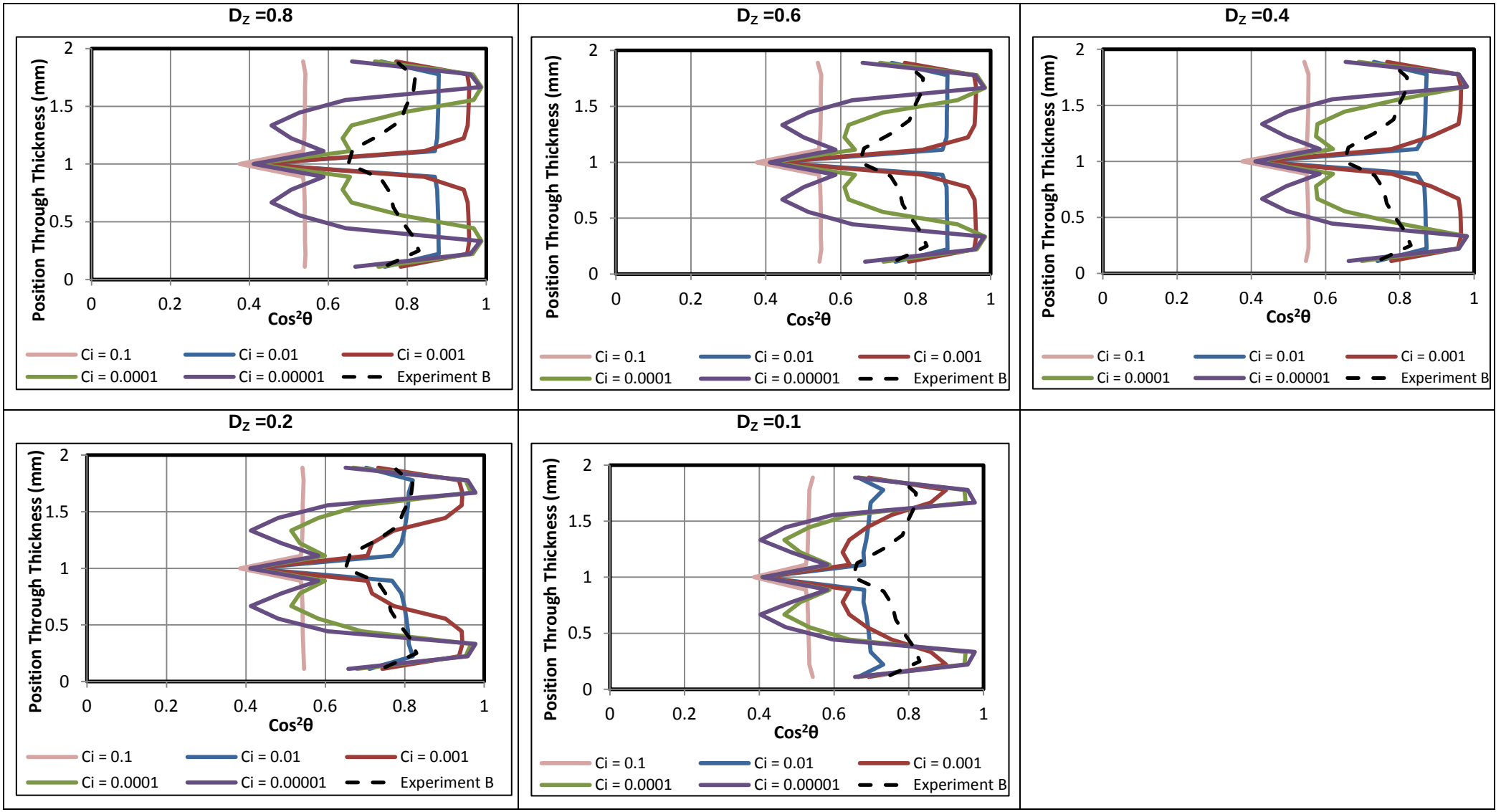

Figure 4.28 The effect of changing the C_I coefficient within the modified Folgar-Tucker model, when varying D_z at 2 mm plate location B

The Folgar-Tucker model (2.13), (1984) is implemented into software packages to predict the fibre orientation within injection moulded composites. The model uses the principles of a single fibre (Jeffery, 1922) and incorporates fibre-fibre interactions. Within this equation C_i is a coefficient of strain rate $\dot{\gamma}$ ($C_I\dot{\gamma}$). A high magnitude of C_i indicates a greater interaction between fibres (increase in concentration or aspect ratio) and this interaction increases magnitude of strain rate term. This diffusivity term $(C_I\dot{\gamma})$ influences the strength and rate of fibre interactions or collisions. Therefore more interactions create a motion of particles, away from a higher orientation towards regions of lower orientation (Brenner, 1974). This explains the change in orientation and size of the shell, which is observed from this study.

$$\frac{DA}{D_t} = (\mathrm{W.A} - \mathrm{A.W}) + \xi(\mathrm{D.A} + \mathrm{A.D} - 2\mathbf{A}\!:\!\mathrm{D}) + 2C_I\dot{\gamma}(\mathrm{I} - 3\mathrm{A}) \qquad \textbf{2.13}$$

Previous research carried out by Bay and Tucker, (1992) indicates that C_i = 0.01 gives a good fit to the FT orientation model for a 3.18 mm plaque and centre-gated disk injection moulded with a 43 wt% of SGF. Another study carried out by Nguyen et al., (2008) concludes that C_i = 0.03 provides the best solution for 40 wt% LGF 3 mm thick centre gate and plaque geometries when applying the RSC (will be discussed shortly) model. The value of C_i = 0.00043 using Tucker and Advani, (1994) proposed empirical expression (2.14). Where V_f = 21%, L = 250 µm and D = 10 µm for this particular study. From the understanding of the D_z and C_i coefficients and the recommendations found in the literature, parameters can be narrowed down to arrive at an enhanced prediction.

$$c_i = 0.0184\exp\left(-0.7148V_f\frac{\mathrm{L}}{\mathrm{D}}\right) \qquad \textbf{2.14}$$

Figure 4.29 and Figure 4.30 represent the FOD prediction for the FT models against the measured FOD at location A and B for the 2 mm plate. The model use the best and default parameters (selected by Moldflow) to predict FOD. The most fitting parameter for both Folgar-Tucker models, namely Classic FT C_i= 0.03 and modified FT D_z = 0.15 C_i = 0.0057. The Classic FT C_i = 0.0057 and modified FT D_z = 0.3214 C_i

= 0.0008, represent the default values selected by ASMI 2014. The default value selected by ASMI 2014 for C_i is dependent upon the material and fibre concentration.

The thickness of the core is reduced for all solutions as a result of the wide shell layer. Apart from the over-prediction at the core, the MFT model (D_z = 0.15 C_i = 0.0057) accurately predicts the orientation at the shell for both locations. Although the FT model (D_z = 1 C_i = 0.03) is a good approximation of the measured FOD, the $\cos^2\theta$ is predicted lower at the skin and shell. The orientation is over-predicted by the default solution at both locations at the shell and core layers. Figure 4.29 and Figure 4.30 show the $\cos^2\theta$ at the core does not change at location A and B for varying C_i and D_z parameters.

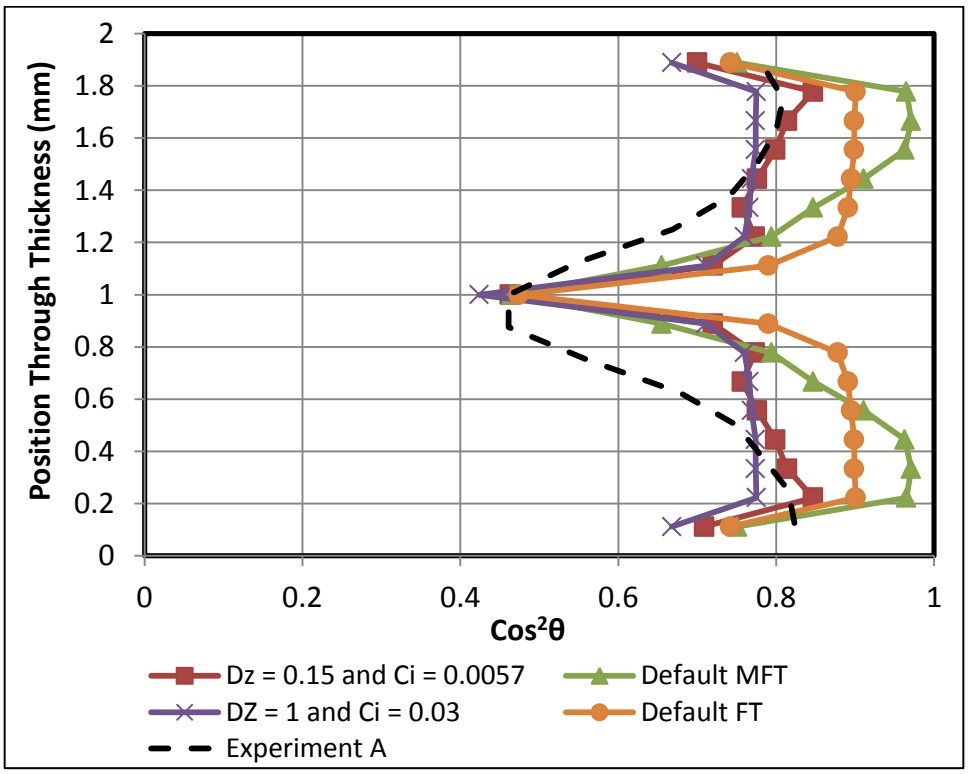

Figure 4.29 Enhanced and default prediction from both Folgar-Tucker models against 2 mm plate average FOD at location A

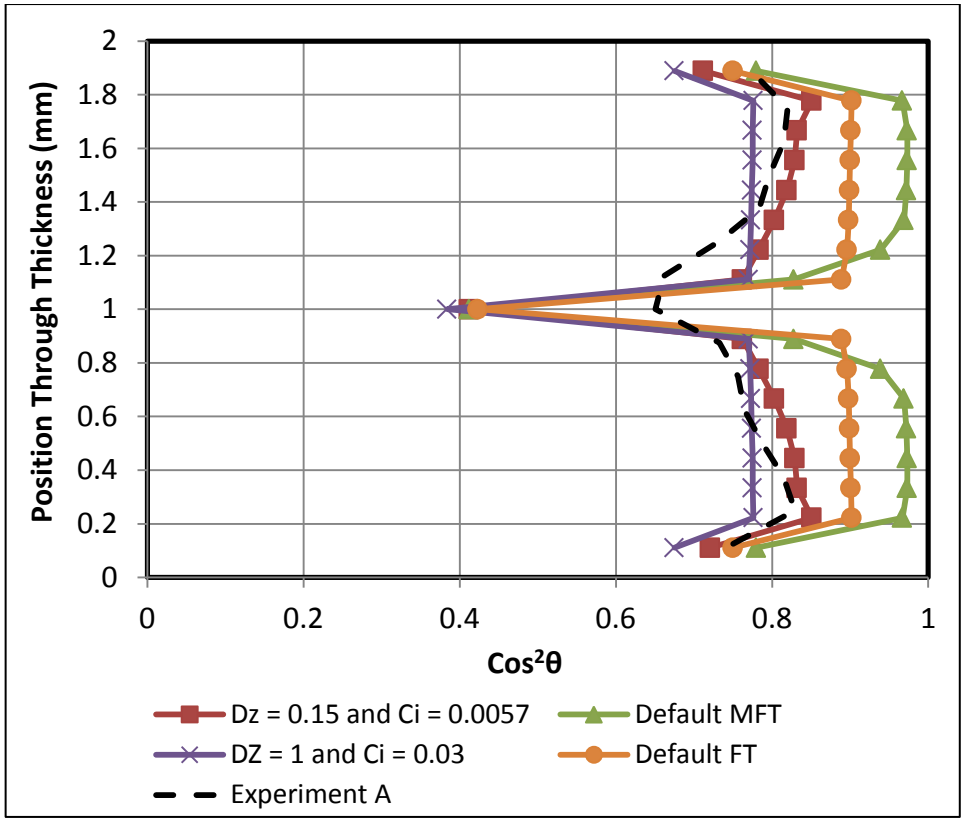

Figure 4.30 Enhanced and default prediction from both Folgar-Tucker models against 2 mm plate FOD at location B

4.3.2.2 RSC

Various (reduced strain factor) k and (coefficient of interaction) C_i values are examined for the RSC (Reduced Strain Closure) model (Equation 2.16) shell model. The findings from the 2 mm plate at location A were then used to tailor the solutions for the different geometries. The examined parameters are specified in Section 3.4.2 Extracting Predicted FOD.

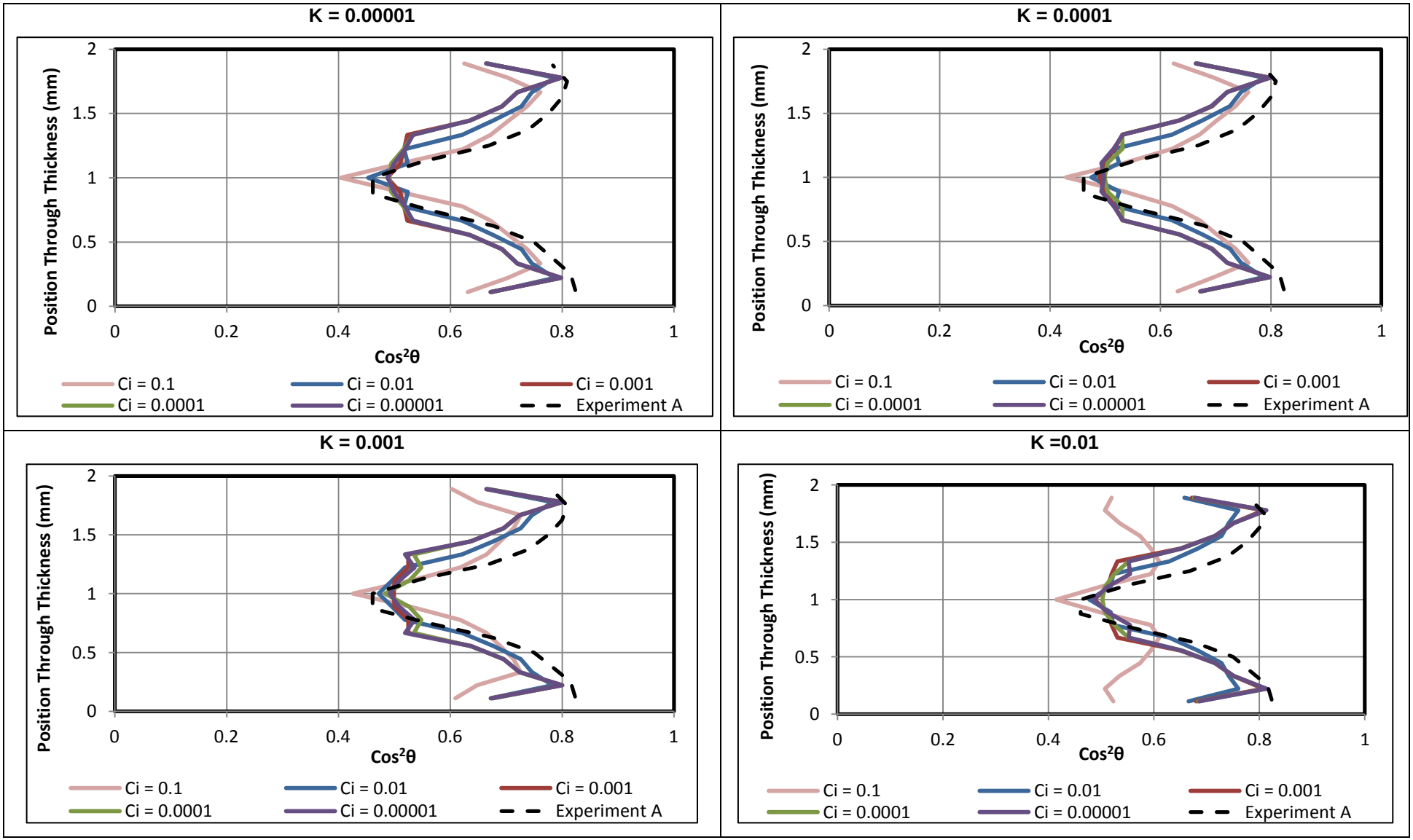

Figure 4.31 Effect of changing the C_i parameter within the RSC model, for different K values for 2 mm plate at location A

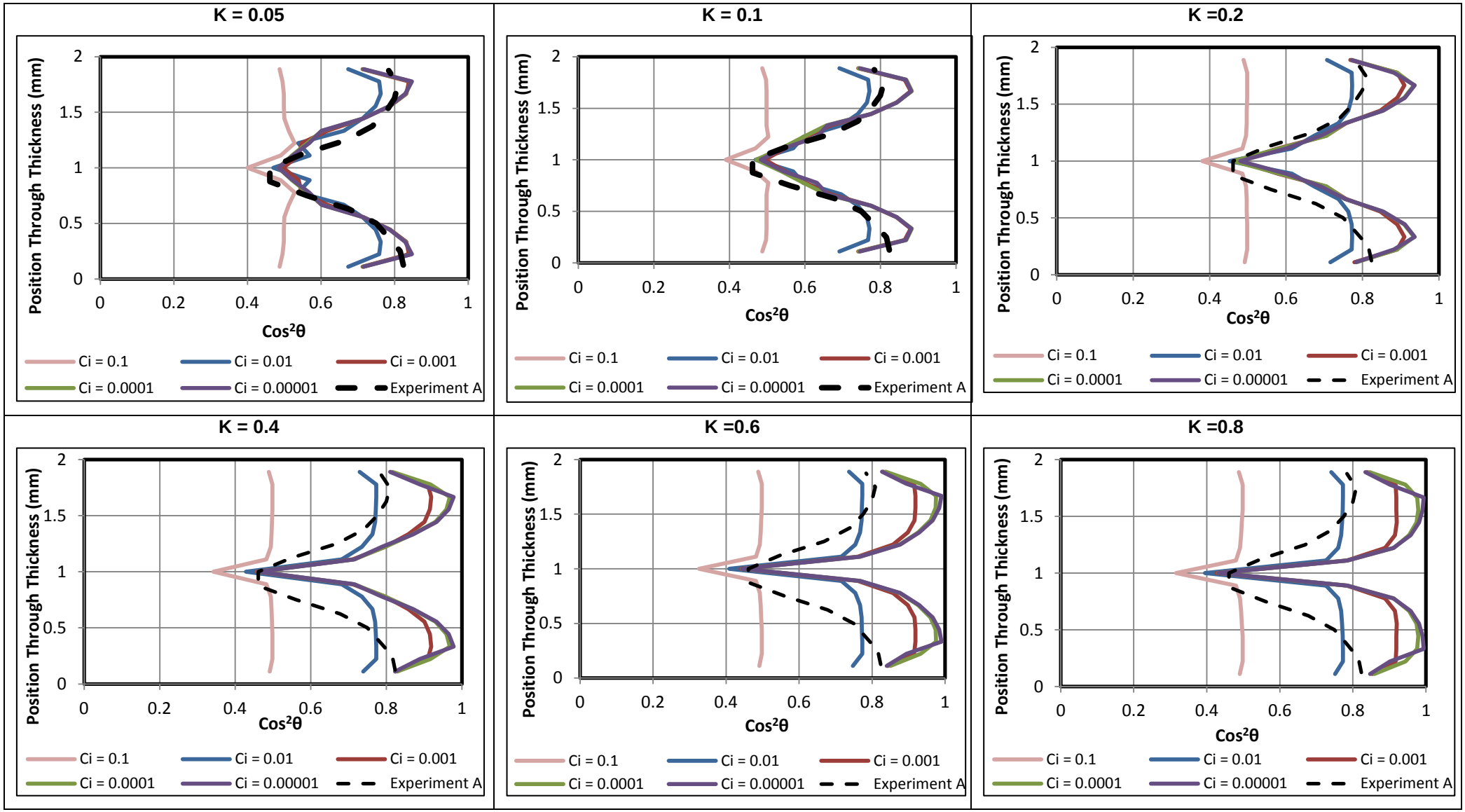

Figure 4.32 Continuation of changing the C_i parameter within the RSC model, for different K values for 2 mm plate at location A

Table 4.4 contains the width of the core and the average FOD ($\cos^2\theta$) for the skin, shell and core layers for the alternating k (0.00001 - 0.8) parameter within the RSC model for C_i between 0.00001 - 0.1 in Figure 4.31 and Figure 4.32. For values of k between 0.00001 - 0.1 the thickness of the core is at the maximum with values between 0.4 - 0.1 mm for the various C_i solutions and the shell layer is aligned in the direction of flow and the orientation at the core is random and does not vary. When the reduced strain factor starts to increase or when k > 0.2 the thickness of the core starts to reduce, the thickness of the shell layer increases and average FOD increases within the shell and skin layers. The orientation at the core becomes more transverse as the factor increases (k > 0.2). A RSC solution for the 2 mm plate at location A would lie between 0.01 - 0.1. ASMI 2014 recommends using a k value of 0.05 to obtain a good solution. All the C_i solutions follow a typical trend apart from C_i = 0.1. The orientation in the shell and skin layers becomes increasingly random and the width of the core increases when the k value is above 0.01.

k	C_i	Skin	Shell	Core	Core Thick (mm)
0.00001	0.1	0.63	0.76	0.4	0.2
0.00001	0.01	0.67	0.79	0.45	0.2
0.00001	0.001	0.67	0.8	0.49	0.35
0.00001	0.0001	0.67	0.8	0.49	0.35
0.00001	0.00001	0.63	0.8	0.49	0.35
0.0001	0.1	0.63	0.76	0.4	0.2
0.0001	0.01	0.67	0.79	0.45	0.1
0.0001	0.001	0.67	0.8	0.49	0.35
0.0001	0.0001	0.67	0.8	0.49	0.35
0.0001	0.00001	0.67	0.8	0.49	0.35
0.001	0.1	0.6	0.73	0.43	0.2
0.001	0.01	0.67	0.78	0.47	0.1
0.001	0.001	0.67	0.8	0.49	0.1
0.001	0.0001	0.67	0.8	0.49	0.1
0.001	0.00001	0.67	0.8	0.49	0.1
0.01	0.1	0.52	0.61	0.42	0.3
0.01	0.01	0.66	0.76	0.48	0.2
0.01	0.001	0.68	0.81	0.49	0.1
0.01	0.0001	0.68	0.81	0.49	0.1

0.01	0.00001	0.68	0.81	0.49	0.2
0.05	0.1	0.49	0.5	0.4	0.35
0.05	0.01	0.67	0.76	0.47	0.05
0.05	0.001	0.71	0.84	0.49	0.05
0.05	0.0001	0.72	0.85	0.48	0.05
0.05	0.00001	0.72	0.85	0.48	0.01
0.1	0.1	0.52	0.61	0.42	0.4
0.1	0.01	0.67	0.76	0.48	0.05
0.1	0.001	0.68	0.81	0.49	0.02
0.1	0.0001	0.68	0.81	0.5	0.05
0.1	0.00001	0.69	0.81	0.49	0.05
0.2	0.1	0.49	0.5	0.38	0.3
0.2	0.01	0.72	0.77	0.45	0.1
0.2	0.001	0.78	0.94	0.48	0.1
0.2	0.0001	0.78	0.94	0.46	0.1
0.2	0.00001	0.78	0.94	0.48	0.1
0.4	0.1	0.49	0.5	0.34	0.3
0.4	0.01	0.82	0.77	0.43	0.1
0.4	0.001	0.82	0.92	0.46	0.08
0.4	0.0001	0.82	0.97	0.46	0.08
0.4	0.00001	0.82	0.98	0.46	0.08
0.6	0.1	0.49	0.5	0.34	0.3
0.6	0.01	0.73	0.77	0.41	0.08
0.6	0.001	0.84	0.92	0.44	0.06
0.6	0.0001	0.84	0.97	0.44	0.06
0.6	0.00001	0.84	0.99	0.44	0.06
0.8	0.1	0.49	0.5	0.32	0.3
0.8	0.01	0.73	0.77	0.4	0.08
0.8	0.001	0.85	0.92	0.43	0.06
0.8	0.0001	0.85	097	0.43	0.06
0.8	0.00001	0.85	0.99	0.43	0.06

Table 4.4 Average FOD at each layer and core width for varying C_i and k parameters

Reference to the RSC model (Equation 2.16) shows the parameter influences the kinetics orientation caused by the fibre interactions and shear flow. The k parameter reduces the fibre orientation kinetics as the magnitude of k

decreases. Therefore as k increases (k ≥ 0.2) the rate of orientation development increases, the thickness of the shell layer increases, there is a decrease in core thickness but the orientation within the core becomes more transverse to the flow direction. From previous literature the value of k was set at 0.05 (Moldflow default) for thin plaque and disk geometries and 0.03 for thick disk geometries (Wang and Jin, 2010).

$$\frac{DA}{D_t} = (\mathrm{W.A} - \mathrm{A.W}) + \xi(\mathrm{D.A} + \mathrm{A.D} - 2[\mathbf{A} + (1-\kappa)(\mathbf{L} - \mathbf{M}:\mathbf{A})]:\mathrm{D}) + 2\kappa C_I\dot{\gamma}(\mathrm{I} - 3\mathrm{A}) \quad \textbf{2.16}$$

4.3.2.3 Summary

Figure 4.33 and Figure 4.34 is a comparison of the best possible solutions for the RSC model and the MFT model. All the predictions are using the parameter C_i = 0.0057, this interaction coefficient is default for this specific material regardless of the reduced strain factor when a C_i value is not input. A clear difference is seen in the thickness of the core between factors k = 0.1 and k = 0.05, there is reduced over-prediction at the core at both locations when k = 0.1 compared to other solutions. All the solutions predict the orientation at the skin accurately. All the solutions from ASMI 2014 over-predict the orientation at the core at location B for the 2 mm plate although the measured average FOD does not have a core.

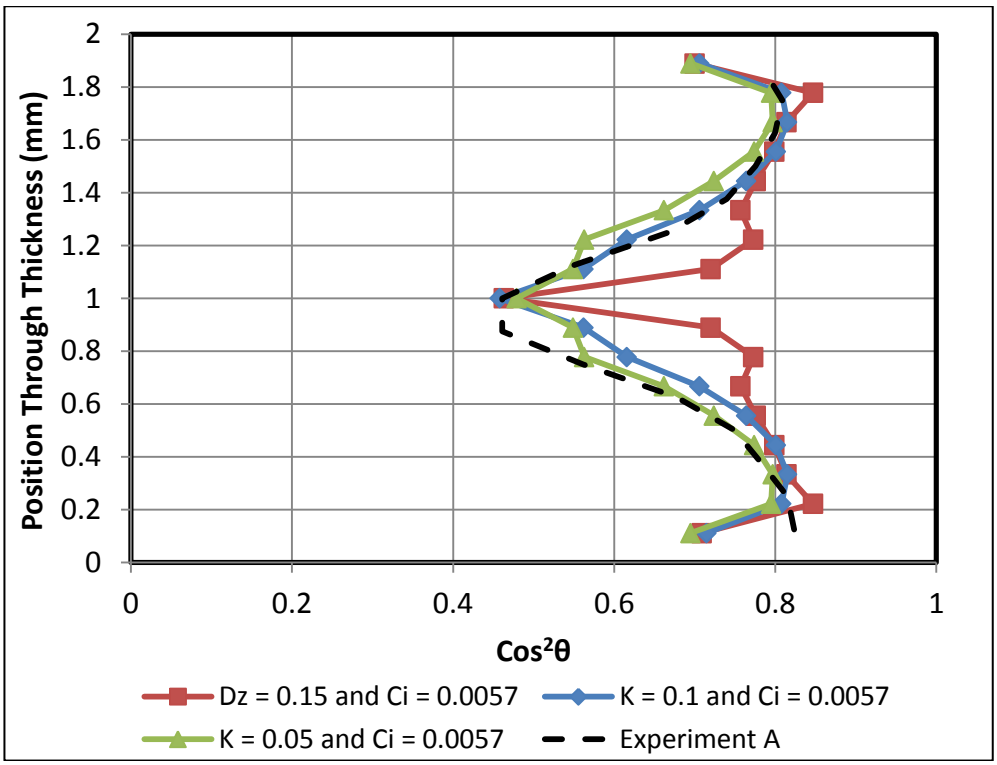

Figure 4.33 Enhanced predictions from RSC and MFT against 2 mm plate FOD at location A

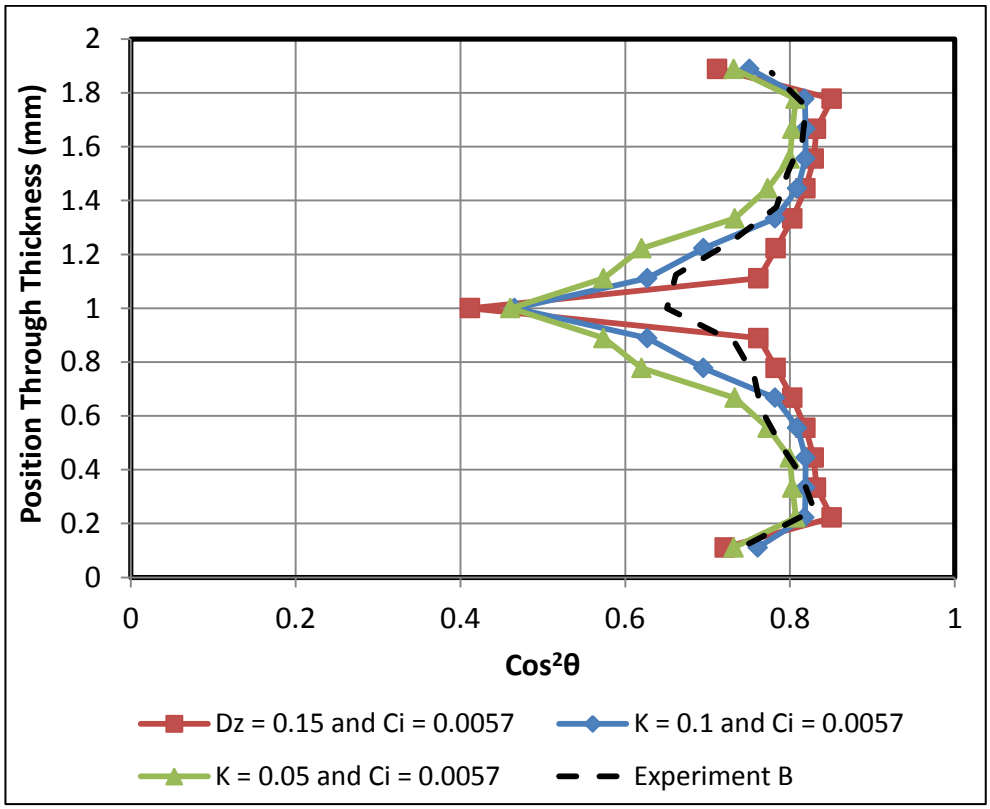

Figure 4.34 Enhanced predictions from RSC and MFT against 2 mm plate FOD at location B

Varying the coefficient of interaction (C_i) within the FT and MFT model primarily affects the alignment and thickness at the shell. When C_i is between 0.00001-0.0001 fibres at the shell align parallel to the flow direction, the thickness of the shell decreases and the thickness of the core increases. However if C_i increases in the range of 0.001- 0.01 the thickness of the shell increases, the thickness of the core decreases and the orientation within the shell layer reduces as fibres become less aligned to the direction of flow. At C_i= 0.1 the orientation within the skin and shell layer is the same (random) and the orientation at the core always remains transverse to the flow direction.

In ASMI 2014 the MFT model predicts the skin and shell layer accurately and there is less over-prediction at the core compared to the FT model when D_Z = 0.15. Reference to the MFT model is made in equation 2.15, within this equation the D_Z parameter affects the orientation which is parallel to the flow direction. Although this parameter shows improvement in the MFT prediction the width of the core still remains small. The findings show that D_Z parameter only impacts the fibre orientation at values below 0.4. Decreasing the D_z parameter decreases the out of plane orientation, the thickness of the core increases and the orientation in the shell reduces.

For the 2 mm plate with the FT model the parameter C_i = 0.03, over-predicts the orientation at the core and under predicts the orientation at the skin and shell. The MFT model provides a closer approximation to the measured results compared to the FT model as shown in Figure 4.29 and Figure 4.30 at both locations for the 2 mm plate. For MFT and RSC predictions the value of C_i = 0.0057 provides the best solution. Published work shows the value C_i = 0.01 (Bay and Tucker, 1992) is recommended solution for 3.18 mm thick plaque with 43 fibre wt%. There is a difference of factor three between the predicted C_i of 0.03 and the recommended value of 0.01 for the FT model, this includes a 3% difference in fibre wt%.

The RSC prediction best fits the measured results compared to the MFT model at location A and B shown in Figure 4.33 and Figure 4.34 for the 2 mm plate. Although the MFT model gives a good prediction for the orientation at the shell and skin the core is over-predicted. The reduced strain factor slows down the

rate of orientation as the factor decreases; this allows the model to predict the thickness of the core with accuracy. The closest approximation to the measured data was found using the parameters k = 0.1 and C_i = 0.0057. The k parameters recommend in the literature include 0.03 and 0.05. The default value of k = 0.05 recommended by ASMI 2014 with C_i = 0.0057 is a secondary solution to predict the orientation within a 2 mm plaque. When in default ASMI 2014 selects C_i = 0.0057 for any reduced strain factor value.

4.3.2.4 Conclusion

The aim of this study is to specify the best possible solution to predict the $\cos^2\theta$ for different geometries and thickness using shell models in ASMI 2014. The values adopted by Moldflow as default for both FT and MFT models, show a great deal of over prediction and inconsistency with the test data. It can be concluded that the RSC model provide a better solution for the 2-d geometry within ASMI 2014. A set of generic rules have been created using the conclusions from investigation of the 2 mm plate at location A and B. These rules will narrow down the possible optimum parameters which would best predict the FOD within any geometry using the FT, MFT and RSC models. These rules will be tested on the 4 mm thick ribbed plaque and the 1 mm, 2 and 4 mm centre gate geometries.

C_i Parameter

1. To generate a shell layer oriented parallel to the flow direction and a large core select a low C_i parameter between 0.00001 - 0.0001.
2. To increase the shell layer thickness, reduce the thickness of the core and to decrease the alignment of fibres within the shell layer select a C_i parameter between 0.001 - 0.01
3. To have a large skin layer with random FOD and a very small core select a high C_i parameter of 0.1.

D_z Parameter

1. To reduce over prediction at the shell and increase the thickness of the core a D_Z parameter less than 0.4 is a good solution. For thin geometries the D_Z parameter is between 0.2 - 0.1.

K Parameter

1. To increase the core thickness and to decrease the shell layer thickness select a k value between 0.00001 - 0.01.
2. To align the fibres in the shell layer in the flow direction select a k value between 0.2 - 0.8.
3. To decrease the core thickness and to align the fibres within the core transverse to the flow direction select a k value above 0.05.

4.3.3 Ribbed plaque 4 mm

Measured 4 mm ribbed plaque FOD is compared to the predicted FOD from both the MFT and RSC models.

4.3.3.1 Folgar-Tucker and Modified Folgar Tucker

To predict the FOD within a thick geometry there is the option to choose a C_i between 0.001 - 0.08 and a small D_z to achieve a wide core. The results in Figure 4.35 and Figure 4.36 compare MFT and FT predictions using different C_i parameters. Although parameters C_i = 0.0057 and D_z = 0.15 predicted the best solution for the 2 mm plate, the default FT (C_i = 0.0057), is over-predicting the orientation at skin/shell/core layers. The average FOD within this 4 mm thick geometry results in a wide core and a small but random orientation within the shell layer. No value of C_i can meet this criteria, however for the MFT and FT models the following parameters C_i = 0.03 and D_z = 0.15 or C_i = 0.06 and D_z = 0.15 and C_i = 0.06 and D_z = 1 offer the best solution at one location with the orientation at the core over-predicted. ASMI 2014 uses as a lower value of C_i (C_i = 0.001 and D_z = 0.1579) as default parameters. The default parameters

increase the core thickness but over-predict the level of orientation within the rest of the layers at both locations. All the predictions are unable to capture the transverse orientation and thickness at the core.

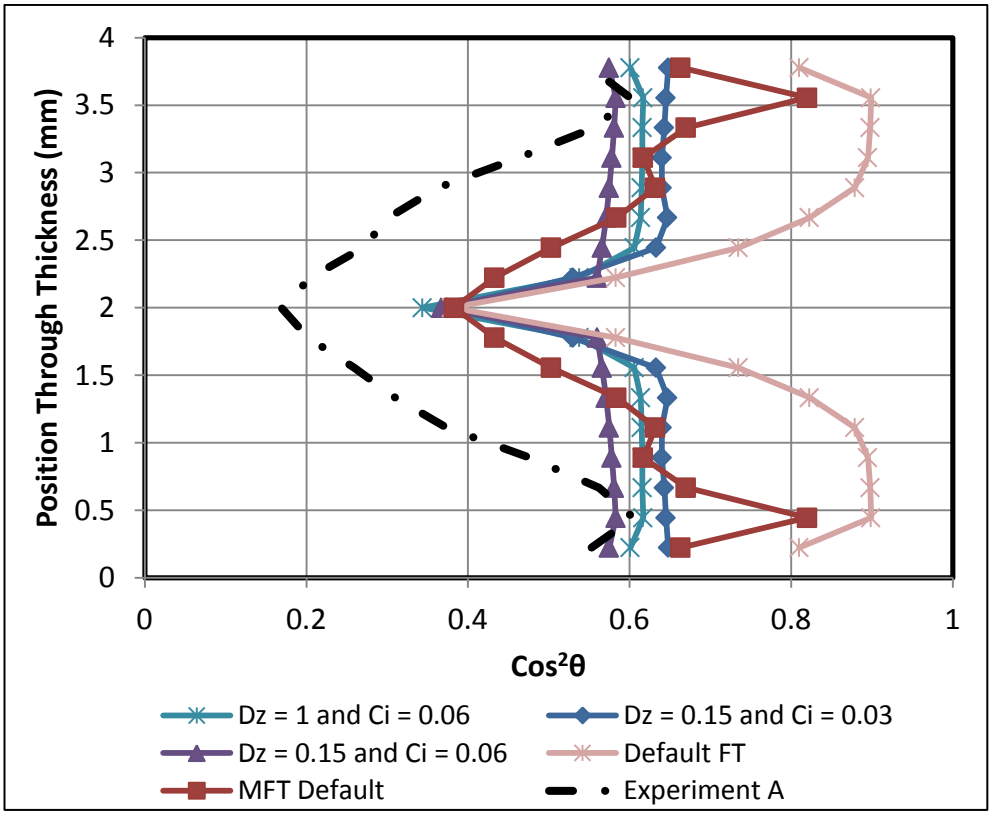

Figure 4.35 Enhanced and default prediction both FT models against 4 mm plate average FOD at location A

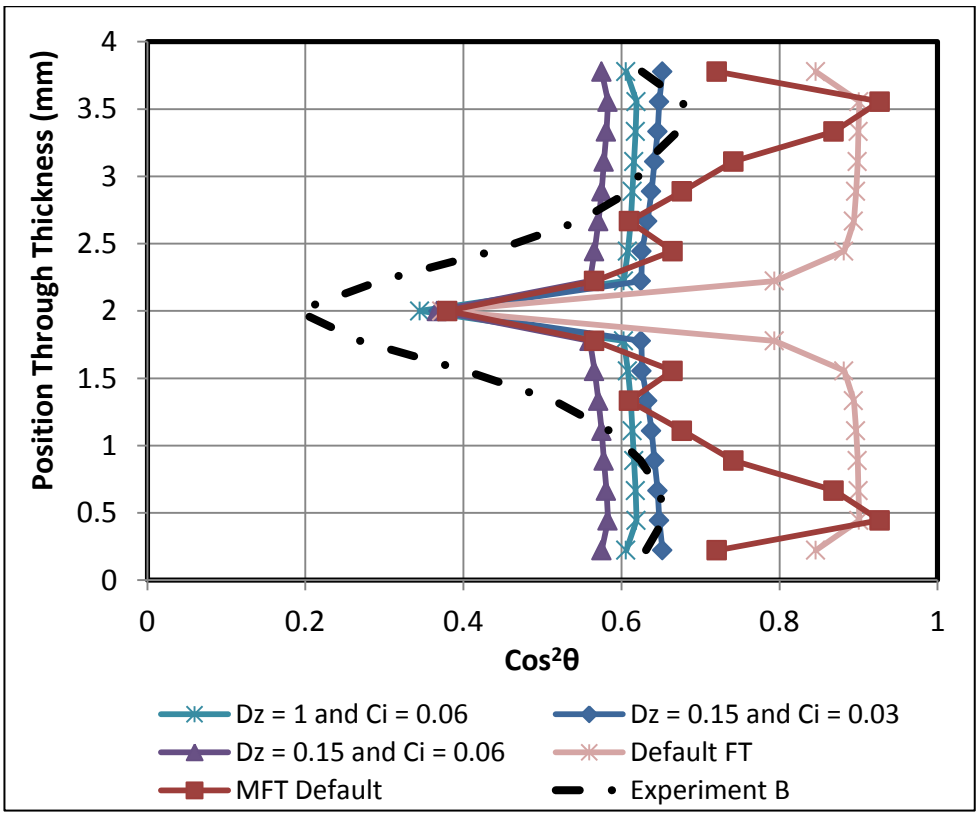

Figure 4.36 Enhanced and default prediction both FT models against 4 mm plate average FOD at location B

4.3.3.2 RSC

Moldflow selects a default value of C_i =0.0057 for any reduced strain factor, in the case where no C_i value is supplied. Applying the RSC model in Figure 4.37 and Figure 4.38 on the 4 mm thick geometry provides a better prediction, with a 0.03 or 0.06 value of C_i compared to a lower magnitude of C_i. The closest approximation to the measured data is given by k = 0.8 and C_i = 0.03, although a higher value of k predicts a transverse core, the shell layer is over-predicted at both locations. When k = 0.1 the orientation at the core is random but there is less over-prediction at the shell layer. For any given solution or model ASMI 2014 appears to over-predict the level of orientation for a thicker geometry, this argument will be confirmed with the 4 mm thick centre gate prediction.

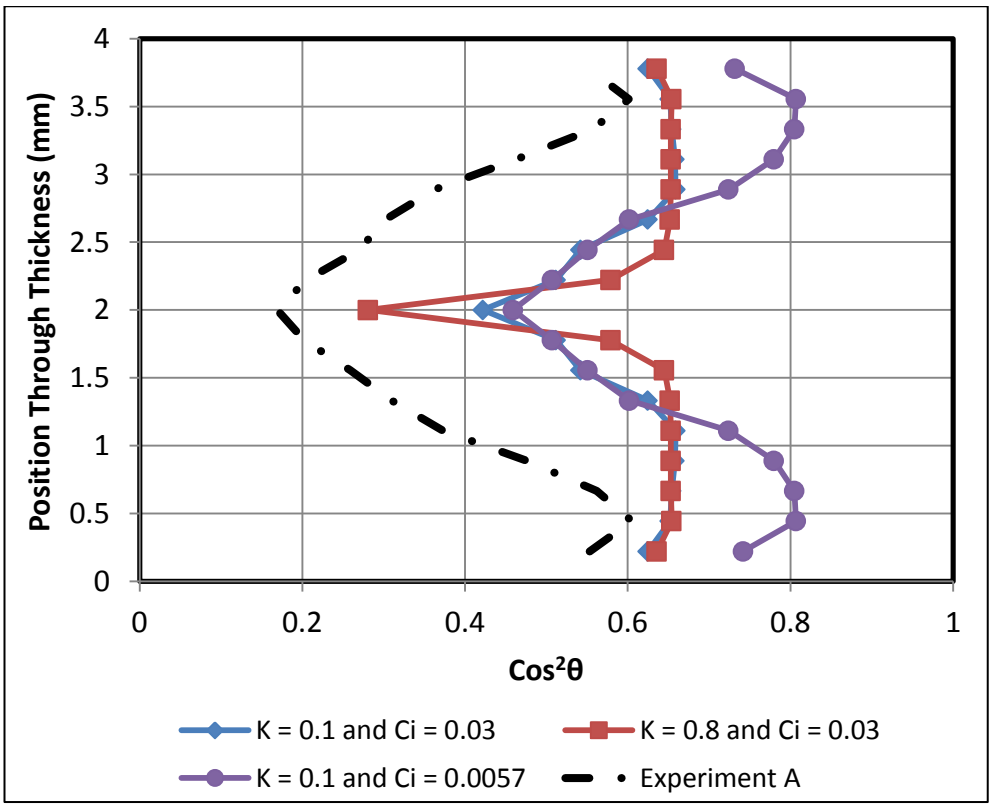

Figure 4.37 Enhanced predictions for RSC against 4 mm plate average FOD at location A

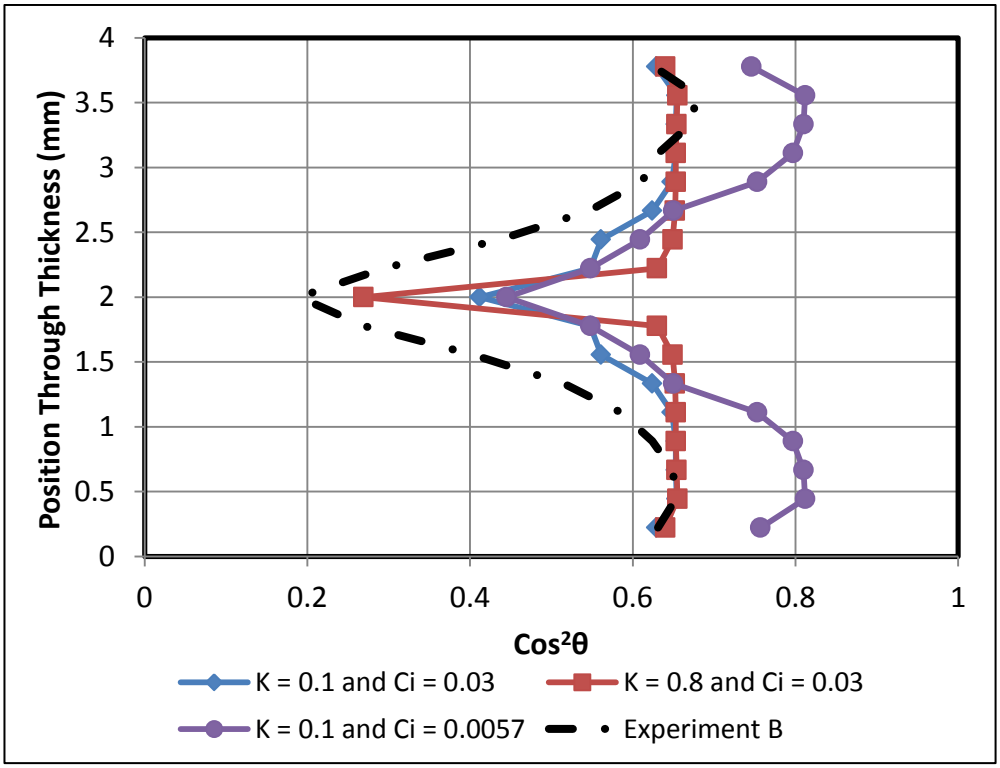

Figure 4.38 Enhanced predictions for RSC against 4 mm plate average FOD at location B

4.3.4 Centre Gate

Measured FOD at 3 locations for the 1 mm, 2 mm and 4 mm centre gate component is compared with FT, MFT and the RSC predictions.

4.3.4.1 1 mm Thick

4.3.4.1.1 Folgar-Tucker and Modified Folgar Tucker

The measured FOD in Figure 4.39, Figure 4.40 and Figure 4.41 has a thin core oriented perpendicular to the direction of flow and the shell is oriented parallel to the direction of flow. To the C_i between 0.001 - 0.01 and the D_Z between 0.2 - 0.15, should predict a thin core and a shell layer oriented in the direction of flow. ASMI 2014 default FT with C_i = 0.0057 predicts the core width but over predicts the orientation at the skin and shell. Lowering the C_i = 0.0035 may increase the width of the core but increases over prediction for the FT model. The most fitting solution within the deviation is given by the MFT model with parameters Ci = 0.0057 and D_z = 0.15, these parameters are identical to 2 mm plate prediction (Ci = 0.0057 and D_z = 0.15). The default MFT model under predicts the orientation with a wide core and highly aligned shell layer, with parameters Ci = 0.0009 and D_z = 0.1409. All the solutions predict (highly transverse core) the orientation at the core, which does not change with varying C_i and D_Z parameters. The transverse core prediction is in the minimum range of the random variation at location A and B. All solutions are unable to predict the random orientation within the skin at location B and C.

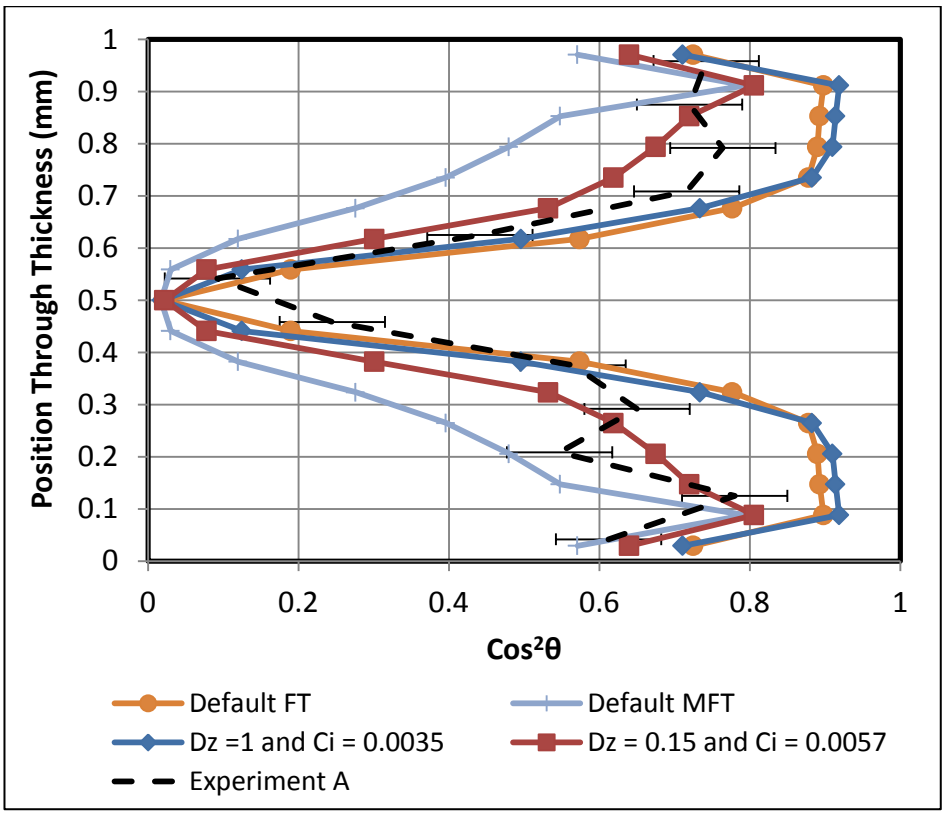

Figure 4.39 Enhanced and default predictions for FT against 1 mm centre gate average FOD at location A

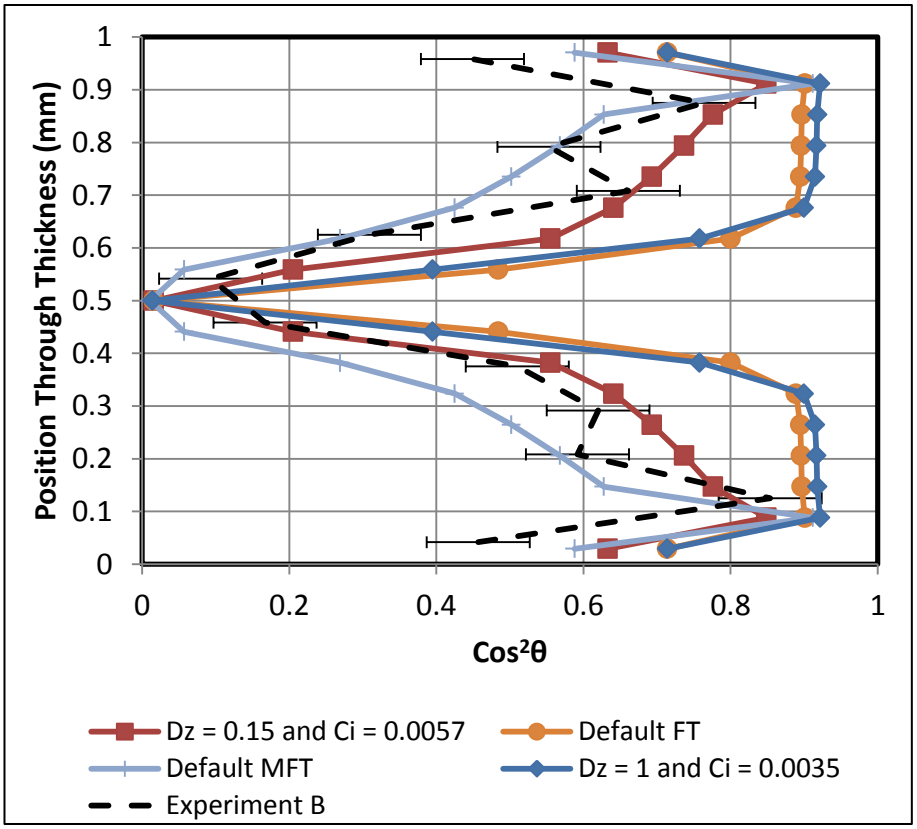

Figure 4.40 Enhanced and default predictions for FT against 1 mm centre gate average FOD at location B

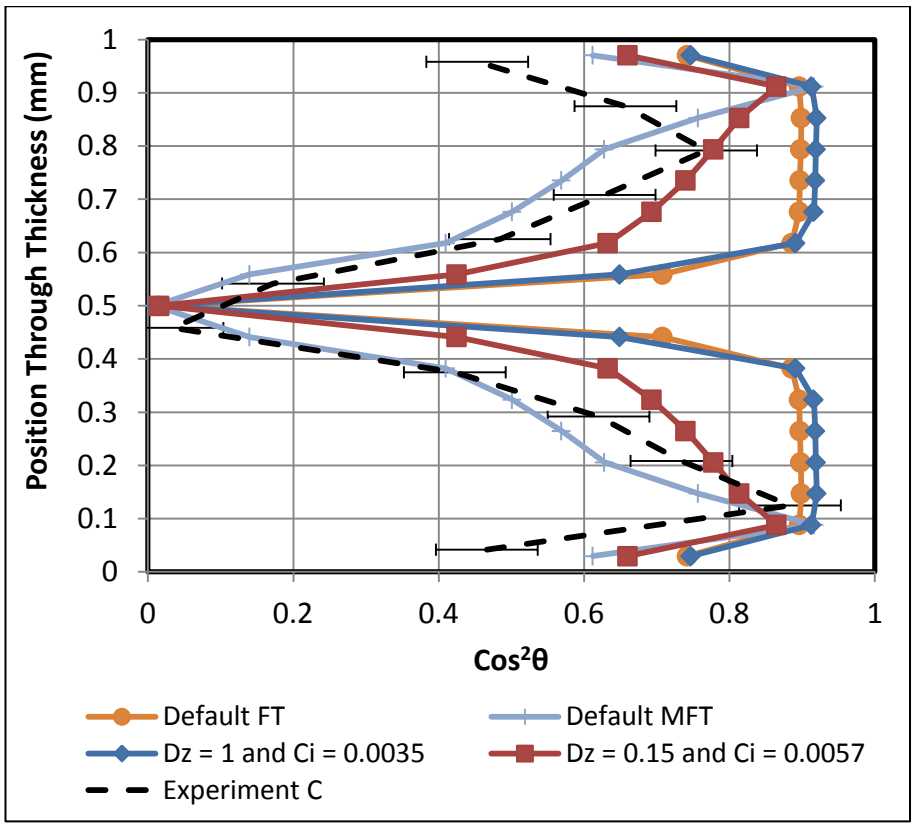

Figure 4.41 Enhanced and default predictions for FT against 1 mm centre gate average FOD at location C

4.3.4.1.2 RSC

A high k factor between 0.4 - 0.6 is required to predict the transverse orientation at the core with the RSC model. The RSC model in Figure 4.42, Figure 4.43 and Figure 4.44 over predicts the orientation at the core unlike the optimum MFT solution which is also shown; it is unable to capture the thickness of the shell and core. Although a small k factor (default 0.05) can capture the wide core the orientation at the core is over predicted. Parameters k = 0.6 and C_i = 0.0057 predict the transverse core better than parameters k = 0.4 and C_i = 0.0057. Moldflow selects a default value of C_i =0.0057 for any reduced strain factor. All RSC solutions are unable to predict the random orientation within the skin at location B and C.

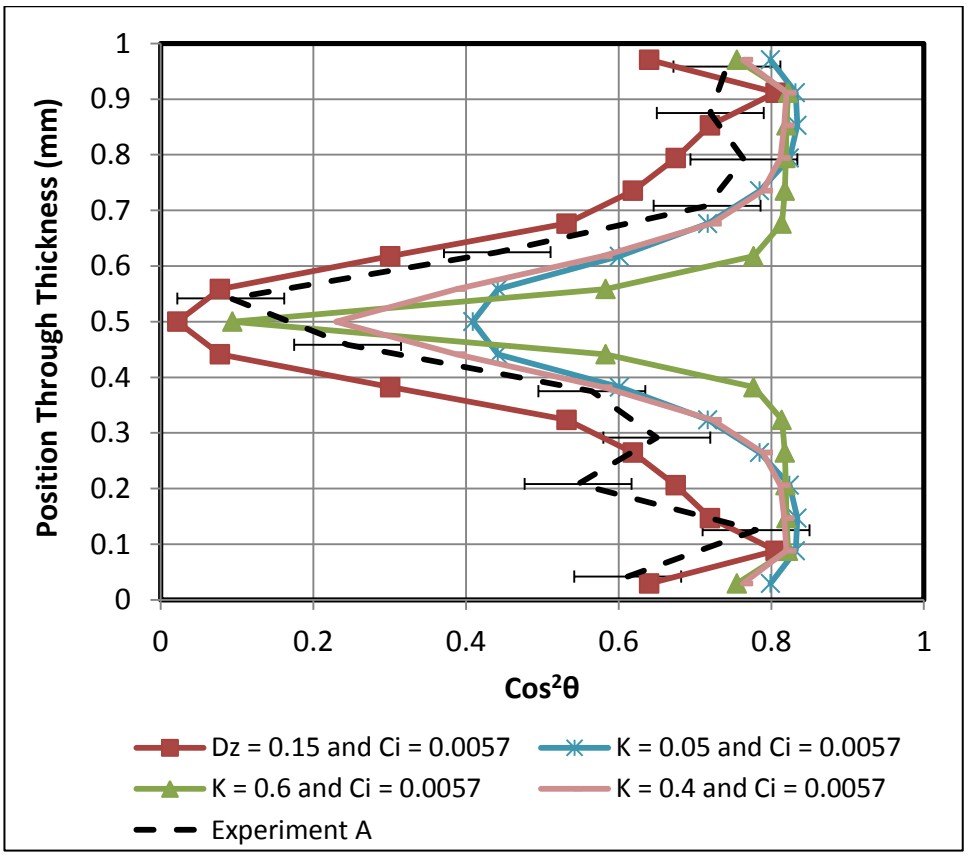

Figure 4.42 Enhanced predictions for RSC and MFT against 1 mm centre gate average FOD at location A

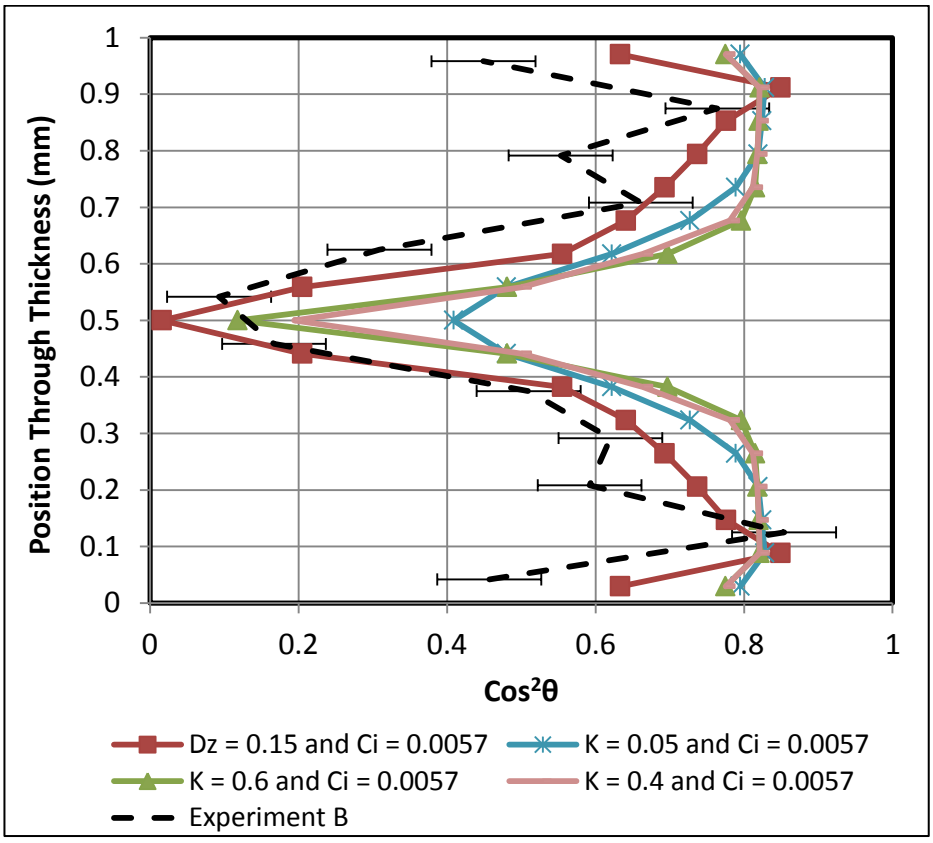

Figure 4.43 Enhanced predictions for RSC and MFT against 1 mm centre gate average FOD at location B

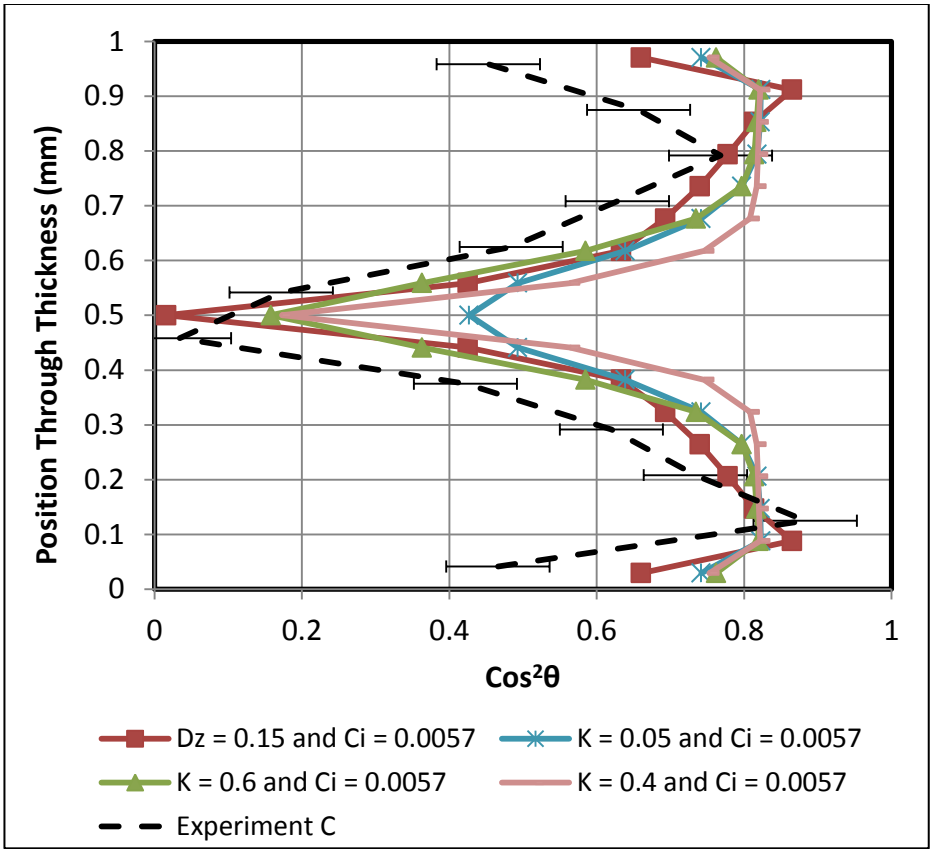

Figure 4.44 Enhanced predictions for RSC and MFT against 1 mm centre gate average FOD at location C

Inlet Condition

Within ASMI 2014 there is the option to change the default inlet profile of the predicted FOD at the injection/gate location. Currently the default input profile is set at 'fibres aligned at the skin and random at the core'. This means the $\cos^2\theta$ at the core starts at around 0.5 (random) and the fibres at the skin/shell are aligned parallel to the flow direction. However there is the option to change the inlet profile to 'fibres aligned at the skin and transverse at the core'. This means the $\cos^2\theta$ at the core starts at around 0.1 (transverse). ASMI 2014 defines the skin/shell and core orientation for both inlet conditions. The points between the skin and core are an interpolation of the cosine function which determines the width of the core.

A change was seen in the RSC prediction whilst evaluating the effect of the inlet profile. The change is shown for location A to C for the 1 mm thick centre gate geometry in Figure 4.45, Figure 4.46 and Figure 4.47. The results predict the

FOD for k= 0.05 and k = 0.4 with varying inlet conditions. The default condition with the RSC model is unable to capture the transverse core. Once the inlet condition changes to 'transverse at the core' the prediction improves. The inlet condition has more influence on smaller k (0.05) values compared to a higher value (0.4). The transverse inlet improves the prediction for k=0.05 and provides a better solution compared to a k =0.04 at location C.

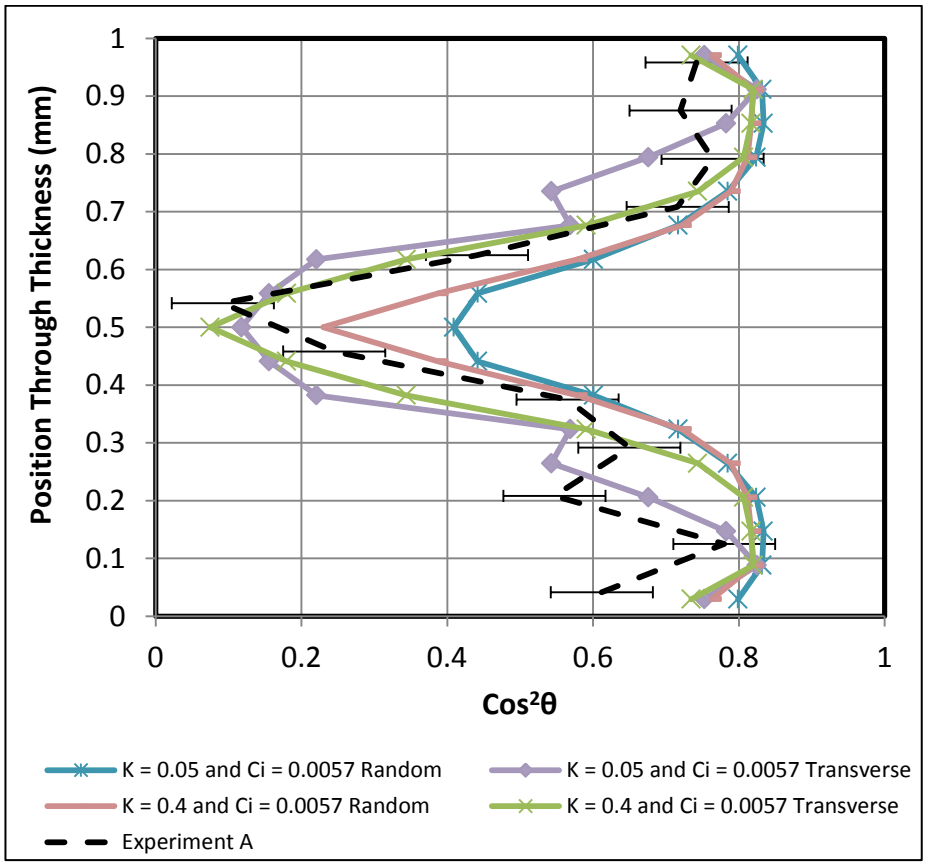

Figure 4.45 Predictions for RSC with varying inlet condition against 1 mm centre gate average FOD at location A

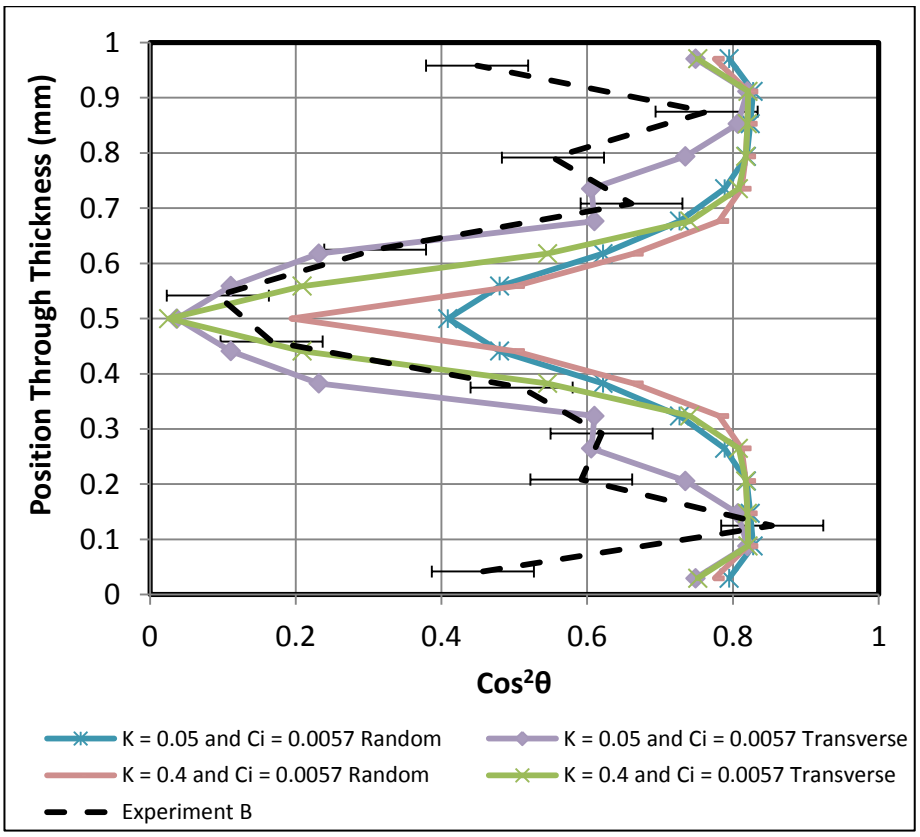

Figure 4.46 Predictions for RSC with varying inlet condition against 1 mm centre gate average FOD at location B

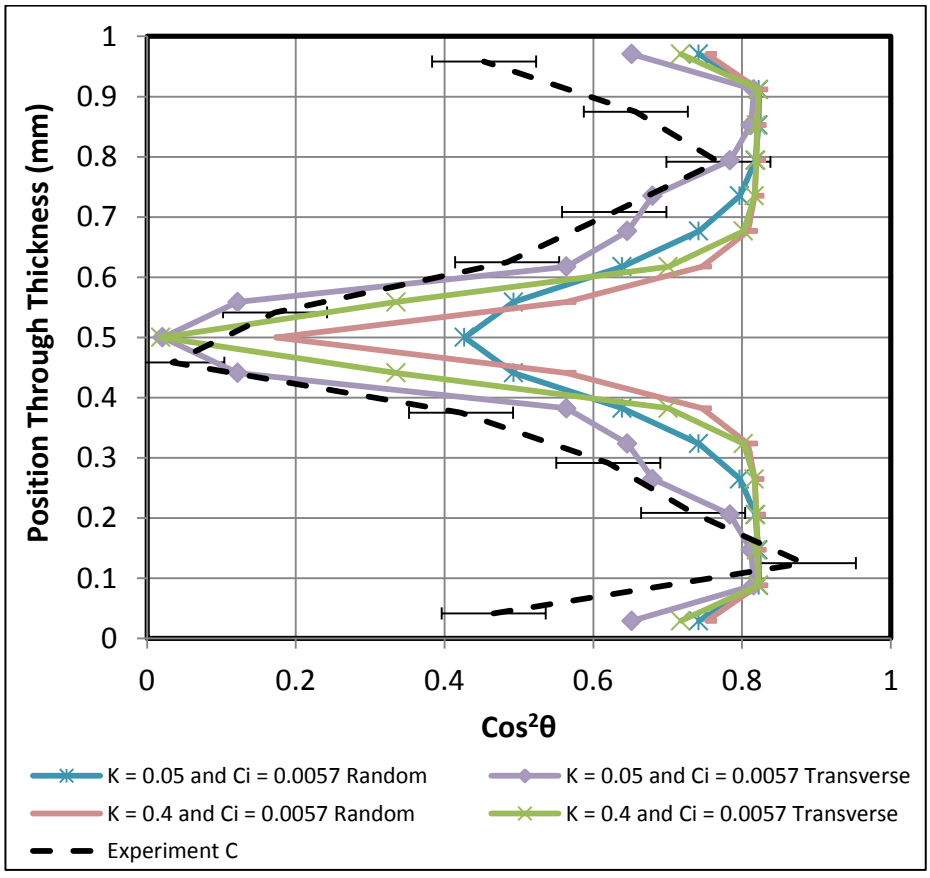

Figure 4.47 Predictions for RSC with varying inlet condition against 1 mm centre gate average FOD at location C

4.3.4.2 2 mm Thick

4.3.4.2.1 Folgar-Tucker and Modified Folgar Tucker

The measured FOD for the 2 mm thin centre gate geometry in Figure 4.48, Figure 4.49 and Figure 4.50 has a wide core oriented perpendicular to the direction of flow and the shell is oriented parallel to the direction of flow. To capture the measured FOD the C_i can range between 0.0005 - 0.001 and the D_Z parameter can range between 0.2 - 0.1. ASMI 2014 default FT uses C_i = 0.0057 to predict the FOD, this parameter over predicts the skin, shell and core layers. Applying C_i = 0.001 to the FT model increases the width of the core but does not predict the FOD better than the MFT model. The default MFT parameters C_i = 0.001 and D_z = 0.1513 and best fitting parameters C_i = 0.001 and D_z = 0.2, predict a wide core and a shell oriented in the direction of flow. All the solutions predict the transverse core within the random variation and the orientation does not change with varying C_i and D_z parameters.

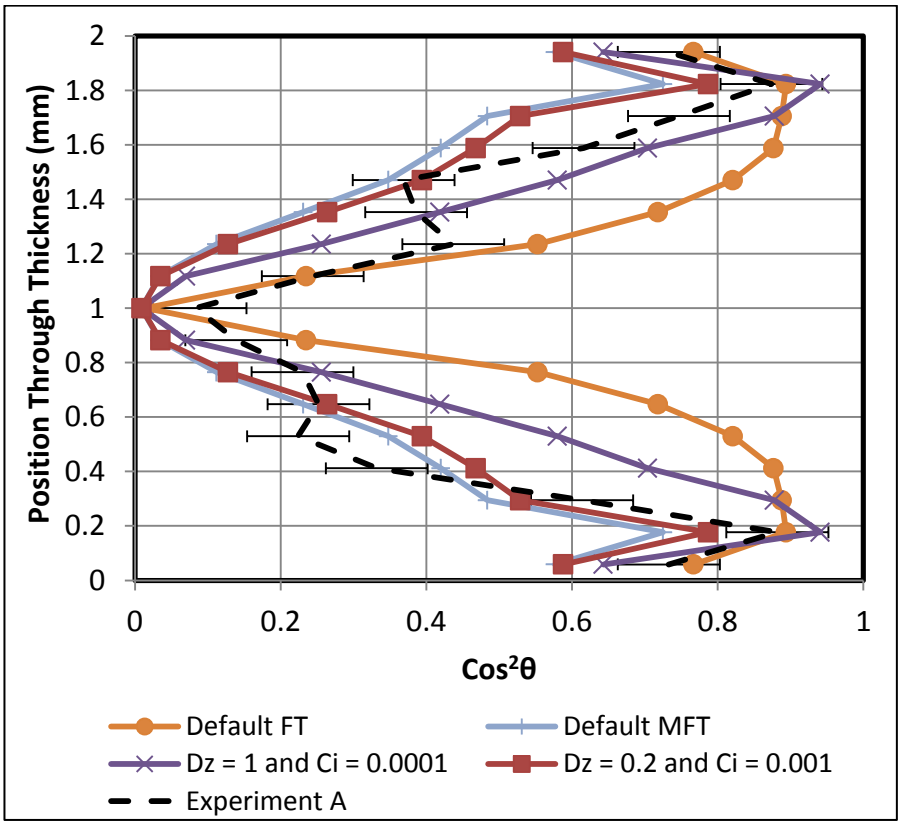

Figure 4.48 Enhanced and default predictions for FT against 2 mm centre gate average FOD at location A

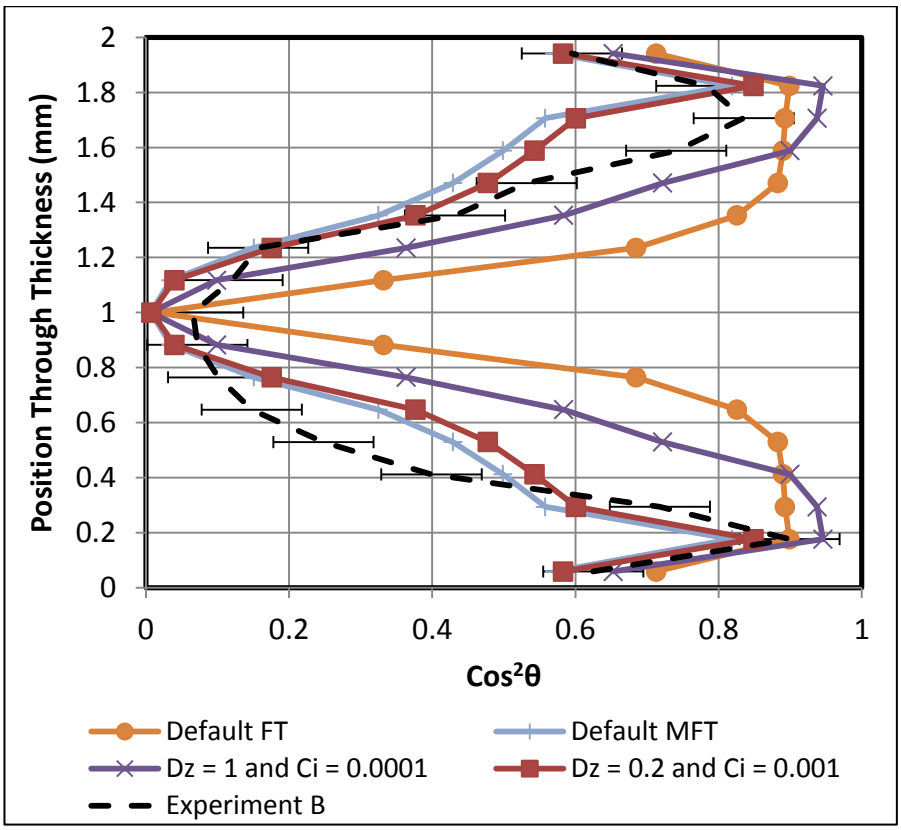

Figure 4.49 Enhanced and default predictions for FT against 2 mm centre gate average FOD at location B

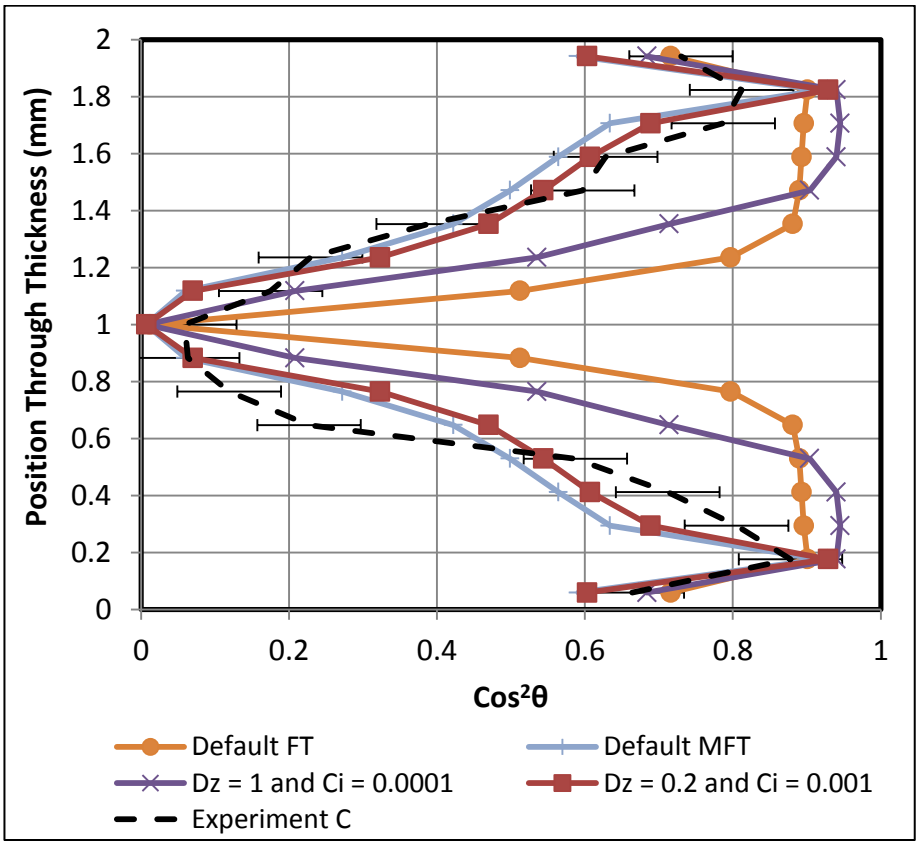

Figure 4.50 Enhanced and default predictions for FT against 2 mm centre gate average FOD at location C

4.3.4.2.2 RSC

A high k factor between 0.6 - 0.8 is required to capture the average FOD of the 2 mm centre gate component with the RSC model. The RSC model with parameter k = 0.8 (Figure 4.51, Figure 4.52 and Figure 4.53) calculates an appropriate orientation at the core but over predicts the core/shell thickness and shell orientation along the radial path. As shown the MFT model provides a better solution than the RSC model. Moldflow selects a default value of C_i =0.0057 for any reduced strain factor.

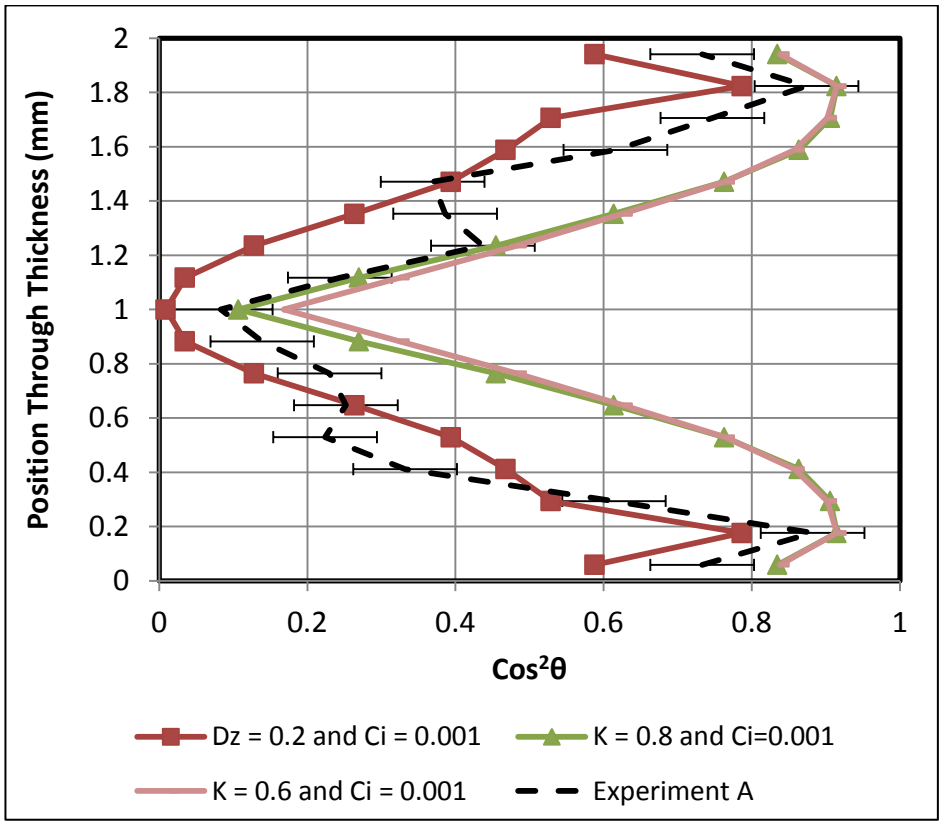

Figure 4.51 Enhanced predictions for RSC and MFT against 2 mm centre gate average FOD at location A

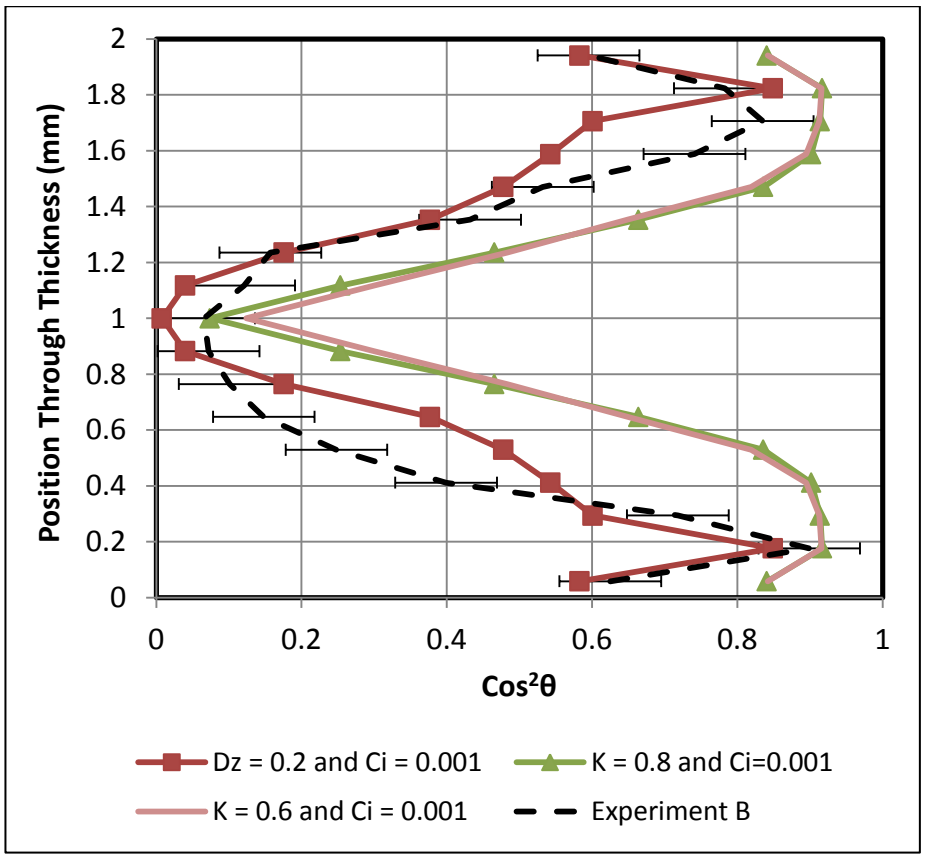

Figure 4.52 Enhanced predictions for RSC and MFT against 2 mm centre gate average FOD at location B

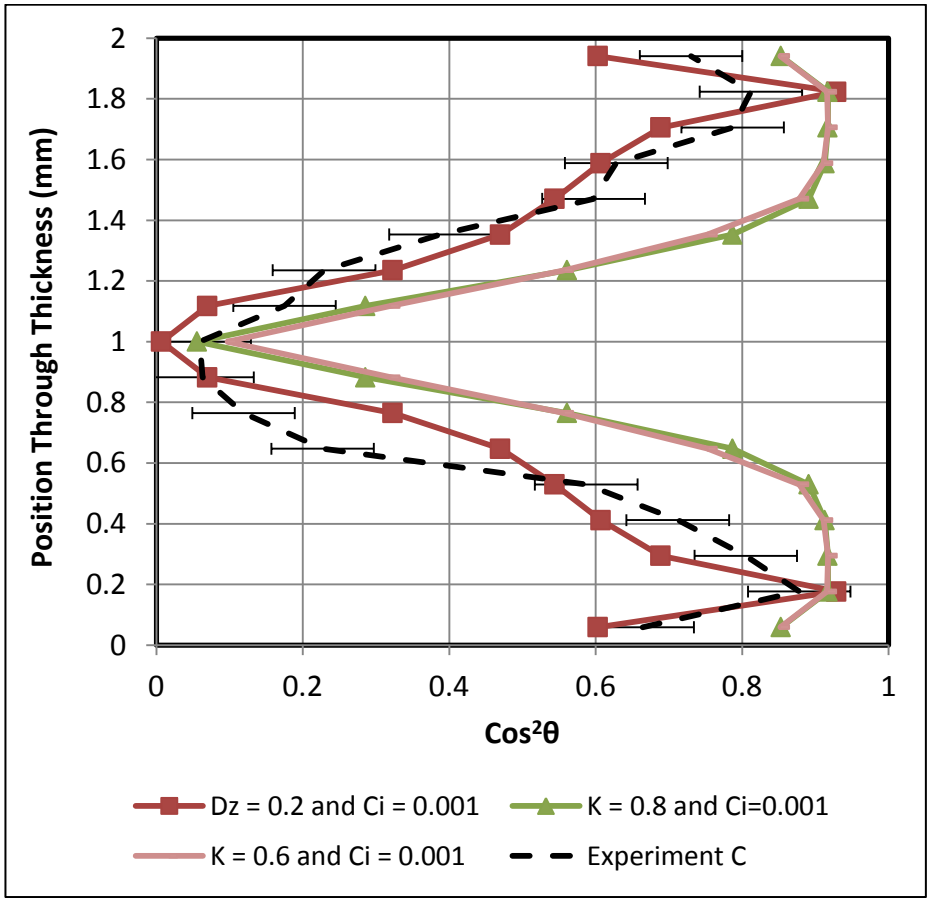

Figure 4.53 Enhanced predictions for RSC and MFT against 2 mm centre gate average FOD at location C

4.3.4.3 4 mm Thick

4.3.4.3.1 Folgar-Tucker and Modified Folgar Tucker

The majority of the fibres are oriented in a random distribution this creates a wide core where fibres are oriented perpendicular to the direction of flow within the 4 mm thick centre gate (Figure 4.54, Figure 4.55 and Figure 4.56). The fibres at the shell are partially oriented in the direction of flow but the size of the shell and skin are very small. Therefore the optimum solution for each model can be achieved using the following parameters; C_i can range between 0.0001 - 0.001 to achieve a wide core, the D_Z parameter could range between 0.2 - 0.1. The default FT uses C_i = 0.0057 to predict the FOD, by decreasing the C_i to 0.00065 the FT prediction improves and the thickness of the core increases. The MFT model provides better solutions with parameters C_i = 0.00065 and D_Z = 0.2 and default MFT C_i = 0.0012 and D_Z = 0.1857, a low C_i value increases the thickness of the core. All the solutions predict (highly transverse core) the orientation at the core, which does not change with varying C_i and D_Z parameters. The transverse core prediction is in the minimum range of the random variation at location A and B.

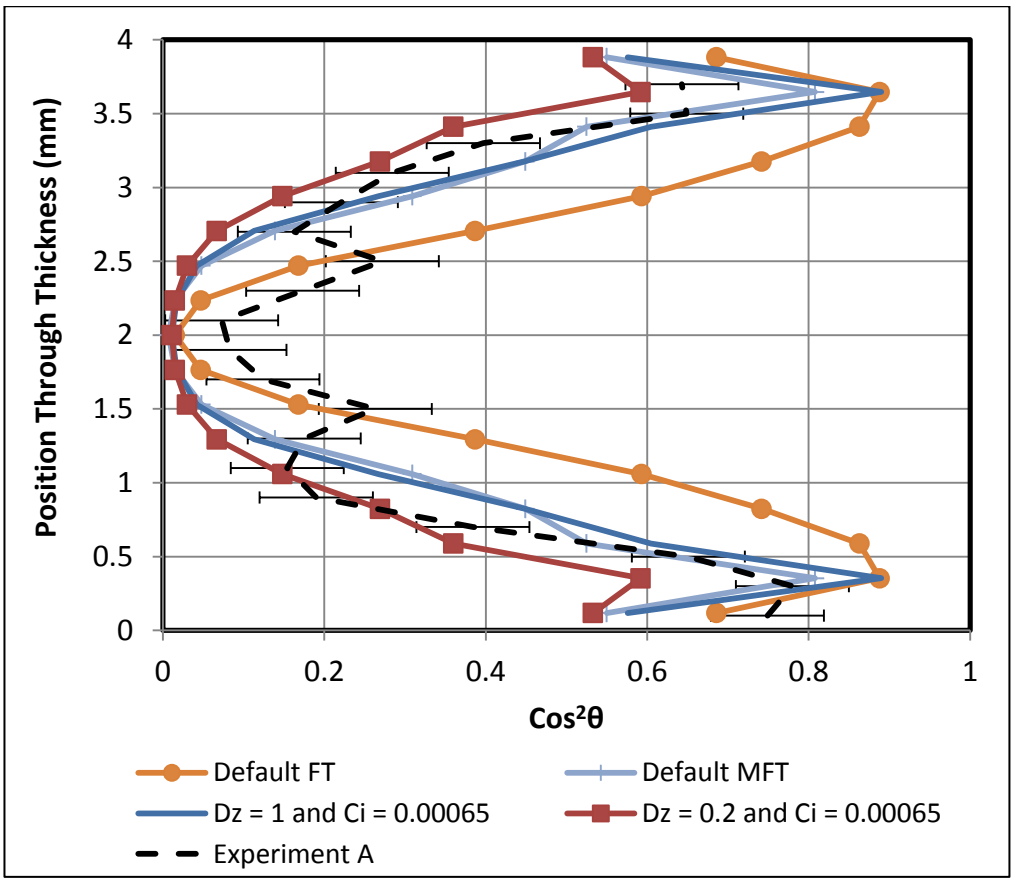

Figure 4.54 Enhanced and default predictions for FT against 4 mm centre gate average FOD at location A

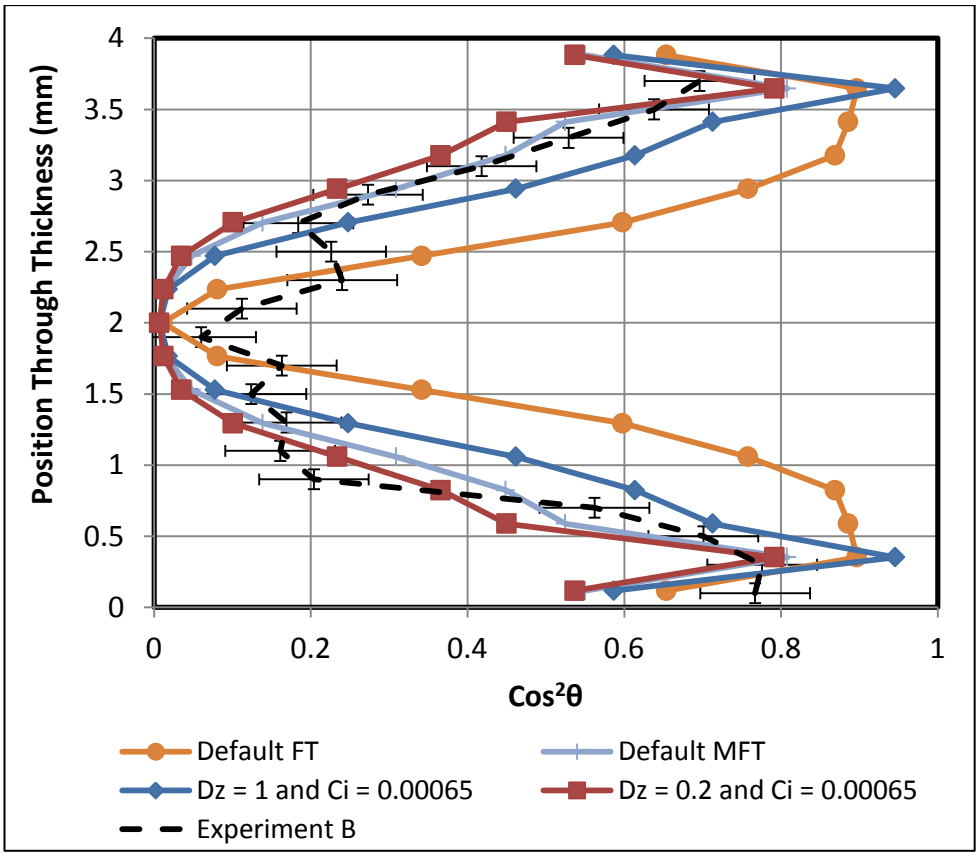

Figure 4.55 Enhanced and default predictions for FT against 4 mm centre gate average FOD at location B

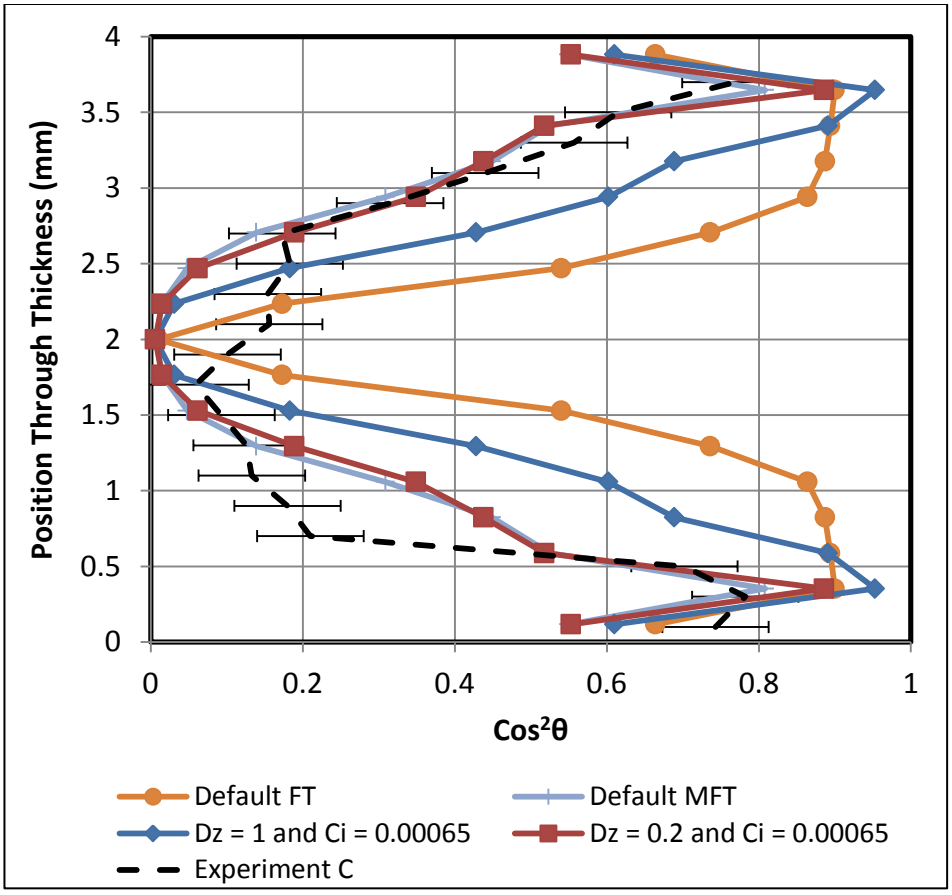

Figure 4.56 Enhanced and default predictions for FT against 4 mm centre gate average FOD at location C

4.3.4.3.2 RSC

Figure 4.57, Figure 4.58 and Figure 4.59 shows the solutions for the MFT and the RSC prediction against the 4 mm centre gate average FOD. The RSC model was investigated with C_i = 0.00065 and the k parameter in the range of 0.6 - 0.8 to predict the transverse core. The RSC model with k = 0.8 accurately predicts the highly transverse orientation at the core but is unable to predict the width of the core. The RSC model with k = 0.8 over predicts the FOD at the skin and shell along the radial direction. Moldflow selects a default value of C_i = 0.0057 for any reduced strain factor, in the case where no C_i value is supplied.

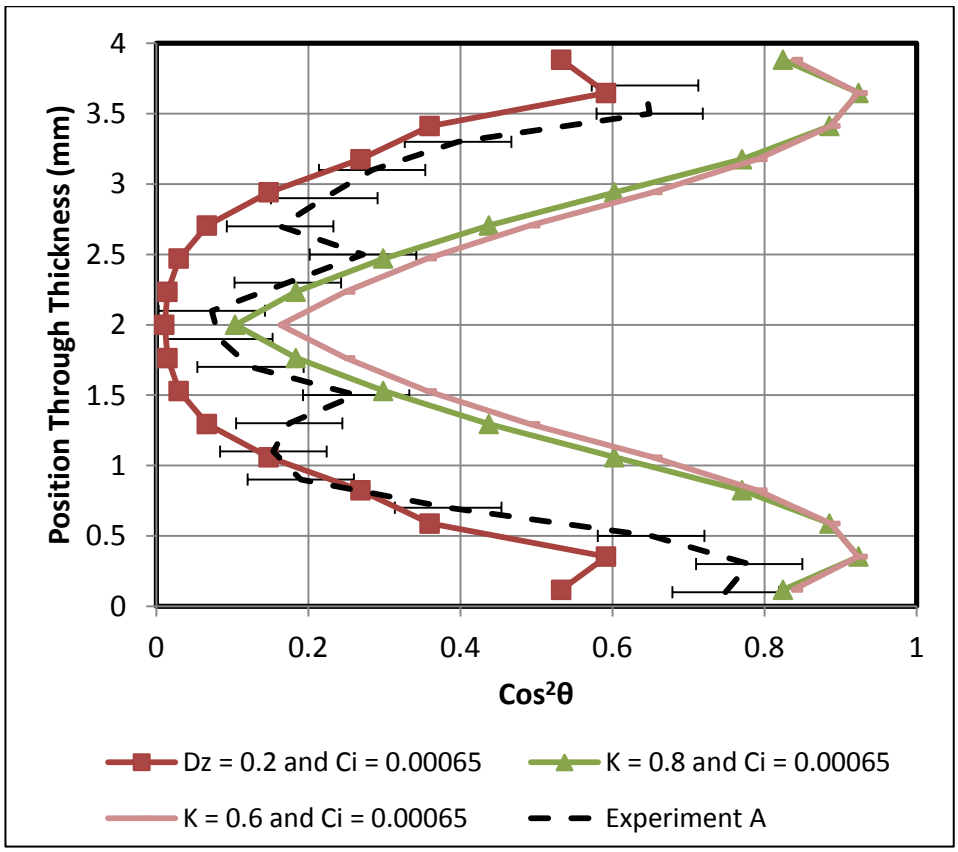

Figure 4.57 Enhanced predictions for RSC and MFT against 4 mm centre gate average FOD at location A

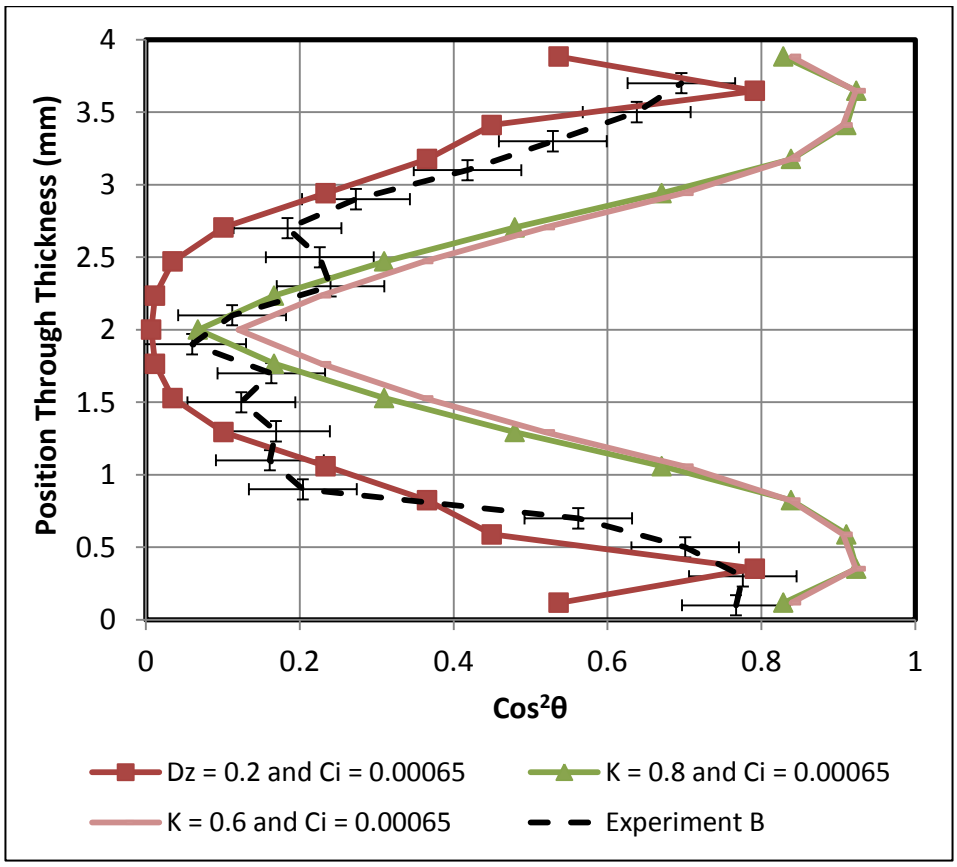

Figure 4.58 Enhanced predictions for RSC and MFT against 4 mm centre gate average FOD at location B

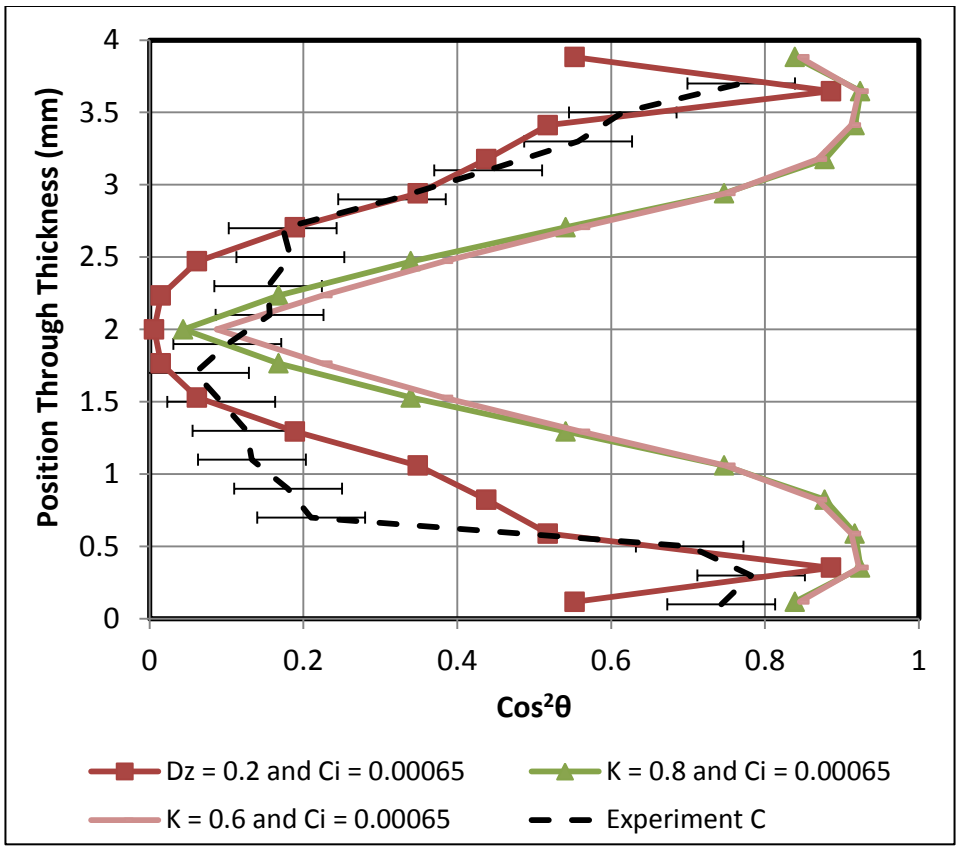

Figure 4.59 Enhanced predictions for RSC and MFT against 4 mm centre gate average FOD at location C

4.3.4.4 Summary

The MFT model reasonably (within the measured random variation) predicts the orientation within skin/shell/core layers of the 1 mm thick centre gate geometry at all 3 locations in the radial direction. The default FT parameter C_i = 0.0057 predicts the orientation at the core but over predicts the orientation at the shell, this value of C_i enhances the RSC prediction for the 1 mm thick plate. The default MFT parameters under predict the level of orientation compared to the best fitting MFT parameters (C_i = 0.0057 and D_Z = 0.2). The RSC model over predicts the level of orientation but predicts the transverse core. A small value of k (0.05) captures the wide core but cannot predict the transverse alignment. The RSC prediction can be improved to capture the core width or orientation by changing inlet condition.

For the 2 mm centre gate the MFT model offers the best solution for the FOD prediction in the radial direction, by changing the D_Z to 0.2 the default MFT prediction with parameters C_i = 0.001 and D_Z = 0.1513 is enhanced. The default FT (C_i = 0.0057) over predicts the level of orientation more than the optimum FT (C_i = 0.001) and RSC (k= 0.8 and C_i = 0.001) models. The RSC model using the default inlet is unable to capture the wide core. The MFT model also offers the best solution for the 4 mm thick geometry. Compared to the default MFT parameters the best fitting MFT parameters Ci = 0.00065 and D_Z = 0.2 over-predict less. The FT (Ci = 0.00065) does not predict the orientation as well as the MFT model but is a better solution compared to the default FT and RSC model.

The MFT model with the right choice of parameters enhances the FOD. This result is seen within the 4 mm thick sample. Although the MFT model predicts a transverse core for each thickness of the centre gate geometries the prediction remains in the random variation. Default (Moldflow) MFT parameters for the 2 and 4 mm centre gate geometries provide a good solution. These findings contradict some of the previous facts drawn from the 2 and 4 mm plate geometries. Below are some key conclusions for both the end gate and centre gate geometries.

4.3.5 Conclusions

- The FOD within the centre gate disc does not change significantly after 16 mm along the radial flow path. The $\cos^2\theta$ reduces at the skin, shell and core layers as the thickness of a plaque increases. As a result of the principal stretching within the centre gate geometry the core is wider, transversely aligned to the direction of flow compared to the plaque where fibres align in the direction of shear flow.

- The MFT and FT model can predict the in-plane stretching motion which orientates the fibres within the 1 mm, 2 mm and 4 mm centre gate geometries. However the previous findings for the end gate geometries suggest the RSC model offers a better solution, especially for the 2 mm

thick plate. Hence the RSC prediction slows down the rate orientation develops in the FT model. At present models within ASMI 2014 are not capable of predicting the FOD within the 4 mm thick plaque.

- ASMI 2014 selects a default value of C_i = 0.0057 regardless of the reduced strain factor for Rhodia Technyl C216 V40, which is 40 wt% short glass fibre. This setting is the same for any geometry or thickness and is imposed by material selection. For any part with a thickness < 1.5 mm the default value of C_i can be set to 0.0057. The optimum coefficients for the centre gate geometry do not match the findings from previous literature.

- The solution found for the C_i = 0.01 in published work is very similar to the solutions found for the fan gate geometries using the FT model. The C_i parameters for the centre geometries are different. The k parameter of 0.05 is found in the published domain and is the recommend default by ASMI 2014. However this value does not provide the best solution for both fan gate and centre gate geometries unless further adjustments are made to C_i.

- For a pin or centre geometry where in-plane stretching is influencing the direction of fibre orientation ASMI 2014 can predict the orientation up to 4 mm thickness. ASMI 2014 is able to agree with measured data up to 2 mm thick for the fan gate geometry hence the limit for accurate prediction could be between 3 - 3.5 mm. Further investigation to find the thickness limits for the fan gate problem is necessary but outside the scope of this project.

Chapter 5 Long Glass Fibre Composites

5.1 Introduction

All the long glass fibre injection moulding studies were done with SABIC® Stamax 30YM240 material. This is a 30% wt reinforced long glass fibre polypropylene material with a 12 mm pellet length. Figure 5.1 shows the FLD of 1290 measurements from a pellet with an average fibre length (L_n) of 12.52 mm. The fibre length measurements range between 12 mm and 12.98 mm. This shows that fibre breakage did not occur during the wire coating process, manufacturing of LGF material or fibre length measurement.

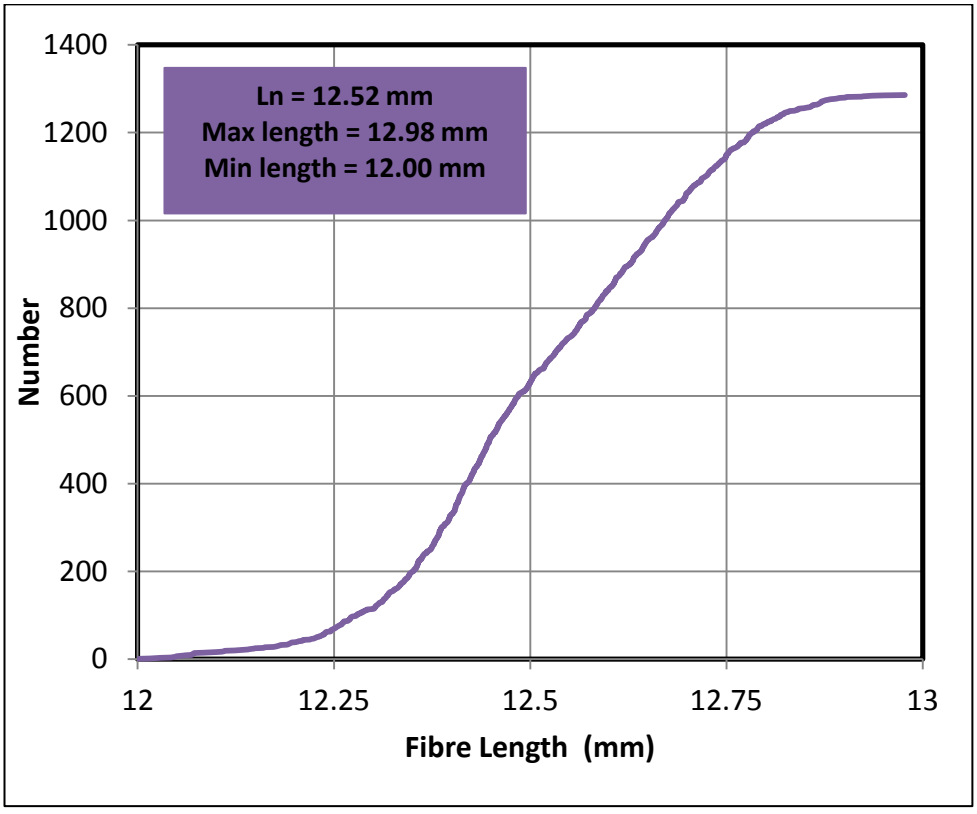

Figure 5.1 Fibre length measurements and average fibre length of the pellet material

5.2 Fibre Length Distribution

5.2.1 Geometry

Fibre length measurements were taken from the extrudate (material which goes into the sprue), top of the sprue and from 2 locations within the 1 mm and 2 mm centre gate components (Figure 5.2). This exercise was repeated for the centre gate component with sprue and nozzle modifications. Refer back to chapter 3 for more information on the sprue and nozzle modifications. The diameter of the original sprue was 3.5 mm this was increased to 6 mm for the modified centre gate geometry. Figure 5.2 is the diagram illustrating where the 12 x 12 mm square specimens were taken. The extrudate was in the form of a strand (varying width) so this was cut down to a length of 12 mm.

The 2-d centre gate geometry was implemented to verify the fibre breakage in ASMI 2014 (Autodesk Simulation Moldflow Insight) and the predicted FLD was extracted from location A and B. The area of A and B in the shell model is representative of the 12 x 12 area shown in Figure 5.2.

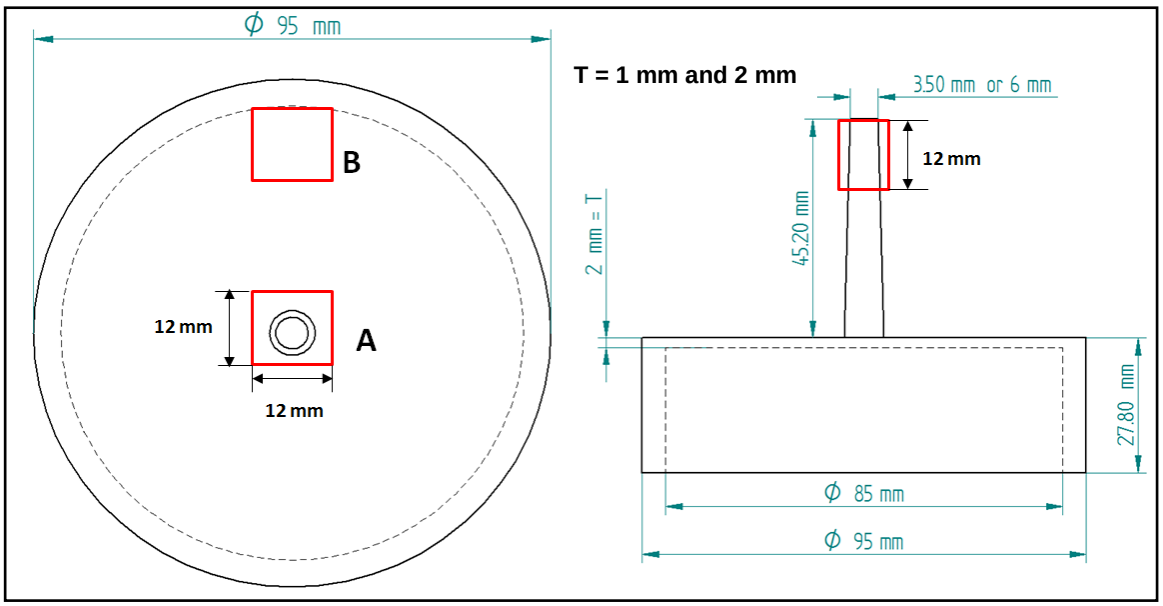

Figure 5.2 Diagram showing experiment locations A, B and sprue for FLD

5.2.2 Measurement Technique

The fibre length measurements in this chapter were carried out using the fibre length measurement technique described in Chapter 3.3 Fibre Length Distribution Measurement. In some cases the number of measured fibres for a single specimen was above 30,000. Therefore the standard procedure was to measure each sample once. Repeats were carried out for 2 samples to verify the small level of error in these large datasets. Sample 1 is a specimen taken at location B from the 1 mm centre gate geometry with a 3.5 mm sprue (Figure 5.2). Sample 2 is a specimen taken at location B from the 1 mm centre gate geometry with a 6 mm sprue (Figure 5.2). Figure 5.3 and Figure 5.4 show the FLD for sample 1 and sample 2 with their repeats, both of the dataset show very small variation in fibre length distribution (FLD) from one sample to another. The samples show a greater variation in the weight average length (L_w) than the number average length (L_n). Long fibres are more susceptible to breakage; this could be a reason for the difference in L_w between the samples. Table 5.1 shows the standard deviation for each sample and an average value of the standard deviation (0.03). The average value for the standard deviation is insignificant this shows there is a small level of error for each sample measurement.

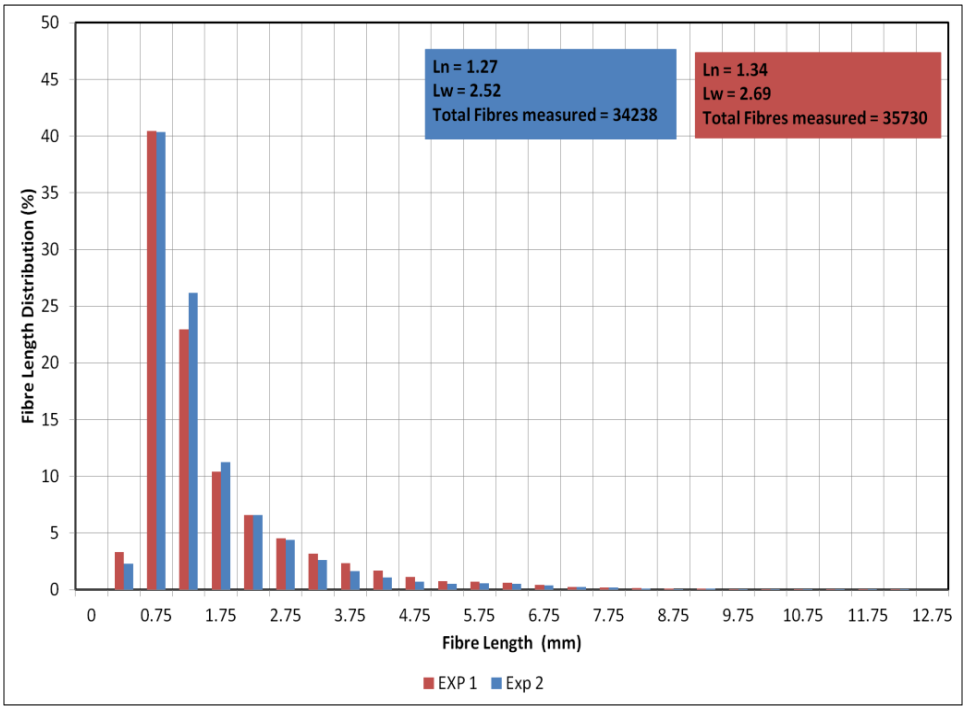

Figure 5.3 FLD for sample 1 including repeat measurement

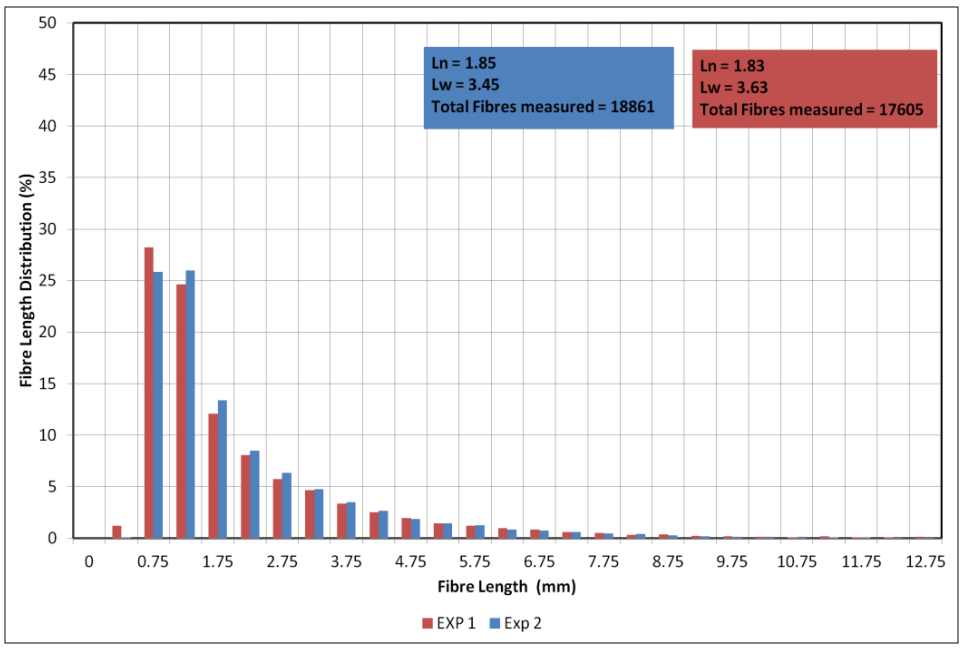

Figure 5.4 FLD for sample 2 including repeat measurement

	Standard Deviation (mm)
Sample 1	0.049
Sample 2	0.013
Average of standard deviation	0.03

Table 5.1 Average standard deviation for sample 1 and 2

To confirm the small level of error another large dataset with 36773 fibres was investigated. Fibre length measurements were taken from the large data set at random and analysed. Measurements were taken at random and added to the initial random set. This process was repeated until the entire data set was analysed. Figure 5.5 from 4530 to 36773 there is little change between the distribution at 16932 and that at 36773. Table 5.2 highlights the change in the L_n and L_w as more fibres are examined. More deviation is seen in the L_w compared to the L_n. Less change is seen in the L_n value after 16932 measurements.

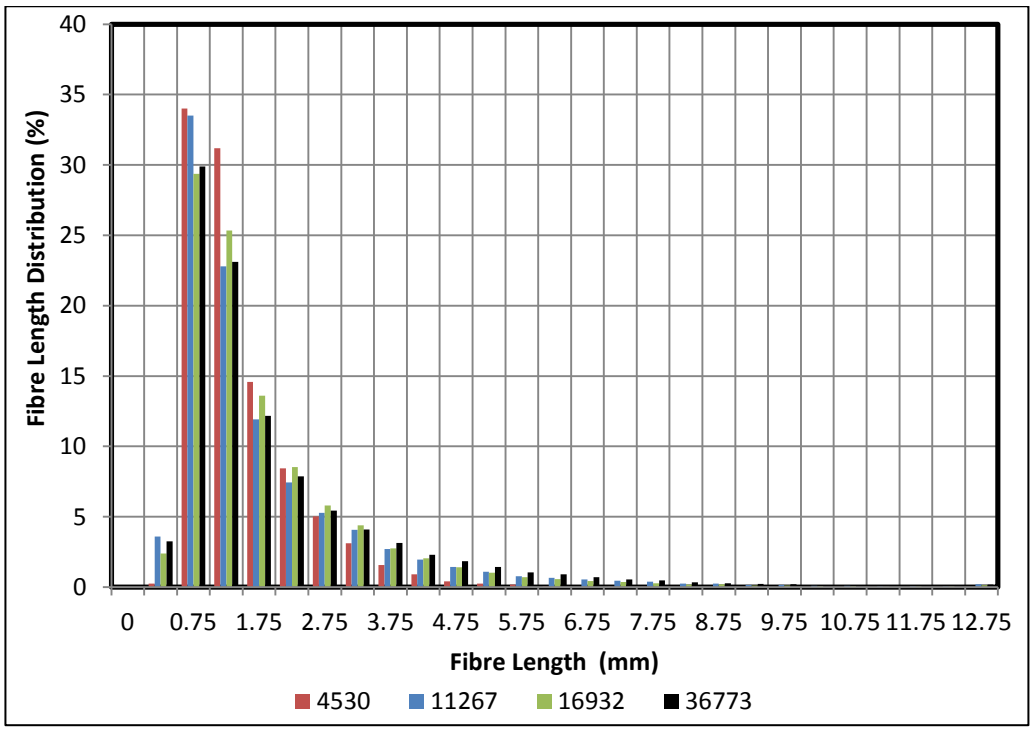

Figure 5.5 Change in FLD depending on random measurements

Number of fibres	Ln	Lw
4530	1.22	1.81
11267	1.58	3.33
13388	1.57	3.15
16932	1.58	3.03
19827	1.69	3.17
23604	1.68	3.17
36773	1.7	3.62

Table 5.2 Change in L_n and L_w as the number of random fibres increases

5.2.3 Sample size

In this study 12 mm by 12 mm square specimens were taken from the centre gate components at specific locations of interest (Figure 5.2). Inevitably fibres will be cut at the edge of the samples; in theory studying a specimen with a bigger area should reduce the proportion of fibres cut at the edge. Part of this study a comparison was made between two sample sizes from the same component. Sample 1 was 12 mm by 12 mm and sample 2 was 18 mm by 18

mm. The specimens were taken at location A from the 1 mm thick centre gate component (Figure 5.2). Figure 5.6 shows the FLD for each sample. There is a greater proportion (8%) of short fibres (< 1.3 mm) in an 18 x 18 mm sample. Apart from this difference there is a small variation in the overall distribution.

To confirm if this difference is a result of other injection moulding factors and independent of the size of the sample, the total number of fibres in the 0.25-0.75 mm fibre length range was divided by the sample area. Figure 5.7 shows the number of fibres in this length range per unit area against the position (centre) of the sample along the radial path. There are two data points for the 12 x 12 mm sample at location A and B (Figure 5.2) and one data point for the 18 x 18 mm sample at location A. Figure 5.7 indicates the proportion of small fibres in the bigger area lies within the close range of two values for the 12 x 12 mm samples along the radius. This suggests that the small difference between the FLD for the large and small specimens at 3 mm and 4.5 mm respectively could be accounted for by fibre breakage between the locations. This suggests cutting fibres at the boundaries is not a significant factor. Therefore in this study 12 x 12 mm specimens will be taken from each region of interest.

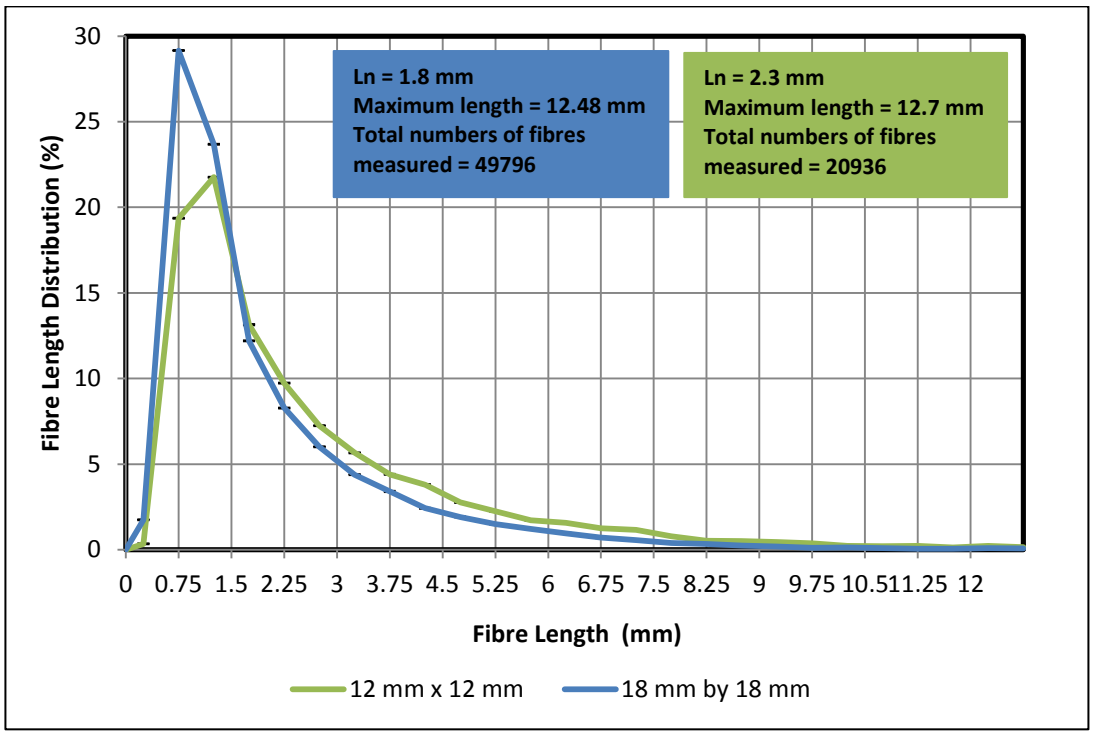

Figure 5.6 Difference in FLD between 2 sample size

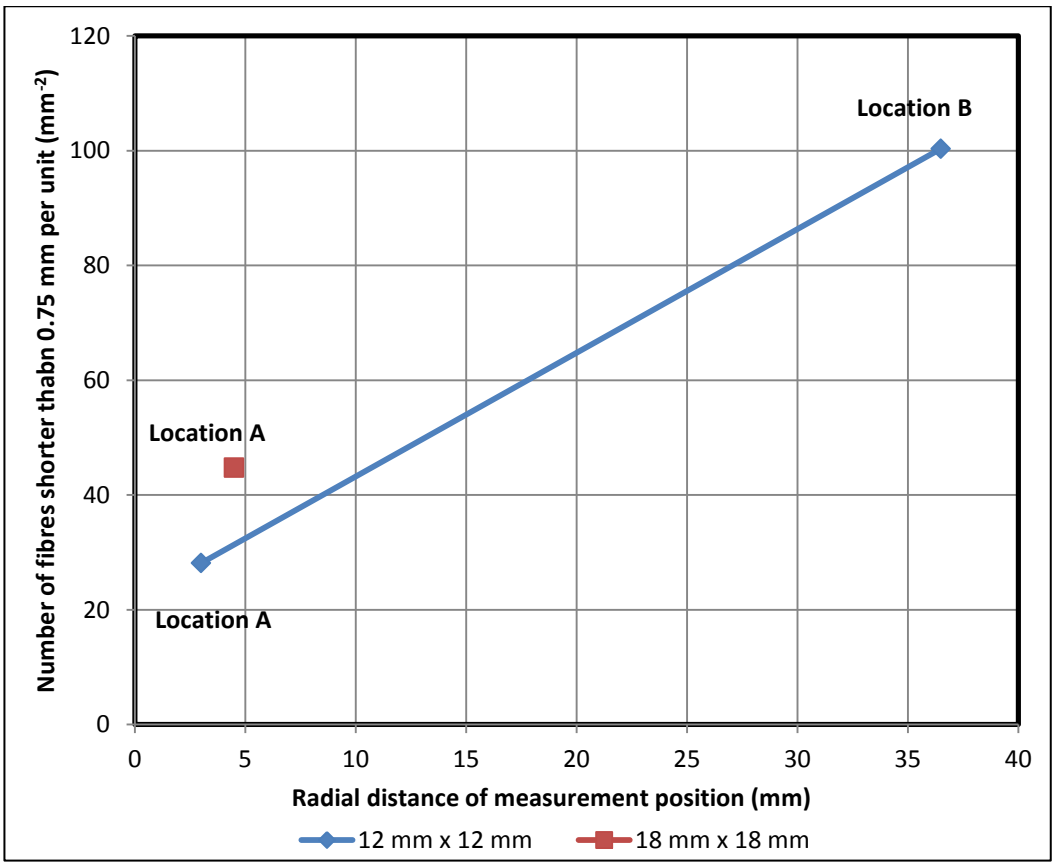

Figure 5.7 Distribution of fibres according to the area and position along radius

5.2.4 Observed curved fibres

The percentage of curved fibres increase from 4 % within the extrudate to 13 % - 33 % at different positions within the centre gate components analysed in this study, this observation was made from the fibre length measurements. The majority of the long glass fibres are sandwiched within the core layer of each injection moulded sample (Bailey and Kraft, 1987). Although the curved fibres expand after the matrix removal, the majority of them still remain curved. Figure 5.8 (a) shows the typical curvature of a long fibre found within an injection moulded component. Figure 5.8 (b) shows another arrangement of a curved fibre but this might only occur once or twice in one sample measurement.

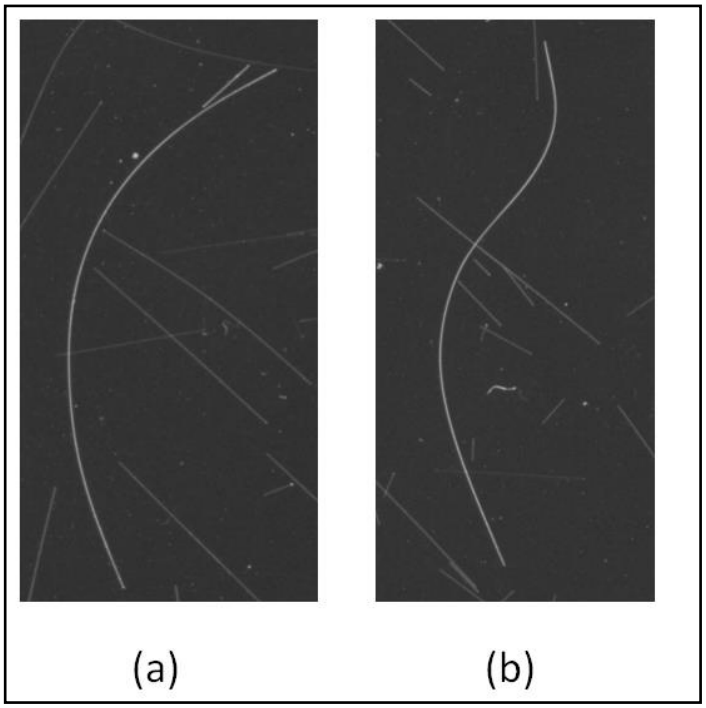

Figure 5.8 The different types of curvature found in fibres after matrix burn off

The length measurement of curved fibres is carried out using the semi-manual technique described in Section 3.3.3.2 Line Detection.

5.2.5 Experiment

5.2.5.1 1 mm Thick Centre Gate
3.5 mm Sprue

Figure 5.9 shows the FLD measured from the extrudate taken from the 3 mm nozzle (refer to Section 3.1.3.2 Modifications), and from the 1 mm centre gate geometry taken from the 3.5 mm sprue and at the two locations A and B within the component (Figure 5.2). Figure 5.10 shows the L_w and the L_n values. Before the material enters the sprue the L_n is 2.37 mm and the L_w is 5.34 mm, and the FLD shows there are more long fibres (> 9 mm) in the extrudate. The L_n is 2.19 mm and the L_w is 4.26 mm in the sprue; as a result of long fibre breakage there is an increase of short fibres with lengths in the range of 0.75 - 2.25 mm. The distribution at the gate (location A) shows relative to the sprue there is an increase of fibres with lengths in the range of 2.25 - 5.25 mm, where

L_n is 2.28 mm and the L_w is 4.20 mm. The difference of 0.09 mm in L_n could be a result of hold pressure applied to the sprue causing fibre breakage as an outcome of greater stress on the fibres. At location B the majority of the long fibres have broken and formed child fibres or short fibres, with the distribution of fibres between 0.75 -1 mm lengths now being above 40%. The L_n is 1.34 mm and the L_w is 2.69 mm at location B and the averages reflect the FLD. The short fibres in the range of 0.1 - 0.25 mm length reduce within the gate and sprue but the proportion increases at location B.

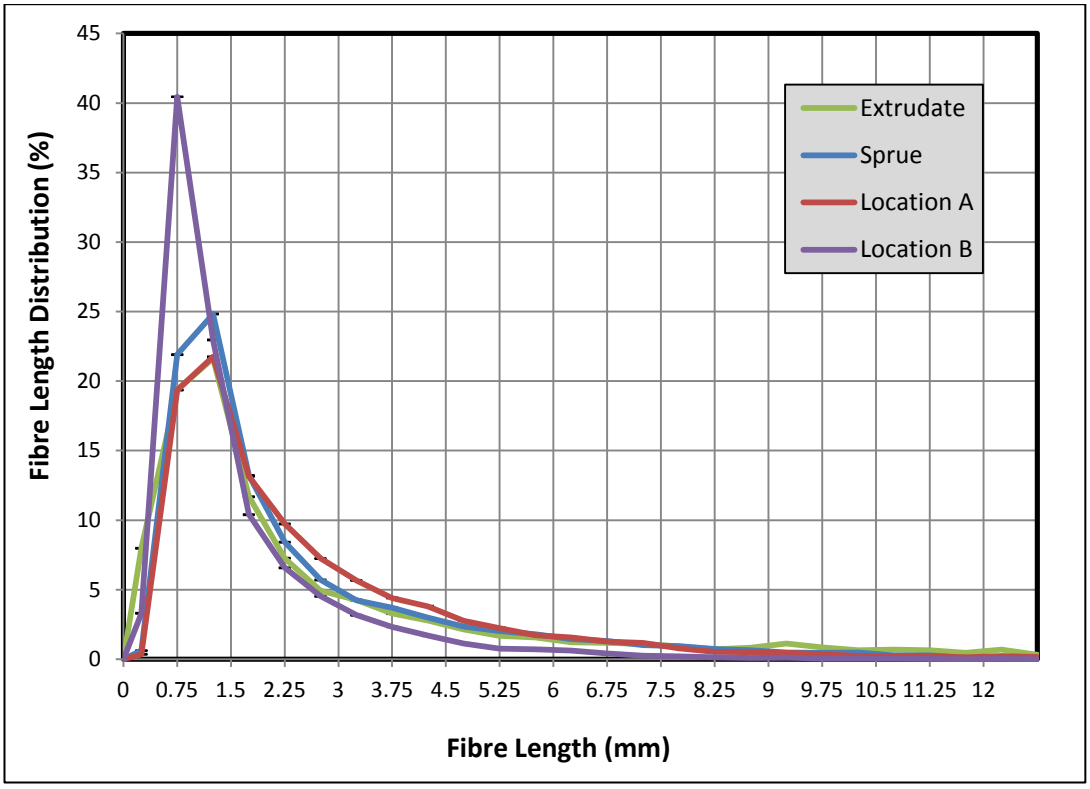

Figure 5.9 FLD measurements for 1 mm centre gate 3.5 mm sprue with error bars

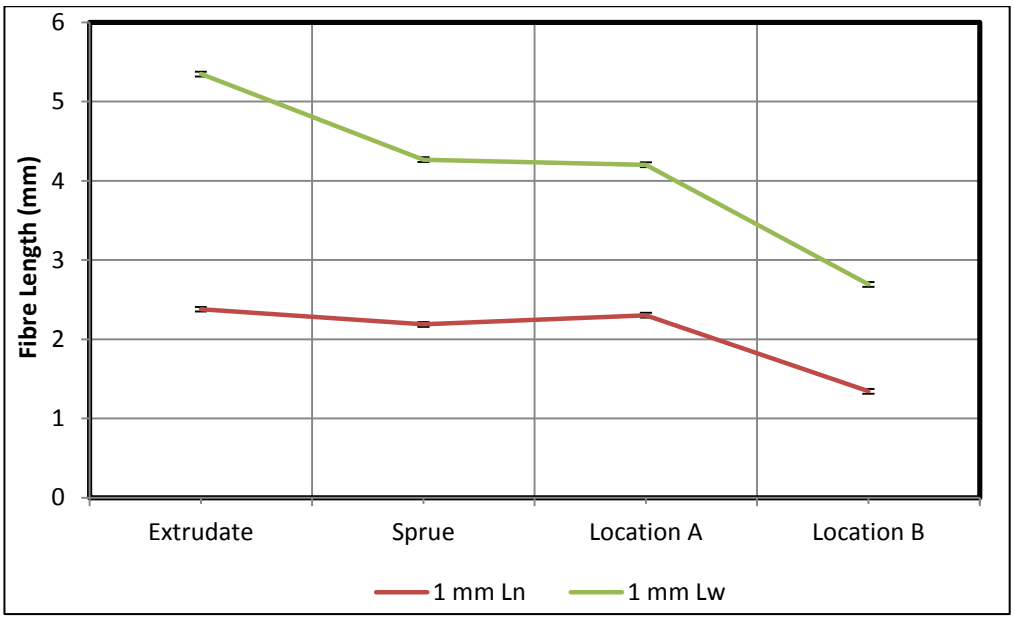

Figure 5.10 Average length for 1 mm centre gate 3.5 mm sprue with error bars

6 mm Sprue

Figure 5.11 shows the FLD once the 1 mm thick component is modified with a 6 mm sprue (Figure 5.2). FLD measured from the extrudate is taken from the 6 mm nozzle (refer to Section 3.1.3.2 Modifications). Figure 5.12 corresponds to an L_n value of 2.31 mm and L_w value of 4.53 mm for the extrudate. The extrudate from a 6 mm nozzle contains a greater distribution of short fibres compared to material from a 3 mm nozzle. Within the sprue the distribution of fibres with the length in the range of 0.75 - 1.5 mm increases; this reduces the L_n to 1.96 mm and the L_w to 4.07 mm. At the gate L_n = 2.17 mm and L_w = 3.96; the FLD of short fibres increases but the distribution of short fibres within the gate remains less than in the sprue. There is a 0.21 mm difference between the L_n of the gate and of the sprue. This finding confirms there is more breakage at the sprue when packing material into a thin cavity. The effect of the hold pressure on the fibres within the sprue is shown in Section 5.2.5.3. The L_n reflects the greater number of short fibres present within the sprue. At location B the long fibres have broken to give an L_n = 1.83 mm and the L_w = 3.62. There is a 0.48 mm difference between the values of L_n in the extrudate and location B; this means there is minor fibre breakage in the cavity.

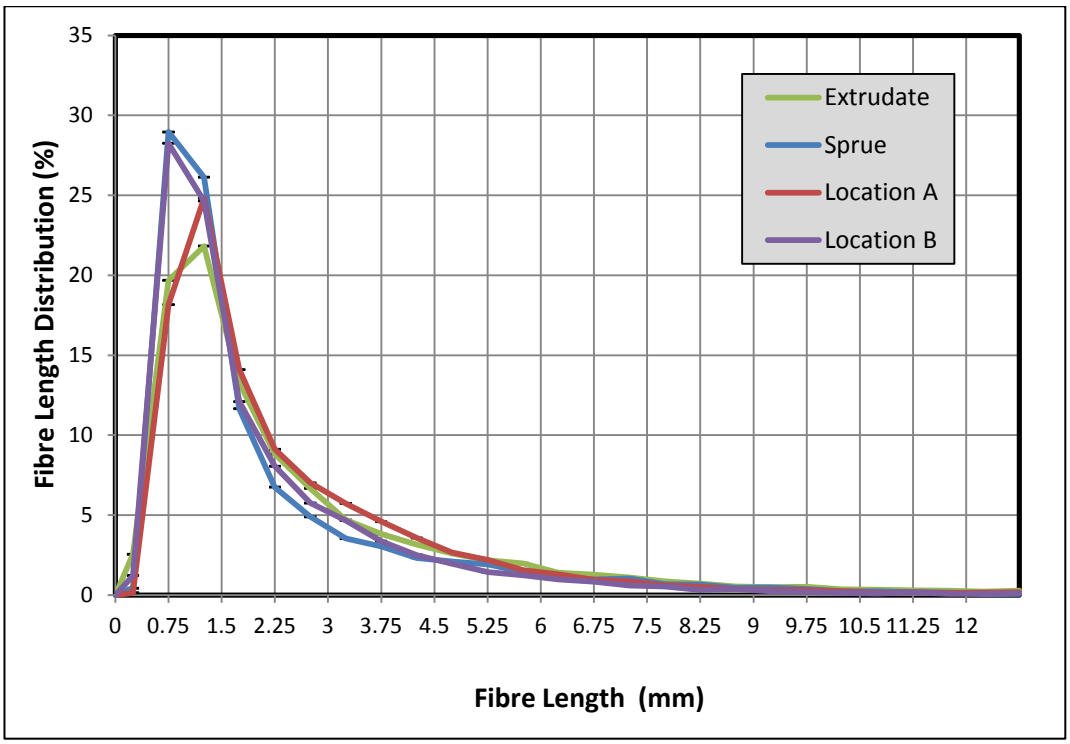

Figure 5.11 FLD measurements for 1 mm centre gate 6 mm sprue with error bars

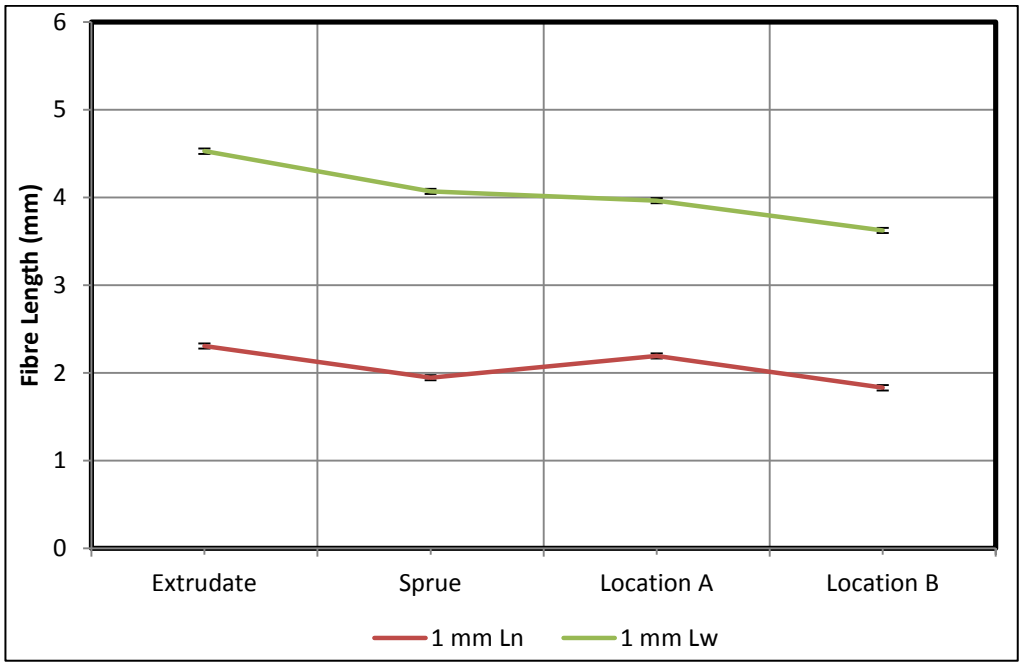

Figure 5.12 Average length for 1 mm centre gate 6 mm sprue with error bars

5.2.5.2 2 mm Thick Centre Gate

3.5 mm Sprue

Figure 5.13 shows the FLD measured from the extrudate taken from the 3 mm nozzle (refer to Section 3.1.3.2 Modifications), 2 mm centre gate geometry with 3.5 mm sprue and the two locations within the component (Figure 5.2). Figure 5.14 shows the L_w and the L_n values. Before the material enters the sprue the L_n is 2.37 mm and the L_w is 5.34 mm, the FLD shows there are more long fibres in the extrudate. The FLD shows a clear trend of long fibres breaking further along the cavity (location B). The L_w and the L_n shows a clear trend in reduction of the fibre length through the sprue to location B. At location B the L_w = 3.05 mm and the L_n = 1.59 mm, there is a 0.79 mm and 2.29 mm difference between the L_n and L_w of the extrudate and location B. This means there is a reasonable amount of fibre breakage within 2 mm thick component. The distribution of very short fibres between 0.1 - 0.25 mm length reduces at the end of the flow path.

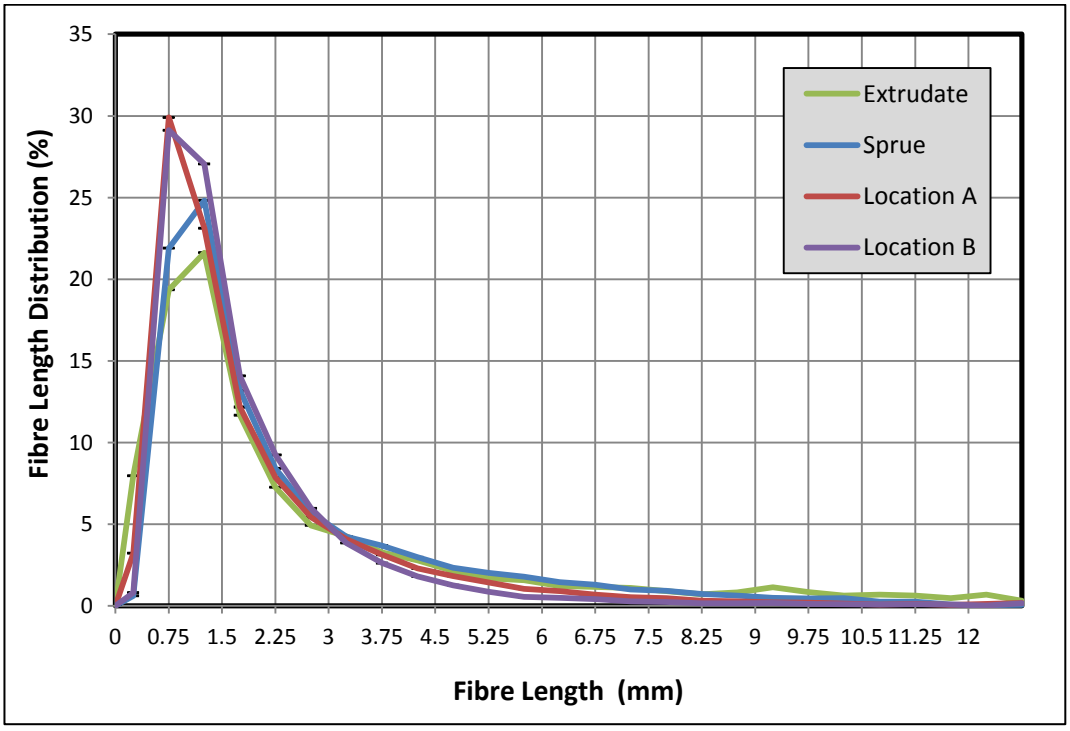

Figure 5.13 FLD measurements for 2 mm centre gate 3.5 mm sprue with error bars

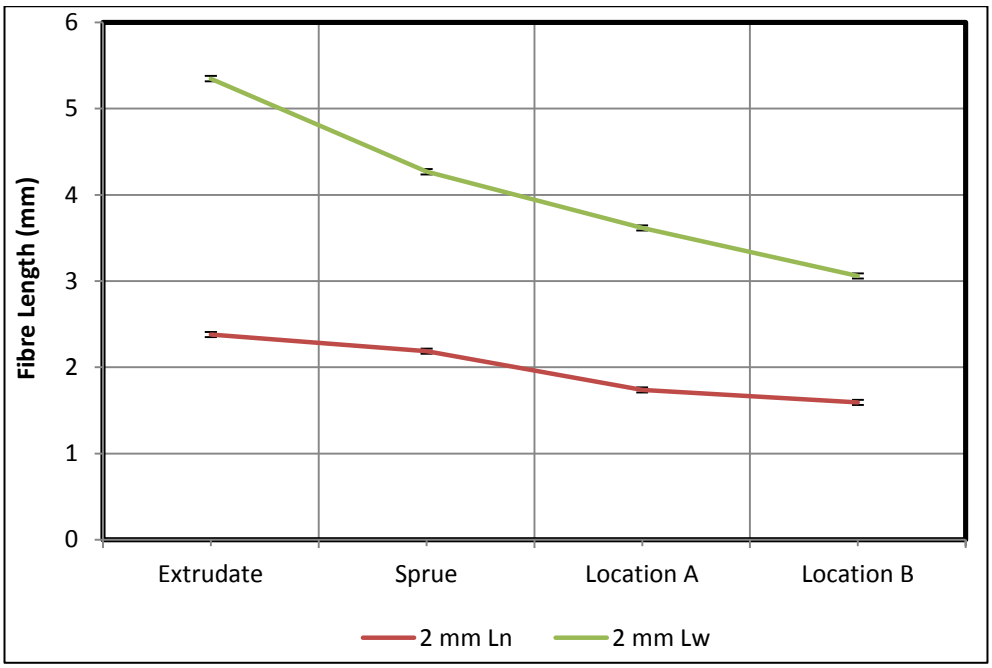

Figure 5.14 Average length for 2 mm centre gate 3.5 mm sprue with error bars

6 mm Sprue

Figure 5.15 shows the FLD once the 2 mm thick component is modified with a 6 mm sprue (Figure 5.2). Figure 5.16 corresponds to an L_n value of 2.31 mm and L_w value of 4.53 mm for the extrudate. The FLD and the average fibre length shows there is very little change or fibre breakage between the sprue where L_n =1.94 mm and at the gate L_n =1.98 mm. There is a greater proportion of short fibres (< 1.5 mm) within the sprue but more long fibres have broken within location A hence a 0.17 mm difference in L_w. As expected the fibre breakage increases at location B. This results in more fibres with the length in the range of 0.75 - 2.25 mm. At location B the L_n =1.78 mm and L_w =3.54 mm, giving a 0.35 mm and 0.99 mm difference between the L_n and L_w respectively of the extrudate and location B. This means there is minor fibre breakage within 2 mm thick component with a 6 mm sprue. The distribution of very short fibres between 0.1 - 0.25 mm length reduces at the end of the flow path.

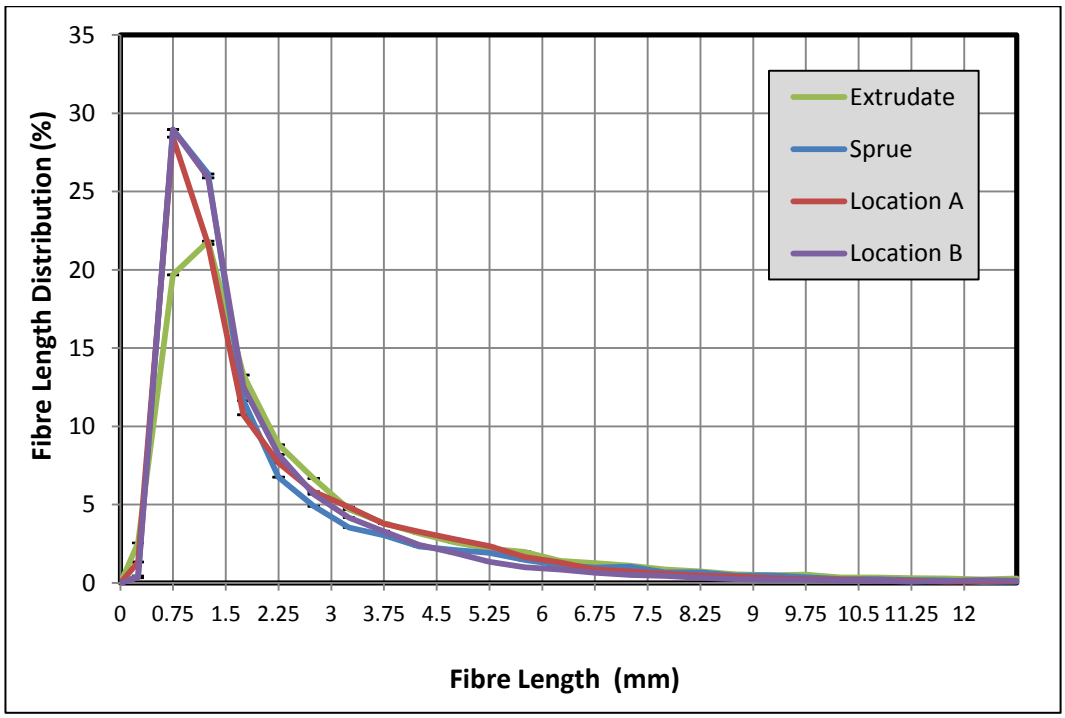

Figure 5.15 FLD measurements for 2 mm centre gate 6 mm sprue with error bars

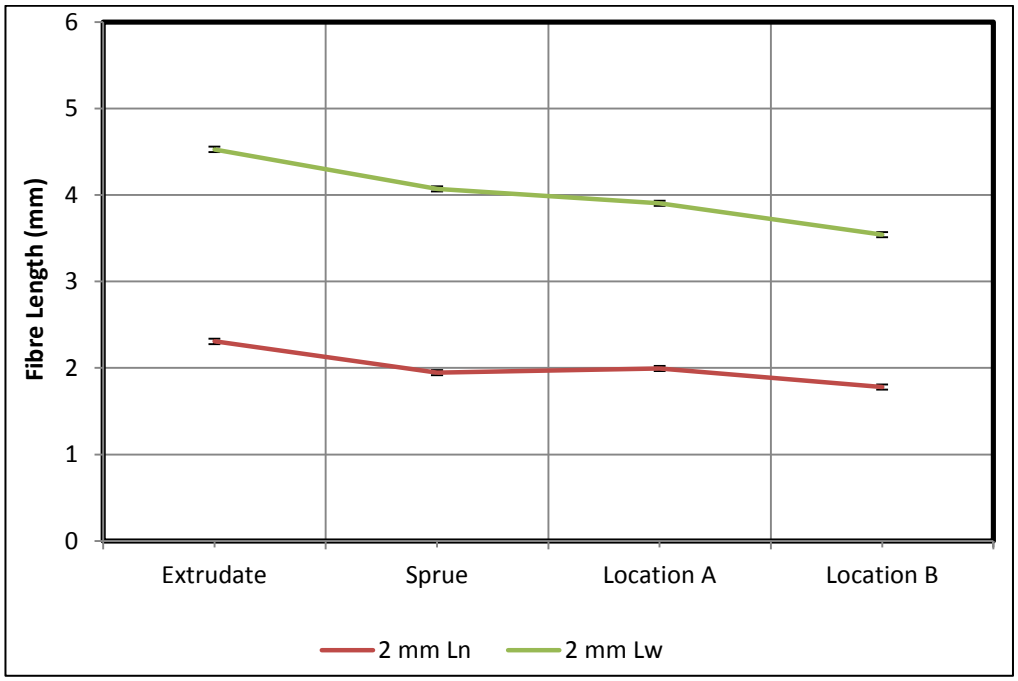

Figure 5.16 Average length for 2 mm centre gate 6 mm sprue with error bars

5.2.5.3 Evaluation

Comparison has been made between the weight-averaged length (L_w) (Figure 5.17) and the number averaged length (L_n) (Figure 5.18) for the 1 mm and 2

mm thick centre gate geometries for the 3.5 mm and 6 mm sprue (Figure 5.2). To calculate the total breakage at location B, a percentage difference was calculated between the L_n within the pellet and the L_n at location B (Equation 5.1). In Equation 5.1 L_p is the number average fibre length in the pellet and L_b is the number average fibre length in the sample at location B.

$$\Delta l = \left[\frac{(L_p - L_b)}{L_P}\right] \times 100 \qquad \textbf{5.1}$$

Figure 5.17 and Figure 5.18 illustrate the total breakage is less in the 2 mm thick centre gate geometry with a 3.5 mm sprue compared to a 1 mm thick geometry where shear flow causes breakage to reach 89.3%, reducing L_n to 1.34 mm and L_w to 2.69 mm. There is more breakage at location B within the 1 mm centre gate geometry compared to 2 mm centre gate geometry. The average fibre length at location B shows more fibres break if the gate is smaller. The total breakage in the 2 mm thick centre gate cavity with a 6 mm sprue is the same as the 1 mm thick geometry. This is indicated by a similar L_n and L_w. However a similar trend is seen at location A between the 1 mm and 2 mm thick geometries with a 6 mm sprue; there is less fibre breakage if the gate is wider.

The number average fibre length within the extrudate from the 6 mm and 3 mm nozzle remains the same; there is a greater volume of long fibres (L_w) present in the 3 mm extrudate. The L_n in the 6 mm sprue is less than the 3.5 mm sprue therefore the increase in the sprue size results in more fibre breakage. The total breakage in a 1 mm thick cavity with a 6 mm sprue is 3.9 % less compared to the 1 mm thick cavity with a 3.5 mm sprue. The average L_w and L_n is similar at location A for the 1 mm cavities. The total breakage in a 2 mm thick cavity with a 6 mm sprue is 2 % less compared to the 2 mm thick cavity with a 3.5 mm sprue. There is a 0.25 mm difference between the L_n at location A for both 2 mm geometries with different sprues, this difference is more compared to the thin cavity. This means a small sprue attached to a 2 mm thick gate results in more fibre breakage as a wider sprue allows higher packing pressure at location A.

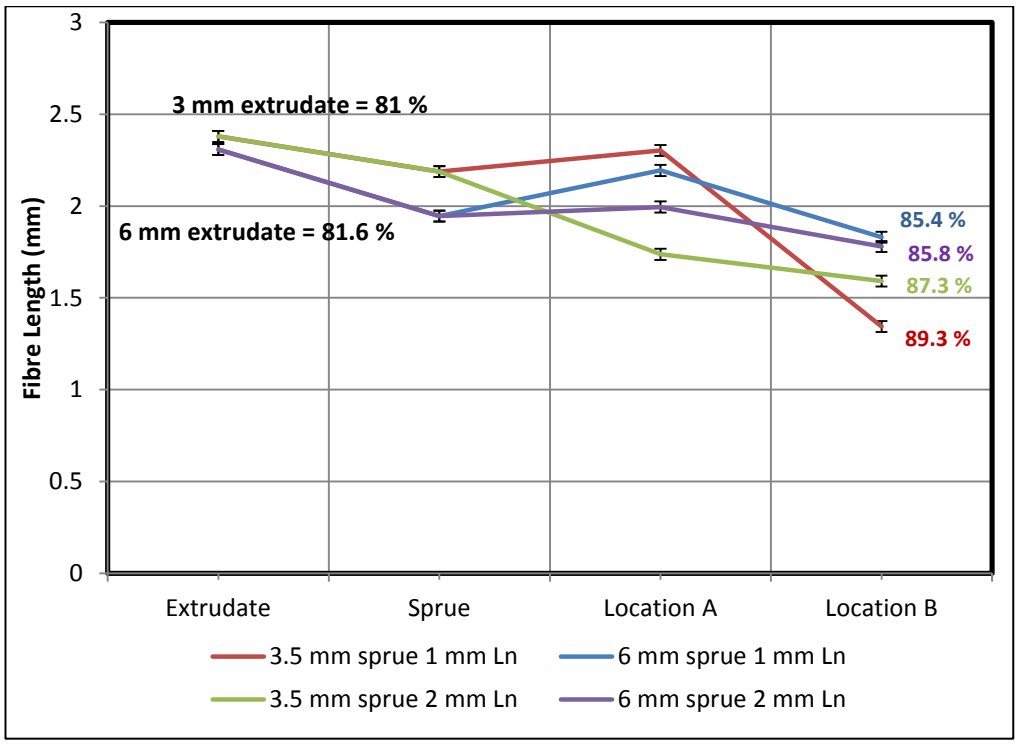

Figure 5.17 Comparison of average length between centre gate geometries. Percentages refer to breakage as defined in equation 1

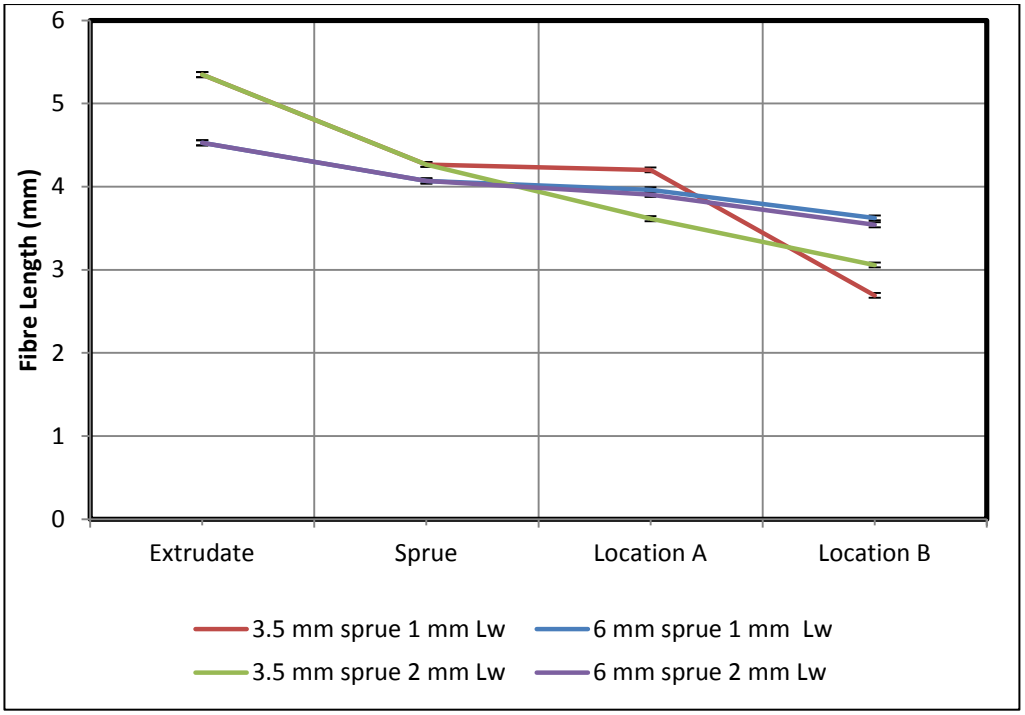

Figure 5.18 Comparison of weighted average length between centre gate geometries

The FLD for the 1 mm components (6 mm and 3.5 mm sprue) shows there are a greater proportion of short fibres, within the sprue in comparison with location

A. The greater proportion of short fibres results in a lower L_n for the sprue compared to location A. To understand if this was a result of the hold pressure applied during injection moulding the FLD was measured from the 3.5 mm sprue geometry before hold pressure. Figure 5.19 shows the difference in the 3.5 mm sprue when there is no hold pressure applied to the 1 mm centre gate geometry. The results show there is breakage of long fibres caused by the hold pressure applied at the sprue. The results before hold pressure for both averages are slightly higher compared to location A (Figure Figure 5.10) where Ln is 2.28 mm and the Lw is 4.20 mm. These results highlight fibre breakage at the sprue after packing material into a thin cavity.

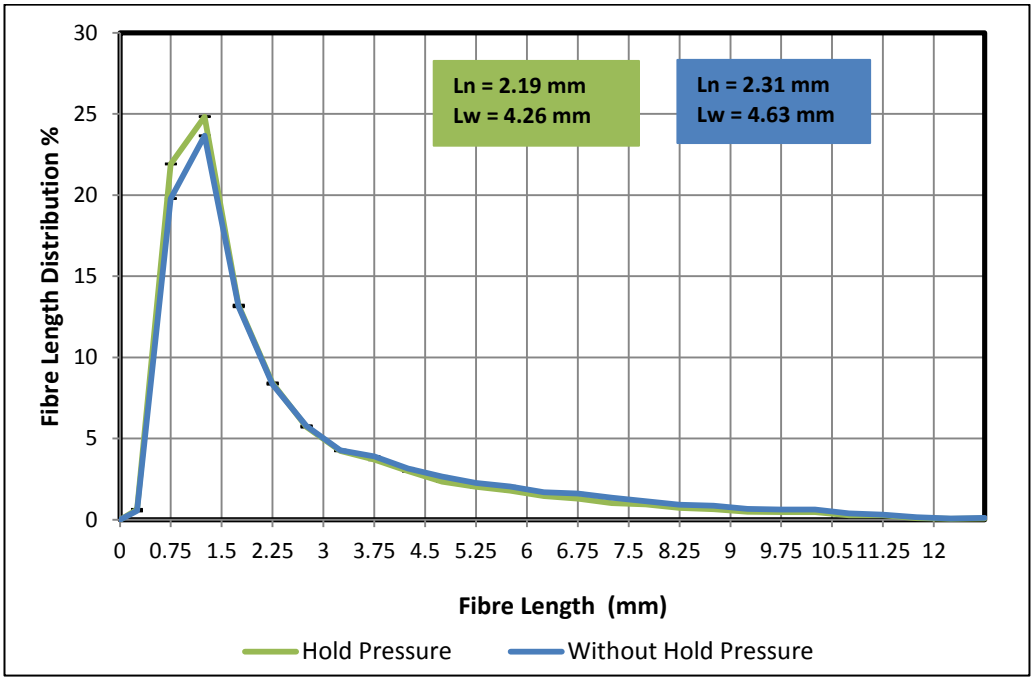

Figure 5.19 Difference in FLD and average length in sprue due to hold pressure

5.2.5.4 Summary

The average fibre length is similar for extrudate extracted from a 6 mm or 3 mm nozzle but there is more breakage within a 6 mm sprue compared to a 3.5 mm sprue (Figure 5.2). This difference could be a result of increase in fibre-fibre interactions. The results show the highest total breakage was within the 1 mm centre gate geometry with a 3.5 mm sprue. If the thickness increases the average fibre length increases at location B. There is less fibre breakage within the 1 mm centre gate with a 6 mm sprue compared to a 3.5 mm sprue. The

average fibre length at location B for the 1 mm and 2 mm geometry with a 6 mm sprue is similar. The fibre breakage reduces at location B if the thickness of the geometry increases to 2 mm with either sprue geometry. There is more breakage when a 3.5 mm sprue is filling a wide gate compared to a 6 mm sprue. A clear trend in fibre breakage is seen in the FLD for the 2 mm centre gate geometries. The FLD for the 1 mm components result in more fibre breakage within the sprue caused by the hold pressure when applied to a thin cavity. A wider sprue reduces the total fibre breakage within the 1 mm thick geometry. The size of the sprue has little influence on the overall fibre breakage within the 2 mm thick geometry.

5.2.6 Prediction

The fibre breakage model (Equation 2.20) in ASMI 2014, can predict the fibre breakage within the component. By default the breakage model uses the initial average fibre length of the pellet (12.5 mm), but there is the option for a user to input the initial fibre length distribution as described in Section 3.4.3.1 Breakage Model. For this study the measured extrudate and sprue FLD was input into ASMI 2014, to predict the FLD at location A (Figure 5.2). To predict the FLD at location B (Figure 5.2) the measured extrudate, sprue and gate FLD was input into ASMI 2014. The prediction from each input will be assessed against the measured FLD. For this exercise the 3 scalar factors will remain default at C_b= 0.002, D_g = 3 and S = 0.25.

5.2.6.1 1 mm Centre Gate
3.5 mm Sprue

Figure 5.20 and Figure 5.21 shows the prediction for each FLD input into the fibre breakage model for the 1 mm centre gate with a 3.5 mm sprue at location A and B (Figure 5.2). Table 5.3 contains the measured and predicted average fibre lengths (L_n) at location A and B. The default FLD (pellet length as input) predicts inaccurate fibre breakage with 60 % and above fibres remaining at 12.5 mm (initial length) at both locations. At location A the FLD prediction from the extrudate input and sprue input is the same and both inputs predict a greater

proportion of fibres between 0.64 and 1.28 mm length. The over -prediction of short fibres at location A results in a L_n much lower compared to the measured average. At location B the over-prediction is reduced when the predicted FLD for the sprue, extrudate or gate is input. The predicted average lengths at location B for all inputs reflect the measured average length. According to the predicted average fibre length in Table 5.3 the L_n at location B is greater than the L_n at location A, but the measured average shows the opposite result. In practice the greater distance from the gate (location A) the more fibres fracture resulting in a lower number average.

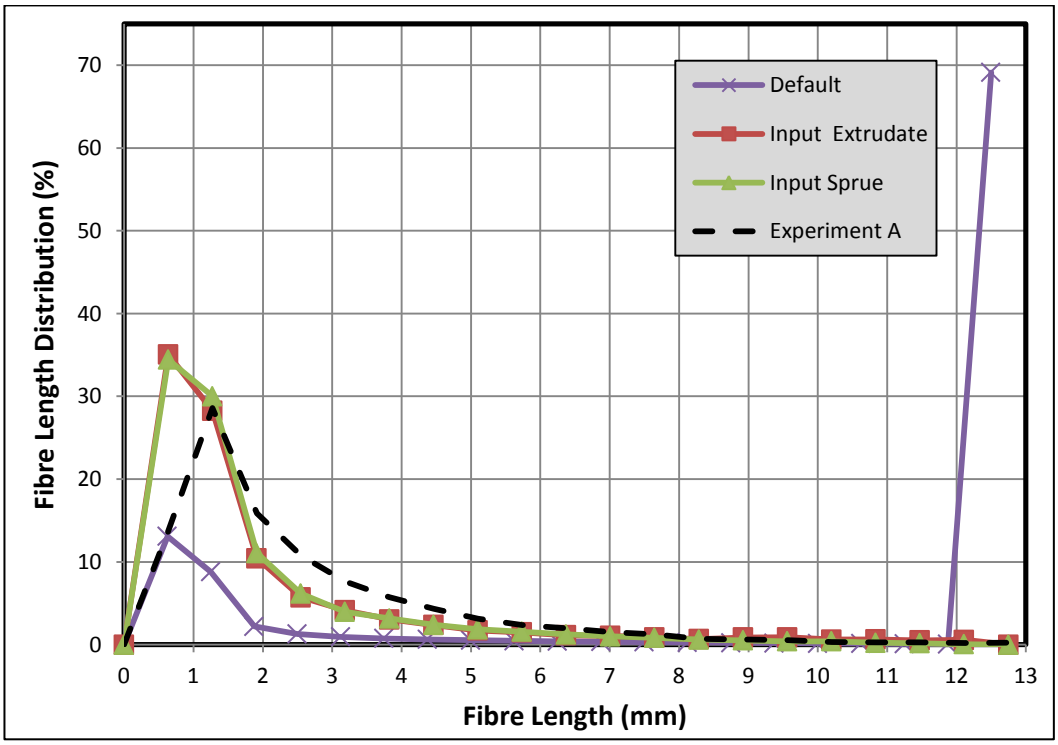

Figure 5.20 Fibre breakage prediction for 1 mm centre gate with 3.5 mm sprue at location A

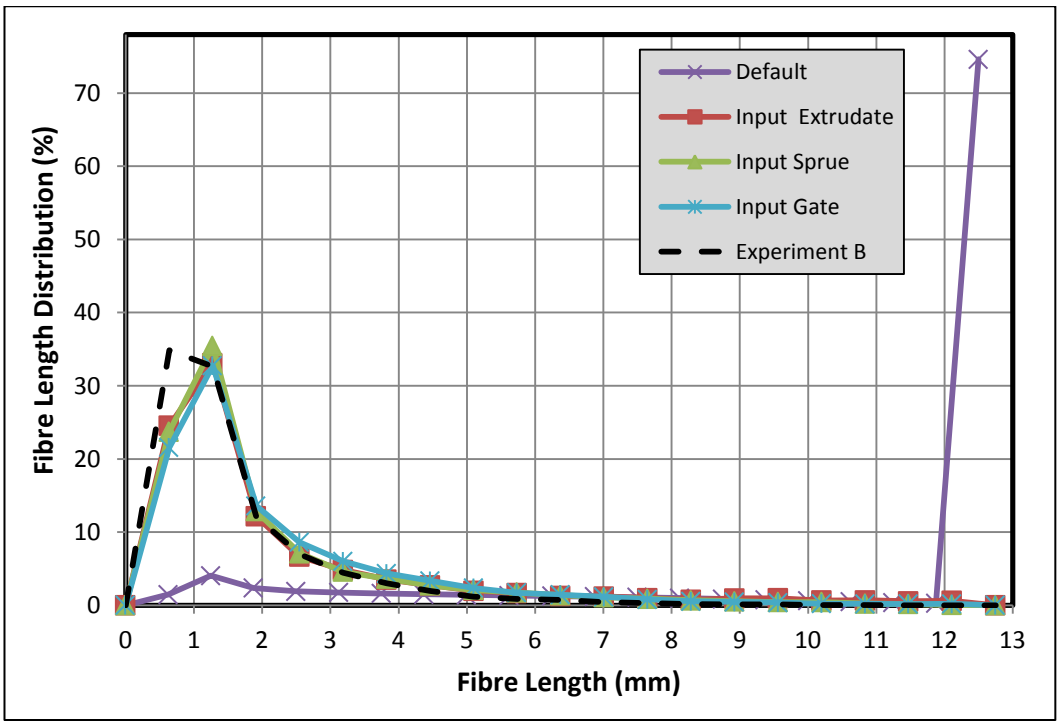

Figure 5.21 Fibre breakage prediction for 1 mm centre gate with 3.5 mm sprue at location B

Location	Default Predicted	Input Extrudate Predicted	Input sprue Predicted	Input Gate Predicted	Experiment average
A	3.85	1.05	1.04	-	2.28
B	5.75	1.22	1.21	1.26	1.34

Table 5.3 Predicted averages compared to the measured average at location A and B for 1 mm centre gate with 3.5 mm sprue

6 mm Sprue

Figure 5.22 and Figure 5.23 shows the prediction for each FLD input into the fibre breakage model for the 1 mm centre gate with a 6 mm sprue at location A and B (Figure 5.2). Table 5.4 contains the measured and predicted average fibre lengths (L_n) at location A and B. The default FLD (pellet length as input) predicts inaccurate fibre breakage with 60 % and above fibres remaining at 12.5 mm (initial length) at both locations. Figure 5.22 shows the FLD prediction at location A, the input extrudate provides the best prediction against the measured FLD. There is over-prediction when the measured sprue FLD is input into the fibre breakage model. The increase in smaller fibres within the sprue results in a lower L_n compared to the measured average. At location B (Figure

5.23) the distribution of fibres with 1.28 mm length has increased but the proportion of fibres shorter than 1.28 mm length is less compared to location A. The predicted L_n from the input extrudate and gate is closer to the measured L_n at location B. ASMI 2014 is predicting a higher L_n at the end of the flow path (location B).

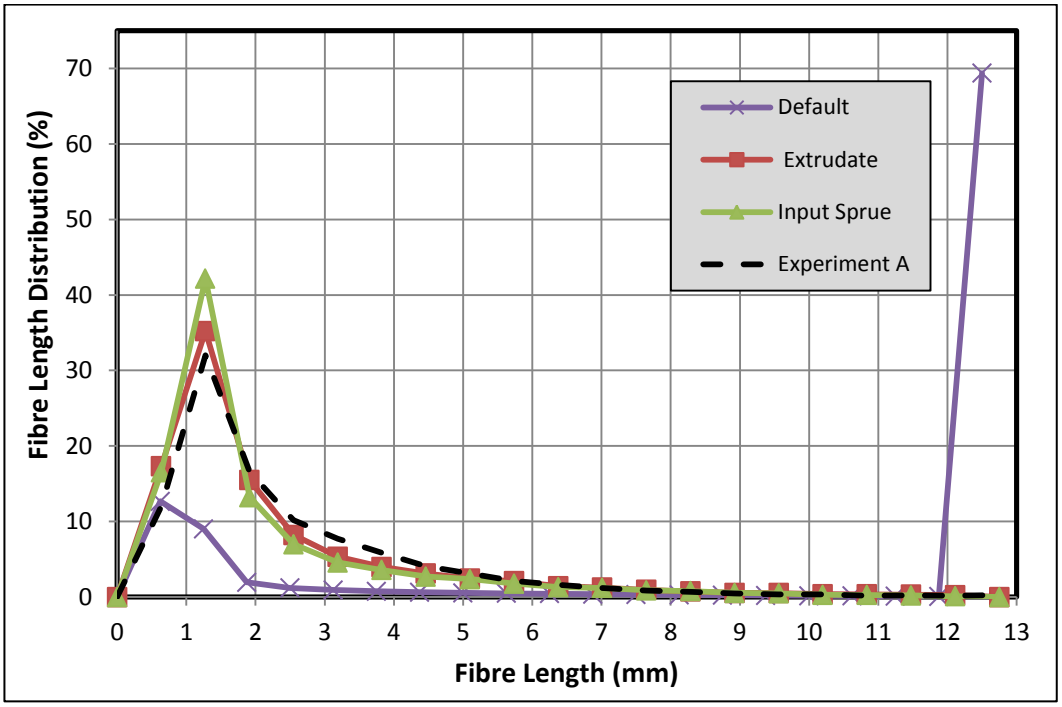

Figure 5.22 Fibre breakage prediction for 1 mm centre gate with 6 mm sprue at location A

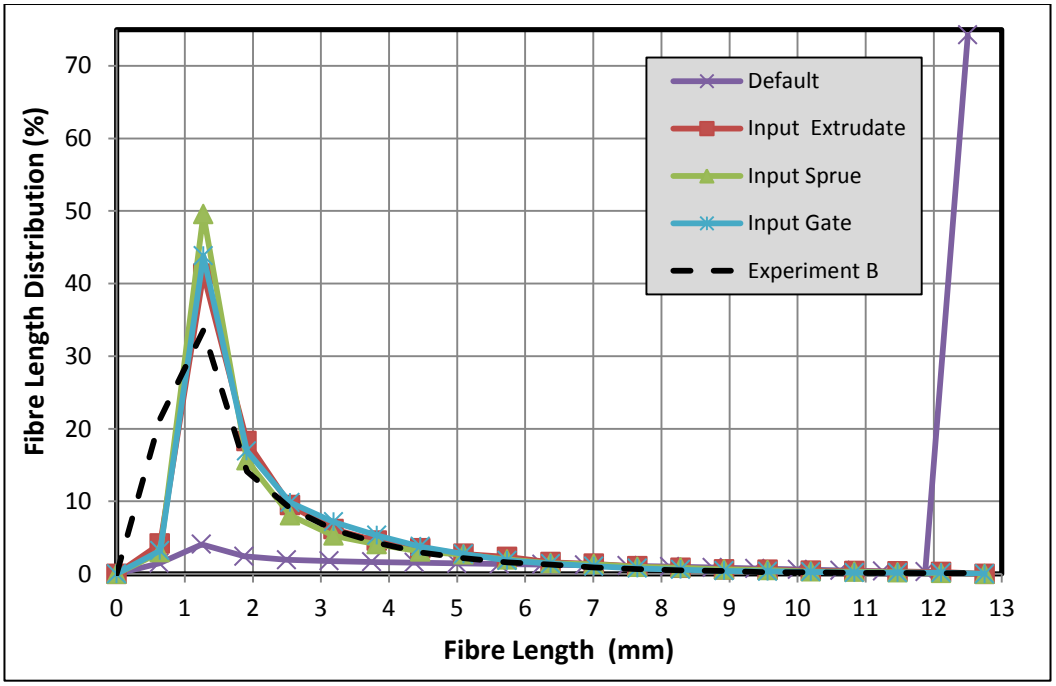

Figure 5.23 Fibre breakage prediction for 1 mm centre gate with 6 mm sprue at location B

Location	Default Predicted	Input Extrudate Predicted	Input Sprue Predicted	Input Gate Predicted	Experiment average
A	3.85	1.35	1.30	-	2.17
B	5.74	1.62	1.58	1.62	1.83

Table 5.4 Predicted averages compared to the measured average at location A and B for 1 mm centre gate with 6 mm sprue

5.2.6.2 2 mm Centre Gate

3.5 mm Sprue

Figure 5.24 and Figure 5.25 shows the prediction for each FLD input into the fibre breakage model for the 2 mm thick centre gate with a 3.5 mm sprue at location A and B (Figure 5.2). Table 5.5 contains the measured and predicted average fibre lengths (L_n) at location A and B. The default FLD with the pellet length as input predicts inaccurate fibre breakage with 70 % and above fibres remaining at 12.5 mm length at both locations. The input extrudate and sprue provide the best prediction for the measured FLD for locations A and B. At location B the input gate is over-predicting the fibre breakage. At location A the predicted L_n for both inputs is similar, the difference between the measured and predicted L_n is less than 0.6 mm. The difference between the measured and predicted L_n is less than 0.3 mm at location B. The model predicts a higher L_n at location B compared to location A.

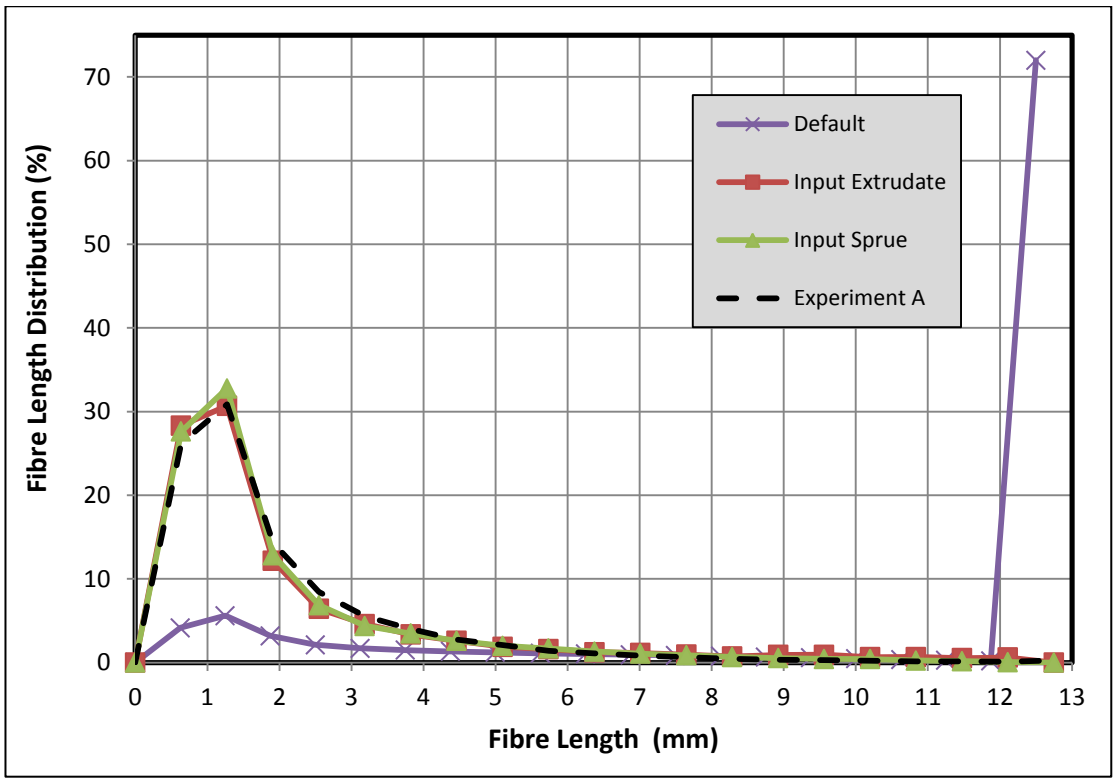

Figure 5.24 Fibre breakage prediction for 2 mm centre gate with 3.5 mm sprue at location A

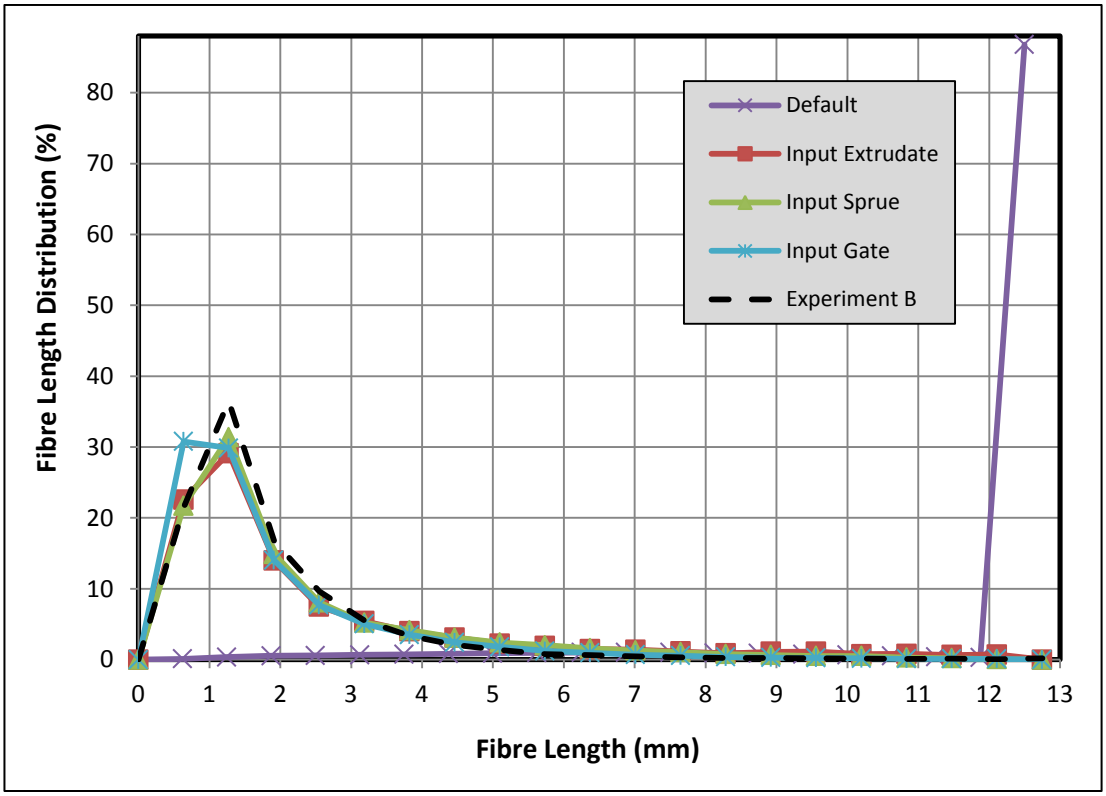

Figure 5.25 Fibre breakage prediction for 2 mm centre gate with 3.5 mm sprue at location B

Location	Default Predicted	Input Extrudate Predicted	Input sprue Predicted	Input Gate Predicted	Experiment average
A	4.72	1.15	1.14	-	1.74
B	8.81	1.33	1.32	1.15	1.59

Table 5.5 Predicted averages compared to the measured average at location A and B for 2 mm centre gate with 3.5 mm sprue

6 mm Sprue

Figure 5.26 and Figure 5.27 shows the prediction for each FLD input into the fibre breakage model for the 2 mm centre gate with a 6 mm sprue at location A and B (Figure 5.2). Table 5.6 contains the measured and predicted average fibre length (L_n) at location A and B. The default FLD with the pellet length as input predicts inaccurate fibre breakage with 70 % and above fibres remaining at 12.5 mm length at both locations. At both locations the input extrudate enhances the FLD prediction; this is reflected by a higher predicted L_n for the extrudate at both locations. The input sprue at both locations and the gate at location B (Figure 5.27) over-predict the fibre breakage with a greater distribution of small fibres (< 1.25 mm). Although the input extrudate generates a better prediction of the FLD, the L_n is 0.8 mm and 0.42 mm less than the measured fibre length at location A and B. For all inputs the fibre breakage model predicts a lower L_n at location A compared to location B, the measured L_n is showing the opposite effect.

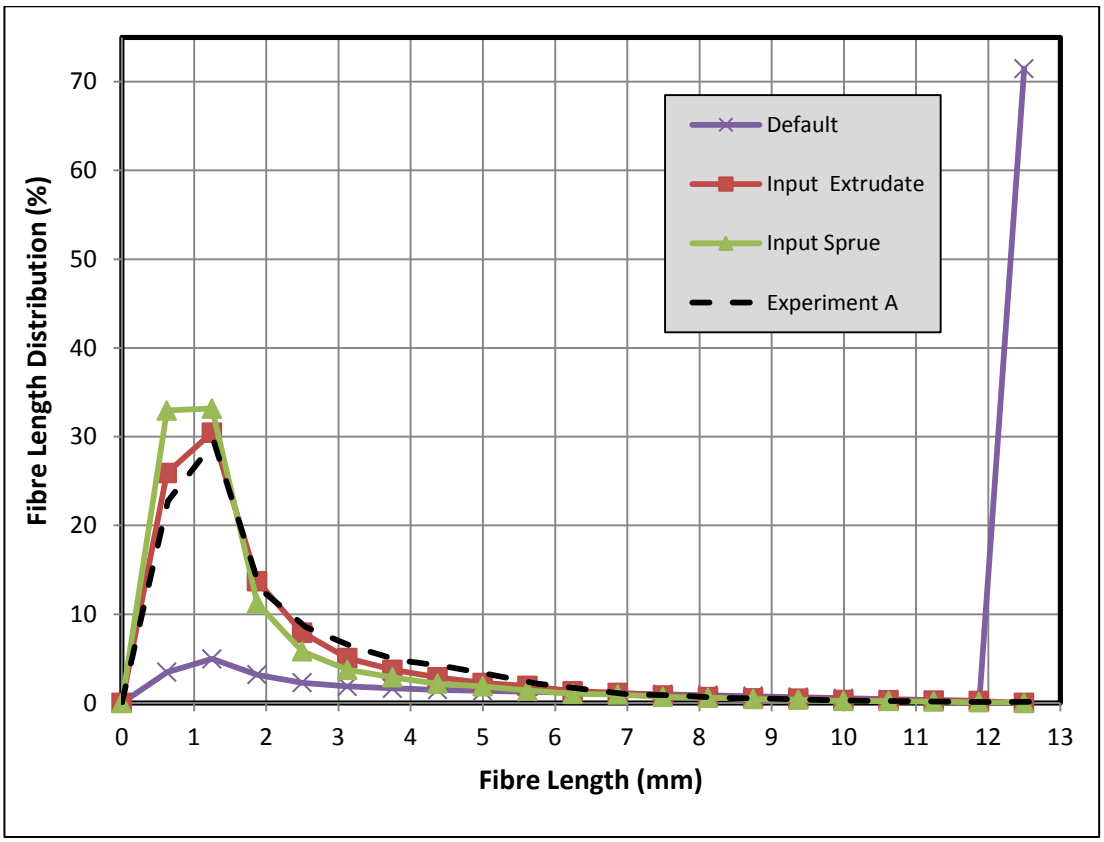

Figure 5.26 Fibre breakage prediction for 2 mm centre gate with 6 mm sprue at location A

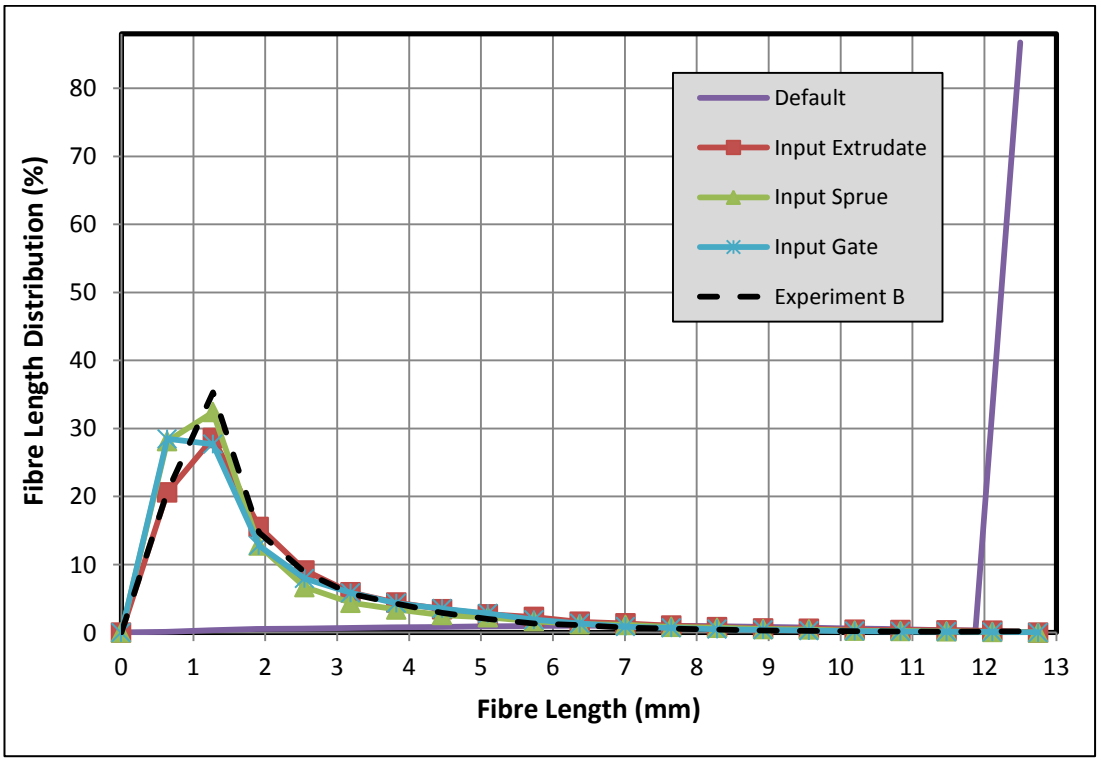

Figure 5.27 Fibre breakage prediction for 2 mm centre gate with 6 mm sprue at location B

Location	Default Predicted	Input Extrudate Predicted	Input sprue Predicted	Input Gate Predicted	Experiment
A	4.97	1.19	1.06	-	1.99
B	8.79	1.36	1.19	1.15	1.78

Table 5.6 Predicted averages compared to the measured average at location A and B for 2 mm centre gate with 6 mm sprue

5.2.6.3 Summary

The breakage model predicts an inaccurate FLD and L_n when the initial pellet length is input into to the model. The FLD illustrates the majority of fibres remain the initial length (12.5 mm) following an injection moulding cycle. The input of the sprue and extrudate enhance the FLD prediction for the 3.5 mm sprue geometries at both locations. For the 6 mm sprue geometries the input extrudate provides a better approximation of measured FLD. In most cases the FLD prediction is a good representation of the measured FLD. However the predicted average fibre length is always less than the measured average length for both locations and geometries. Therefore the model over predicts the fibre breakage in all scenarios. According to ASMI 2014 the predicted average fibre length at location B is always greater than the L_n at location A, but the measured average shows the opposite effect. Fibre breakage occurs due to fibre-fibre interactions and fibre wall interactions as a cavity fills so in hindsight more fibres have broken at location B.

5.3 Fibre Orientation Distribution

5.3.1 Introduction

The long glass fibre ARD-RSC and ARD model has been applied to the 1 and 2 mm thick base centre gate geometries in mid-plane analyses, enhanced solutions were found for the model by comparing fibre orientation distribution from location three locations along the radial flow path. They are shown below in Figure 5.28; Location A (16 mm from sprue); B (25 mm from sprue); and C (36 mm from sprue).

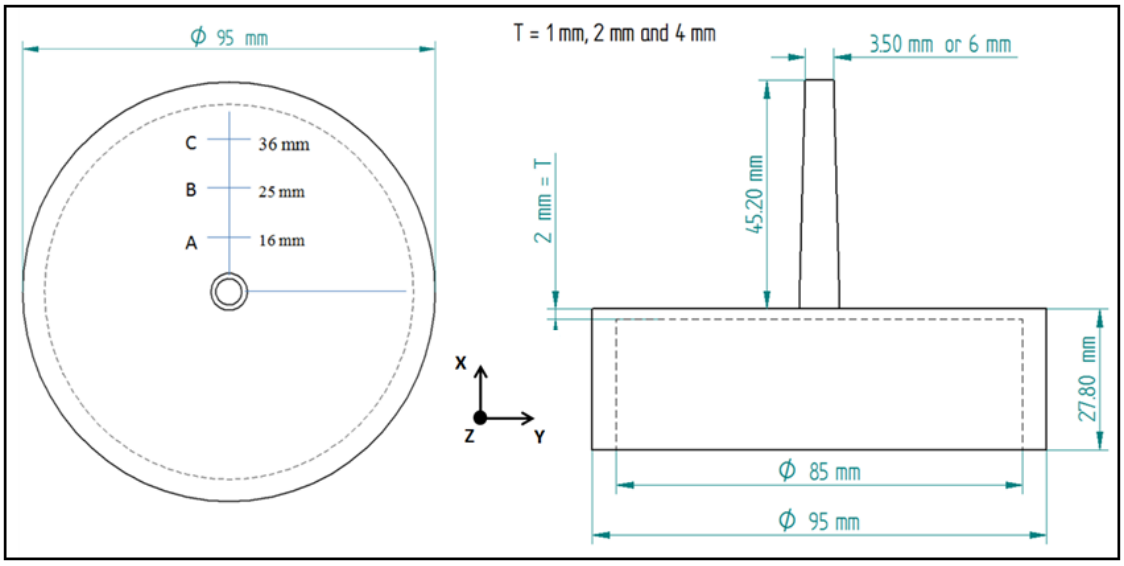

Figure 5.28 Diagram showing experiment locations A, B and C for centre gate

5.3.2 Experiment

The measured FOD was found for the 1 and 2 mm centre gate geometries with either sprue geometry at location A, B and C.

5.3.2.1 Variation

This segment covers the FOD variation within the 6 mm and 3.5 mm sprue centre gate geometries. Fibre orientation measurements were taken from two 1 mm thick LGF samples along the same flow path. These tests were carried out

on the same batch of injection moulded samples. Figure 5.29 and Figure 5.30 show the data for both samples at location A, B and C within the 3.5 mm and 6 mm sprue geometries. Table 5.7 and Table 5.8 show the standard deviation for two measurements at each location and the average standard deviation for both geometries.

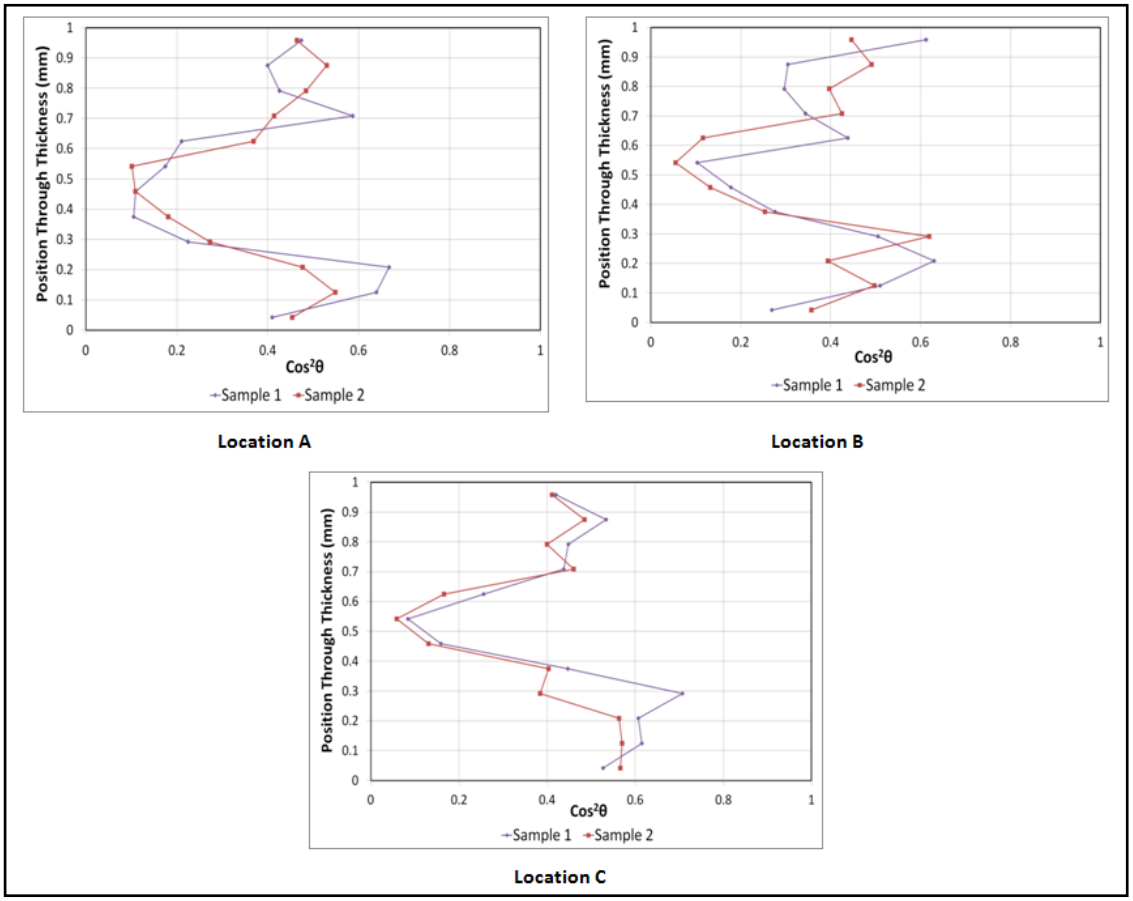

Figure 5.29 Measured average FOD from sample 1 and 2 taken from the LGF 1 mm thick 3.5 mm sprue centre gate at location A, B and C

Location A	Location B	Location C	Average
0.062	0.084	0.045	0.064

Table 5.7 Standard deviation between sample 1 and 2 at location A, B and C

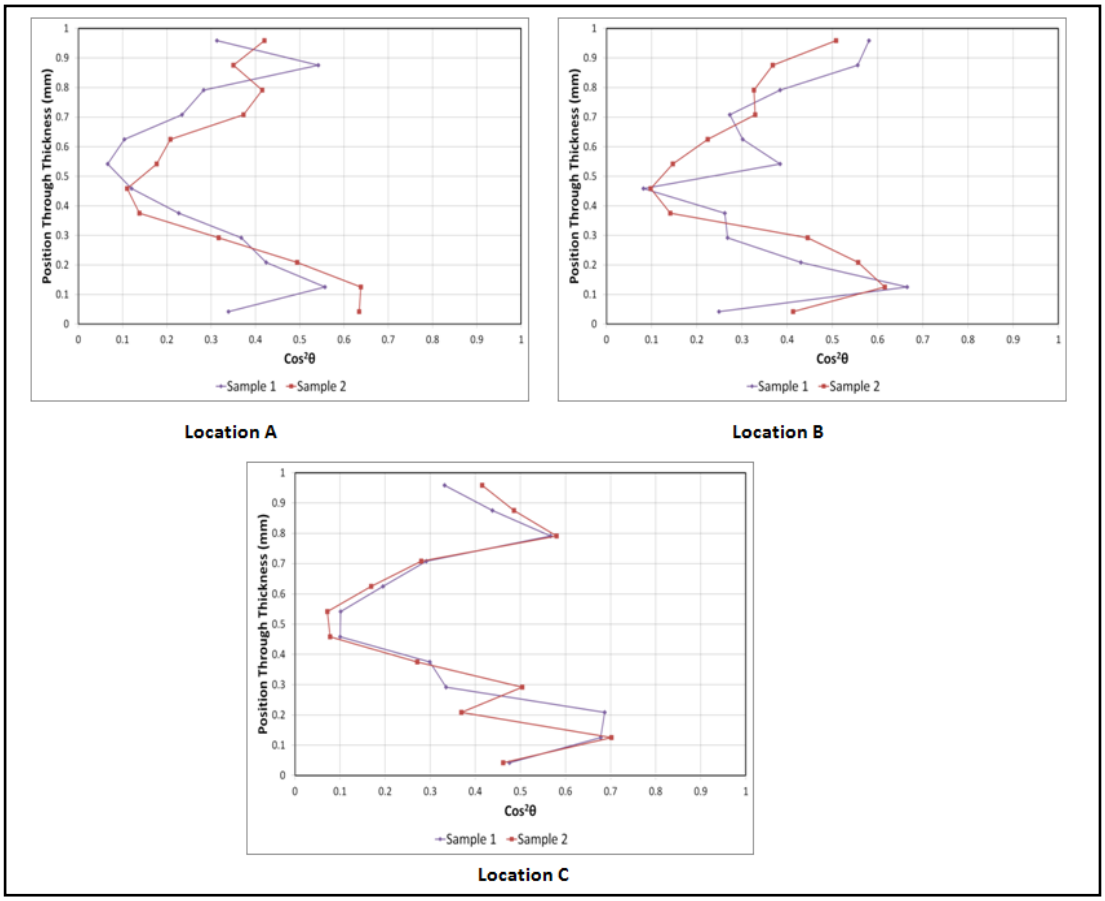

Figure 5.30 Measured average FOD from sample 1 and 2 taken from the LGF 1 mm thick 6 mm sprue centre gate at location A, B and C

Location A	Location B	Location C	Average
0.081	0.079	0.046	0.068

Table 5.8 Standard deviation between sample 1 and 2 at location A, B and C

The variation for either sprue geometry is the same two decimal places as shown in Table 5.7 and Table 5.8. The average variation for both geometries is the same as the variation found for the SGF 1 mm thick injection moulded samples ± 0.07. The average variation includes an error in measurement of ± 0.02 which is a result of the image analysis system (Bubb, 2001). The remaining ± 0.05 random variation can be attributed to the variation in the injection moulding process conditions. Figure 5.29 and Figure 5.30 illustrate majority of the variation occurs at the shell. A consistent pattern is seen for both sprue geometries at location C where the variation reduces.

5.3.2.2 1 mm Thick Centre Gate

3.5 mm Sprue

The average FOD distribution is the same within the ±0.07 variation at the skin, shell and core layers for the 3.5 mm sprue 1 mm thick centre gate geometry between locations A, B and C as shown in Figure 5.31. The orientation at the skin is random with $\cos^2\theta$ varying between 0.4-0.5. Although material fills the thin cavity at high shear the core represents up to 0.5 mm (half) of the total sample thickness at locations A, B and C with fibres aligned perpendicular to the flow direction with $\cos^2\theta$ of 0.1 or below. The orientation is similar at each location this is clearly shown within the contour plots of FOD through thickness in Figure 5.32. However the effect of in-plane stretching reduces towards the end of the flow path and shearing increases at location C, causing the fibres to align parallel to the direction of flow within the shell layers where $\cos^2\theta$ is 0.58.

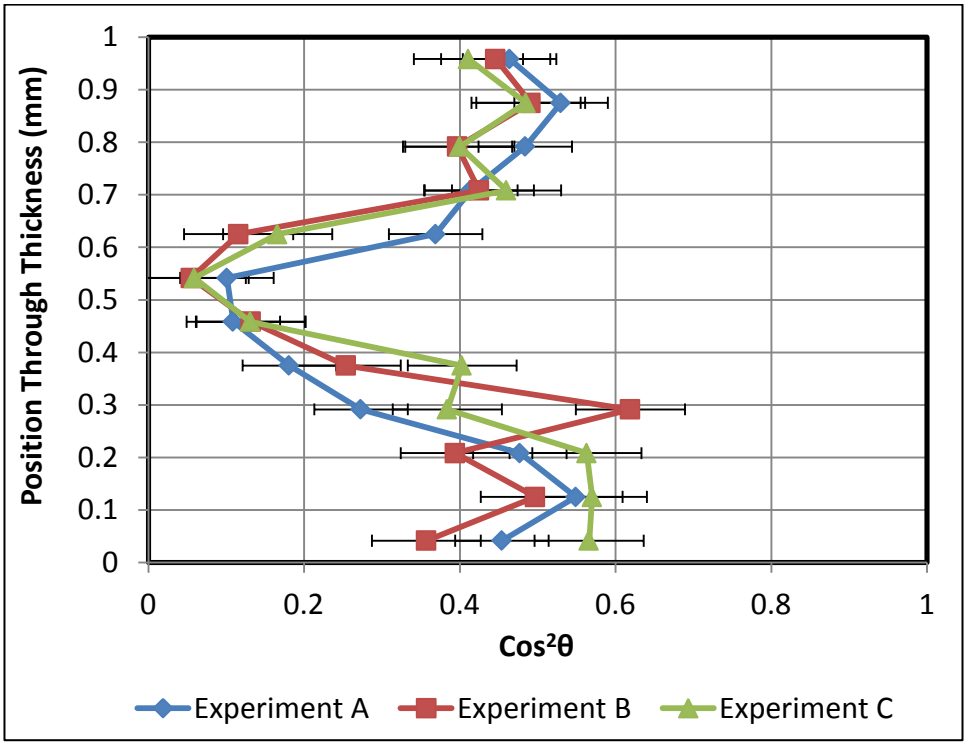

Figure 5.31 Measured average FOD within 1 mm centre gate 3.5 mm sprue at location A, B and C

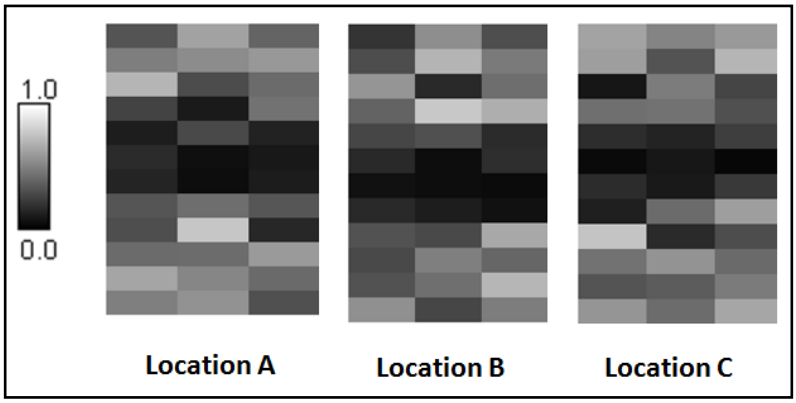

Figure 5.32 Contour plots of 1 mm centre gate 3.5 mm sprue at location A, B and C

6 mm Sprue

The average FOD distribution is qualitatively similar at the skin, shell and core layers within the 6 mm sprue, 1 mm thick centre gate geometry at locations A, B and C as shown in Figure 5.33. The orientation at the skin is random with $\cos^2\theta$ varying between 0.4-0.45 in most circumstances. At location C the fibres align partially parallel to the direction of flow within the shell layers where $\cos^2\theta$ is 0.6 and above. The core represents 0.5 - 0.55 mm of the total thickness of the sample at locations A, B and C with fibres aligned perpendicular to the flow direction with $\cos^2\theta$ of 0.1 or below. The orientation is similar at each location this is clearly illustrated within the contour plots in Figure 5.34.

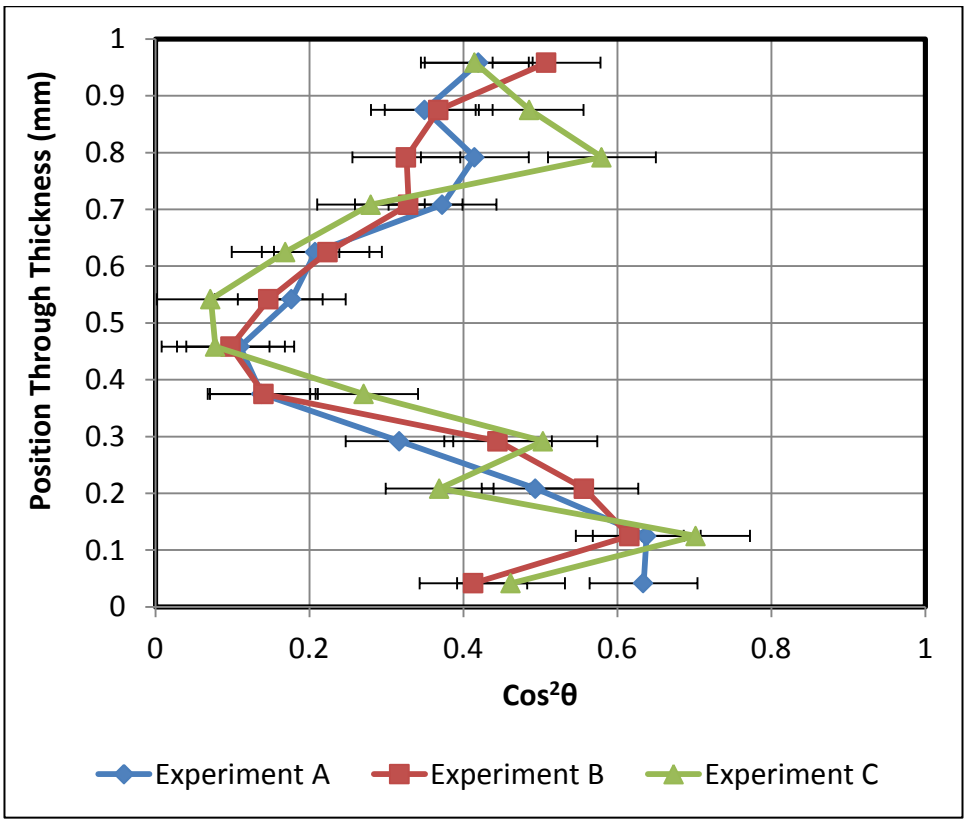

Figure 5.33 Measured average FOD within 1 mm centre gate 6 mm sprue at location A, B and C

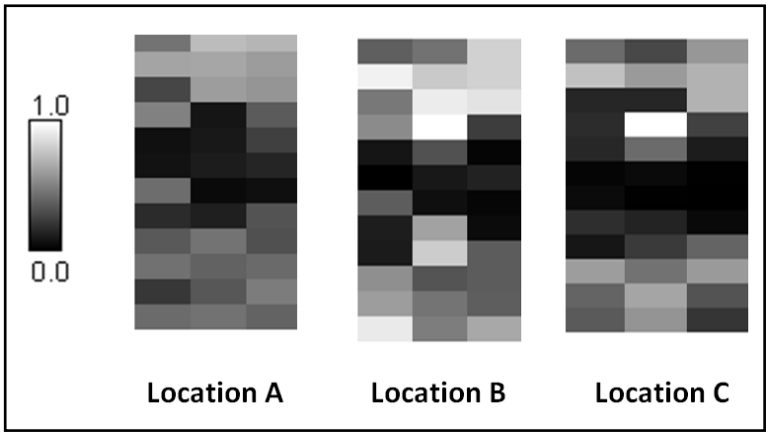

Figure 5.34 Contour plots of 1 mm centre gate 6 mm sprue at location A, B and C

5.3.2.3 2 mm Thick Centre Gate

3.5 mm Sprue

The average FOD does not change significantly across the radial path within the 3.5 mm sprue, 2 mm thick centre gate geometry (Figure 5.35). There is a noticeable change within the position of the core from location A to B this is

illustrated by the contour plots in Figure 5.36. Within the given random variation the average orientation at the skin is between 0.4 - 0.5 and 0.5 or above for the shell layers. The only noticeable change is in the width of the core from location A to B. The thickness of the core remains the same at location A, B and C this is apparent in the contour plots Figure 5.36. The $\cos^2\theta$ of the fibres at the core for all locations is 0.1 or below.

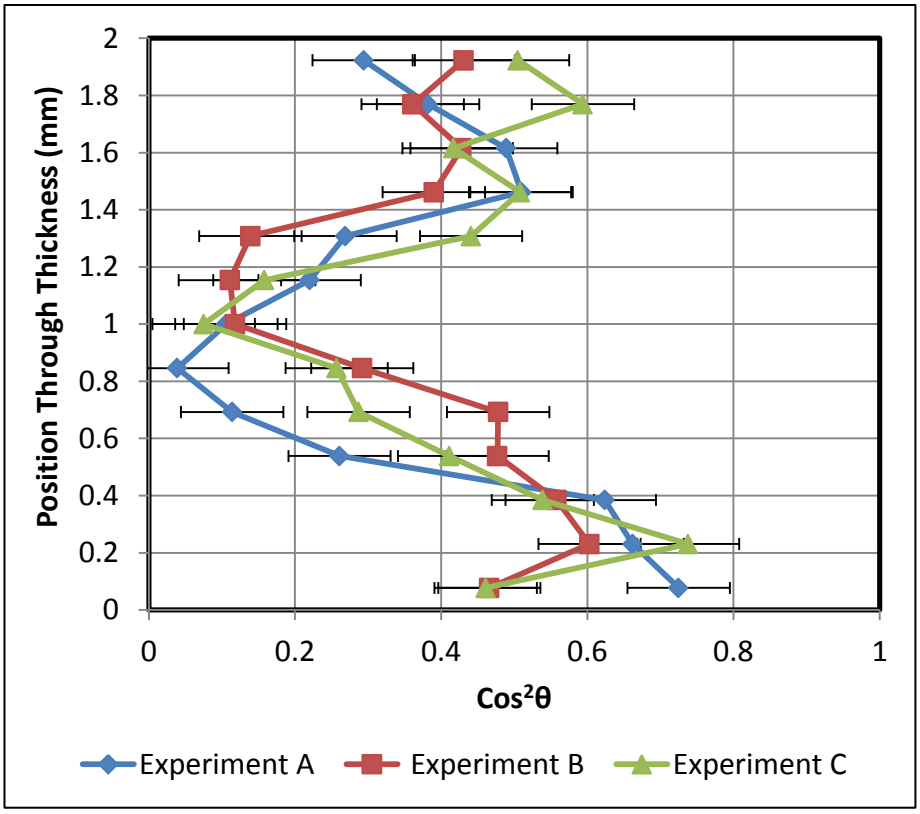

Figure 5.35 Measured average FOD within 2 mm centre gate 3.5 mm sprue at location A, B and C

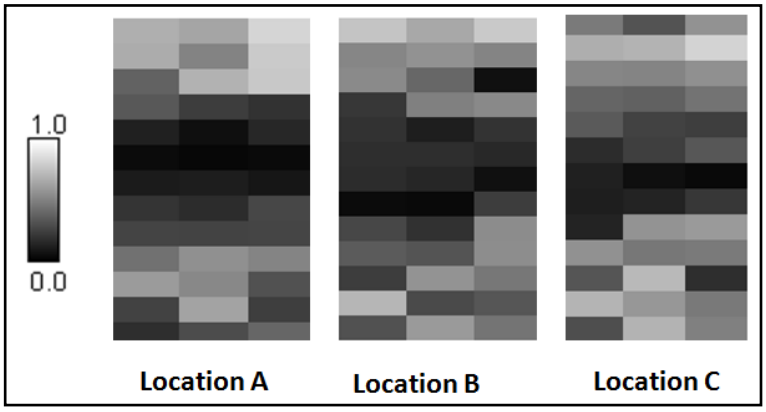

Figure 5.36 Contour plots of 2 mm centre gate 3.5 mm sprue at location A, B and C

6 mm Sprue

The average FOD distribution is qualitatively similar at the skin, shell core layers within the 6 mm sprue, 2 mm thick centre gate geometry between locations A, B and C as shown in Figure 5.37. There is a small change within the position of the core from location B to C this is illustrated by the contour plots in Figure 5.38. The orientation at the skin and shell layer is different at the top and bottom of the sample. The orientation at the shell layer $\cos^2\theta$ is 0.6 at the bottom of the sample and 0.4 at the top. The core represents up to 1.20 mm of the total thickness of the sample at locations A, B and C with fibres aligned perpendicular to the flow direction with $\cos^2\theta$ of 0.1.

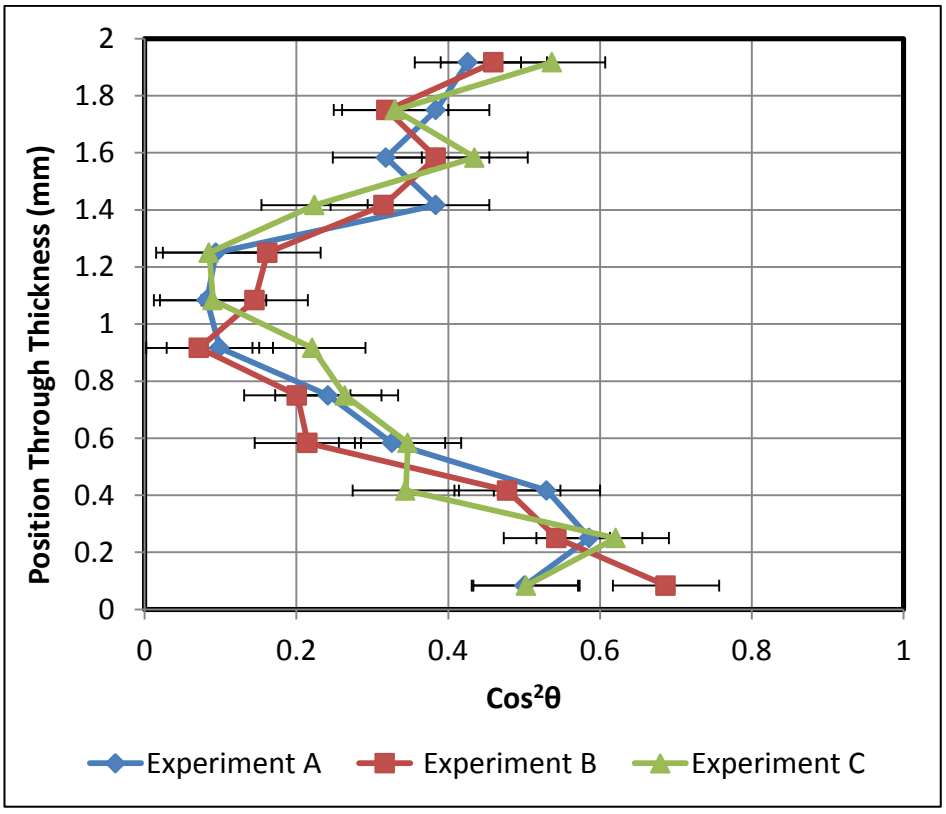

Figure 5.37 Measured average FOD within 2 mm centre gate 6 mm sprue at location A, B and C

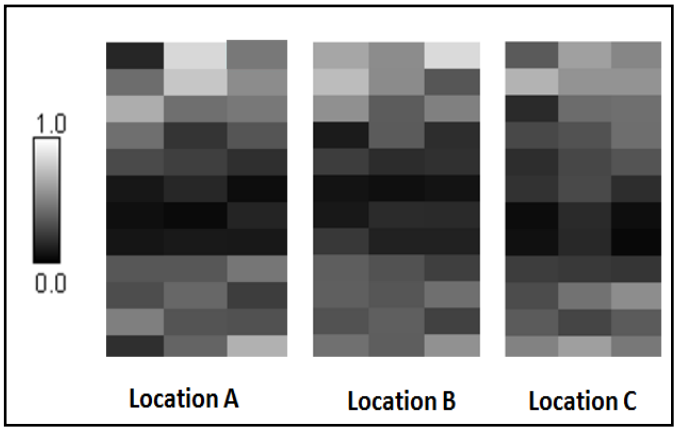

Figure 5.38 Contour plots of 2 mm centre gate 6 mm sprue at location A, B and C

5.3.2.4 Evaluation

5.3.2.4.1 Influence of Geometry

Previous findings in this chapter have shown the average orientation does not change within the centre gate geometries through the radial flow path. A comparison has been made between the same width but different sprue (3.5 mm and 6 mm) geometries at location C. Figure 5.39 shows the average FOD for the 1 mm thick centre gate for both sprue geometries. The average orientation is similar at the skin and shell and core layers. The core width is the same for the 6 mm sprue and the 3.5 mm sprue. The comparison between the average FOD for the 2 thick mm centre gate for 6 mm sprue and the 3.5 mm sprue is shown in Figure 5.40. The average orientation is very similar at the skin, shell and core layers. There is a maximum 0.2 mm difference in the core width between the 6 mm sprue. From the findings in the previous Section 5.2.5.3, the average fibre length is greater in the 6 mm sprue geometries. Therefore the slightly wider core could be a result of the higher average fibre length. However these findings and published work (Hine et al., 2014) on STAMAX LGF material confirms the average FOD, is not sensitive to changes in average fibre length when studying the same geometry.

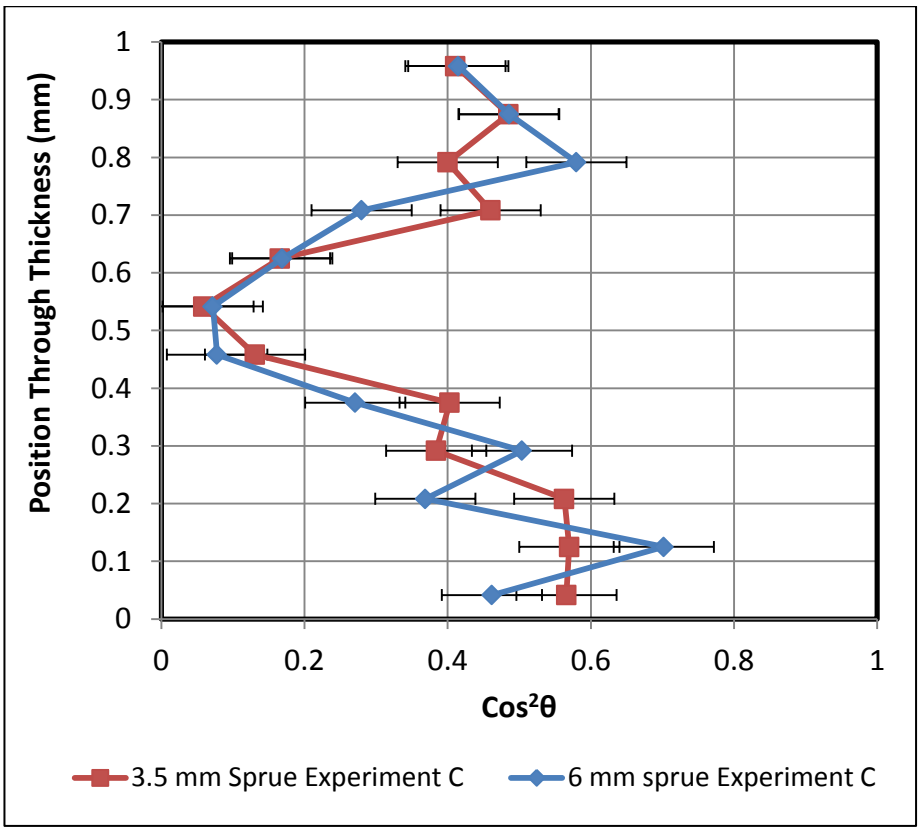

Figure 5.39 Comparison of average FOD between 3.5 mm and 6 mm sprue geometries for the 1 mm centre gate at location C

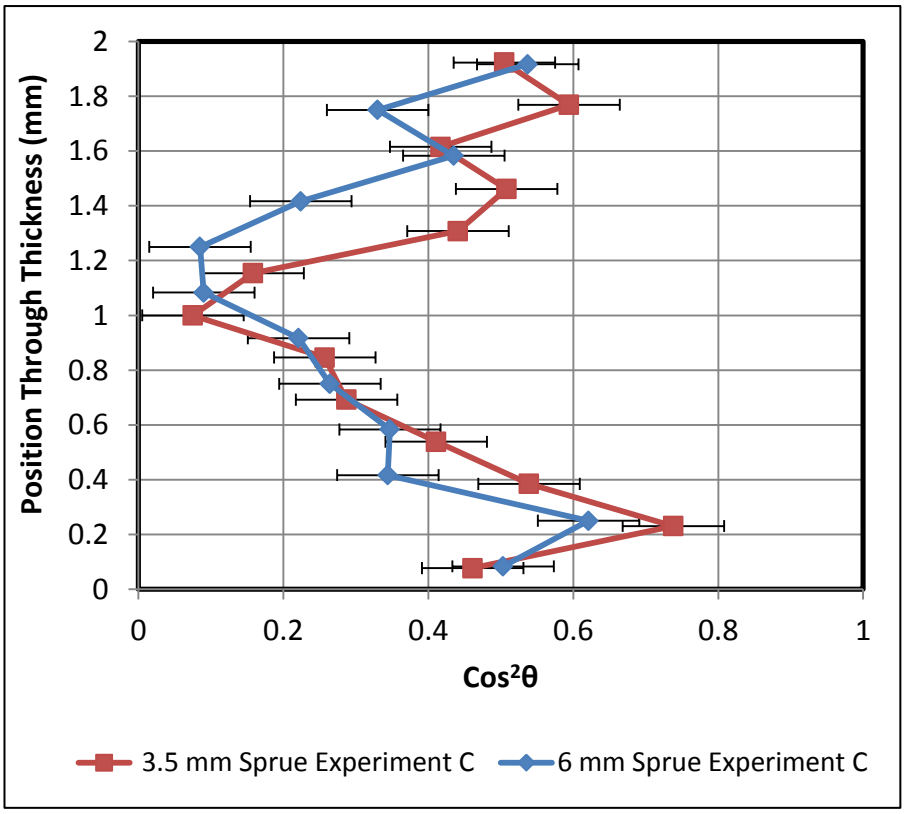

Figure 5.40 Comparison of average FOD between 3.5 mm and 6 mm sprue geometries for the 2 mm centre gate at location C

5.3.2.4.2 Influence of Geometry Thickness

The difference between the average FOD of the 1 mm and 2 mm centre gate geometries with the 3.5 mm sprue is illustrated in Figure 5.41. The $\cos^2\theta$ at the skin and core layer is similar for both geometries. The $\cos^2\theta$ at the skin for the 2 mm thick is 0.6 and above this means the fibres at the skin are aligned partially parallel to the direction of flow. The core thickness amounts to 50 % of the total thickness (1 mm) of the 2 mm centre gate compared to 45 % of the total thickness (0.45 mm) of the 1 mm centre gate. The proportion the core width occupies is similar for the 1 mm and 2 mm centre gate LGF samples. This difference is 20 % less compared to the SGF 1 and 2 mm thick centre gate samples (4.2.7.1 Influence of Geometry Thickness). Evaluating the LGF FOD with SGF FOD would provide a better understanding of this difference.

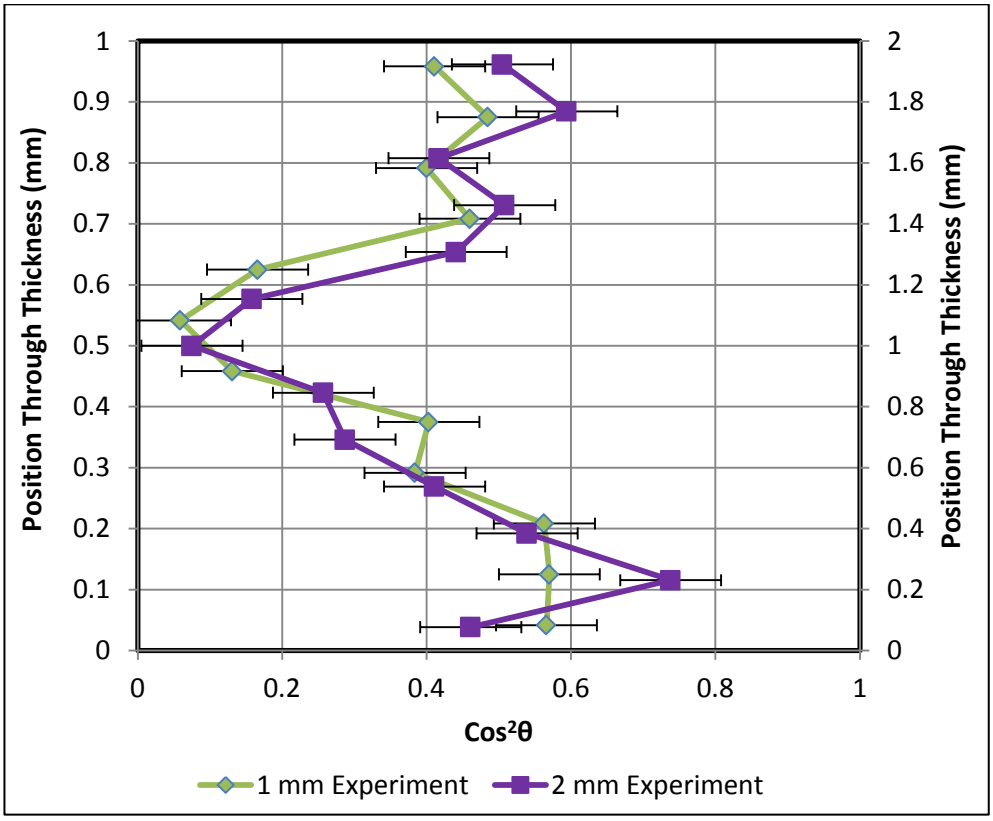

Figure 5.41 Difference in average FOD between 1 mm and 2 mm centre gate 3.5 mm sprue at location C

5.3.2.4.3 Short Glass Fibre vs Long Glass Fibre

Figure 5.42 and Figure 5.43 evaluates the LGF against SGF average FOD for the 1 mm thick and 2 mm centre gate geometries (3.5 mm sprue). The average FOD within the long glass fibre samples is not symmetrical. This creates a shell layer with a slightly higher $\cos^2\theta$ on the bottom compared to the top. Both 1 and 2 mm thick LGF samples have a lower $\cos^2\theta$ at the shell layer compared to the SGF samples. The fibres are oriented in a random distribution within the LGF shell layer compared to fibre oriented parallel to the direction of flow in the SGF shell layer. The difference in $\cos^2\theta$ between the LGF and SGF skin is less in comparison to the shell layer. The average orientation at the core of 0.1 does not change as a result of material. The core width is 0.2 mm greater within the LGF 1 mm thick sample compared to the SGF 1 mm thick sample. There is a 0.1 mm difference between the core thicknesses of the 2 mm thick LGF sample compared to the 2 mm thick SGF sample. The results show the core width increases in a LGF sample but the change is more evident in a thin cavity or the 1 mm thick centre gate.

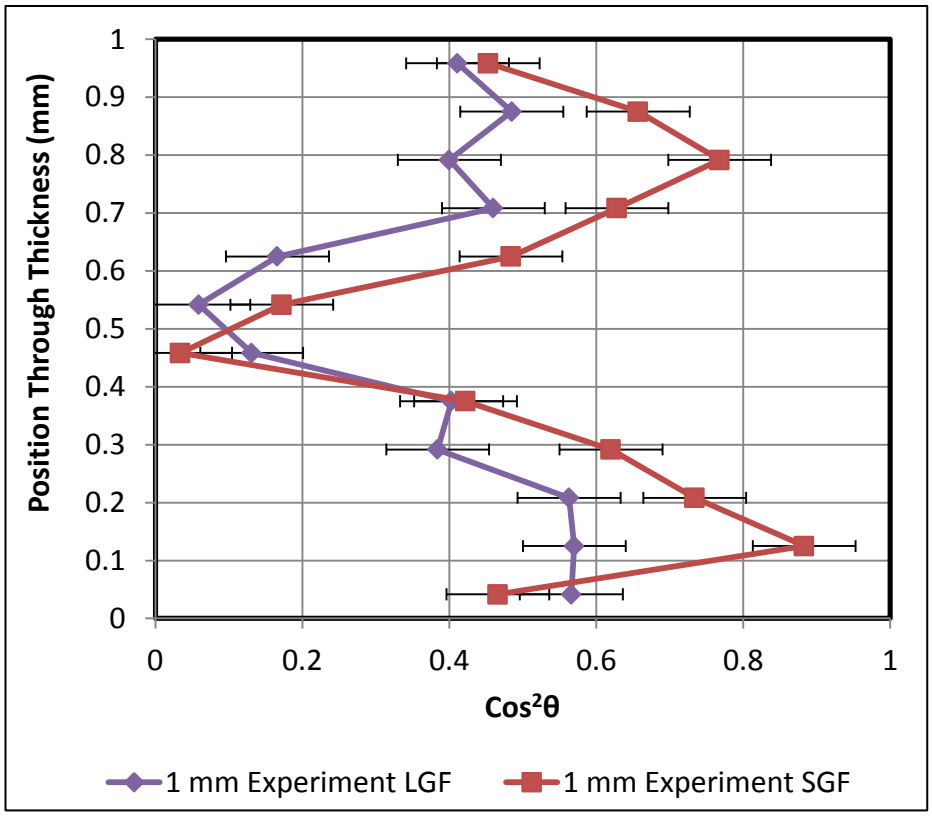

Figure 5.42 Difference in average FOD between LFG and SGF 1 mm centre gate at location B

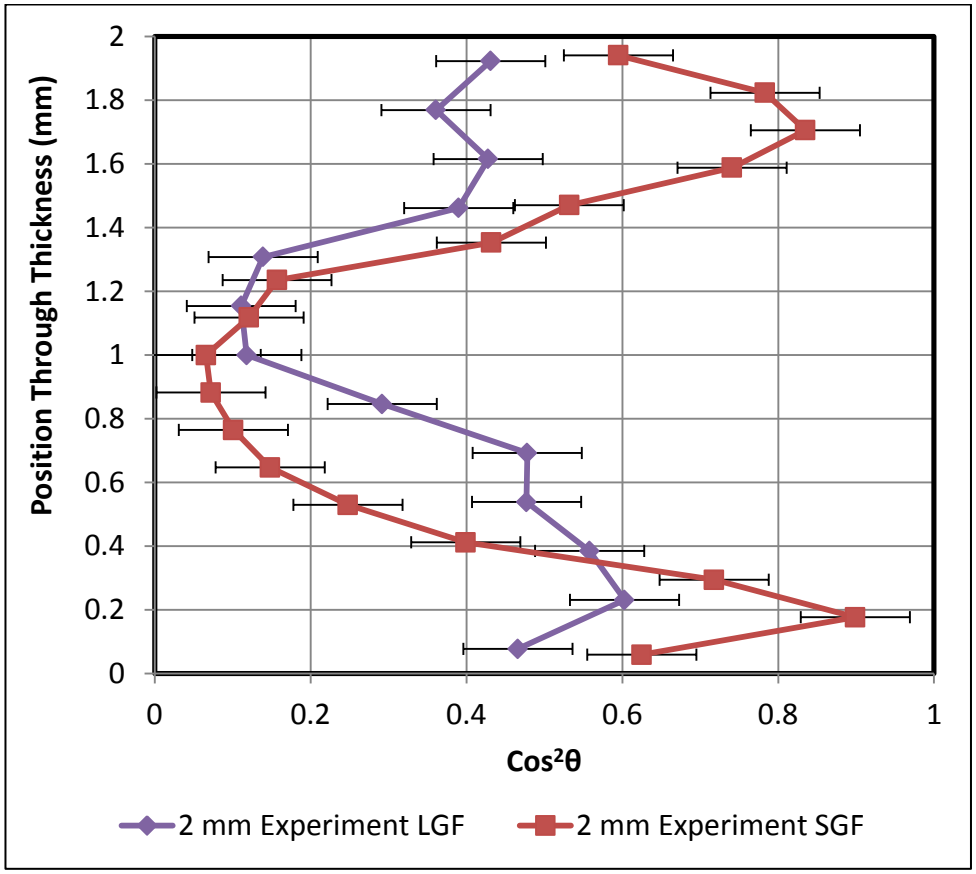

Figure 5.43 Difference in average FOD between LFG and SGF 2 mm centre gate at location B

5.3.2.5 Summary

The average FOD remains similar along the radial flow path for LGF 1 and 2 mm thick centre gate geometries for both 6 mm and 3.5 mm sprues. An increase in the average fibre length does not change the average FOD within the LGF component. The $\cos^2\theta$ is the same for a 1 mm and 2 mm thick LGF centre gate geometry where the core width is a similar proportion. In comparison to a thin SGF centre gate a thin LGF centre gate has random orientation at the shell and skin but the orientation at the core is the same. The difference in the core width for the SGF and LGF samples is more apparent in a 1 mm thick centre gate.

5.3.3 Prediction

ASMI 2014 uses the ARD (Equation 2.17) or ARD-RSC (Equation 2.19) model to predict the orientation within a long glass fibre injection moulded component. To slow the rate of orientation development the k parameter is introduced into the ARD-RSC model from the SGF RSC model. The k parameter reduces the fibre orientation kinetics as the magnitude of k decreases. If the value of k is equal to 1 the ARD-RSC model reverts back to the ARD model. From investigating the SGF RSC model generic rules were found to select a k factor which improves FOD prediction. These rules should be the same for the ARD-RSC model if the k factor behaves as the k factor within the RSC model. Predicting the measured FOD of the 1 mm and 2 mm centre gate geometries with a 3.5 mm sprue should confirm the RSC rules.

K Parameter Rules

1. To increase the core thickness and to decrease the shell layer thickness select a k value between 0.00001 - 0.01.
2. To align the fibres in the shell layer in the flow direction select a k value between 0.2 - 0.8.
3. To decrease the core thickness and to align the fibres within the core transverse to the flow direction select a k value above 0.05.

5.3.3.1 1 mm Centre Gate

Figure 5.44, Figure 5.45 and Figure 5.46 shows the long fibre prediction against the average FOD with the measured deviation for the 1 mm centre gate at location A, B and C. Various (reduced strain factor) k are examined for the ARD-RSC (Equation 2.19) shell model. The examined parameters are specified in Section 3.4.2 Extracting Predicted FOD. The measured FOD has a wide core oriented perpendicular to the direction of flow and a shell layer with reasonably aligned fibre in the direction of flow. To predict this orientation the k needs to be between 0.6 -0.8. From the trial of various k parameters in the ARD-RSC model it can be concluded the k parameter does follow the generic

rules compiled for the RSC model. Apart from increasing the shell layer thickness the $\cos^2\theta$ within the shell layer decreases with a k value between 0.2 - 0.8. The ARD-RSC and ARD model over-predict orientation above the deviation within the skin and shell. The width of the core is over-predicted but the ARD model predicts the orientation at the core at all 3 locations. The over-prediction at the shell layer does reduce at location C. The ARD (k = 1) and ARD-RSC with k parameter 0.8 are better solutions compared to the ASMI 2014 default with k parameter of 0.05. The 5 scalar parameters within the ARD model are set at default values, reference of these can be made from Section 2.7.2.1 ARD Model.

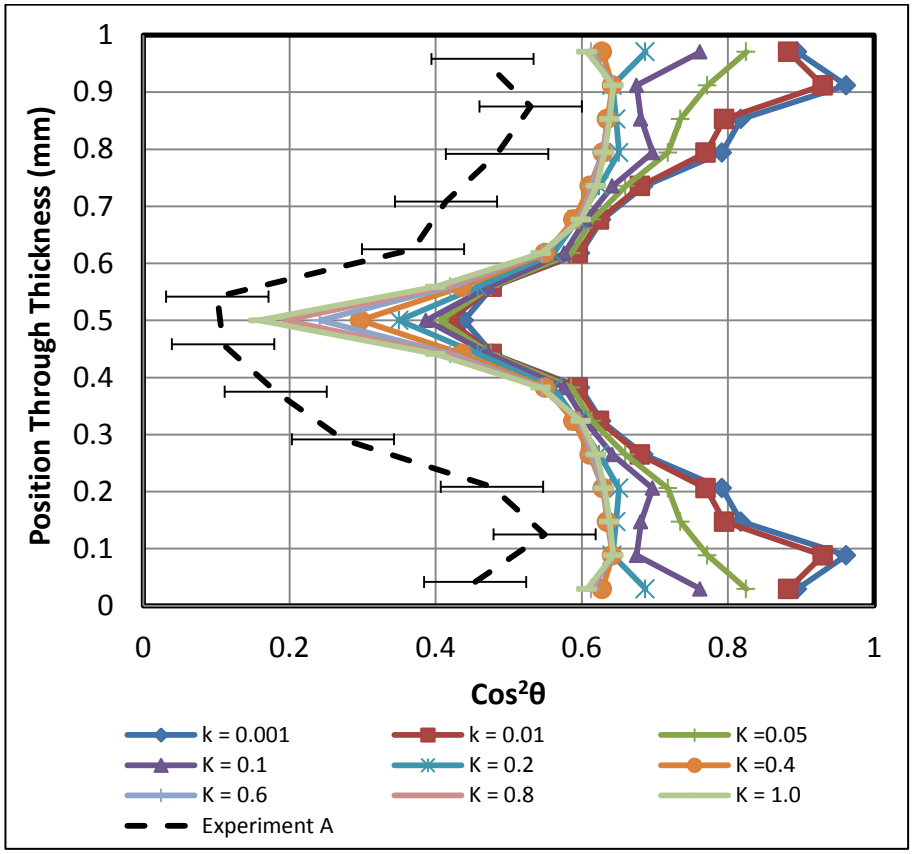

Figure 5.44 Predictions for the ARD and ARD-RSC model against 1 mm centre gate average FOD at location A

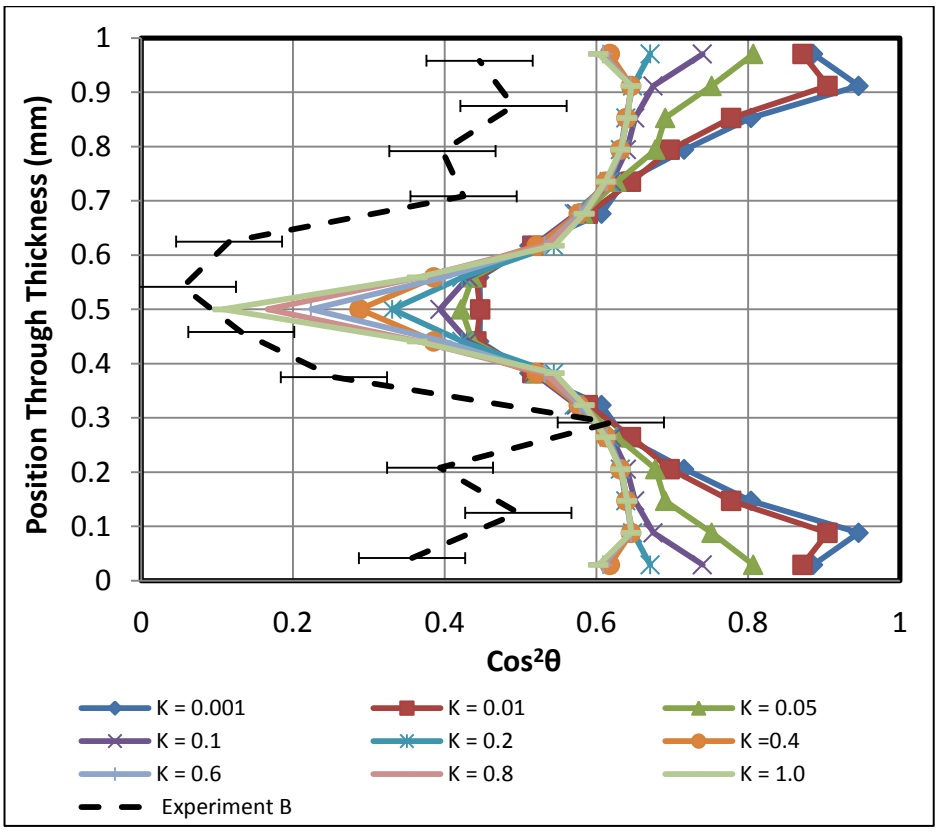

Figure 5.45 Predictions for the ARD and ARD-RSC model against 1 mm centre gate average FOD at location B

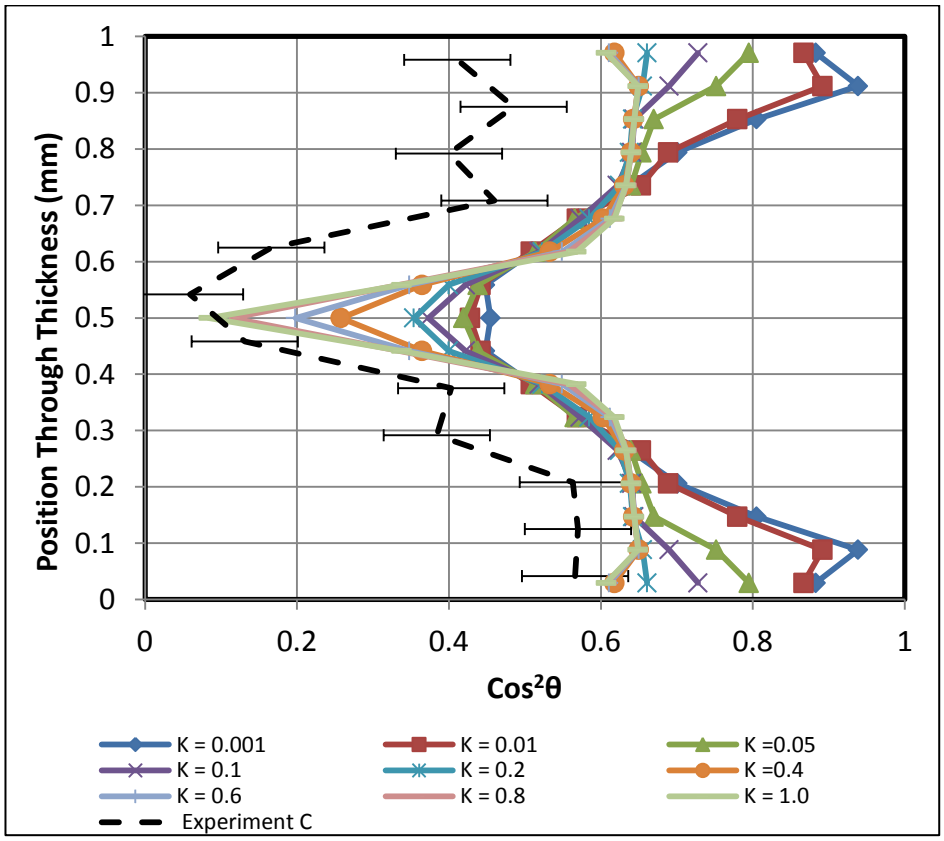

Figure 5.46 Predictions for the ARD and ARD-RSC model against 1 mm centre gate average FOD at location C

5.3.3.2 2 mm Centre Gate

From the above findings and the understanding of the LGF FOD within the 2 mm centre gate, a very high k parameter for the ARD-RSC model or the ARD-RSC model is required to predict the average FOD. Figure 5.47, Figure 5.48 and Figure 5.49 shows the long fibre prediction against the average FOD for the 2 mm centre gate at location A, B and C. The ASMI 2014 default k parameter of 0.05 is over-predicting the level of orientation. Both the ARD models over-predict the core orientation and width. Within the measured deviation the ARD-RSC with k parameter 0.8 and the ARD model provide the best solution for the core and skin. The 5 scalar parameters within the ARD-RSC model are set at default.

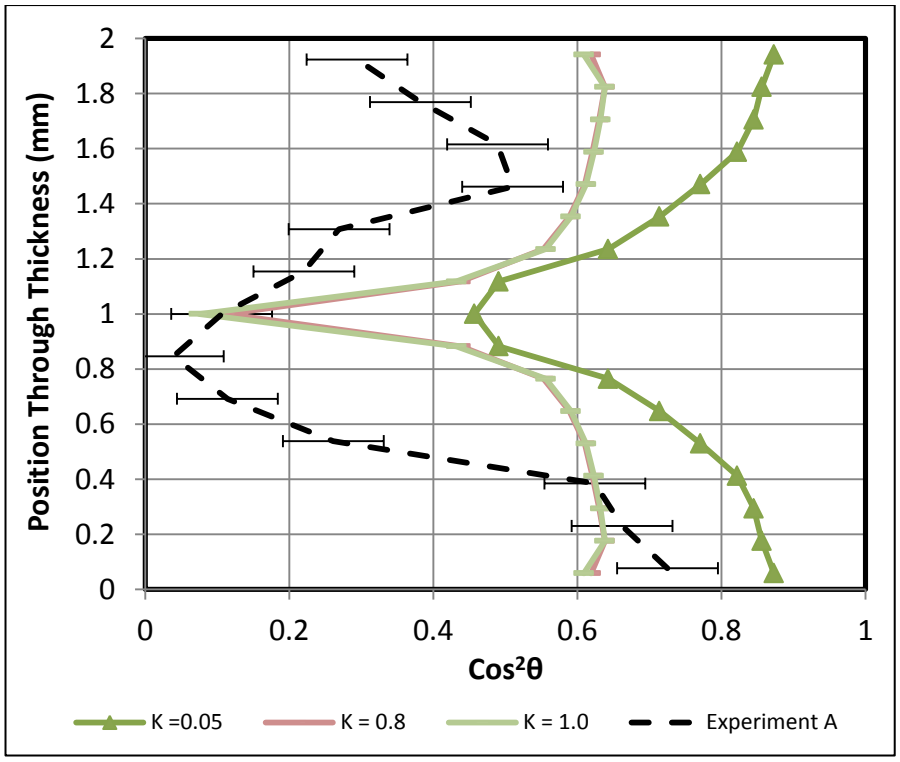

Figure 5.47 Predictions for the ARD and ARD-RSC model against 2 mm centre gate average FOD at location A

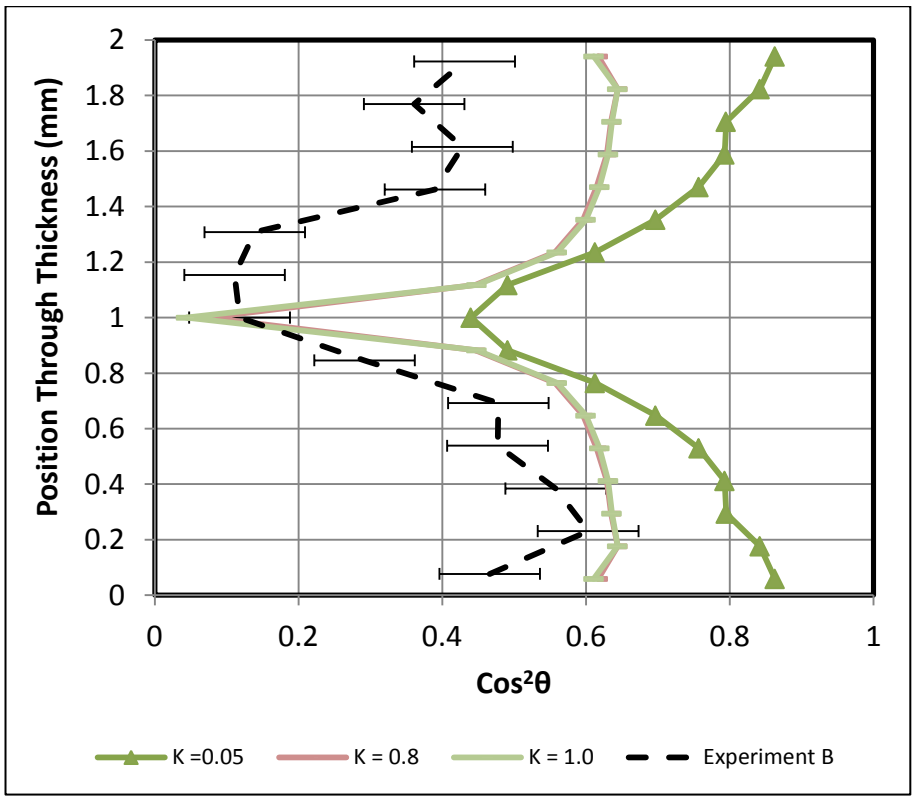

Figure 5.48 Predictions for the ARD and ARD-RSC model against 2 mm centre gate average FOD at location B

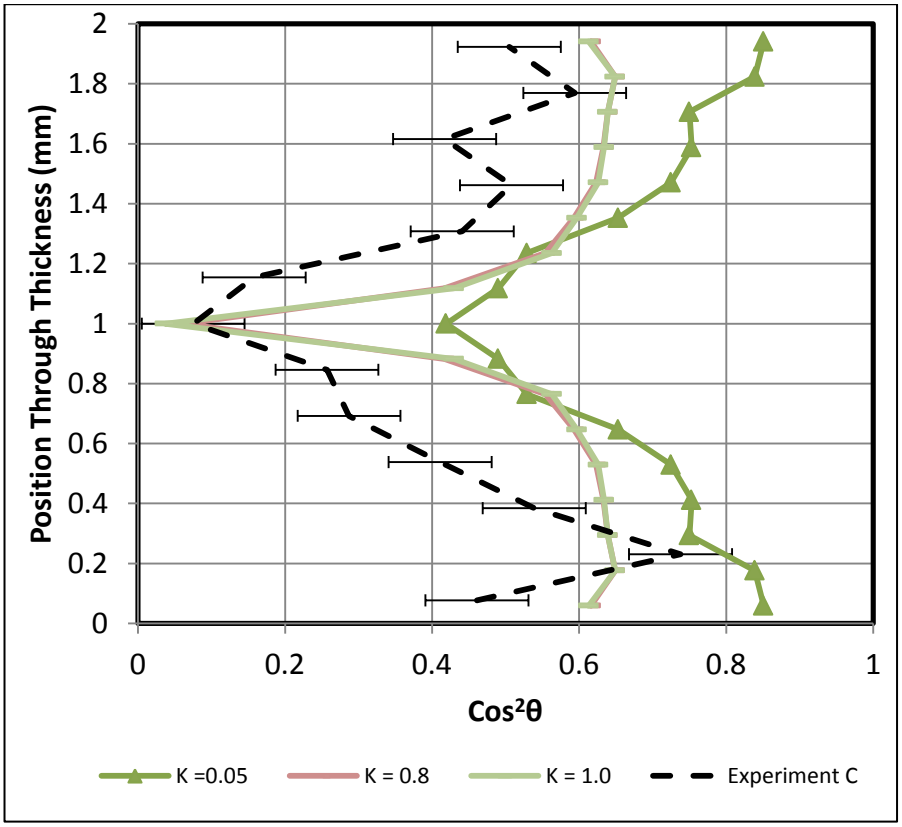

Figure 5.49 Predictions for the ARD and ARD-RSC model against 2 mm centre gate average FOD at location C

The 5 parameters are set as defaults in ASMI 2014 as follows; $b_1 = 0.0001924$, $b_2 = 0.005839$, $b_3 = 0.04$, $b_4 = 1.168 \times 10^{-5}$ and $b_5 = 0$. Although it is not recommended to change these scalar parameters, for this study two of these were changed to give $b_1 = 0.0001924$, $b_2 = 0.005839$, $b_3 = 0.04$, $b_4 = 3$ and $b_5 = 4$. The prediction is implementing the ARD model (k = 1) so there is no influence of the k factor. The model is predicting the average FOD at location A and B of the 2 mm centre gate. Figure 5.50 demonstrates the under prediction (non-physical behaviour) which occurs in the orientation upon the change of 2 scalar parameters. The prediction improves using the default parameters. A better understanding is required of each scalar parameter before a better solution is established.

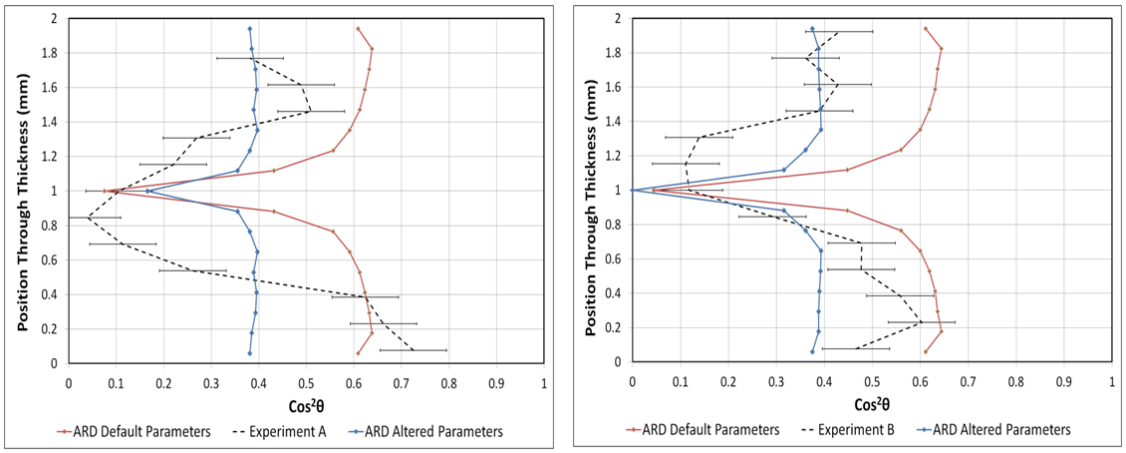

Figure 5.50 Predictions for the ARD default and ARD altered parameters against 2 mm centre gate average FOD at location A and B

5.3.3.3 Summary

The generic rules created for the k factor in the RSC model are applicable to the ARD-RSC model with the addition of the change seen in the shell layer.

Updated K Parameter Rules for ARD-RSC Model

1. To increase the core thickness and to decrease the shell layer thickness select a k value between 0.00001 - 0.01.

2. To increase the shell layer thickness and reduce $\cos^2\theta$ select a k value between 0.2 - 0.8.
3. To decrease the core thickness and to align the fibres within the core transverse to the flow direction select a k value above 0.05.

Both the ARD models over-predict the orientation at the skin and shell layers for both 1 mm and 2 mm centre gate geometries. The core width is over-predicted but the models can predict the transverse alignment of fibres in the core. For the 1 and 2 mm thick centre gate the ARD model or the ARD-RSC with a high k parameter provides the best solution. The solutions predict the orientation at the skin for the 2 mm thick centre gate. Changing the scalar parameters will adjust the ARD prediction. Better understanding is required of each parameter to enhance the prediction, but this problem is outside the scope of this study.

5.4 Conclusions

- Insignificant amount of fibres are cut at the edges when studying the FLD of a 12 x 12 mm specimen compared to an 18 x 18 mm specimen from the LGF centre gate.

- The distribution of curved fibres in the investigated samples is between 13 % and 33 %.

- A large distribution of small fibres is created within the 1 mm centre gate with a 3.5 mm sprue, but the average fibre length increases if the thickness of the sample increases. The fibre breakage is reduced and the average fibre length increases if the sprue size increases to 6 mm. There is more breakage when a 3.5 mm sprue is filing a thick gate compared to a 6 mm sprue. The FLD for the 1 mm components result in more fibre breakage within the sprue caused by the hold pressure when applied to a thin cavity.

- Measured FLD from the extrudate or the sprue is required to enhance the fibre breakage prediction. Even though measured FLD is input into

ASMI 2014 the model over-predicts the fibre breakage within all the components, this is confirmed by the lower average fibre length compared to the measured average fibre length at both locations. The model predicts more fibre breakage at location A compared to location B, which is opposite to the experimental findings.

- The increase in the average fibre length does not change the FOD when studying the centre gate geometry. The size of the core remains in a similar proportion for the 1 mm and 2 mm thick LGF centre gate. A higher orientation is found at the skin within 2 mm thick LGF centre gate.

- The LGF centre gate has a lower orientation at the shell (randomly oriented) and a wider core compared to a SGF centre gate. The difference in the core width between a LGF and SGF specimen is more apparent in a 1 thick mm centre gate compared to the 2 mm thick geometry.

- The long glass fibre FOD model (ARD or ARD-RSC) over- predicts the measured average orientation at the skin and shell layer for the 1 mm and 2 mm thick centre gate. The models predict the transverse core but over-predict the core width. The K parameter in the ARD-RSC model follows the same rules as the K parameter in the SGF RSC model.

- Better understanding is required of the 5 scalar parameters embedded into the ARD model, the wrong choice of parameters can significantly change the prediction.

Chapter 6 Discussion and Conclusion

6.1 Overall Discussion

6.1.1 Experimental Technique

The reflective microscopy system was developed to measure the fibre orientation distribution within SGF composites. For this study the system was used to investigate LGF as well as SGF injection moulded samples. The core within the LGF centre gate geometries is wider in comparison to the SGF samples and the majority of fibres within the core are aligned in the radial direction by the in-plane stretching. The majority of the fibres within LGF samples have the same appearance as short fibres and so the reflective microscopy system can be applied in the same way. The fibres which were over 1 mm in length as well as curved crossed over 2 frames. The image analysis system is capable of capturing a long fibre passing over two adjacent frames. The particle is stored as a fibre which is flat in the measurement plane or a fibre aligned perpendicular to the flow direction. The LGF components investigated in this study consist of 33 % to 13 % of curved fibres at different positions within the centre gate components. In this study there was no method of confirming if the ellipse particle was in fact a curved fibre.

Although the 2-d image analysis system was successful in capturing the average FOD of the centre gate geometry, it may fail to capture the average FOD within other flow patterns. Currently there is no practical and cost-effective solution which can describe the fibre orientation accurately for a long glass fibre sample. A study carried out by Bernasconi et al., (2012) shows very small differences in the measured FOD of a short glass fibre specimen; captured using micro-CT and the optical method. The results from the study show the optical method has a low level of accuracy when measuring the orientation angles of fibres almost perpendicular to the flow. Micro-CT 3-d image analysis is a potential solution to capture the orientation distribution of curved fibres but this involves expensive facilities and lengthy data analysis.

Fibre length measurements were made using the semi-automatic fibre length measurement system. The image analysis detects and measures the length of each straight fibre but the curved fibres were measured manually. As a result of analysing a large dataset the level of error for each specimen measurement was very small. Although the manual measurements of curved fibres was a time consuming exercise, the system is capable of measuring thousands of straight fibres. The system is suitable for measuring the fibre length of short glass fibre samples and requires further development to detect and measure curved fibres.

6.1.2 Modelling

In this study 2-d geometries were created to assess the accuracy of the fibre prediction models. Mid-plane solver consists of a 2-d mesh, which collapses the 3-d model into a number of mid-planes. In essence the flow is symmetric about the mid-plane and the z- axis is equal to zero within the 2-d solver. Therefore the mid-plane solution is unable to calculate the velocity and pressure fields in 3-d features such as corners, gates and ribs. An alternative solution to the mid-plane solver is the 3-d solver, which represents the solid geometry by filling the volume of the model with 4-noded tetrahedral 3-d elements. The overall results suggest that the mid-plane solver is a good solution for investigating simple geometries; the results are achieved with less computational time and speed compared to 3-d models. However the 3-d solver is a solution extensively applied in industry as it is capable of evaluating micro-macro geometries with large differences in dimensional scales (Tofteberg and Andreassen, 2009).

Figure 6.1 shows a comparison between the mid-plane and a latest 3-d solver FOD prediction against the measured 1 mm centre gate SGF average FOD at location A and C. Both geometries are made of elements with an edge length of 1 mm and are applying the SGF RSC model with parameters $k = 0.4$ and $C_i = 0.0057$. The results show the 3-d model predicts the orientation better at the beginning (location A) compared to location C. However the shell model is a better solution to predict the average FOD through the radial flow path. It is

known from the literature that both models use different flow predictions. The 3-d solver technology is still undergoing major development. In the future it could be used to find an accurate solution to the fibre orientation and breakage prediction in any kind of geometry.

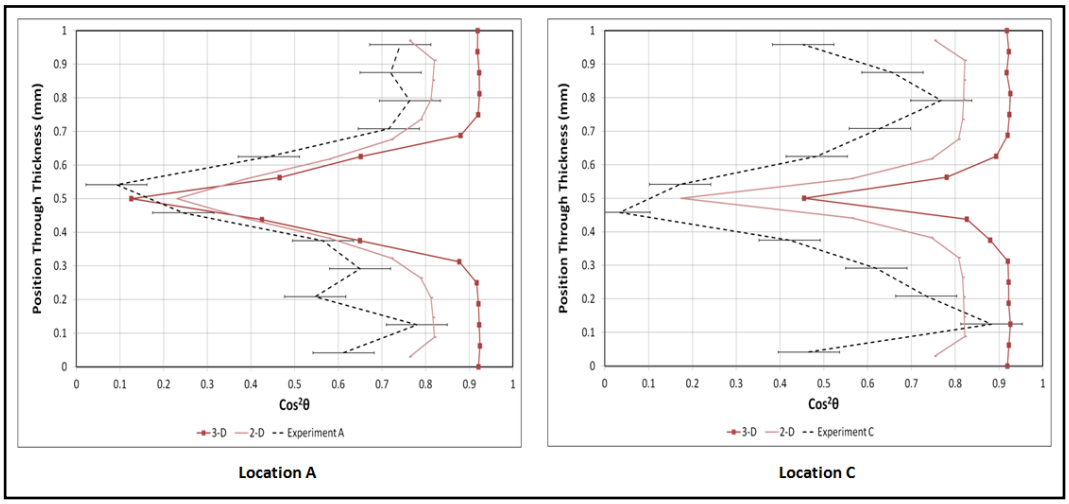

Figure 6.1 Difference in average SGF FOD between the 3-d and 2-d for the 1 mm centre gate geometry

6.1.3 Fibre Orientation Distribution

The discussion for the FOD results is broken down into two sections including measured average FOD and predicted FOD for the fan-gate and centre gate geometries.

6.1.3.1 Experiment

The SGF fibres within thin fan-gate geometry align with the shear, resulting in fibres aligned parallel to the direction of flow towards the end of the plaque. The flow changes in a thick plaque resulting in a wider and transverse core. The average FOD within the SGF centre gate geometry does not vary along the radial flow path for any given thickness. In the centre gate geometry the shell is highly aligned in the direction of flow and the core is aligned perpendicular to the direction of flow by the in-plane stretching. If the thickness of the centre gate geometry increases the core width increases. The core is wider and aligned transverse to the direction of flow within a 2 mm thick SGF centre gate geometry compared to a 2 mm thick plaque.

The average FOD [2mm thick centre gate geometry is different for SGF and LGF systems. In comparison to the SGF the core of a LGF system is wider and the fibres in the shell layer are oriented in a random formation. The difference between the core width of a 1 mm thick and 2 mm thick LGF is negligible in comparison to the change seen in SGF component. When the thickness of the part increases the change noticed in core width is less within the LGF orientation compared to the SGF orientation. Increasing the average length within the LGF centre gate does not change the average FOD. The FOD measurements were not taken from the 5 mm thick section which protrudes from the base of the centre gate geometry. However it would be interesting to investigate the FOD within this section in the future.

6.1.3.2 Prediction

6.1.3.2.1 Short Glass Fibre Orientation

There are user defined parameters for each SGF orientation prediction model assessed in this study. Generic rules have been created for each parameter within these models, which narrow down the possible solutions which could enhance the FOD prediction for each parameter. The rules were applied to the 4 mm plaque and the 1, 2 and 4 mm centre gate measured data and functioned well. The generic rules apply against the measured average SGF FOD. The parameters found for the geometries in this study are possible solutions for other geometries when processing a similar material. The recommended parameters found for each model are not the same as the recommended parameters in the published domain.

The FT model is not as accurate as the RSC and MFT models. The majority of the default parameters chosen by ASMI 2014 do not predict a better solution compared to the recommended parameters. The solutions for the centre gate geometries are a closer approximation to the measured FOD (including 4 mm centre gate) compared to the fan-gate solutions. The recommended parameters for each SGF prediction model are summarised in Table 6.1. The best solution for each SGF 40 wt% injection moulded geometry is highlighted in grey in Table 6.1.

Geometry	FT	MFT	RSC
2 mm plaque	$C_i = 0.03$	$C_i = 0.0057$ and $D_z = 0.15$	$C_i = 0.0057$ and $K = 0.1$
4 mm plaque	$C_i = 0.06$	$C_i = 0.03$ and $D_z = 0.15$	$C_i = 0.0057$ and $K = 0.8$
1 mm centre gate	$C_i = 0.0057$	$C_i = 0.0057$ and $D_z = 0.15$	$C_i = 0.0057$ and $K = 0.6$
2 mm centre gate	$C_i = 0.001$	$C_i = 0.001$ and $D_z = 0.2$	$C_i = 0.001$ and $K = 0.8$
4 mm centre gate	$C_i = 0.00065$	$C_i = 0.00065$ and $D_z = 0.2$	$C_i = 0.00065$ and $K = 0.8$

Table 6.1 Recommended parameters for each SGF FOD model

Clearly the existing theories cannot accurately model the 4 mm thick plate. It would be of interest to investigate similar plates of thicknesses ranging between 0.5 and 3.5 mm to determine the limits of accurate prediction. However the MFT model can accurately model the orientation within the 4 mm thick SGF centre gate geometry. Each fibre orientation prediction model is suitable if the right parameters are selected when studying expansion flow. However in the case of shear dominated flow this only applies to geometries 2 mm thick.

6.1.3.2.2 Long Glass Fibre

The long glass FOD (ARD and ARD-RSC) models over-predict the average measured FOD. Although a high value of the k parameter can predict the transverse core the models are unable to predict the core width. The ARD model is dependent on 5 scalar parameters which influence the prediction. More research is required to understand these parameters; there is no published work to explain the effect each parameter has on the orientation prediction. To improve the mathematical model and to predict the orientation of a curved fibre, more research could be carried out on LGF injection moulded composites. Further LGF FOD measurements need to be carried out on various LGF material and injection moulded cavity shapes. Additional investigations need to be carried out using different measurement techniques including the optical technique. Any new measurement technique will assess the limitations of the optical FOD measurement system.

6.1.4 Fibre Length

The discussion for the FLD of long glass fibre is broken down into two sections including measured FLD and predicted FLD for the centre gate geometries.

6.1.4.1 Experiment

The design of the sprue and the thickness of the base were configured for the centre gate geometry. Increasing the size of the sprue increases the average fibre length within a 1 mm thick centre gate. Changing the sprue size has very small significance within the 2 mm thick part. Hence the overall fibre breakage (at location B in Figure 5.2) is similar within the 2 mm component with either sprue geometry. The average fibre length does not change within the extrudate (material from the barrel) if the size of the nozzle increase. The overall breakage within the centre gate geometry reduces as the thickness increases. Approximately 30,000 fibres were measured for each specimen. A large dataset allows an accurate comparison between the predicted and the measured FLD or average length at location A and B of the centre gate component.

6.1.4.2 Prediction

The fibre breakage predictions improve significantly with the input of measured FLD. The FLD prediction for the 2 mm thick centre gate is a better prediction to the measured FLD in comparison to the 1 mm thick centre gate. However the predicted average in each scenario is lower compared to the measured number average fibre length. The lower average fibre length indicates the model is over-predicting the fibre breakage. The model under-predicts the fibre breakage which occurs at location B (further along the flow path). The predicted results are using the default ASMI 2014 defined parameters. The fibre breakage prediction may be improved further by validating the parameters against the measured FLD.

6.2 Conclusions

The conclusions derived from this thesis are listed below; these conclusions outline the objectives to validate long and short fibre orientation and breakage models, with measured FLD and FOD measurements. Measurements were taken from long and short injection moulded components. Limitations and possible solutions are outlined to improve predictions of fibre length and orientation.

- The FOD within the centre gate disc does not change significantly after 16 mm along the radial flow path. The $\cos^2\theta$ reduces at the skin, shell and core layers as the thickness of a plaque increases. As a result of the stretching within the centre gate geometry the core is wider, transversely aligned to the direction of flow compared to the plaque where fibres align in the direction of shear flow.

- The MFT and FT model can predict the in-plane stretching motion which orients the fibres within the 1 mm, 2 mm and 4 mm centre gate geometries.

- Findings for the end gate geometries suggest the RSC model offers a better solution, especially for the 2 mm thick plate. Hence the RSC prediction slows down the rate at which orientation develops in the FT model. At present models within ASMI 2014 are not capable of predicting the FOD within the 4 mm thick plaque.

- ASMI 2014 selects a default value of C_i = 0.0057 regardless of the reduced strain factor for Rhodia Technyl C216 V40, which is 40 wt% short glass fibre. This setting is the same for any geometry or thickness and is imposed by material selection.

- For any part with a thickness < 1.5 mm the default value of C_i can be set to 0.0057. For the thin geometries the parameter Ci = 0.0057 is a good solution for both the MFT and RSC models. The optimum coefficients

for the centre gate geometry do not match the findings from previous literature.

- A significant increase in the average fibre length does not change the average FOD when studying the LGF centre gate geometry.

- When studying the average FOD the size of the core remains in a similar proportion for the 1 mm and 2 mm thick LGF centre gate.

- The average FOD for the LGF has a lower orientation at the shell (randomly oriented) and a wider core compared to a SGF centre gate. The difference in the core width between the LGF and SGF average FOD is more apparent in a 1 mm centre gate compared to the 2 mm wide geometry.

- A higher orientation is found at the skin within 2 mm thick LGF centre gate.

- Reducing the sprue size from 6 mm to 3 mm increases the overall fibre breakage within a 1 mm thick centre gate cavity.

- The size of the sprue has little influence on the overall fibre breakage within the 2 mm thick centre gate geometry.

- The FLD for the 1 mm thick centre gate components result in more fibre breakage within the sprue, caused by the hold pressure when applied to a thin cavity.

- Insignificant amount of fibres are cut at the edges when studying the FLD of a 12 x 12 mm specimen compared to an 18 x 18 mm specimen from the LGF centre gate.

- The fibre breakage model under-predicts the FLD and L_n when the initial pellet length (12.5 mm) is input into to the model. In the case of the

centre gate geometry the model predicts more fibre breakage closer to the gate compared to location B (further along the flow path), which is opposite to the experimental findings.

- The measured FLD at the end of plastification is input into ASMI 2014 to enhance the predicted FLD and L_n.

- The long glass fibre FOD model (ARD or ARD-RSC) over-predicts the measured average FOD for the 1 mm and 2 mm thick centre gate.

- Better understanding is required of the 5 scalar parameters embedded into the ARD model, the wrong choice of parameters can significantly change the prediction.

Chapter 7 Future Work

Areas where there is a deficient amount of knowledge have been found from the established conclusions. Below is a brief outline of each idea which could be examined further.

- There is opportunity for further refinement and optimisation of the latest fibre orientation and length prediction models, which have been incorporated into Autodesk Moldflow. These models include the LGF orientation model (ARD-RSC), which has been developed by Phelps, (2009) and is based upon the orientation of LGF. The fibre breakage model introduced by Tucker et al., (2010) is based upon the initial length of LGF material. Both of these models are over-predicting in comparison to the measured findings. The fibre breakage prediction improves dramatically if measured FLD at the end of plasticization is input. Further investigation is required into the parameters which influence the LGF prediction models.

- In order to optimise the LGF FOD prediction model, reliable test data is required for the FOD. The long glass fibre specimens contain long fibres in a specimen which have a tendency to curve. To overcome the problem of distinguishing curved fibres from straight the specimen can be investigated using micro-CT. This technique will create a 3-d image reconstruction of the specimen at a micrometer scale. Algorithms then need to be developed to calculate the FOD of each fibre. A comparison of the optical and micro-ct image analysis techniques shall point out limitations of the optical technique.

- The LGF components were injection moulded using the recommended back pressure, screw speed and injection speed parameters. A separate study could be carried out to investigate the effect varying injection moulding parameters has on the fibre length and mechanical properties. The injection speed, screw speed and back-pressure are the parameters which could be investigated.

- Clearly the existing theories cannot accurately model the FOD within the 4 mm thick plate. A solution is required to improve the SGF FOD prediction for the thick plaque geometry. For future studies the geometry should have a thicknesses ranging between 0.5 and 3.5 mm to determine the limits of accurate SGF FOD prediction.

- The mid-plane solver provides a good solution to investigate the fibre prediction models. However in the future the 3-d solver could be applied to study complex geometries.

- It would be useful to measure and predict the FOD and FLD around ribs and corners for both short and long glass fibre material. The 5 mm thick section protruding from the base of the centre gate geometry is a good example for the study.

References

Advani. S.G. and Tucker III. C.L. (1987). 'The use of tensors to describe and predict fiber orientation in short fiber composites'*. J. Rheology*, 31 (8), pp. 751–784.

Ahmadi. Z., Gaffarian. R.S. and Amiri. D. (2000). 'Continuous melt impregnation Process: Materials Parameters'. *Iranian Polymer Journal,* 9 (2), pp. 125-129.

Akay. M. and Barkley. D. (1991). 'Fibre orientation and mechanical behaviour in reinforced thermoplastic injection mouldings'. *Journal of Materials Science*, 26(10), pp. 2731-2742.

Altan. M.C., Subbiah. S. and Güçeri. S.I. (1990). 'Numerical prediction of three-dimensional fiber orientation in Hele-Shaw flows'. *Journal of Polymer Composites,* 30 (14), pp. 848-859.

Au. C.K. (2005). 'A geometric approach for injection mould filling simulation'. *Journal of Machine Tools & Manufacture Design Research and Application*, 45(1), pp. 15 – 124. Autodesk Simulation Moldflow Insight, Help Guide, 2014.

Bailey. R.S. and Kraft. H. (1987). 'Study of fibre attrition in processing of long fibre reinforced thermoplastics'. *Journal of Polymer Processing*, 2, pp. 94-101.

Bailey. R.S., Davies. M. and Moore. R.D. (1989). 'Processing property characteristics for long glass fibre reinforced polyamide'. *Journal of Composite*, 20 (5), pp. 453-460.

Bates. P. J. and Wang. C. Y. (2003). 'The effect of sample preparation on the mechanical properties of nylon 66'. *Journal Polymer Engineering & Science*, 43 (4), pp. 759-773.

Bay. R. S. and Tucker III. C. L. (1992). 'Stereological measurement and error estimates for three-dimensional fiber orientation'. *Polymer Engineering and Science*. 32, pp. 240-253.

Bay. R.S. and Tucker III. C.L. (1992). 'Fiber orientation in simple injection moldings. Part I. Theory and numerical methods'. *Journal of Polymer Composite*, 13 (4), pp. 317–331.

Bay. R.S. and Tucker III. C.L. (1992). 'Fiber orientation in simple injection moldings. Part II. Experimental Results'. *Journal of Polymer Composite*, 13 (4), pp. 332–342.

Bernasconi. A. (2008). 'Local anisotropy analysis of injection moulded fibre reinforced polymer composites'. *Journal of Composite Science and Technology*, 68 (12), pp. 2574-2581.

Bernasconi. A., Cosmi. F. and Hine. P.J. (2012). 'Analysis of fibre orientation distribution in short reinforced polymers: A comparison between optical and

tomographic methods'. *Journal of Composite Science and Technology*, 72 (16), pp. 2002-2008.

Bernie. A.O and Martin. E.D. (2001). 'Practical injection moulding'. New York: Marcel Dekker.

Bijsterbosch. H. and Gaymans. R. J. (1995). 'Polymaide 6-long glass fibre injection mouldings'. *Journal of Polymer Composite'*, 16(5), pp. 363 -369.

Brenner. H. (1974). 'Rheology of a dilute suspension of axisymmetric Brownian particles'. *International Journal of Multiphase Flow*, 1 (2), pp. 195-341.

Bright. P. F., Crowson. R. J. and Folkes. M. J. (1978). 'A study of the effect of injection speed on fibre orientation in simple mouldings of short glass fibre-filled polypropylene'. *Journal of Materials Science*, 13(11), pp. 2497-2498.

Bright. P.F. and Darlington. M.W. (1980*).'* Factors influencing fibre orientation and mechanical properties in fibre reinforced thermoplastics injection mouldings'. *International Conference on Practical Rheology in Polymer Processing*. Loughborough, Ed: Computers & Chemical Engineering. pp 14.1-14.10

Brydson. J. A. (1970). 'Flow Properties of Polymer Melts'. 2nd edn. Great Britain: Butterworth Group.

Bubb. S.L. (2001). 'Fibre orientation in injection moulded composites'. PhD. Thesis. University of Leeds.

Cardozo. D. (2008). 'Three models of the 3-d filling simulation for injection moulding: A brief review'. *Journal of Reinforced Plastics and Composites*, 27 (18), pp. 1963–1974.

Cheremisinoff, N.P. (1993). 'An introduction to polymer rheology and processing'. Florida: CRC Press, Inc.

Cintra. J.S. and Tucker. C.L. (1995). 'Orthotropic closure approximations for flow-induced fibre orientation'. *Journal of Rheology*, 39(6), pp. 1095-1122.

Clarke. A.R. and Eberhardt. C. (1999). 'The representation of reinforcing fibres in composites as 3-d space curves'. *Journal of Composite Science and Technology*, 59 (8), pp. 1227-1237.

Clarke. A.R., Archenhold. G. and Davidson. N.C. (1995). 'A novel technique for determining the 3-d spatial distribution of glass fibres in polymer composites'. *Journal of Composite Science and Technology*, 55 (1), pp. 75-91.

Cooper. G.A. and Kelly. A. (1969). 'Role of interface in the fracture of fibre-composite materials'. Interfaces in composites ASTM STP 452. American Society for Testing and Materials, pp. 30-106

Dahl. J., Blanchard. P., Latimer. T., Sudrla. J. and Henshaw. J. 'A method for characterizing fiber length distribution in random fiber composites'.

Proceedings of the 11th Annual SPE Automotive Composites Conference and Exposition. 2011.

Darlington. W.M. and Mcginley. L.P. (1975). 'Fibre orientation distribution in short fibre reinforced plastics'. *Journal* of *Materials Science*, 10 (5), pp. 906-910.

Davidson, N.C., 'Image analysis for fibre orientation measurements', PhD Thesis, University of Leeds, 1993.

Davidson. N.C. and Clarke. A.R. (1999). 'Extending the dynamic range of fibre length and fibre aspect ratios by automated image analysis'. *J. of Microscopy*, 196 (2), pp. 266-272.

Davidson. N.C., Clarke. A.R. and Archenhold. G. (1997). 'Large-area, high-resolution image analysis of composite material'. *J. of Microscopy*, 185 (2), pp. 233-242.

Dinh. M.S. and Armstrong. R.C. (1984). 'A rheological equation of state for semi-concentrated fibre suspensions'. *Journal of Rheology*, 28 (3), pp. 207-227.

Downey. R.A. (1987). *International conference on reinforced injection processing thermoplastic and thermosets*. Solihull, 24 – 25 February 1987. Ed: Plastics and Rubber Institute. England: Science and Technology Publisher Ltd. pp 1.1 – 1.7, 4.1 – 4.19, 6.1 – 6.10, 7.1 – 7.7, 13.1 – 13.12, 14.1 – 14.5

Egitto. F.D. (1990). 'Plasma etching and modification of organic polymer'. *Journal* of *Applied Chem,* 62 (9), pp. 1699-1708.

Eshelby. J.D. (1957). 'The determination of the elastic field of an ellipsoidal inclusion, and related problems'*. Proc. Royal Society of London A*, 241, pp. 376-396.

Fan. X., Phan-Thien. N. and Zheng. R. (1998). 'A direct simulation of fibre suspensions'. *Journal of Non-Newtonian Fluid Mechanics*, 74, pp. 113-135.

Folgar. F. and Tucker III. C.L. (1984). 'Orientation behaviour of fibers in concentrated suspensions. *Journal of Reinforced Plastic and Composite'*, 3 (2), pp. 98–119.

Fu. Y.S., Lauke. B., Mader. E., Yue. Y.C. and X. Hu. (2000). 'Tensile properties of short-glass-fibre and short-carbon-fibre reinforced polypropylene composites'. *Composites Part A: Applied Science and Manufacturing*, 31(10), pp. 1117-1125.

Fu. Y.S., Mai. W.Y., Ching. C.Y.E. and Li. K.Y.R. (2002). 'Correction of the measurement of fiber length of short fiber reinforced thermoplastics'. *Composites Part A: Applied Science and Manufacturing*, 33(11), pp. 1549-1555.

Gauthier. M. M. (1995). 'Engineered Materials Handbook, Desk Edition'. ASM International: Taylor Francis.

Gonzalez. R.C. and Woods. R.E. (1993). 'Digital Image Processing'. Prentice Hall.

Greszczuk, L.B. (1969). 'Theoretical studies of the mechanics of the fiber-matrix interface in composite'. *Interfaces in Composites ASTM STP 452 American Society for Testing and Materials*, pp. 42-58.

Groover. P.M. (2010). 'Fundamentals of modern manufacturing: materials, processes and system'. U.S.A: John Wiley and Sons Ltd, p. 162, fig. 8.9.

Gupta. V. B., Mittal. R. K., Sharma. P. K., Mennig. G. and Wolters. J. (1989). 'Some studies on glass fiber-reinforced polypropylene. Part II: Mechanical properties and their dependence on fiber length, interfacial adhesion, and fiber dispersion'. *Journal of Polymer Composite*, 10, pp. 16–27

Gupta. V. B., Mittal. R. K., Sharma. P. K., Mennig. G. and Wolters. J. (1989). 'Some studies on glass fiber-reinforced polypropylene. Part I: Reduction in fiber length during processing'. *Journal of Polymer Composite*, 10, pp. 8–15.

Hand. G. L. (1962). 'A theory of anisotropic fluids'. *Fluid Mech*, 13, pp. 33 - 46.

Hayes. B.S. and Gammon. (2010). 'Optical microscopy of fiber-reinforced composites'. (OH) USA: ASM International, Materials.

Hieber. C.A. and Shen. S.F. (1980). 'A finite-element/finite-difference simulation of the injection-molding filling process'. *J. Non-Newtonian Fluid Mech*. 7, pp. 1–32.

Hine, P.J. and Dukett, A.R. (2004). 'Fiber orientation structures and mechanical properties of injection molded short glass fiber reinforced ribbed plates'. *Polym. Compos*ite, 25 (3), pp. 237–254.

Hine. P.J., Davidson. N.C, Dukett. A.R and Ward. I.M . (1995). Measuring the fibre orientation and modelling the elastic properties of injection-moulded long-glass-fibre-reinforced nylon. *Composite Science and Technology*, 53 (2), 125-131.

Hine. P.J., Dukett. A.R., Davidson. N.C. and Clarke. R.A. (1993). Modelling of the elastic properties of fibre reinforced composites. I: Orientation measurement. *Composite Science and Technology*, 47 (1), 65-73.

Hine. P.J., Duckett.R.A., Caton-Rose. P. and Coates, P.D. (2004). 'Fibre orientation structures and their effect on crack resistance of injection moulded transverse ribbed plate'. *Journal of Plastics, Rubbers and Composite,* 33 (1), pp. 43-53.

Hine. P.J., Duckett.R.A., Caton-Rose. P., Coates, P.D., Jittman. P., Chapman. C. and Smith.G (2005). 'Fibre orientation: measurement, modelling and knowledge based design'. *Journal of Plastics, Rubbers and Composite,* 34 (9), pp. 417- 424.

Hine. P.J., Parveen. B., Brands. D. and Caton-Rose. P. (2014). 'Validation of the modified rule of mixtures using a combination of fibre orientation and fibre length'. *Journal of Composite Part A,* 64 (13), pp. 70-78.

Hofmann. J. T., Vélez-Garcia. G. M., Baird. D. G. and Whittington. A. R. (2013). 'Application and evaluation of the method of ellipses for measuring the orientation of long, semi-flexible fibers'. Journal *of Polymer Composite*, 34, pp. 390–398.

Hofmann. J.T., Meyer. K.J. and Baird. D.G. (2008). 'The effect of glass fibre length on orientation distribution within center and end gated injection molded composite' *Proceedings of the Annual Automotive Composites Conference and Exhibition'*, SPE ACCE, 9 pages.

Hoshen Pricision and Plastic. (2009). 'The plastic injection moulding system'. Available at: http://www.mold-china.net/en_us/news/show?id=3 (Accessed: 27 February 2014).

Huilier. D. and Patterson. W.I. (1991). 'Simulation of the packing and cooling phases of thermoplastic injection moulding'. In: Isayev. A.I., Utracki. L.A. and Singh. A. Modelling of polymer processing recent developments. Oxford University Press. pp 172 – 203.

Jeffery. G.B. (1922). 'The motion of ellipsoidal particles immersed in a viscous fluid'. *Proceedings of Royal Society. A*, 102, pp. 161–179.

Jin. X. and Jin. W. 'Fibre breakage calculation for injection molded long fiber composite'. SPE annual technical conference - ANTEC. Boston (USA), 2011.

Kagan. V.A., Mcpherson. R. and Chung, J.S. (2003). 'An advanced high modulus (HMG) short glass – fibre reinforced nylon 6: Part 1 – role of fibre – glass reinforcement'. *Journal of Reinforced Plastics and Composites*, 22 (11), pp. 1035 – 1044.

Kamal. M.R., Song. L. and Singh. P. (1986). 'Experimental measurement of fiber and matrix orientations in fiber reinforced composites'. *Journal of Polymer Composites,* 7 (5), pp. 323-329.

Kastner. J., Plank. B. and Salaberger. D. *(2012). 'High resolution X-ray computed tomography of fibre- and particle filled polymers'. 18th world conferecne of nondestructive testing. South Africa (Durban), 16-20 April 2012.*

Kelly. A. and Davis. G.J. (1965). 'The principles of the fibre reinforcement of metals'. *Metallurgical Reviews*, Vol. 10, pp. 1-77.

Kelly. A. and Tyson. R.W. (1965). 'Tensile properties of fibre-reinforced metals: copper/tungsten and copper/molybdenum'. *Journal of the Mechanics and Physics of Solids,* 13(6), pp. 329-338.

Keshtkar. M., Heuzey. M.C., Carreau. P.J., Rajabian. M. and Dubois. C. (2010). 'Rheological properties and microstructural evolution of semi-flexible fiber suspensions under shear flow'. *Journal of Rheology,* 54 (2), pp. 197-222.

Koch. D.L. (1995). 'A model for orientational diffusion in fiber suspensions'. *Phys. Fluids*, 7, pp. 2086-2088.

Kunc. V., Frame. B., Nguyen. B.N., Tucker. C.L. and Valez-Garcia.G. 'Fiber length distribution measurement for long glass and carbon fiber reinforced injection molded thermoplastics'. *Proceedings of the 7th Annual SPE Automotive Composites Conference and Exposition*. 2007.

Lafranche. E., Krawczak. P., Ciolczyk. J.P. and Maugey. J. (2005). 'Injection moulding of long glass fibre reinforced polyamide 66: Processing condition/microstructure/flexural properties relationship '. *Advances in Polymer Technology*, 24(2), pp. 114-131.

Lafranche. E., Krawczak. P., Ciolczyk. J.P. and Maugey. J. (2007). 'Injection moulding of long glass fibre reinforced polyamide 6-6: guidelines to improve flexural properties'. *Express Polymer Letters*, 1 (7), pp. 456-466.

Mallick. K.P. (2000).' Particulate and short fiber reinforced polymer composites'. In: Kelly. A. and Zweben. C. Comprehensive Composite Materials. Pergamon, Oxford, pp. 291-331.

Matthews. F.L. and Rawlings. R.D. (1994). 'Composite Materials: Engineering and Science'. London: Chapman and Hall.

McCrum. N.G., Buckley. C.P. and Bucknall. C.B. (1997). 'Principles of Polymer Engineering'. 2nd edn. New York: Oxford University Press Inc.

McGrath. J.J. and Wille. J.M. (1995). 'Determination of 3-d fiber orientation distribution in thermoplastic injection molding'. *Journal of Composite Science and Technology*, 53 (2), pp. 133-143.

Monnich. S., Glockner. R. and Becker. F. *(2004). 'Analysis of fibre orientation using µCT data'. 8th European LS-DYNA Conference , 15 pages.*

Nassehi. V. (2002). 'Practical aspects of finite element modelling of polymer processing'. England: John Wiley and Sons, Inc.

Navier. C. L. M. H. (1823). Mem acad. R. sci. paris, Vol. 6 pp 389-416.

Nelson. W.E. (1976). 'Nylon Plastic Technology'. London: Newnes-Butterworth for Plastics and Rubber Institute.

Nguyen. B.N., Bapanapalli. K.S., Holbery. D.J., Smith. T.M., Kunc. V., Frame. J.B., Phelps. J.H. and Tucker. C.L. (2008). 'Fiber length and orientation in long-fiber injection-molded thermoplastic – Part 1: modelling of microstructure and elastic properties'. *J.Composites Material*, 42 (10), pp. 1003-1029

Nguyen. B.N., Holbery. D.J., Johnson. I.K. and Smith. T.M. (2005). 'Long-fiber thermoplastic injection molded composites: From process modelling to property prediction'. *Proceedings of the 5th Annual Automotive Composites Conference and Exhibition'*, SPE ACCE, 9 pages.

Nguyen. B.N., Jin. X., Wang. J., Phelps. J.H., Tucker. C.L., Kunc. V., Bapanapalli. K.S. and Smith. T.M. (2010). 'Implementation of new process

models for tailored polymer composite structures into processing software packages'. Pacific Northwest National Laboratory: U.S. Department of Energy.

Nomoto. M., Tanaka. T., Yoshihiko. A. and Inoue, A. (2012). 'Study on the effect of screw geometries on fiber length and dispersion of GFRTP in injection moulding'. *Procedings of polymer processing society.* Niagara Falls (Canada), 21-24 May.

Olmsted. A. B. and Davis. E.M. (2001). 'Practical Injection Moulding'. New York: Marcel Dekker.

O'Regan, D. and Akay. M. (1996). 'Distribution of fibre lengths in injection moulded polyamide composite components'. *Journal of Material Processing Technology*, 56, pp. 282-291.

Osher. S. and Sethian. A.J. (1988). 'Fronts propagating with curvature-dependent speed: algorithms based on Hamilton-Jacobi formulations'. *Journal of computational physics*, 79, pp. 12–49.

Parham. A.R. and Church. O John. (1977). 'On the calculation of weighted average fibre length in paper'. *IPC Technical Paper Series*, Number 44.

Park. M.J. and Park. J.S. (2011). 'Modelling and simulation of fiber orientation in injection moulding of polymer composite'. *Hindawi publishing corporation*, Volume 2011, pp. 14.

Parveen. B. (2010). 'Automotive Pedal Analysis', BEng Project, University of Bradford.

Patcharaphun. Somjate, and Opaskornkul. Grand. (2008). 'Characterization of fiber length distribution in short and long glass-fiber reinforced polypropylene during injection moulding process'. *Natural Science*, 42 (5), pp. 392-397.

Phan-Thien. N., Fan, X., Tanner. I.R. and Zheng. R. (2002). 'Folgar-Tucker constant for fibre suspension in a Newtonian fluid'. *Journal Non-Newtonian Fluid Mech*, 103, pp. 251-260.

Phelps. J.H. (2009). 'Processing-microstructure models for short-and long-fibre thermoplastics composites'. PhD. Thesis. University of Illinois at Urbana-Champaign.

Phelps. J.H. and Tucker III. C.L. (2008). 'An anisotropic rotary diffusion model for fiber orientation in short and long –fiber thermoplastic'. *Journal of Non-Newtonian Fluid Mechanics*., 256 (3), pp. 165–176.

Piggot. R.M. and Harris. B. (1980). 'Factors Affecting the compression strength of aligned fibre composites'. In: Bunsell. R.A., Bathias. C., Martrenchar. A., Menkes. D. and Verchery. G. Proceedings of Metallurgical Society of Canadian Institute of Mining and Metallurgy. Pergamon Oxford. pp.305 – 312.

Powell. C.P. and Ingen Housz. J.A. (1998). 'Engineering with polymers'. Cheltenham: Stanley Thornes. Proceedings of Metallurgical Society of

Canadian Institute of Mining and Metallurgy. Pergamon Oxford. pp. 259 – 274.Piggot, R.M. (1989). 'Fundamental Concepts of Reinforced Polymers'. In: Wilkinson, S.D.

Reddy. J.N. (1993). 'An Introduction to the Finite Element Method'. 2nd edn. U.S.A: McGraw-Hill.

Rhodia Technical Data Sheet. (2011): Technyl C 216 V40 Black. Solvay Rhodia

Rochow. G. T. and Tucker. P. A. (1994). 'Introduction to Microscopy by Means of Light Electrons, X Rays, or Acoustics'. 2nd edn. New York: Plenum Press.

Rohde. M., Ebel. A., Wolff-Fabris. F. and Altstadt. V. (2011). 'Influence of processing parameters on the fiber length and impact properties of injection molded long glass fiber reinforced polypropylene'. *Journal of the Polymer Processing*, 26 (3), pp. 292-303.

Rostato. V.D. (1996). 'Injection moulding higher performance reinforced plastic composites'. *Journal of Vinyl and Additive Technology*, 2 (3), pp. 216-220.

Sabic Injection Moulding Guide. (2011): STAMAX Long Fibre Polypropylene. Sabic Europe

Sabic Technical Data Sheet. (2013): STAMAX Long Fibre Polypropylene. Sabic Europe

Salaberger. D., Kannappan. A.K., Kastner. J., Reussner. J. and Auinger. T. (2011). 'Evaluation of computed tomography data from fibre reinforced polymers to determine fibre length distribution'. *Journal of Polymer Processing*, 26 (3), pp. 285-291.

Sawyer. C.L and Grubb. T.D. (1987). 'Polymer Microscopy'. London: Chapman and Hall.

Schijve. W. (2000). 'High Performance at medium fibre length in long glass fibre polypropylene'. *Journal of Plastic, Additives and Compounding,* 2 (12), pp. 14-21.

Schijve. W. (2010, May). Long fibre PP: understand the properties, and know how to design and simulate application. [PowerPoint slides]. Presented at Sabic Global Application Technology.

Shen. Changyu., Zhai. Ming. and Gu. Yuanxian. (2005). 'An improved algorithm for the simulation of injection-molding filling process'. *Journal of Reinforced Plastics and Composites,* 34 (7), pp. 691-698.

Sims. D.G. and Broughton. R.W. (2000). 'Glass fiber reinforced plastics—properties'. In: Kelly. A. and Zweben. C. Comprehensive Composite Materials. Pergamon, Oxford, pp. 151-197.

Steinbach. J. (2002). 'Variational inequality approach to free boundary problems with application in mould filling'. Switzerland: Birkhauser Verlag.

Talwar. K., Costa. F., Rajupalem. V., Antanovski. L. and Friedl. C. 'Three-dimensional simulation of plastic injection moulding'. SPE annual technical conference - ANTEC*.* Atlanta (Georgia), 1998.

Templeton. A.P. (1990). 'Strength predictions of injection molding compounds'. *Journal of Reinforced Plastics and Composites,* 9 (3), pp. 210-225.

Thattaiparthasarathy. K.B., Pillay. S., Ning. H. and Vaidya. (2008). 'Process simulation, design and manufacturing of long fiber thermoplastic composite for mass transit application'. *Journal of Composite: Part A*, 39, pp. 1512-1521.

Thomason. J.L. (2002). 'The influence of fibre length and concentration on the on the properties of glass-fibre reinforced polypropylene: 5. Injection moulded long and short fibre PP'. *Composites Part A: Applied Science and Manufacturing*, 33 (12), pp. 1641-1652.

Thomason. J.L. (2005). 'The influence of fibre length and concentration on the properties of glass fibre reinforced polypropylene. 6. The properties of injection moulded long fibre PP at high fibre content'. *Composites Part A: Applied Science and Manufacturing*, 36 (7), pp. 995-1003.

Thomason. J.L. (2007). 'The influence of fibre length and concentration on the properties of glass fibre reinforced polypropylene: 7. Interface strength and fibre strain in injection moulded long fibre PP at high fibre content'. *Composites Part A: Applied Science and Manufacturing*, 38, pp. 210-216.

Thomason. J.L. (2008). 'The influence of fibre length, diameter and concentration on the impact performance of long glass-fibre reinforced polyamide 6, 6'. *Composites Part A: Applied Science and Manufacturing*, 40 (5), pp. 625-634.

Thomason. J.L. and Schoolenberg. G.E. (1994). 'An investigation of glass fibre/polypropylene interface strength and its effect on composite properties'. *Journal of Polymer Composite*, 25 (3), pp. 197-203.

Thomasset. J., Carreau. J.P., Sanschagrin. B., and Ausias. G. (2004). 'Rheological properties of long glass fiber filled polypropylene'. *Journal of Non-Newtonian Fluid Mechanics*, 125, pp. 25-34.

Ticona Injection Moulding Guide. (2011): Celstran Long Fibre Reinforced Thermoplastic. Technical data sheet, Ticona GmbH

Tofteberg. T.R. and Andreassen.E. (2009). 'Multiscale simulation of injection molding of parts with low aspect ratio microfeatures*. SINTEF Materials and Chemistry,* Oslo (Norway).

Toolcraft Plastics. (2014). 'Basic explanation and schematic view - injection moulding process'. Available at: http://www.toolcraft.co.uk/help-injection-moulding-process.htm (Accessed: 27 February 2014)

Tucker. C.L. (2013, December). Fibre orientation and length modelling: the concept behind the calculations. [PowerPoint slides]. Presented at Autodesk University at Las Vegas.

Tucker. C.L. and Advani. S.G. (1994). 'Processing of short-fiber systems'. In: Advani, S.G. Flow and Rheology in Polymer Composites Manufacturing. Elsevier Science, 147-202.

Tucker. C.L., Phelps. J.H., Abd El-Rahman. A.I., Kunc. V. and Frame. B.J. 'Modelling fibre length attrition in molded long-fibre composites'. Proceedings of Polymer Processing Society 26th - PPS-26. Banff (Canada), 2010.

Tucker. C.L., Phelps. J.H., Abd El-Rahman. A.I., Kunc.V., and Frame. B.J. (2010). 'Modelling fiber length attrition in molded long-fiber composites'. *Procedings of polymer processing society 26th annual meeting.* Banaff (Canada), 4-8 July 2010.

Vaxman. A. and Narkis. M. (1989). 'Short-fiber-reinforced thermoplastics. Part 3: Effect of fiber length on rheological properties and fiber orientation. *Journal of Polymer Composite*, 10, pp. 454-462.

Vélez-García. G.M., Mazahir.S., Hofmann. J., Wapperom. P., Baird. D., Zink-Sharp. A. and Kunc.V. *(2010). 'Improvement in orientation measurement for short and long fiber injection molded composites'. Proceedings of the 10th Annual Automotive Composites Conference and Exhibition, SPE ACCE, 11 pages.*

Velez-Garcia. G.M., Wapperom. P., Kunc. V., Baird. D.G. and Zink-Sharp. A. (2012). 'Sample preparation and image acquisition using optical-reflective microscopy in the measurement of fiber orientation in thermoplastic composites'. *Journal of Microscopy*, 248(1), pp. 23-33.

Verleye. V. and F. Dupret. 'Prediction of fiber orientation in complex injection Molded Parts'. Proc. ASME Winter Annual Mtg. New Orleans (LA), 1993.

VerWeyst. B.E., Tucker. C.L., Foss. P.H. and O' Gara. J.F. (1999). 'Fiber orientation in 3-d injection molded features: Prediction and Experiment'. International Polymer Processing, (4), pp. 409-420.

Vincent. M. and Agassant. J. F. (1986). 'Experimental study and calculations of short glass fiber orientation in a center gated molded disc'. *Journal of Polymer Composites,* 7 (2), pp. 76-83.

Wambua. P., Ivens. J. and Verpoest. I. (2003). 'Natural fibres: can they replace glass in fibre reinforced plastics?'. *Journal Composites Science and Technology*, 63 (9), pp. 1259-1264.

Wang. J. and Jin. X. (2010). 'Comparison of recent fiber orientation models in Autodesk Moldflow Insight simulations with measured fiber orientation data'. *Procedings of polymer processing society 26th annual meeting.* Banaff (Canada), 4-8 July 2010.

Wang. J., O'Gara, J.F. and Tucker III. C.L. (2008). 'An objective model for slow orientation kinetics in concentrated fiber suspensions: Theory and rheological evidence'. *Journal of Rheology*, 52 (5), pp. 1179-1200.

Ward, S. and Challahan, C. (1993). 'Proceeding of the 9th Annual ASM/ESD Advanced Composite Conference'. ESD The Engineering Society ESD The Engineering Society. Dearborn (OH), pp. 551-563

Ward. I.M. and Sweeney. J. (2013). 'Polymer Composites: Macroscale and Microscale, in Mechanical Properties of Solid Polymers'. 3rd edn. U.K: John Wiley and Sons Ltd.

Whiteside. B.R. (2001). 'Simulation and validation of fibre orientation in injection mouldings: simulation and experimental validation of short glass fibre orientation and resultant mechanical properties for injection moulded polyamide components of increasing complexity'. PhD. Thesis. University of Bradford.

Wolf. J.H. (1994). 'Screw plasticating of discontinuous fiber filled thermoplastic: Mechanisms and prevention of fiber attrition'. *Journal of Polymer Composites,* 15 (5), pp. 375-383.

Yu. G.H. and Thomas. R. (1997) Method for modelling three dimension objects and simulation of fluid flow. United States Patent 6096088, Appl. 17th Sept 1997, Acc. 1st August 2000.

Zhou. H. (2013). 'Computer modelling for injection molding: simulation, optimization and control'. England: John Wiley and Sons, Inc.

Zhou. H. and Li. D. (2001). 'A numerical simulation of the filling stage in injection molding based on a surface model'. *Advances in Polymer Technology*, 20 (2), pp. 125–131.

Zhou. H., Geng. T. and Li. D. (2005). 'Numerical filling simulation of injection molding based on 3-d finite element model'. *Journal of Reinforced Plastics and Composites*, 24 (8), pp. 823–830.

Zhu. Y.T., Blumenthal. W.R. and Lowe. T.C. (1997). 'Determination of non-symmetric 3-d fibre-orientation distribution and average fibre length in short-fibre composites'. *Journal of Composite Materials,* 31 (13), pp. 1287-1301.

Appendix 1: Injection Moulding Parameters

Injection moulding settings for settings for 4 mm ribbed plaque

Machine	Battenfeld
Injection Time (seconds)	0.8
Hold Pressure (bar)	45
Hold Time (seconds)	15
Melt Temperature (ºC)	270
Mould Temperature (ºC)	90
Cooling Time (seconds)	15

Injection moulding settings for settings for 2 mm plaque

Machine	Battenfeld
Injection Time (seconds)	0.37
Hold Pressure (bar)	40
Hold Time (seconds)	8
Melt Temperature (ºC)	270
Mould Temperature (ºC)	90
Cooling Time (seconds)	15

Injection moulding settings for the centre gate geometries with Rhodia Technyl C216 V40.

Machine	Battenfeld		
Thickness Geometry (mm)	1	2	4
Injection time (mm)	0.47	0.57	0.59
Injection rate (mm/s)	79.5	79.5	79.5
Screw speed (rpm)	75	86	58
Hold Pressure (bar)	40	40	40
Hold Time (seconds)	10	15	10
Melt Temperature (ºC)	270	270	270
Mould Temperature (ºC)	85	85	85
Cooling Time (seconds)	90	90	90

Injection moulding settings for 3.5 mm sprue centre gate geometry for Stamax material.

Machine	Battenfeld	
Thickness Geometry (mm)	1	2
Injection time (mm)	0.67	0.71
Injection rate (mm/s)	45.6	45.6
Screw speed (rpm)	49.5	49.5
Back Pressure (bar)	3	3
Hold Pressure (bar)	35	40
Hold Time (seconds)	10	15
Melt Temperature (ºC)	250	250
Mould Temperature (ºC)	60	60
Cooling Time (seconds)	60	60

Injection moulding settings for 6 mm sprue centre gate geometry for Stamax material.

Machine	Battenfeld	
Thickness Geometry (mm)	1	2
Injection time (mm)	0.67	0.74
Injection rate (mm/s)	45.6	45.6
Screw speed (rpm)	49.5	49.5
Back Pressure (bar)	3	3
Hold Pressure (bar)	25	25
Hold Time (seconds)	5	10
Melt Temperature (ºC)	250	250
Mould Temperature (ºC)	60	60
Cooling Time (seconds)	60	60

Appendix 2: List of Publications

Hine.P, Parveen.B, Brands.D. and Caton-Rose.P. (2014). 'Validation of the modified rule of mixtures using a combination of fibre orientation and fibre length'. Journal of Composite Part A, 64 (13), pp. 70-78.

Parveen.B, Caton-Rose.P, Costa.F, Jin.X. and Hine.P. (2014). Study of injection moulded long glass fibre-reinforced polypropylene and the effect on the fibre length and orientation. AIP Conference Proceedings, 1593, 432-435.

Caton-Rose.P, Hine.P, Costa.F, Jin.X. and Parveen.B. Fibre orientation predictions for short glass fibre reinforced injection moulding. PPS-29, Germany (15-19 July 2013).

Caton-Rose.P, Hine.P, Costa.F, Jin.X, Wang.J. and Parveen.B. Review of short glass orientation prediction models for injection moulding. PPS-26, Niagara Falls (2012).

Hine.P, Parveen.B. and Caton-Rose.P. The effect of fibre length on fibre orientation structures in injection moulded glass fibre reinforced polypropylene plates. 15th European Conference on Composite Materials (ECCM), Venice (2012).

Caton-Rose.P, Hine.P, Costa.F, Jin.X, Wang.J. and Parveen.B. Measurement and prediction of short glass fibre orientation in injection moulding components. 15th European Conference on Composite Materials (ECCM), Venice (2012).

Autodesk University, Vegas (2011)

UK, Moldflow user group, Warwick (2011)